VALLEYS, ESTUARIES, AND LAGOONS: PALEOENVIRONMENTS AND REGRESSIVE-TRANSGRESSIVE ARCHITECTURE OF THE UPPER CRETACEOUS STRAIGHT CLIFFS FORMATION

by

Brenton Michael Chentnik

A thesis submitted to the faculty of
The University of Utah
in partial fulfillment of the requirements for the degree of

Master of Science

in

Geology

Department of Geology and Geophysics

The University of Utah

May 2015

The University of Utah Graduate School

STATEMENT OF THESIS APPROVAL

The thesis of **Brenton Michael Chentnik**

has been approved by the following supervisory committee members:

		Date Approved
Cari Johnson	, Chair	**10/06/2014**
Lisa Stright	, Member	**10/06/2014**
Lauren Birgenheier	, Member	**10/06/2014**

and by **John Bartley** , Chair/Dean of

the Department/College/School of **Geology and Geophysics**

and by David B. Kieda, Dean of The Graduate School.

ABSTRACT

Facies and stratigraphic analysis of the John Henry Member of the Upper Cretaceous Straight Cliffs Formation, exposed in the northern Kaiparowits Plateau of southern Utah, reveals deposition of four regressive-transgressive (R-T) cycles. Each of the four R-T cycles is discussed in detail, with emphasis on the transgressive phases of deposition. Fifteen lithofacies (LF) are grouped into four facies associations (FAs): FA-1: wave-dominated shorefaces; FA-2: coastal plain; FA-3: tide-influenced coastal margin; FA-4: low-energy bay/lagoon. Regressive deposits preserve FA-1 and FA-2, whereas FA-3 and FA-4 comprise transgressive intervals. Seven bounding surfaces and elements define the regressive-transgressive architecture: 1) maximum regressive surface (mRs); 2) process change from wave- to tide-dominated processes (pCt); 3) tidal ravinement surface (tRs); 4) wave ravinement surface (wRs); 5) flooding surface (FS); 6) tide- to fluvial-dominated process change (pCf); and 7) the subaerial unconformity (SU).

At Main Canyon, a stepped, forced regression is associated with the development of shore oblique incised valleys. A composite stratigraphic surface (SU/mRs/tRs), referred to here as the "lower John Henry Member sequence boundary," separates regressive shorefaces from overlying high-energy, transgressive estuarine and back-barrier deposits. Basinward, the correlative conformity is preserved as sharp-based wave-dominated, river-influenced shorefaces. Overlying R-T cycles are not associated with valley incision, but instead preserve sand-rich back-barrier and tidal channel deposits which are overlain distributary mouth bars, fluvial channels and coastal plain fines, which record infilling of the back-barrier. The preservation of >30 m thick accumulations of back-barrier deposits indicate an accretionary shoreline trajectory with balanced rates of high sediment supply and accommodation.

Regional correlation across the northern Kaiparowits Plateau indicate 47% expansion of the John Henry Member occurring over ~14 km from southwest to northeast, with a steep topographic gradient of 0.011. These results suggest structural deformation of the foredeep was occurring from Coniacian to Campanian time, controlling sediment transport, and depositional patterns across the Kaiparowits subbasin. Allogenic and autogenic processes are considered as controls on the stratigraphic architecture for successive regressive-transgressive cycles. This study adds to the growing body of literature documenting the complex nature of transgressive deposits, which will aid in the prediction and management of analogues subsurface reservoirs.

“I have no special talents. I am only passionately curious.”
-Albert Einstein

TABLE OF CONTENTS

LIST OF FIGURES

LIST OF TABLES

ACKNOWLEDGEMENTS

I would like to begin by thanking my friend and advisor Cari Johnson for the countless hours she committed to this project. I am undoubtedly a better geologist having worked with her over these past two years. Many thanks go to Lisa Stright and Lauren Birgenheier for serving on my committee, thoughtful conversations, and critical reviews throughout this project. Thanks to the Grand Staircase Escalante National Monument, the BLM, and Dixie National Forest for providing permits to conduct field work. Chevron, ConocoPhillips, Hess, Shell, and Statoil provided funding.

I cannot begin to express my gratitude to all the brilliant geologists who assisted me in the field: Ryan Purcell, Julia Mulhern, Jonathan Primm, Gavin Ferguson, Alex Lowe, Gabby St. Pierre, Heather Judd, and Robyn Lyons. This project is more yours than mine. Anton Wroblewski provided entertainment in the field in addition to helping identify tidal facies and trace fossils. To the many friends I have made on this journey: Alex Gonzalez, Marco Gorenc, Bianca Maibauer, David Wheatley, Leah Toms, Karenth Dwrosky, Allie Jackson, Thomas Etzel, and many others, thanks for all the wonderful memories. Tyler Szwarc and Alex Turner are not only great friends, but also provided critical feedback throughout this project.

My geologic journey to graduate school began many years ago when a good friend of mine provided an uncertain and lost high school student a chance to see the world. Scott Johnson, I cannot thank you enough for everything you have done for me.

Support and guidance from fiancée Kimble Slonaker is the reason I made it through this process. Thank you for always being patient and understanding, especially when I would disappear into the field for weeks on end. Finally, thanks to my family for always encouraging me to follow my dreams and instilling in me, a love and appreciation for nature.

INTRODUCTION

Despite recent attention, the internal architectures and facies variability of transgressive deposits are still poorly understood relative to their regressive counterparts (Cattaneo and Steel, 2003; Sixsmith et al., 2008; Allen and Johnson, 2011, Kieft et al., 2011). Some of the most well-studied transgressive deposits are estuarine incised valley fills (Allen, 1991; Dalrymple et al., 1992; Allen and Posamentier, 1993; Zaitlin et al., 1994; Boyd et al., 2006). Valleys that form during forced regressions act as zones of bypass that convey sediment to lowstand deltas (Van Wagoner et al., 1990) and submarine fan systems (Posamentier et al., 1991) further basinward. Lowstand fans and deltas form significant petroleum reservoirs (Bhattacharya and Willis, 2001). Consequently, incised valleys have been heavily researched over the past 20 years in order to understand the up dip stratigraphic relationships and controls between fans and the sediment supplying valleys. Additionally, incised valley fills themselves are host to significant petroleum reservoirs (e.g., the Lower Cretaceous Muddy Sandstone in Wyoming). Several questions still exist in regards to the internal architecture, facies distribution, and controls on incised valley development and preservation.

The margins and walls of incised valleys are typically thought to be a chronostratigraphic surface, separating older from younger strata across an unconformity (i.e., sequence boundaries), with regional significance. Recent field studies (Blum and Aslan, 2006; Li and Bhattacharya, 2013) and laboratory experiments (Strong and Paola,

2008) challenge this idea, and indicate that the basal incised valley unconformity is formed throughout various stages of the relative sea level cycle, thus representing a composite stratigraphic surface. Additionally, occupying rivers tend to continually widen the valley as the channel migrates laterally during infilling, resulting in stratigraphic valleys that do not represent any single geomorphic valley in time (Strong and Paola, 2008). Tidal currents are known to remove the basal fluvial deposits within valleys (Allen and Posamentier, 1993; Boyd, Robert W. Dalrymple, et al., 2006a; Plink-Björklund and Steel, 2006), yet their potential to alter the initial valley dimensions is not well understood.

Tidal deposits are common along sections of the coast undergoing transgression (Dalrymple, 2010). Incised valleys are among the first zones along the coast to be flooded (becoming estuaries), and thus are the first areas to experience the effects of tidal energy. Estuaries focus the tidal prism, resulting in stronger tidal currents (Plink-Björklund, 2008; Steel et al., 2012). These currents have the potential to modify the basal unconformity complicating both local and regional correlations. Ravinement is most commonly associated with tidal inlets (Swift, 1968; Demarest and Kraft 1987; Reinson 1992; Allen and Posamentier, 1993), but can also occur at the base of tidal channels within estuaries (Cattaneo and Steel, 2003; Plink-Björklund and Steel, 2006) and back-barrier platforms (Sixsmith et al., 2008). Therefore, the architecture of transgressive tidal deposits is complex because of the migration and stacking of successive channels and the presence of erosional surfaces of several different orders (Dalrymple and Choi, 2007). Additional complications arise when the underlying antecedent topography, upon which transgressive deposits are built, cause lateral variations in accommodation that vary throughout the transgression. Incised valleys generate topographic lows that have the potential to control the position of developing barrier islands. Thus, documenting the orientation of the shoreline and any valley systems present is critical for piecing together the paleogeography, sediment dispersal patterns, and stratigraphic correlations for marginal marine systems.

This study investigates the detailed stratigraphic architecture and depositional environments of the lower and middle John Henry Member of the Straight Cliffs Formation, exposed at Main Canyon in the Kaiparowits Plateau of southern Utah, USA. We focus on the formation and preservation of composite stratigraphic surfaces and the role of antecedent topography on the formation and preservation of transgressive tidal deposits. Additionally, this study expands regional correlations, documents along strike variability along a mixed wave- and tide-dominated shoreline, and discusses allogenic and autogenic process governing stratigraphic architecture preserved within the John Henry Member at Main Canyon. Furthermore, this study adds to the growing body of literature documenting the complex nature of transgressive deposits, which will aid in the prediction and management of analogues subsurface reservoirs

GEOLOGIC BACKGROUND AND PREVIOUS WORK

The Turonian–early Campanian Straight Cliffs Formation was deposited in the foredeep of the Cretaceous Western Interior Basin. Subduction of the Farallon plate beneath the western margin of the North America plate from Jurassic to Eocene time resulted in west-east crustal shortening that culminated in development of the Sevier fold-thrust belt during the Late Cretaceous (Armstrong, 1968; Coney, 1972; Dickinson, 1974; DeCelles and Coogan, 2006). Flexural subsidence, in response to crustal loading within the actively deforming thrust belt (Jordan, 1981), in addition to dynamic mantle-driven subsidence (Liu et al., 2011, 2014), produced an asymmetric foreland basin to the east of the active fold-thrust belt. Global greenhouse conditions and elevated rates of sea floor spreading persisted throughout the Cretaceous, resulting in a global eustatic high-stand (Haq et al., 1987; Miller et al., 2005), that caused flooding of the foreland basin and formed the Cretaceous Western Interior Seaway (Kauffman, 1977; Hancock and Kauffman, 1979).

Upper Cretaceous strata of the Kaiparowits Plateau are composed of siliciclastic detritus derived from the Sevier fold-thrust belt to the west, the Mogollon Highlands to the southwest, and the Cordilleran Volcanic Arc (Eaton, 1991; Lawton et al., 2003; Szwarc et al., in press) (Fig. 1). Distributary fluvial systems draining the Sevier fold-thrust belt and the Mogollon Highlands supplied sediment to a northeast-flowing axial fluvial system that delivered sediment to the Kaiparowits Basin (Szwarc et al., in press).

The Straight Cliffs Formation records coeval deposition of fluvial, paralic-coastal plain, and marginal marine strata along the western margin of the Western Interior Seaway.

Peterson (1969a, b) produced the earliest stratigraphic correlations of the Straight Cliffs Formation and subdivided the formation into four formal units: the Tibbet Canyon, Smoky Hollow, John Henry, and Drip Tank Members (Fig. 2). The lowermost Tibbet Canyon Member consists of shoreface sandstones and offshore mudstones that overlie the Tropic Shale, recording the transition from offshore marine mudstone deposition to more proximal shoreface and nonmarine sedimentation. The Smoky Hollow Member comprises carbonaceous floodplain mudstones and thin coals interbedded with isolated fluvial channels (Peterson 1969b). Amalgamated, coarse-grained fluvial channels of the Calico Bed commonly form the top of the Smoky Hollow Member. The focus of this study is the overlying John Henry Member, which forms the bulk of the Straight Cliffs Formation and preserves the fluvial to marine transition zone in the study area (Fig. 3).

The John Henry Member comprises siliciclastic sandstones, mudstones, and coal, and it outcrops extensively throughout the northern Kaiparowits Plateau (Fig. 3). Peterson (1969b) noted irregular thickening of the John Henry Member from ~200 m in the southwest plateau to over 330 m in the northeast, and recent studies extend this to >500 m thick at Buck Hollow (Mulhern et al., 2014; Fig. 2). In general, the western Kaiparowits Plateau preserves fluvial and coastal plain strata (Peterson, 1969a; McCabe et al., 1988; Shanley and McCabe, 1991, 1994; Shanley et al., 1992; Hettinger et al., 1993; Gallin et al., 2010; Gooley, 2010; Pettinga, 2013; Turner et al., in review), whereas the eastern plateau preserves shoreface and lagoonal deposits (Allen and Johnson, 2011; Dooling, 2013). Peterson (1969b) named seven shoreface deposits along Fifty Mile

Mountain “A” to “G,” in stratigraphic order (Fig. 2). Extensive coals occur in the center of the plateau and have been the focus of numerous studies to document their nature, distribution, and economic potential (e.g., Vaninetti, 1979; Hettinger, 1995, 2000). These are termed the Lower, Christensen, Rees, and Alvey coal zones in stratigraphic order (Fig. 2).

Shanley (1991) and Shanley and McCabe (1991, 1992, 1993, 1994, 1995) conducted the first sequence-stratigraphic studies of the Straight Cliffs Formation, and linked changes in alluvial architecture to down-dip trends in marginal marine strata. In this body of work, they identified four sequence boundaries (Fig. 2) in the Straight Cliffs Formation: 1) the Tibbet Canyon sequence boundary, located at the top of the Tibbet Canyon Member; 2) the Calico sequence boundary, located at the base of the Calico Bed; 3) the “A- sequence boundary,” in the lower John Henry Member at the top of the A-shoreface; and 4) the Drip Tank sequence boundary, located at the base of the Drip Tank Member.

Allen and Johnson (2010, 2011) revisited the John Henry Member and identified six transgressive-regressive shoreface cycles at Rogers Canyon (Fig. 1). In their analysis, the “A,” “B,” and “C” shorefaces of the lower John Henry Member are strongly progradational. Additionally, their study recognized a larger basinward shift in facies between the “B” and “C” shorefaces (15 km) than the “A” to “B” (4 km), and this notion is supported by other studies (e.g., Hettinger 1996; Gallin et al., 2010; Gooley, 2010; Dooling et al., 2012; Mulhern et al., 2014).

Along Highway 12 (Fig. 3), Hettinger et al. (1993) performed detailed stratigraphic analysis on transgressive deposits within the Calico sequence, and documented the detailed architecture of the overlying highstand shoreface strata within the John Henry Member. The Calico Bed is interpreted as a braided fluvial sheet deposited during a period of decreased accommodation relative to sediment supply (Bobb, 1991). Shanley and McCabe (1991) interpreted a sequence boundary at the base of these braided fluvial deposits and related it to a late-Turonian base-level fall. However, new detrital zircon data indicate that the Calico Bed is early Coniacian in age (Szwarc et al., in press), which does not correspond with a major eustatic sea level fall (Hardenbol et al., 1998; Miller et al., 2005). Other studies have noted major erosion and an unconformity at the top of the Calico Bed (Bobb, 1991; Shanley and McCabe, 1991; Gooley, 2010). In Upper Valley (Fig. 3), the Calico Bed is >45 m thick (Bobb, 1991) and is overlain by heterolithic tidal deposits interpreted by Hettinger et al. (1993) as estuarine backfill, recording the initial transgression following deposition of the Smoky Hollow Member. Additionally, their study briefly discussed transgressive deposits occurring above the “A sequence boundary,” which they interpreted as estuarine backfill of an incised valley. These deposits are reconsidered in the current study, which examines them in a parallel outcrop section in Main Canyon, ~3 km north of Upper Valley (Fig. 3).

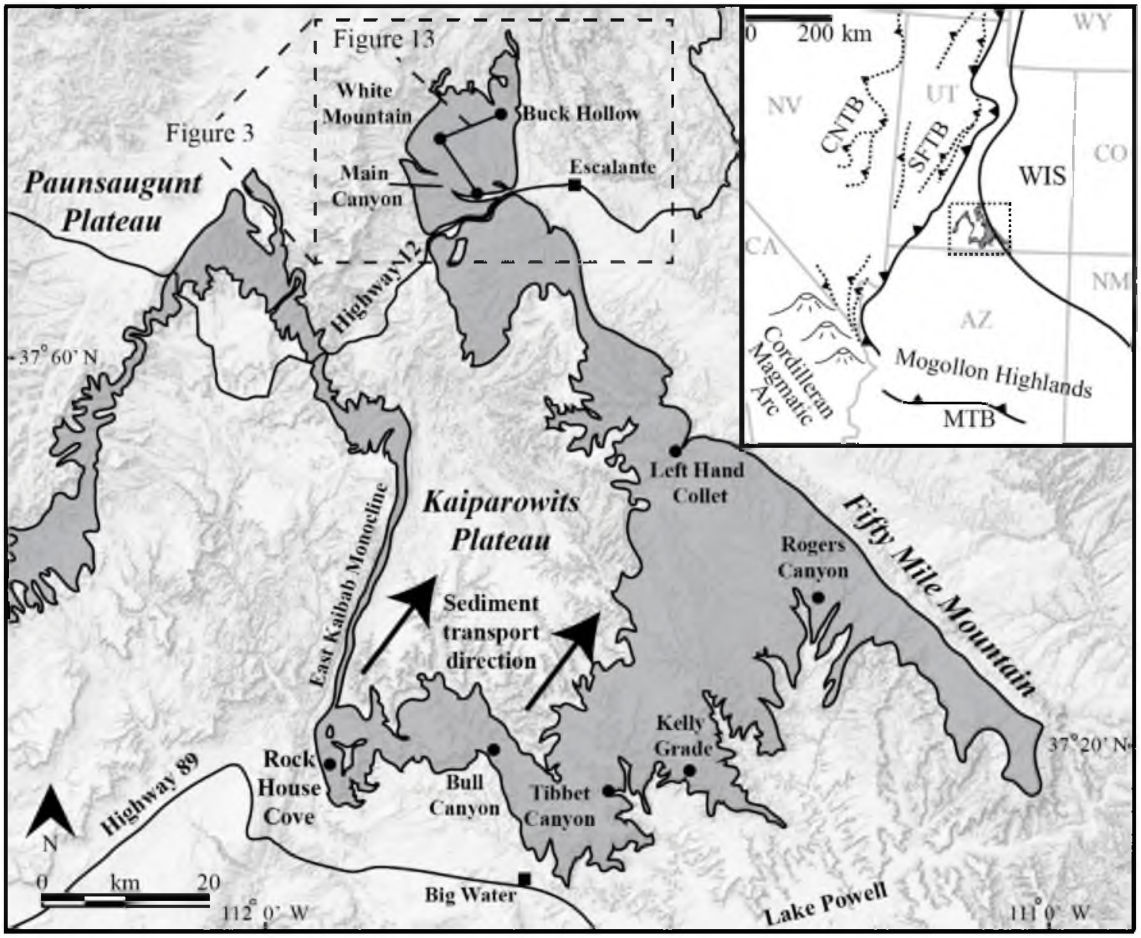

Figure 1. Regional map of the Kaiparowits Plateau of southern Utah. Outcrops of the Straight Cliffs Formation are shaded gray with locations of previous studies focused on the John Henry Member highlighted. Arrows indicate the general proximal to distal facies relationships in the John Henry Member, ranging from fluvial on the western margin to marine on the eastern margin, with tidal and paralic facies in between. Abbreviations: CNTB-Central Nevada Thrust Belt, SFTB-Sevier fold-thrust belt, WIS-Western Interior Seaway, MTB-Maria Thrust Belt. Location of preliminary stratigraphic correlation (Fig. 13) is shown. Modified from Szwarc et al. (in press).

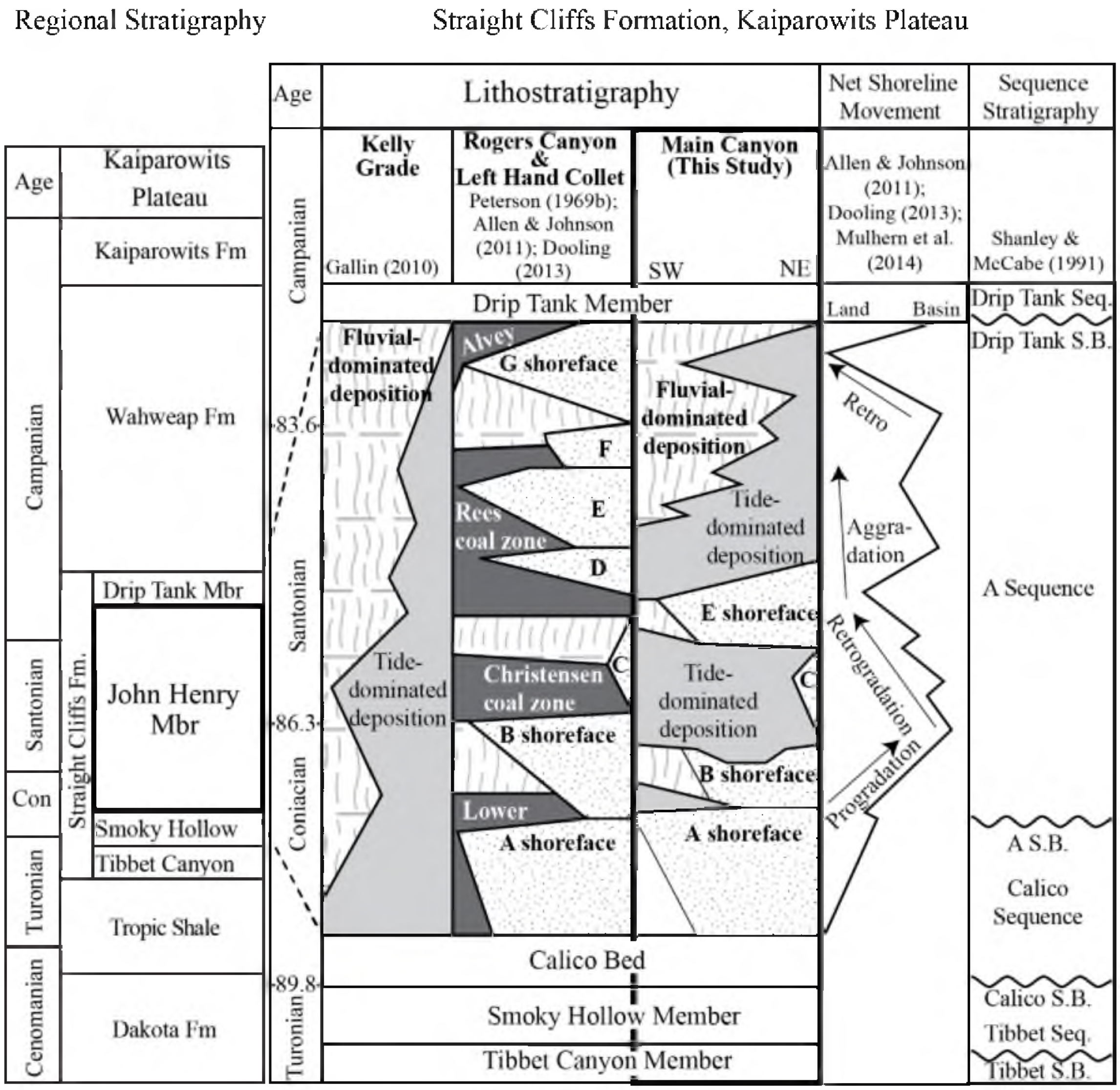

Figure 2. Stratigraphic summary chart of the Turonian-Campanian Straight Cliffs Formation, including previous lithostratigraphic and sequence stratigraphic interpretations. Seven marine sandstone packages were named “A-G” by Peterson (1969a) that pinch out landward into coal zones and coastal plain facies. Net shoreline movements are based on shoreface pinchouts and marginal marine facies distributions at Left Hand Collet (Dooling, 2013) and Rogers Canyon (Allen and Johnson, 2011).

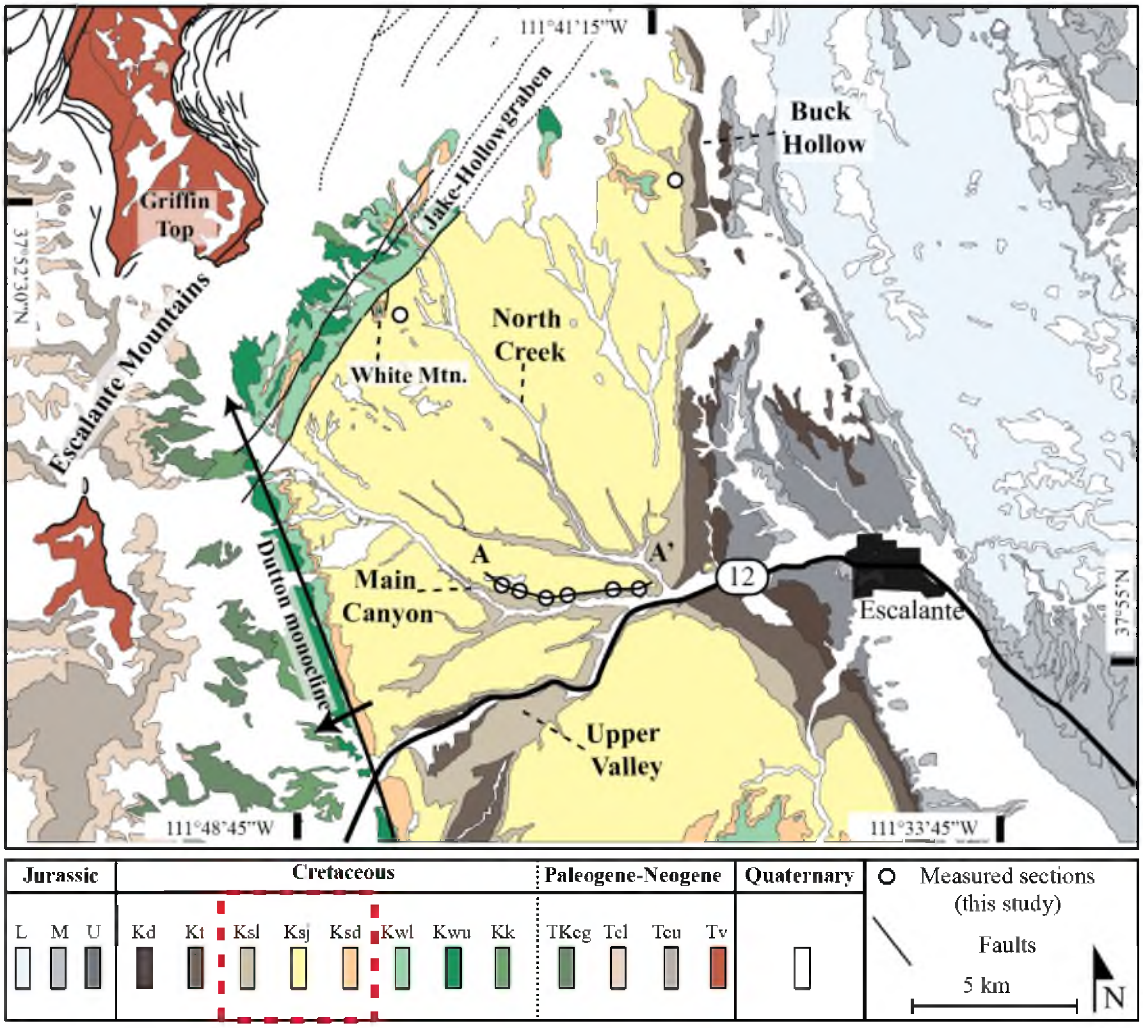

Figure 3. Simplified geologic map of the northern Kaiparowits Plateau illustrating the extensive outcrops of the John Henry Member, locations of measured sections used in this study, and the position of correlation A to A' depicted in Figure 8. Abbreviations: L-Lower, M-Middle, U-Upper, Kd-Dakota, Kt-Tropic Shale, Ksl-lower Straight Cliffs Fm., Ksj-John Henry Member, Ksd-Drip Tank Member, Kwl-lower Wahweap Fm., Kwu-Upper Wahweap Fm., Kk-Kaiparowits Fm., TKcg-Grand Castle Fm., Tcl-lower Claron Fm., Tcu-upper Claron Fm., Tv-Tertiary volcanics undifferentiated. Quaternary deposits are undifferentiated and shaded white. Modified from Doelling and Willis (1999).

METHODS

A total of seven sections were measured in and near Main Canyon (Fig. 3), plus multiple detailed sections to capture facies variability. Six of the sections are from the northern wall of Main Canyon, and span the lower to middle John Henry Member, with the base of most sections occurring on a correlative flooding surface at the top of the Calico Bed at the base of "A" sandstone interval, and the top of exposures within a burned coal zone (the Rees coal zone). One additional section was measured ~9 km north of Main Canyon, near White Mountain, from a flooding surface at the base of the "E" sandstone interval in the middle John Henry Member up to the base of the Drip Tank Member.

All sections record vertical changes in grain size, sorting, texture, sedimentary structures, bedding geometries, trace and body fossils, and paleocurrent indicators. Key facies and bounding surfaces were walked-out to document lateral variability and facies transitions. Photomosaics assisted correlations between measured sections and across inaccessible outcrops. A differential GPS unit paired with a laser rangefinder was used to map bounding surfaces and the geometries of sand bodies and facies belts. Paleocurrent data (n=1,017) were collected on the axes of trough cross-stratification, planar cross-stratification, ripple-laminations, and flute casts. Water depths of both fluvial and tidal channels were estimated using measurements of mean cross-set height (hm) and applying the methods of Leclair and Bridge (2001). The minimum (six times the cross-set height) and maximum (ten times the cross-set height) water depth estimates from this analysis are presented for key stratigraphic intervals.

Data from Main Canyon and White Mountain are used in conjunction with a complete section of the Straight Cliffs Formation from Buck Hollow (Mulhern et al., 2014) to discuss regional correlations, sedimentation trends, paleogeography, and basin evolution. Aerial photographs taken along Fifty Mile Mountain and canyons throughout the northern plateau assisted regional correlations.

FACIES ANALYSIS

An assemblage of 15 lithofacies (LF) is identified based on lithology, primary bedding structures, trace and body fossils, bedding geometries, paleocurrent measurements, and their vertical and lateral associations with other facies. Characteristics of each lithofacies, along with its interpreted depositional environment(s) are summarized below and in Table 1. Lithofacies are grouped into four facies associations (FAs): wave-dominated shoreface (FA-1), coastal plain (FA-2), tide-influenced coastal margin (FA-3), and low-energy lagoonal/bay facies (FA-4). Each facies association reflects the dominant processes that controlled deposition (e.g., waves and storms, tidal currents, rivers, and suspension settling), with each FA commonly occurring within either regressive or transgressive phases.

Facies Association 1 - Wave-Dominated Shoreface

Description. Facies association 1 (Fig. 4) comprises the bulk of the lower and middle John Henry Member in the study area. Lithofacies 1.1 consists of planar-laminated gray mudstones and siltstones interbedded with hummocky cross stratified (HCS), heavily bioturbated sandstones. Mudstones and laminated siltstones contain abundant terrestrial plant material, and coarsen upward to capping sandstone beds between 0.2–1.0 m thick. These sandstones are in turn overlain by finer-grained deposits. Packages coarsen and thicken upwards into very fine- to fine-grained hummocky and swaley cross-stratified (SCS) sandstones of lithofacies 1.2 (Fig. 4). HCS is abundant at the base of these sandstone units with SCS becoming progressively more abundant in the upper intervals. Bioturbation within these amalgamated sand-rich units is minor and typically consists of *Ophiomorpha* and *Schaubcylindrichnus* (Fig. 4). Within the lower John Henry Member, cross-stratified quartzite pebbles occur as lags (Fig. 4F) that correlate basinward (east) to flooding surfaces. Lithofacies 1.2 (Table 1) transitions basinward to lithofacies 1.1 over <5 km at Main Canyon.

Interpretation. Deposits assigned to FA-1 record deposition on a wave- and storm-dominated shelf. Interbedded mudstones and siltstones record deposition in offshore and distal lower shoreface marine environments (LF 1.1); hummocky cross-stratified sandstones (LF 1.2) record shelfal transportation and reworking during storm events (Walker and Plint, 1992; Clifton, 2006). Abundant terrestrial plant debris and sharp-based shorefaces suggest the presence of nearby distributary channel(s) supplying sediment to a wave and storm-dominated coast (Walker and Pint, 1992). Coarsening upward packages record shallowing environments as shorefaces prograded, and these are bound by flooding surfaces (i.e., parasequences of Van Wagoner et al., 1988). In places, lithofacies 1.2 includes basinward-inclined planar laminations recording foreshore deposition. However, these sections are commonly truncated by the overlying flooding surface of the next parasequence and therefore poorly represented throughout the section. Trace fossils are typical of marine environments, but their rarity suggests high sedimentation rates that generally outpaced burrowing (MacEachern and Pemberton, 1994; Pemberton et al., 2001). Additionally, burrows are usually vertical and lined, indicative of a high-energy environment. The unusually thick (>25 meter) accumulations of shoreface deposits indicate a high accommodation and high sediment supply setting (Allen and Johnson, 2011).

Facies Association 2 – Coastal Plain

Description. Deposits of FA-2 (Fig. 5) occur throughout the section at Main Canyon but comprise a significant portion of the deposits of the middle and upper John Henry Member. These deposits are laterally and vertically associated with deposits of the other three facies associations, across both unconformable and conformable contacts. Lithofacies 2.1 consists of well-sorted, upward-fining cross-stratified sandstones which are commonly tabular and not confined to distinct channels. Where channelized, the sandstone bodies have 1–2 m of basal scour relief. Paleocurrents from lithofacies 2.1 show predominantly northeast flow. Plant fragments and leaf impressions are common, and the upper parts of the sandstones commonly contain root traces. Lithofacies 2.1 laterally transitions to, and also erosively overlies, lithofacies 2.2, which itself contains massive and planar-laminated carbonaceous siltstones, mudstones, and coals with abundant root traces indicating pedogenesis. Rippled siltstones and very-fine grained sandstones are interbedded within the carbonaceous shales. These coarser-grained beds are most common at the bottoms of sandstone bodies of lithofacies 2.1.

Channelized medium- and coarse-grained sandstones, and channelized lithic-clast breccias, form the most internally-complex deposits identified in the study area. These channelized deposits are assigned to lithofacies 2.3 (Table 1) and are only identified along a single 100–200 m stretch of outcrop above the “B” shoreface in the study area. Channelized breccias are matrix supported, poorly sorted, and discontinuous over 10 to

20 m (Fig. 5C). No trace fossils were observed within this facies.

Inclined, erosionally-based, lenticular cross-stratified sandstones comprise lithofacies 2.4. Internal scouring and trough-cross stratification is common within individual lenticular bodies and there is limited bioturbation in the form of *Teredolites* bored wood fragments (Table 1). Lithofacies 2.4 is laterally associated with deposits of FA-1 (shorefaces) and FA-4 (lagoon fill) within two intervals of the John Henry Member at Main Canyon. The channelized deposits overlie shoreface strata in the "A' sandstone interval in the western part of the study area (Figs. 4A, 5BC). In the middle John Henry Member, sand bodies transition laterally into carbonaceous shales and channelized sandstones over tens to hundreds of meters and amalgamate to form 5 to 10 m thick complexes.

Interpretation. Facies association 2 (Fig. 5) contains the most proximal deposits of the John Henry Member at Main Canyon, recording deposition on a paralic coastal plain dissected by distributary channels. Lithofacies 2.1 records deposition within fluvially-dominated distributary channels preserved as channel belts (Bridge, 2003), whereas lithofacies 2.2 (Table 1) record the interdistributary, overbank deposits. Scour surfaces, barform accretion surfaces, and unidirectional trough cross-stratification are indicative of fluvial channels (Miall, 1985). Crevasse splay deposits are recorded as siltstones and rippled sandstone beds, their increased abundance at the bases of sandstones records increasing proximity to laterally migrating channel belts. In the middle John Henry Member, these units are heavily brecciated and baked from coal fires, making correlations and facies identification difficult. Lenticular sandstone bodies of lithofacies 2.4 occur at the basinward reach of distributary channels (where they transition into lagoon fill of FA 4), and are interpreted as distributary mouth bars. Where laterally-amalgamated, these units form mouth-bar complexes (Fielding et al., 2005; Fielding, 2010). The lack of marine trace fossils and presence of scarce *Teredolites* bored wood fragments indicate brackish water conditions.

Lithofacies 2.3 (Table 1) is interpreted as recording bank collapse and debris flows within an erosionally-confined valley. Abrupt lateral pinch outs (Fig. 5BC) of channels and abrupt lateral facies transitions suggest that these deposits were left behind as abandoned terraces during a period of active fluvial incision. Lateral migration of incising channels undercut valley margins and produced bank instability (Schumm, 1993a). High-discharge storm events could have triggered bank failure and temporally increased stream power to levels high enough to transport boulder-sized clasts downstream. The highly angular clasts indicate a relatively short transport distance, further supporting the debris flow interpretation. Deposits of lithofacies 2.3 are included within FA-2 because no tidal indicators or marine trace fossils were observed and paleocurrents are unidirectional to the northeast (Table 1). Similar deposits are found at the base of the fluvial-dominated incised valley fills in the Lower Cretaceous Fall River Formation (Willis, 1997). In an alternative interpretation, these debris flows may have resulted from lateral migration and bank collapse of tidal channels within an estuary or back-barrier lagoon environment.

Facies Association 3 – Tide-Influenced Coastal Margin

Description. The deposits that comprise FA-3 (Fig. 6) overlie FA-1 shoreface strata across both unconformable and conformable contacts. Landward, FA-3 deposits transition to coastal plain strata of FA-2; while the basinward expression of FA-3 is not preserved in the study area. The deposits are a complex assemblage of sandstones (Fig. 6A) and heterolithic strata with wavy and lenticular bedding (Fig. 6B), organized into packages that generally fine upwards, and contain sparse bioturbation (Fig. 6C; Table 1).

Strata assigned to lithofacies 3.1 are channelized and sigmoidal sandstone bodies that contain abundant bidirectional paleoflow indicators (trough, planar, sigmoidal and herringbone cross-stratification), soft sediment deformation features, and carbonaceous mud drapes (Fig. 6D; Table 1). Paleocurrents indicate flow (Fig. 6E) to the northeast and southwest (Figure 6A; Table 1). Bioturbation is most abundant within the heterolithic sections (Fig. 6F) and consists of small, unlined horizontal burrows (*Planolites*). Sandstones and heterolithic deposits amalgamate to form complexes that locally exceed 30 m in thickness. These complexes interfinger with and are overlain by carbonaceous shales (LF 4.1), and also locally interfinger with rhythmically-bedded deposits of lithofacies 3.6 (Fig. 6A). In the upper section, channels erosively overlie the “E” shoreface and are laterally equivalent to deposits of lithofacies 3.6 and lithofacies 4.1. Channels correlate basinward (northeast) to a 10–20 m thick, laterally continuous (>10 km along both depositional strike and dip) sandstone sheet deposit of lithofacies 3.5 (Fig. 6A).

Lithofacies 3.2 consists of amalgamated, well sorted, very fine- to fine-grained sandstone bodies. Primary sedimentary structures are dominated by upper plane beds and trough cross-stratification. It is distinguished from other deposits within FA-3 by lacking more heterolithic, wavy and lenticular-bedded deposits, and by its limited lateral extent defined by a concave-up basal surface of erosion. Amalgamated sandstone bodies form complexes >15 m thick that are dominated by northeast directed paleocurrents with subordinate flow to the southwest (Table 1). Vertically, these deposits become progressively heterolithic and transition to lithofacies 3.1 and lithofacies 4.1.

Deposits assigned to lithofacies 3.3 consist of inclined heterolithic strata that unconformably overlie the “B” shoreface in the western part of Main Canyon (Fig. 6F). Reactivation surfaces occur within mud-draped planar and trough cross-stratified sandstones. The thinly bedded nature of these deposits, in conjunction with their lateral transition to more heavily amalgamated channel bodies of lithofacies 3.1, warrants classification as a separate facies. Due to limited exposures above shoreface cliffs, these deposits could only be examined in detail along a small length of outcrop (Fig. 6F).

Lithofacies 3.4 comprises interbedded fine- to coarse-grained sandstones and gravels, and is observed at the mouth (east) of Main Canyon. These deposits overlie and transition westward into deposits of FA-4. Paleocurrent data are bimodal (Table 1) with southwest (paleolandward) dominated currents and subordinate flow to the northeast (paleobasinward). A continuous ~ 5 cm thick oxidized layer separates tan-colored barforms from overlying white tidal deposits assigned to lithofacies 3.5.

Lithofacies 3.5 consists of characteristically white, well-sorted, medium-grained, sheet-like, sandstone-dominated deposits. Above the "B" shoreface, paleocurrents display strong bidirectionality with southwest dominated flow and subordinate flow to the northeast (Table 1). In the "E" sandstone interval paleocurrent data display similar trends

(Fig. 6; Table 1). Several distinctions exist between this facies and lithofacies 3.4; lithofacies 3.5 has better sorting, fewer mud rip-up lags and gravels, and forms a laterally extensive (>5 km along depositional strike and >2.5 km along depositional dip) sheet across the study area. In contrast, sandstones and gravels of lithofacies 3.4 become more heterolithic in a paleolandward (southwest) direction. This facies may have an erosive base or conformably overlie shoreface deposits.

The final lithofacies (LF 3.6) discussed within FA-3 comprises rhythmically bedded (Fig. 6G), planar-laminated sandstones and siltstones that are observed in the middle John Henry Member along the western section of Main Canyon. Here, these deposits laterally correlate to large (>30 m thick) sand-rich complexes with sigmoidal and channel shaped sandstones of lithofacies 3.1, and fine-grained carbonaceous shale and laminated grey siltstone and mudstone deposits of lithofacies 4.1.

Interpretation. Facies Association 3 is interpreted as tide-influenced sandstones and heterolithic strata deposited and shaped by sediment transport associated with tidal channels housed within estuaries and tide-dominated back-barrier lagoons (Table 1). Lithofacies 3.1 records deposition within tidal channels, creeks (Hughes, 2012), and elongate tidal bars (Dalrymple et al., 2012). Lithologically, tidal channels and creeks have the same characteristics as elongate tidal bars, hence their presentation here as the same lithofacies. The only major difference between them is the scale of the barforms, sigmoidal-shaped elongate bars reach heights in excess of 15 m, whereas individual bars within tidal channels and creeks are between 1–5 m in size. Tidal channels and elongate tidal bars within a larger incised container suggest an estuarine association, whereas tidal channels above a relatively conformable surface could represent back-barrier deposits.

Elongate tidal bars are common along the outer reaches of modern tide-dominated estuaries (Dalrymple et al., 2012) and can have relief in excess of 20 m from the bar crest to the bottom of the adjacent tidal channel.

Deposits of lithofacies 3.2 record the basal fill of an incised valley network within upper flow regime sand flats and ebb channels (Dalrymple et al., 2012). Sand-dominated, multistory channel belts developed in response to lateral confinement within a valley and display northeast dominated paleoflow (Table 1). This basinward dominance in flow direction with subordinate flow to the southwest indicates fluvial processes prevailed, with minor flood-tidal influence. The highly aggradational nature of these deposits, coupled with the lack of heterolithic strata common in other tidal deposits, suggest a high-energy environment with few periods of slackwater (Reineck and Wunderlich, 1968). Additionally, the dominance of plane parallel laminations within well-sorted fine-grained sandstones indicate that upper-flow-regime conditions dominated, consistent with deposition in the braided sand-flats of a tide-dominated estuary (Dalrymple et al., 1990; Dalrymple et al., 2012).

Lithofacies 3.3 (Fig. 6F) is interpreted as tidally-influenced fluvial point bars. Similar inclined heterolithic strata have been described throughout the Kaiparowits Plateau in the John Henry Member (Shanley et al., 1992; Gallin, 2010; Gooley, 2010; Pettinga, 2013) and are commonly thought to occur during transgressive intervals. Rhythmic interbedding and draping of mud and sandstone (Fig. 6F) form under conditions of fluctuating current energy (Thomas et al., 1987; Shanley et al., 1992) and can occur in fluvial deposits that are not influenced by tidal currents. However, the presence of *Teredolites* borings indicate brackish water conditions (Bromley et al., 1984) and its occurrence with other marine trace fossils further indicates marine influences. These factors combine to suggest mudstone deposition occurred during periods of slackwater between tidal cycles (Thomas et al., 1987; Shanley et al., 1992; Dalrymple and Choi, 2007). Alternatively, lithofacies 3.3 may record tidal reworking of a bayhead delta along the landward reach of an estuary (Dalrymple et al., 1992). The lateral correlation to upper flow regime tidal flats and ebb channels make this a viable interpretation. It is unlikely, however, given that an up-section increase in sandstone is not observed within these deposits, which would be expected within a bayhead delta (Boyd, 2010). In either case, tidal currents were strong enough to remobilize and transport sand-sized sediment, and the intervening slackwater periods were long enough to allow suspension settling of clay- and silt-sized particles.

Lithofacies 3.4 comprises prograding flood-tidal deltas on the sheltered side of a barrier island. Lateral and vertical relationships with lithofacies 4.1 and lithofacies 4.2, combined with flood-dominated paleocurrents (Table 1), an abundance of tidal indicators, an upward increase in grain-size, amalgamation, and the presence marine body fossils support this interpretation (Hayes, 1979; Israel, 1987; Allen and Johnson, 2010). Flood-tidal deltas form along weaknesses generated in the barrier island by washovers that are subsequently exploited by tidal inlets (Barwis et al., 1990; Allen and Johnson, 2011). The presence of swaley-cross stratification indicates that wave-reworking of the tidal barforms occurred. Allen and Johnson (2010) proposed a micro- to mesotidal environment for similar deposits observed to the southeast at Rogers Canyon and Left Hand Collet, respectively. The continuous oxidized horizon that separates lithofacies 3.4 from lithofacies 3.5 may represent a short-lived period of subaerial exposure of the flood tidal delta during a high-frequency drop in relative sea-level.

The lateral continuity, high-energy sedimentary structures, and sheet-like geometry of lithofacies 3.5 are indicative of deposition within a migrating tidal inlet or a sand-rich back barrier. Where these deposits occur as a capping unit overlying lithofacies 3.4 and deposits of FA-4, with an erosive base, they represent tidal inlet fill. When conformably overlying shoreface deposits (Fig. 6A), they are interpreted to reflect migration of dunes and barforms in a sandy back barrier setting. In this latter case, sand bodies record migration on a subtidal-to-intertidal platform landward of the barrier island (Sixsmith et al., 2008). These sheet deposits are coeval with tidal channels of lithofacies 3.1 that occur in the paleolandward part of the study area. Adjacent to these tidal channels, rhythmically bedded, centimeter thick beds of sandstone with mudstone, and carbonaceous partings record declining tidal current energy along the lower to middle intertidal flats over many tidal cycles (Davis and Dalrymple, 2012). These deposits comprise lithofacies 3.6. Local scours dissect these deposits and were likely generated by tidal creeks that eroded gullies into the tidal flats and marshes (Hughes, 2012). The lateral correlation with tidal channels and carbonaceous lagoonal and bay-fill further indicate the influence of tidal currents on deposition.

Facies Association 4 – Low-Energy Bay/Lagoon

Description. Lithofacies 4.1 (Fig. 7A) is comprised of fissile siltstones and mudstones with varying carbonaceous content, and subbituminous coals. Coals typically occur as capping units at the tops of carbonaceous shale packages where the concentration of terrestrial organic material progressively increases vertically. Oyster shell fragments are common throughout, and occasionally occur as thin (10 cm) lags. Bioturbation is limited to small-diameter *Planolites* burrows within the carbonaceous shales. Lithofacies 4.2 is interbedded with lithofacies 4.1 throughout the section and is composed of well-sorted sandstones containing landward (southwest) inclined planar-laminations, landward directed ripples, and small-scale trough cross stratification (Fig. 7; Table 1). Sandstone beds are typically <1 m thick (Fig. 7B) and laterally extensive for around 100 m. Along the eastern part of Main Canyon, these sandstones are observed vertically and laterally transitioning into more laterally extensive bidirectional sands and gravels of lithofacies 3.4 (Fig. 7B). Marine body fossils of oysters, inoceramids, gastropods (Fig. 7C), and sharks' teeth occur within sandstones along with *Skolithos*, *Ophiomorpha*, *Planolites*, and *Lockeia* traces.

Interpretation. Facies association 4 records deposition within a sheltered back-barrier lagoon, low-energy bay, or the middle stretches of an estuary. Shells and trace fossils of marine organisms, along with lateral associations with sandy tidal deposits, distinguish lithofacies 4.1 from coastal plain carbonaceous shales (LF 2.2). Furthermore, an impoverished trace-fossil assemblage implies brackish conditions. The basinward decrease in organic material further suggests increasing marine influence, which is supported by the presence of flood-tidal delta deposits in the eastern part of the study area. This facies represents subaqueous deposition in low-energy back-barrier lagoons or restricted bays, with flanking swamps that supplied abundant carbonaceous material (McCabe et al., 1988; Hettinger, 2000).

Thinly-bedded sandstones of lithofacies 4.2 contain landward-directed paleocurrents and inclined laminations (Fig. 7D). This, plus a marine trace fossil assemblage and marine body fossils, indicate storm-driven deposition of washover fans on the landward sides of barrier islands. Barrier islands that migrate landward are made up of coalescing washover fans or washover terraces that form when storm waves overtop the barrier, transport sand from the beach, and then deposit it on the backside of the barrier (Hayes and FitzGerald, 2013). Planar laminations within washovers record upper plane bed sedimentation during the initial stages of flooding followed by waning flow, small-scale ripples, and troughs (Barwis and Hayes, 1985; Allen and Johnson, 2010).

Table 1

Lithofacies descriptions and environmental interpretations

Lithofacies	Description and Architecture	Trace/Body Fossils	Environment
Facies Association 1 - Wave-Dominated Shorefaces			
1.1 - Interbedded light brown-gray mudstones, siltstones, fine-grained sandstones	Planar-laminated mudstones and siltstones, 1–10 cm thick, occasional symmetric wave ripples. Sandstone beds are 0.2–1 m thick, sharp-based, and contain abundant hummocky cross-stratification (HCS). Packages coarsen upward from silt to very fine-grained sandstone in 0.5–4 m sections.	Small shell fragments, abundant plant fragments. *Ophiomorpha, Thalassinoides, Chondrites, Zoophycos, Planolites, Palaeophycus.* BI = 0–3	**Offshore and distal lower Shoreface**
1.2 - Hummocky and swaley cross stratified sandstones	Cliff-forming very fine- to fine-grained sandstones, form sharp-based coarsening-upward packages, separated by finer-grained sands or marine mudstones. Amalgamated sandstone units can be >25 m thick and laterally continuous >10 km. HCS and swaley-cross stratification (SCS) are abundant. Locally, SCS grades into zones of planar laminations that are gently inclined to the east.	Minor inoceramid and oyster shell fragments. *Ophiomorpha, Thalassinoides, Schaubcylindrichnus, Skolithos.* BI = 0–1	**Proximal lower and middle shoreface**
Facies Association 2 – Coastal Plain			
2.1 - Channelized upward-fining cross-stratified sandstones	Coarse- to medium-grained, cross-stratified sandstones containing: gravel lags, leaf impressions, plant fragments, basal mud rip-up lags, coaly debris, internal scouring, and erosive bases with up to 2 m of relief. Channels range in thickness from 0.5–3 m, and can amalgamate to form complexes up to 15 m thick. Sandstone continuity ranges from 10s to 100s of m. Sandstones interfinger with carbonaceous shales of lithofacies 2.2 and lenticular sandstones of lithofacies 2.4.	Traces are uncommon; only a few small *Planolites* were found on bases of beds and sporadic root traces in the tops of sandstones. BI = 0–1	**Distributary channels** 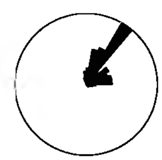 **n=86**
2.2 - Rooted carbonaceous mudstones and coals	Massive and planar-laminated siltstones and mudstones with minor interbeds of very fine-grained ripple-laminated sandstones and coal. The organic content of carbonaceous shales increases vertically at the bed scale, with thin (typically < 0.5 m) coals typically occurring as capping units. Siltstone and rippled sandstones are most commonly observed at the bases of sandstone bodies of lithofacies 2.1.	Root traces were the only fossils observed. BI = 0–1	**Swampy interdistribut-ary coastal plain**

Table 1 (continued)

Lithofacies	Description and Architecture	Trace/Body Fossils	Environment
2.3 - Channelized sandstones and matrix supported, lithic-clast breccias	Laterally confined, channelized lithic-clast breccias, channelized medium-grained sandstones, and planar-bedded sandstones and siltstones. Individual channels are continuous for tens of meters. Lithic clasts are composed of laminated gray-brown mudstones, tan siltstones, and laminated sandstones. Clasts can be as large as boulders (> 26 cm in diameter) and are supported by a predominantly sandstone matrix. Breccia channels and sandstone channels truncate and erode up to 1 m into older deposits. Sandstone channels include unidirectional north-northeast-directed, 5–20 cm scale trough cross-stratification. Planar-bedded sandstones and siltstones contain trough and planar cross-sets, flame structures, and convolute bedding.	Small pieces of shell fragments occur on the tops of a few sandstone beds, with chert and quartzite pebbles. BI = 0	**Debris flows**  **n=32**
2.4 - Inclined lenticular cross-stratified sandstones	Erosionally-based fine- to medium-grained sandstones organized into inclined (5°–20°) sharp-based lenticular bars. Individual bars are typically around 1.5 m thick with abundant internal scouring and trough cross-stratification. Form 5–10 m thick complexes.	Sparse oyster shell fragments; Wood fragments bored by *Teredolites* are observed in lags with mud rip-ups at the bases of sand bodies. BI = 0–1	**Distributary mouth bars** 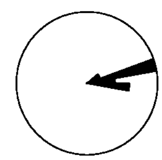 **n=20**
Facies Association 3 –Tide-Influenced Coastal Margin			
3.1 - Channelized, bidirectional sandstones	Laterally confined sigmoidal bars and channel-shaped sandstones. Bars and channels can be in excess of 5 m thick and continuous over the order of 100 m, amalgamating to form complexes up to 30 m thick. Granual lenses 1–5 cm thick occur throughout but are not ubiquitous. Sandstones typically fine upwards and contain primary sedimentary structures of: low-angle planar laminations, wavy-lenticular-flaser bedding, convolute beds, bidirectional planar and trough cross-stratification with double mud drapes and abundant reactivation surfaces.	Pervasive, inoceramid and oyster shell fragments, can also occur as lags at the bottom of channels with clay rip-ups and wood fragments; Trace fossils are scarce but include: *Teredolites, Skolithos, Lockeia, Gyrochorte, Planolites,* and *Diplocraterion.* BI = 0–3	**Tidal channels and elongate tidal bars** 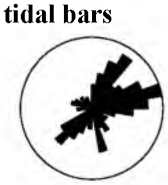 **n=311**

Table 1 (continued)

Lithofacies	Description and Architecture	Trace/Body Fossils	Environment
Estuarine association			
3.2 - Ebb-dominated multistory sandstones	Multistoried very fine- to fine-grained sandstones dominated by upper plane beds, trough cross-stratification, and minor zones with reactivation surfaces. Mud drapes occur but are not pervasive. These form amalgamated complexes > 15 m thick.	Inoceramid and oyster shell fragments scattered throughout; Traces include: *Teredolites, Skolithos, Planolites.* BI = 0–1	**Estuarine ebb channels and upper flow regime sand flats**  **n=169**
3.3 – Inclined heterolithic strata	Thinly interbedded very fine-grained sandstone and mudstone. Beds are inclined between 7° and 20°. Inclined beds are between 0.1–1.5 m thick, and laterally interfinger with tidal channels of lithofacies 3.1 and carbonaceous shales assigned to lithofacies 4.1. Double mud drapes occur along foresets of low-angle trough cross-stratification.	Shell and wood fragments were found with marine trace fossils; Wood borer *Teredolites, Lockeia, Planolites,* and *Skolithos.* BI = 0–2	**Tidally influenced point bar and/or tidally influenced bayhead delta**
Barrier-island association			
3.4 - Amalgamated, cross-stratified sandstones and gravel conglomerates	Fine- to coarse-grained, tan sandstones and gravels range in thickness from 1–3 m and contain a diverse assemblage of planar, trough, sigmoidal, herringbone cross-stratification, double mud and carbonaceous drapes, light gray mud rip-ups, reactivation surfaces, and plant fragments. Swaley cross-stratification occurs within sandstone bodies, and are more abundant in a basinward direction. Sandstones and gravel conglomerate bodies are organized into lenticular barforms amalgamate to form 20 m thick packages. Soft sediment deformation is pervasive.	Body fossils include large inoceramid shells, oysters, and sharks' teeth; Trace fossils include: *Ophiomorpha, Schaubcylindri-chnus,* and rare *Skolithos.* BI = 0–2	**Flood tidal delta**  **n=161**
3.5 - Tabular, bidirectional cross-stratified sandstones	Forms laterally extensive 3–15 m thick white sheets that can be traced for over 10 km. This facies can have either an erosive base with 1–2 m of relief or conformably overlie shoreface deposits. Medium-grained, well-sorted sandstones contain abundant reactivation surfaces, planar, trough, sigmoidal, and herringbone cross-stratification, mud and carbonaceous draped cross-sets, and ball-pillow and flame soft-sediment deformation features. No bioturbation.	Shell fragments of inoceramid and oysters fragments are common, with minor amounts of terrestrial plant debris observed scattered throughout. BI = 0	**Tidal inlet**  **n=41** **Sand-rich back-barrier** 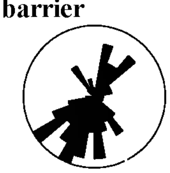 **n=106**

Table 1 (continued)

Lithofacies	Description and Architecture	Trace/Body Fossils	Environment
3.6 - Rhythmically bedded, sandstones and siltstones	5–10 cm thick rhythmically bedded planar-laminated sandstones, siltstones, and minor gray mudstones with minor sections containing ripple laminations. Local scours with 1 m of relief are filled with these rhythmic deposits.	No body fossils were observed: Trace fossils are sparse to absent with very small diameter (2–5 mm) *Planolites* burrows occuring along double mud drapes. BI = 0–1	**Sand rich tidal flat**
Facies Association 4 – Low-Energy Bay/Lagoon			
4.1 - Carbonaceous shales and laminated gray siltstones and mudstones	Fissile noncarbonaceous to carbonaceous shales and thin subbituminous coals comprise lithofacies 4.1. Organic content increases through these deposits with 5- 20 cm thick coals capping 5–10 m thick successions. Organic content of the carbonaceous shales increases to the west. In the east, fine-grained deposits consist of laminated gray mudstones with little to no organic content, with the exception of small plant fragments.	Oyster shell fragments occur throughout and occasionally occur as thin (<10 cm) lags; The only trace fossils observed were *Planolites.* BI = 0–1	**Restricted bay/lagoon**
4.2 - Planar-laminated, bioturbated sandstones	Fine- to medium-grained sandstones with minor erosion at their bases. Beds are typically less than 1 m thick and extend laterally for around 100 m. Beds display slight fining upward trends, and typically, a vertical transition from landward dipping planar-laminations to ripple-laminations, with occasional small-scale trough cross-stratification. Paleocurrent measurements on ripple laminations and trough cross-stratification indicate southwest directed flow. Occasionally, beds are highly bioturbated and all primary sedimentary structures are obliterated.	Includes oysters, inoceramid clams, gastropods, and sharks' teeth; Trace fossils include: *Skolithos, Lockeia, Planolites,* and rare *Ophiomorpha.* BI = 0–5	**Washover fans**  **n=16**

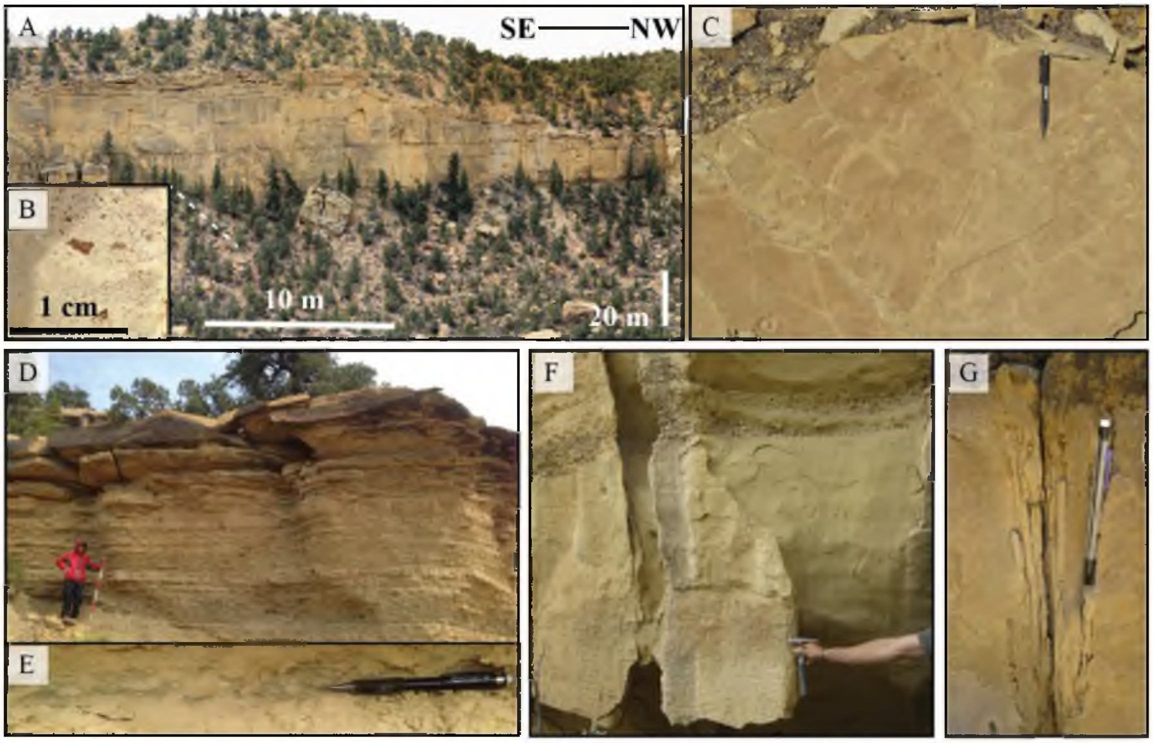

Figure 4. Representative field photos of FA-1 (wave-dominated shoreface). A) The lower John Henry Member is characterized by coarsening upwards parasequences stacked progradationally. Note the high-relief incision into the amalgamated shorefaces; B) Close-up view of offshore mudstones containing abundant terrigenous plant material, suggesting proximity to a fluvial output; C) *Planolites*, *Thalassinoides*, and *Ophiomorpha* burrows are common in sharp-based hummocky sands; D) Typical succession through distal lower shoreface deposits; E) *Chondrites*, *Zoophycos*, and *Planolites* burrows in offshore mudstones; F) Quartzite and chert conglomerate lenses in swaley cross-stratified proximal lower shoreface deposits of the "A" shoreface; G) *Schaubcylindrichnus* dwelling burrow in swaley cross-stratified shoreface sands.

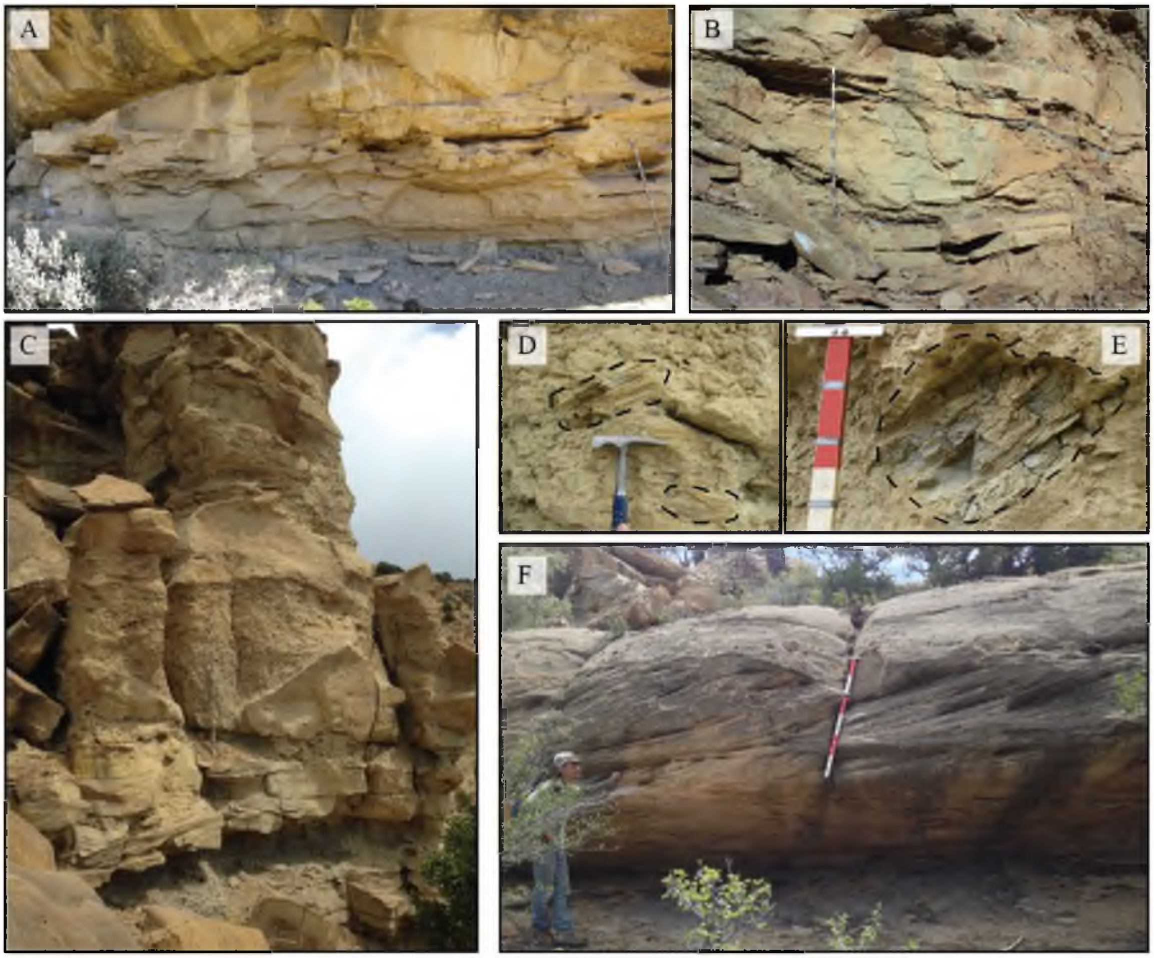

Figure 5. Field photos representing FA-2 (coastal plain). A) Distributary mouth bar overlying the “A” shoreface (Jacob staff intervals = 10 cm); B) Medium-grained sandstone channel within lithofacies 2.4. Channels pinch out out over tens of meters; C) Matrix-supported breccia channel truncating an underlying sandy channel; D) Planar-laminated sandstone and mudstone clasts within a sandstone matrix; E) Boulder-sized gray mudstone clast floating in a sand matrix; F) Unidirectional trough cross-stratification within a channel belt sandstone in the middle-upper John Henry Member.

Figure 6. Field photos illustrating the diversity of tide-influenced coastal margin deposits (FA-3) at Main Canyon. A) Aerial photograph of a sheet-like tidal sandstone (Facies 3.5) conformably overlying the “E” shoreface north of Main Canyon. Paleocurrents collected throughout this sheet-form are bidirectional with dominate southwest and subordinate northeast flow; B) Wavy and lenticular bedding at the base of a tidal channel; C) Isolated *Ophiomorpha* burrows in high-energy deposits of lithofacies 3.3; D) Double mud drapes at the base of a tidal barform; E) Herringbone cross-stratification common in lithofacies 3.4 and lithofacies 3.5; F) Inclined heterolithic strata erosively overlying the “B” shoreface; G) Rhythmically bedded tidal flat deposits of lithofacies 3.6 (Jacob staff intervals = 10 cm); H) *Teredolites* wood borings in a channel lag; I) *Lockeia*, *Palaeophycus*, and *Gyrochorte* traces on the base of a lenticular tidal bar.

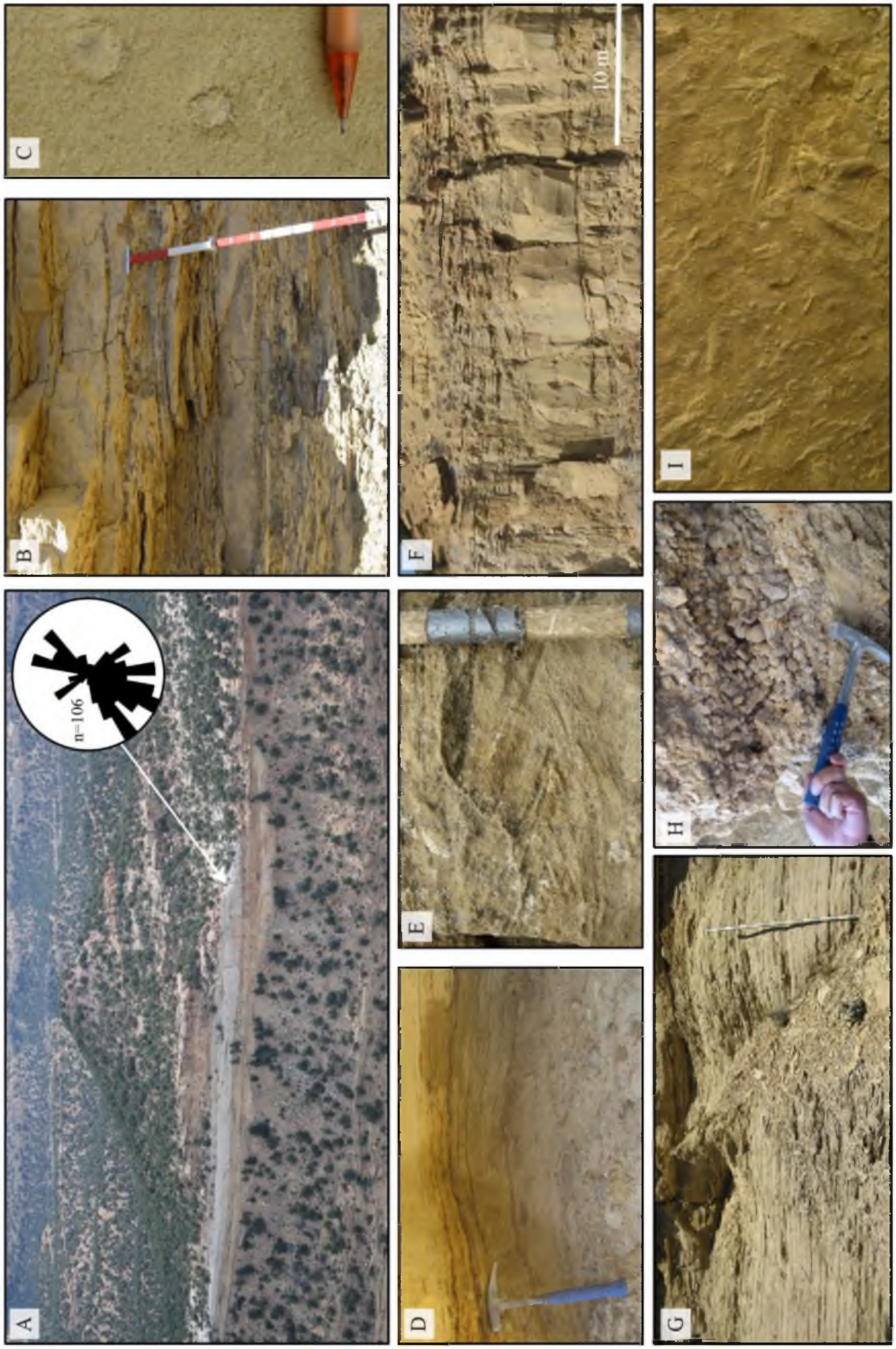
A
n=106
B
C
D
E
F
10 m
G
H
I

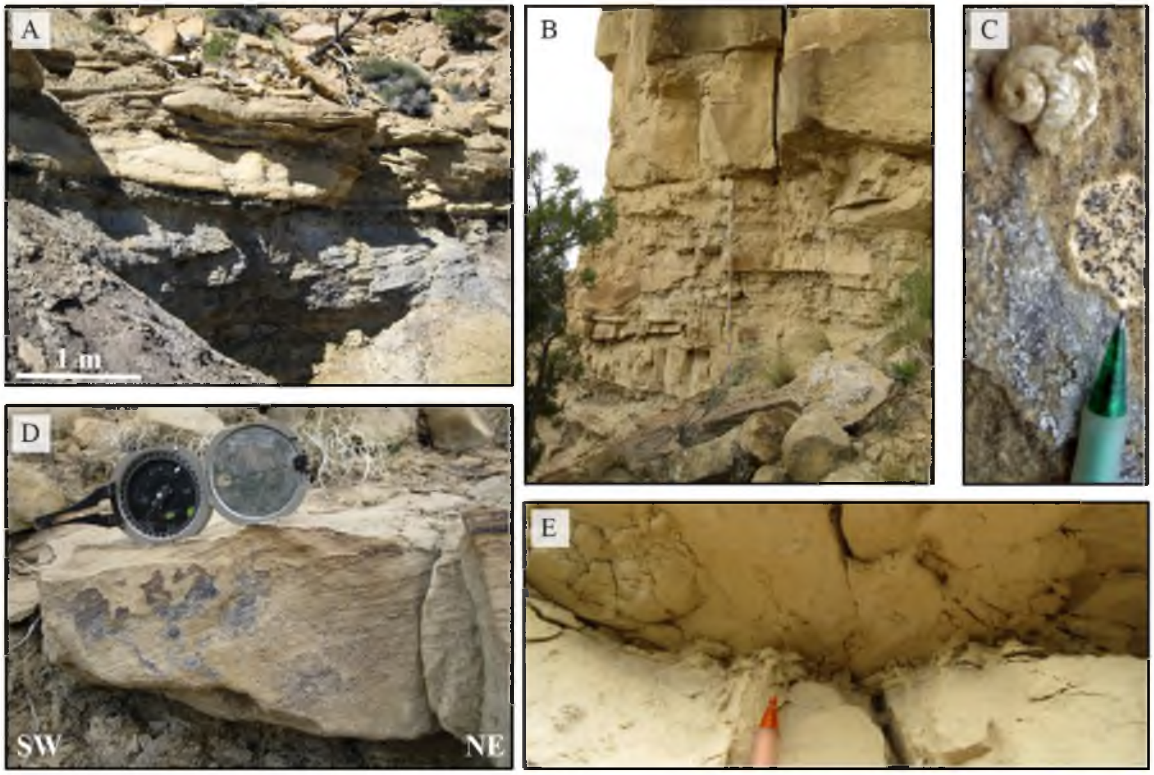

Figure 7. Field photos illustrating low energy bay/lagoon fill of FA 4. A) Carbonaceous shale capped by a thin <20 cm coal that is in turn overlain by an erosive-based tidal channel; B) Interbedded bay-fill mudstones (LF 4.1) and washover fans (LF 4.2) overlain by amalgamated flood tidal delta bars (LF 3.4) (Jacob staff intervals = 10 cm); C) Gastropod shell from a washover fan; D) Typical washover fan with landward-inclined planar laminations that transition into ripple laminations and small scale trough cross-stratification; E) *Lockeia,* a bivalve resting trace, is commonly observed on the bases of thin sandstone beds.

DISCUSSION

A complex assemblage of offshore, shoreface, estuarine, back-barrier, and coastal plain facies is preserved within the John Henry Member at Main Canyon. These strata reflect temporal changes and spatial variability in the dominance of waves, rivers, and tides on sediment transport and deposition. Facies and bounding surfaces have geometries and architectures that reflect deposition within distinct regressive and transgressive cycles (Curray, 1964; Swift, 1968; Nummedal and Swift, 1987; Devine, 1991; Olsen et al., 1999; Cattaneo and Steel, 2003; Sixsmith et al., 2008; Kieft et al., 2011). Allen and Johnson (2011) interpreted analogous deposits within the John Henry Member at Rogers Canyon (Fig. 1) to be approximately fourth to fifth order parasequences (Van Wagoner et al., 1990; Plint et al., 1992). It is reasonable to assume the deposits at Main Canyon are also fourth and fifth order cycles.

Regressive deposits are composed of facies associations 1 and 2, and record deposition along wave-dominated shorelines and the adjacent coastal plain, respectively. In contrast, transgressive intervals preserve laterally and stratigraphically-varying estuarine and back-barrier deposits (FA 3 and FA 4). These deposits contain evidence for both marine (e.g., shells and burrows, landward-directed paleocurrents, and tidal facies) and nonmarine (terrestrial plant fragments, shoreline-directed paleocurrents, and mixed tidal-fluvial facies) influence. Two such transgressive intervals are well exposed along depositional strike and dip near Main Canyon, permitting detailed analysis of their facies architecture.

The cycles and their internal bounding surfaces are first discussed in stratigraphic order, then synthesized in a depositional model with an emphasis on the formation of compound erosional surfaces and the preservation of tide-dominated transgressive deposits in this and analogous settings. The stratigraphy at Main Canyon is then related to regional stratigraphic trends and the paleogeography of the Kaiparowits Plateau.

Regressive-Transgressive Architecture

Bounding surfaces. Seven distinct bounding surfaces are used to describe the regressive-transgressive cycle architecture, and these are divided into two groups, A and B (Table 2; Allen and Johnson, 2011). Type A surfaces occur at the base of transgressive units and can be conformable or erosive and unconformable. The surface of maximum regression (mRs) forms an unconformable contact between the underlying shoreface strata and overlying transgressive deposits, recording the onset of transgression (Helland-Hansen and Martinsen, 1996). A shift from wave-dominated to tide-dominated processes occurs along a process change surface (pCt), and records a relatively conformable contact with the underlying shoreface. Additionally, this surface is used to separate two stacked transgressive units across a gradational and conformable zone occurring within a coal zone (Allen and Johnson, 2011). Tidal ravinement (tRs) generates an unconformable contact between underlying regressive shoreface deposits and overlying tidal channel deposits. Tidal erosion occurs by channel thalweg-scouring during migration of tidal channels during transgressions (Swift, 1968).

Type B surfaces are found at the base of regressive units (Table 2). Wave erosion during shoreface retreat generates a wave ravinement surface (wRs) that separates underlying transgressive deposits from overlying regressive shoreface strata (Swift, 1968). Flooding surfaces (FS) separate shoreface parasequences with minimal erosion (Van Wagoner et al., 1988, 1990), thus implying an intervening transgression between stacked regressive units. Landward of the shorefaces, the distinction is marked by the appearance of transgressive deposits (e.g., bounding surface B2 of Allen and Johnson, 2011). In this case, relative deepening or flooding along this surface continues along the wRs. A surface marks a process change from tide-dominated to fluvial-dominated energy (pCf), and forms a diachronous zone separating underlying lagoonal deposits from overlying coastal plain facies. Lastly, the subaerial unconformity (SU) forms as a result of fluvial erosion or bypass under subaerial conditions (Van Wagoner et al., 1990).

The beginning of a regressive-transgressive cycle can be placed at the base of transgressive units (Embry and Johannessen, 1993). In this study, however, we recognize evidence for significant tidal ravinement occurring at the base of transgressive units (Cattaneo and Steel, 2003; Sixsmith et al., 2008), which complicates their recognition. Throughout the Kaiparowits Plateau, the subaerial unconformity forms a regionally-traceable, significant boundary (Shanley and McCabe, 1991). However, in the Main Canyon study area, this surface (discussed in detail below) represents a compound subaerial unconformity (SU) modified by tidal ravinement. Consequently, this surface is highly diachronous, forming over various stages of the relative sea-level cycle. Correlation along this boundary (to define R-T cycles) could result in misinterpreted time lines.

Due to this complexity, wave ravinement (wRs) and flooding surfaces (FS) that record the maximum transgression and process changes from tide-dominated to fluvial-dominated processes (pCf) (i.e., the regressive turn-around), are selected as bounding surfaces for R-T cycles of the John Henry Member at Main Canyon. Wave-ravinement and flooding surfaces are relatively flat across the study area, with erosional relief on the order of 10s of cm. Total erosion from wave ravinement is likely on the order of 10 m, corresponding to fair weather wave base (Saito, 1994; Cattaneo and Steel, 2003), and this provides more accurate correlations at a local scale. In intervals where the shoreline did not retreat landward far enough to develop a well-defined maximum transgressive surface, the base of the cycle is placed at the top of the last sign of marine influence on the system (Shanley et al., 1992). In the following section, facies distributions and bounding surfaces that define each of the four R-T cycles near Main Canyon are discussed in detail.

R-T cycle 0. A basal wave ravinement surface (wRs (1); Fig. 8), marks the base of R-T cycle 0 and is characterized by a well-developed quartzite pebble conglomerate overlying tidally-influenced estuarine strata within the Calico Bed interval (Hettinger et al., 1993). This surface marks the base of the John Henry Member and is relatively flat and traceable throughout adjacent canyons. A 1–2 m thick, swaley cross-stratified, tabular-bedded sandstone (LF 1.2) immediately overlies wRs (1). This tabular sandstone is overlain by up to 45 m of stacked wave- and storm-dominated parasequences (Fig. 8), comprised of offshore mudstones, siltstones, and hummocky cross-stratified sandstones (LF 1.1). Parasequences stack regressively and contain stratified gravel lenses, some of which correlate basinward (east) to flooding surfaces. Throughout the eastern Kaiparowits Plateau, extensive lags are found within the “A” shoreface. Paleolandward (west), proximal lower shoreface sands amalgamate, forming units > 25 m thick (e.g., Fig. 4A), while basinward (east), sand-rich units transition to finer-grained deposits of lithofacies 1.1 over a distance of only 2–3 km (Fig. 8). Mapping of shoreface sand bodies around Main Canyon indicates the shoreline was roughly north-south trending at this time. The upper parasequence of R-T cycle 0 is locally overlain by distributary mouth bars (Fig. 5A) of lithofacies 2.2, with up to 2 m of erosion occurring into the shoreface. Paleocurrents collected on these lenticular sandstone bodies indicate unidirectional flow to the east (Fig. 8). Mouth bars are overlain by a thin flooding surface and renewed deposition of proximal lower shoreface sandstones. Basinward, this flooding surface is characterized by a pebble lag.

R-T cycle 1. R-T cycle 1 begins on the basal flooding surface overlying the "A" shoreface, and is itself overlain by a west to east building regressive shoreface ("B" shoreface) parasequence that locally exceeds 25 m in thickness (Fig. 4A). To the southwest, in Upper Valley (Fig. 3), this flooding surface separates a thin wedge of transgressive strata from the overlying shoreface (Hettinger et al., 1993; Allen, 2009), implying a minor intervening transgression occurred and is preserved at Main Canyon as a flooding surface. This basinward transition of a transgressive interval to a flooding surface separating two regressive shorefaces, is consistent with regressive-transgressive architecture described by Allen and Johnson (2011), making this bounding surface B2 of their terminology.

Preservation of transgressive deposits landward (southwest) of Main Canyon indicates the start of a new R-T cycle. Throughout Main Canyon, the overlying shoreface ("B" shoreface) contains southwest- to northeast-trending incisions with varying amounts of relief (Fig. 9). Incisions were mapped and correlated across Main Canyon with the assistance of a differential GPS paired with a laser range finder. These incisions trend subparallel to the underlying shoreline of R-T cycles 0 and 1 (Fig. 4A). Strata overlying this erosional surface are comprised of tide-dominated estuarine (LF 3.1, 3.2, 3.3), flood-tidal delta (LF 3.4), tidal inlet (LF 3.5), lagoonal (FA 4), debris flows (LF 2.3), and patchy fluvial deposits (LF 2.1). Facies architecture varies along this boundary within two distinct zones from west to east in Main Canyon (Fig. 8), discussed separately below.

R-T cycle 1, western zone. The western zone of Main Canyon (Fig. 9) contains N-northeast-trending high-relief incisions that truncate the underlying “B” shoreface and locally penetrate completely through the “B” and into upper parts of the “A” shoreface (R-T cycle 0) (Figs. 4, 8). Maximum relief along this surface locally exceeds 22 m (Fig. 4A). Incisions are overlain by channelized tidal facies of FA-3. In general, the channelized tidal facies progressively fine upwards into carbonaceous shales (LF 4.1) that are dissected by discontinuous tidal channels (LF 3.1) (Fig. 7A) and washover fans (LF 4.2). Deposits vary from <25 m to >35 m in thickness based on their position relative to local high-relief scours (Fig. 9).

Highly amalgamated, multistory, channel sandstones (LF 3.2) immediately overlie the incisions at the western end of the canyon and contain paleocurrent indicators dominated by east/northeast flow (Fig. 9). These thick sandstone packages are laterally continuous for ~500 m and are limited to zones of high relief (>10 m) along the basal erosional surface. Tidal influence on these channels is apparent from subordinate landward-directed paleocurrents. Vertically and eastward, these deposits grade into more heterolithic tidal channels (LF 3.1) and carbonaceous shales (LF 4.1). To the east of these highly amalgamated tidal channels, erosive based tidal channels and elongate sigmoidal tidal bars downlap onto the shoreface (Fig. 10ABC), forming a tidal ravinement surface (tRs). Paleocurrents are bidirectional to the southwest-northeast with a small population of data indicating subordinate flow to the northwest (Fig. 8).

A multistory, heterolithic tidal complex (Fig. 10D) that is >25 m thick erodes up to 15 m into the "B" shoreface and contains channelized sandstones with gravel and mud-rip up lags. Channels scour and erode into successive fills, creating a complex internal architecture (Fig. 10D). Immediately adjacent to this complex are heavily channelized debris flows of lithofacies 2.3 (Fig. 5BC). The transition from tidal complex to debris flows occurs across a sharp lateral boundary (Fig. 8), and the deposits themselves are only observed along a 100–200 m stretch of outcrop. Overall, transgressive deposits of R-T cycle 1, in the western zone, display a progressive fining-upwards trend and contain abundant indicators of flow reversal and periods of slackwater (Fig. 9). Carbonaceous shales are thickest (~10 m) to the west, thinning to the east, across the western zone (Fig. 8). A capping wave ravinement surface (Fig. 8; wRs (2)) creates a planar surface of erosion with a pebble lag, marking the top of R-T cycle 1 in the western part of Main Canyon (Figs. 8, 9). The boundary between the western and eastern zones occurs adjacent to the terraced debris flows (Fig. 8).

<u>R-T cycle 1, eastern zone</u>. Towards the mouth (east) of Main Canyon, (Fig. 11) a distinct change in the nature of tidal deposits within R-T cycle 1 occurs. Deposits within western stretches of R-T cycle 1 progressively fine upward and become more heterolithic to the east/northeast, whereas deposits in the east coarsen upward (Fig. 11) and become heterolithic in a paleolandward (southwest) direction. Additionally, the erosional surface

(SU) changes character along this zone and becomes relatively flat (Fig. 8) to the east, with no high-relief incisions occurring into the underlying shoreface strata. Erosion into the shoreface is limited to basal channel scours with only decimeters of relief.

Gray, laminated lagoonal (LF 4.1) mudstones immediately overlie the "B" shoreface (Figs. 8, 11) in the eastern zone. These lagoonal deposits are interbedded with washover fans (LF 4.2) that display unidirectional landward- directed (southwest) paleocurrents and inclined laminations (Fig. 7D; Table 1). Lagoonal fines (LF 4.1) and washover fans (LF 4.2) transition vertically into flood-tidal delta sandstones and gravels that display highly bidirectional paleocurrents with dominant southwest-directed flow and subordinate northeast flow (Fig. 11; Table 1). A 2–5 m thick package of tidal inlet sandstones (LF 3.5) erodes into the underlying barforms, forming a capping sheet across the mouth of the canyon. This unit is present in adjacent canyons and pinches out to the west, 2.1 km from the mouth of Main Canyon (Fig. 12). Deposits of FA-3 and FA-4 erosively overlie fluvial terrace deposits (LF 2.3) and form the lateral boundary between the western and eastern zones (Figs. 8, 11, 12). These tidal inlet deposits are overlain by wRs (2) that marks the top of R-T cycle 1 in the eastern part of Main Canyon.

In summary, transgressive deposits of R-T cycle 1 consist of fining-upward estuarine strata in the western part of Main Canyon (Fig. 9), and coarsening upwards flood-tidal delta and tidal inlet facies in the east (Figs 8, 11). This difference in depositional style is attributed to the presense of a southwest-northeast trending incised valley. Estuarine strata comprise the western transgressive fill of Main Canyon, whereas back-barrier lagoonal deposits accumulated along the seaward flank of the valley system.

R-T cycle 2. The regressive portion of R-T cycle 2 consists of 20–30 m of shoaling-upwards, distal lower shoreface deposits (LF 1.1), which overlie a wave ravinement surface (wRs (2); Fig. 8). Deposits stack regressively and grade into swaley cross-stratified sandstones, characteristic of lithofacies 1.2. The proximal lower shoreface ("E" shoreface) thickens from 5 m in the southwestern part of Main Canyon to >20 m in adjacent canyons to the northeast.

The "E" shoreface is capped by a surface that has a variable expression throughout the study area. In the paleolandward (southwest) part of the study area, a firm ground, bored by *Gastrochaenolites,* typical of the *Glossifungites* ichnofacies (MacEachern et al., 1992), caps the shoreface. This burrowed surface is overlain by tide-dominated deposits (FA-3) and shelly and carbonaceous lagoonal and bay-fill (FA-4) that locally truncate the underlying "E" shoreface (Fig. 8). To the northeast, the firm ground surface becomes conformable, locally characterized by a thin shell lag separating a 10–15 m thick sheet-like tidal sandstone (LF 3.3) from the underlying shoreface (Fig 3A). The extensive, tabular deposits correlate paleolandward to tidal flats (LF 3.6) and tidal channels (LF 3.1) (Fig. 10F). Tidal channels are locally characterized by tidal ravinement with relief up to 10 m occurring at their bases (Figs.8; 10F). Overall, the surface overlying the "E" shoreface records a process change from wave-dominated to tide-dominated processes (pCt).

Tidal channels in the southwestern study area form sand-rich complexes in excess of 30 m thick (Fig. 10F) that rapidly transition to flanking tidal flats (LF 3.6) and carbonaceous lagoon deposits (LF 4.1). Overall, tidal strata within R-T cycle 2 become progressively finer-grained and more carbonaceous moving up-section. The position of these sandy back-barrier sheets (LF 3.5), tidal channels (LF 3.1), shelly carbonaceous shales (LF 4.1), and tidal flat (LF 3.6) deposits between two regressive units indicates deposition occurred during a rise in relative sea-level, making them transgressive deposits.

R-T cycle 3. Fluvial channel belts (LF 2.1), distributary mouth bars (LF 2.4), and rooted carbonaceous shales and coals (LF 2.2) form a gradational contact (pCf) with underlying tidal and lagoonal deposits, marking the base of R-T cycle 3 (Fig. 8). These organic-rich facies are heavily altered from coal fires, but where better preserved, rooted carbonaceous mudstones, coals, rippled crevasse splays, and isolated channelized fining-upward sandstones are recognized.

Regressive fluvial and coastal plain facies are at least 40 m thick at Main Canyon where they form the top exposures throughout the canyon. Based on aerial photography correlations, these coastal plain facies are laterally continuous for >40 km along strike to the southwest. At the White Mountain section (where the full upper John Henry Member is preserved; Fig. 13) fluvial and coastal plain deposits are 90 m thick and overlain by 40 m of tidal channels, washover fans, and carbonaceous lagoonal/bay fill that form the upper transgressive deposits of R-T cycle 3. The regional correlation of these deposits to the northwest is discussed in detail below.

R-T cycle 4. A final gradational regressive boundary (pCf; Fig. 13) is placed at the last sign of tidal influence in R-T cycle 3 and marks the base of the final R-T cycle of the John Henry Member in the study area. Fluvial channel belts become increasingly amalgamated both laterally and vertically moving up section into the Drip Tank Member, marking the top of the study interval. These deposits are interpreted here to be part of the "G" shoreface interval, based off of a major flooding surface present at the base of the

"G" shoreface at Buck Hollow (Fig. 3). Although the internal architecture of this cycle was not studied in detail, its recognition is important for regional correlations as discussed below (Fig. 13).

Depositional Model

A depositional model for the development of the regressive-transgressive stratigraphy preserved at Main Canyon is summarized next and in Figure 14. Successive R-T cycles are discussed in stratigraphic order, along with associated environments of deposition that characterize each cycle.

R-T cycles 0-1 ("A" and "B" shorefaces): Regressive, river-influenced shorefaces. The basal section of the John Henry Member at Main Canyon preserves heavily bioturbated marine mudstones and siltstones that grade upward to thick hummocky and swaley cross-stratified shoreface sandstones. Deposits that overlie the basal wave ravinement surface (wRs (1); Fig. 8) reflect deposition on a wave- and storm-dominated shelf. The thick (>25 m) accumulations of shoreface sandstones indicate deposition within a high sediment supply, high accommodation setting (Allen and Johnson, 2011).

Although deltaic deposits are not directly observed in the study area, fluvial output of sediment at the shoreline is evidenced by terrestrial plant fragments and thick, sharp-based shorefaces, as well as the prevalence of offshore directed cross-stratification (Fig. 8; Table 1) within mouth bar deposits (Bhattacharya and Giosan, 2003; Olariu and Bhattacharya, 2006; Fielding, 2010). Further basinward, sediment from distributary channels would have been reworked and transported south via longshore drift. Previous studies indicate that southward longshore drift is likely along the western margin of the Western Interior Seaway, given paleogeographic and paleoclimatic parameters (Ericksen and Slingerland, 1990; Fielding, 2010). Southward-deflected mouth bar deposits are documented in the John Henry Member along Fifty Mile Mountain (Allen and Johnson, 2010), and provenance data including detrital zircon geochronology provide additional evidence for longshore drift in this section (Allen and Johnson, 2010; Szwarc et al., in press).

The “A” and “B” shoreface successions stack in a strongly progradational pattern from west to east (Fig. 14), indicating the rate of sediment supply outpaced accommodation at the shoreline (Posamentier et al., 1992). Thick (>25 m) packages of proximal lower shoreface sandstones rapidly pinchout over 2–3 km to the east into offshore mudstones (Fig. 12). This stacking pattern is interpreted to be the result of a relatively steep (>0.001) depositional profile (Cattaneo and Steel, 2003) receiving high sediment supply within a high accommodation setting. This interpretation is supported by estimating the gradient of shoreface profiles using the up-dip and down-dip expressions of flood surfaces within the lower John Henry Member in Upper Valley, which yield gradients (Table 3) ranging from 0.006–0.013 (cf., Fig. 2 of Hettinger et al., 1993). A steep regressive foundation has implications on the preservation and distribution of the overlying deposits, as discussed in detail below.

Two aspects of these shorefaces are particularly significant to regional correlations: 1) The west-to-east depositional profile is highly oblique to the erosional surfaces and valley system that overlies these units; and 2) The interpretation of these as the “A” and “B” shorefaces, which are overlain by a compound set of unconformable, tidally-modified erosional surfaces (i.e., valley fill), implies that the “A” sequence boundary of Shanley and McCabe (1991) is not present, and/or is superseded by a more significant, younger bypass/erosion and transgressive fill event above the “B” shoreface (Allen and Johnson, 2011).

We propose that the major subaerial unconformity surface be renamed the lower John Henry Member sequence boundary (Fig. 8). Throughout the Kaiparowits Plateau, the lower John Henry Member displays a strongly progradational shoreface stacking pattern through the “A-B-C” intervals that we interpret as having occurred during a stepped forced regression (Posamentier et al., 1992; Li et al., 2011; Zhu et al., 2012; Li and Bhattacharya, 2013). The thick accumulations of offshore mudstones in the northern plateau, in conjunction with a thin interval of transgressive deposits, supports the interpretation that the amalgamated shorefaces observed at Main Canyon are the “A” and “B” shorefaces rather than two parasequences within the “A” interval. A separating transgressive interval, combined with the regional evidence (Gallin et al., 2010; Allen and Johnson, 2011; Dooling, 2013) for a larger (>14 km) basinward shift of the shoreline at the top of the “B” shoreface, in comparison to the ~4 km basinward shift observed at the transition between the “A” and “B” shorefaces, supports this new regional correlation.

Evidence for structural control on drastic stratigraphic thickening in the northern Kaiparowits Plateau is addressed below with regard to regional correlations. Known thrusting events in the Sevier fold-thrust belt to the west overlap roughly with deposition of the lower John Henry Member (Szwarc et al., in press), so tectonism certainly must be considered. However, base level shifts in the lower John Henry Member have also been assigned to at least partial eustatic controls (Shanley and McCabe, 1995). The basinward shift recorded in the "A-B-C" shorefaces may be related to minor eustatic excursions near the Coniacian-Santonian boundary (Hardenbol et al., 1998; Miller et al., 2005). However, rapid (fourth- and fifth-order), high amplitude (>20 m), fluctuations in eustatic sea level during the Late Cretaceous are enigmatic (Miller et al., 2005). Global greenhouse conditions are generally thought to have inhibited the formation of large ice sheets, the primary driver of high-frequency eustatic fluctuations in more recent ice house climates. However, some studies suggest ice sheets may have developed in restricted areas of Antarctica during the Late Cretaceous (Miller et al., 2003). Moderate rates of eustatic sea level change in greenhouse climates may result in longer valley formation and fill time scales, favoring the formation of composite stratigraphic surfaces and compound fills.

R-T cycle 1 (Top "B" shoreface): Shore-parallel valley incision. The lower John Henry Member sequence boundary at Main Canyon contains southwest-northeast trending incisions (Figs. 8, 14) within R-T cycle 1, interpreted as a subaerial unconformity (SU) developed by incising fluvial channels in response to a fall in relative sea level. The basinward shift in depositional facies, regional extent of the surface (discussed above), the erosive nature of the overlying strata, and the magnitude of incision (>20 m) support this interpretation (Posamentier et al., 1988; Van Wagoner et al., 1990; Shanley and McCabe, 1994; Dalrymple and Zaitlin, 2006). Subaerial unconformities and associated incised valleys develop when the shoreline trajectory is migrating across a surface that is significantly steeper than the adjacent alluvial plain (Helland-Hansen and Gjelberg, 1994). Valley incision typically initiates at river mouths, propagates upstream via knick-point migration (Posamentier, 2001), and continues until the river's reach restores its equilibrium profile (Lane, 1955; Schumm, 1993b).

Our findings support the interpretation of incised valley formation, followed by estuarine deposition (Fig. 14). However, paleocurrent measurements, facies distribution, and regional correlations indicate a change in depositional dip from west-east (R-T cycle 0 and regressive shoreface deposits of R-T cycle 1) to southwest-northeast occurred across this boundary. Therefore, the incised valley was oriented subparallel to the underlying, north-south trending shorelines (Fig. 8). Additionally, this study recognizes lateral partitioning of tide-dominated deposits along the erosional boundary. For example, in the eastern part of Main Canyon (Fig. 11), Hettinger et al. (1993) describe 15–20 m of tide-dominated facies, which they interpreted as estuarine fill (e.g., Fig. 3 sections 13 and 14 of Hettinger et al., 1993). In this study, we have reinterpreted sand bodies originally described as upper shoreface in their study as flood-tidal delta and tidal inlet facies. Consequently, the transgressive portion of R-T cycle 3 is over 39 m thick at the mouth of Main Canyon. These new correlations result in drastically differing shoreline geometries, sand-body distributions, and call into question the time-significance of the "A" sequence boundary (Fig. 14).

Incised valleys at Main Canyon are interpreted to have formed subparallel to the underlying shoreline (Fig. 14). Shore-parallel valley incisions, although less pervasive in the literature than their orthogonal counterparts, are documented in both modern and ancient settings (e.g., the modern Neuse River estuary of Eastern North Carolina (Fig. 15), and in the Lower Cretaceous Basal Quartz Unit of the Western Canada basin (Ardies et al., 2002; Zaitlin et al., 2002). Valleys typically form perpendicular to the shoreline due to the tendency of distributary channels to remain straight as they approach the receiving body of water and pass through the zone of backwater effects (Gouw and Berendsen, 2007; Chatanantavet et al., 2012). However, features such as raised coal mires, local highs generated from fault movement, or differential sediment compaction can produce topographic features that control the position of distributary channels entering the recieving basin (Fig. 16).

Additional factors controlling valley orientation are basin-scale drainage and thickness patterns. The John Henry Member thickens significantly from south to north (~240 m at Bull Canyon, ~255 m at Left Hand Collet, ~350 m between Main Canyon and White Mountain, and >500 m at Buck Hollow (Fig. 13)). Furthermore, provenance data from the Straight Cliffs Formation indicate that sediment was supplied from a northeast-flowing fluvial system (Szwarc et al., in press) that ran axial to the Sevier fold-thrust belt and entered the Kaiparowits subbasin obliquely (Fig. 1). This oblique approach to the shoreline likely played a role in determining the position of avulsing distributary channels.

One hallmark of incised valleys is the presence of numerous smaller tributary valleys (Fig. 15) developed on the abandoned flood plain, that drain into a trunk valley (Posamentier, 2001). It is possible, though we think unlikely, that the deposits at Main Canyon were tributary valleys that fed into a larger trunk valley further down depositional dip (northeast). Time-correlative, high-relief, west to east trending incision surfaces are not present north of the study area. Furthermore, the scale of tributary valleys is much smaller, commonly between 1–2 km in width, (Posamentier, 2001; Simms et al., 2006) than the region in which the incisions are mapped around Main Canyon (>5km).

<u>R-T cycle 1 (“C-D” interval): Tidal ravinement, incised valley modification,</u>

estuarine deposition. Incised valleys are important because their bases are thought to be sequence boundaries with chronostratigraphic significance, separating younger and older deposits (Posamentier and Vail, 1988; Van Wagoner et al., 1988; Wagoner et al., 1990; Shanley and McCabe, 1994). The chronostratigraphic significance of sequence boundaries has been challenged by both field data and flume studies (Holbrook and Bhattacharya, 2012). Strong and Paola (2008) demonstrate how the basal discontinuity of incised valleys is continuously redefined through erosion and deposition over several relative sea-level cycles. Thus, the preserved valley surface, while having a valley shape, does not represent any individual geomorphic surface.

Field studies of incised valleys on the modern Texas coastal plain show that four episodes of relative sea-level rise and fall have generated compound incised valleys containing stepped fluvial terraces. These terraces onlap a basal erosional surface that is time-transgressive in both cross- and down-valley directions (Blum, 1993; Blum and Törnqvist, 2000; Blum and Aslan, 2006; Blum et al., 2013). Similar compound incised valley fills have recently been documented in the Upper Cretaceous Ferron Sandstone Member of the Mancos Shale (Li and Bhattacharya, 2013). These studies recognize the importance of fluvial process in defining and reshaping the incised valley dimensions through time, however, relatively few studies highlight the importance of tidal currents during the initial stages of relative sea-level rise in redefining the valley container (Allen and Posamentier, 1993; Willis, 1997; Willis and Gabel, 2003; Li and Bhattacharya, 2013).

The abundance of tide-dominated facies and the paucity of fluvial deposits within the valley fill at Main Canyon (Fig. 8) indicate that tidal currents heavily modified the basal surface (i.e., the subaerial unconformity) during the initial stages of relative sea-level rise (mRs). Incised valley fill is commonly dominated by deposits that are tidal-estuarine in origin, partly because previous stages of falling relative sea level favor incision and scouring, which create topography that increases the tidal prism upon flooding (e.g., Plink-Björklund and Steel, 2006; Steel et al., 2012). Elongate sand bars and compound tidal dunes (e.g., LF 3.1 and 3.2) are common in tide-dominated estuaries and contain reactivation surfaces and master bedding planes that are typically inclined in the direction of dominate flow. The paucity of trace fossils observed within estuarine bars in the John Henry Member is consistent with those observed in modern sand-rich estuarine stretches. Rapidly shifting bedforms and a thick mobile layer inhibit benthic organisms from inhabiting these sand bars (Gingras and MacEachern, 2012).

Water depth estimates of 2.2–5.8 m were made using cross-set measurements (6 and 10 times the mean cross set height) on estuarine tidal bar forms. Dalrymple and Choi (2007) note that the accuracy of applying the approach of Leclair and Bridge (2001) to tidal deposits has yet to be investigated, but state that it should give rough estimates of water depths. Results calculated from cross-set data yield different results than taking measurements on individual sigmoidal barforms, which indicate deeper water depths of >15 m (Fig. 10). These results may correspond with the maximum current speed during the tidal cycle, not the water depth at high tide (Dalrymple and Rhodes, 1995; Dalrymple et al., 2012).

Apart from poorly preserved falling-stage terrace deposits (Fig. 8), no fluvial-dominated facies are observed within the basal valley fill of R-T cycle 1 of the John Henry Member. This is interpreted to be the result of extensive reworking and erosion by tidal currents during the transgressive infilling of the valley (Allen, 1991; Allen and Posamentier, 1993; Zaitlin et al., 1994; Willis, 1997; Posamentier, 2001; Holbrook and Bhattacharya, 2012). During the early stages of relative sea-level rise, the maximum regressive surface (mRs) (e.g., transgressive surface of Allen and Posamentier, (1993) and Posamentier et al. (1988)) formed as the valley was initially transgressed (Fig. 14). This surface is diachronous, becoming younger in an up-valley direction as flooding progresses. High basal tidal energy accompanied this surface as supported by erosion at the base of tide-dominated deposits that make up the valley fill.

Strong tidal currents occur within tidal channels and are likely to have the highest erosion potential in mixed energy settings (Zaitlin et al., 1994). The John Henry Member at Main Canyon displays patterns typical of mixed wave- and tide- dominated estuaries undergoing transgression, with the majority of tidal currents usually channelized parallel to the axis of the estuarine valley (Dalrymple et al., 2012). At Main Canyon, the valley was oriented southwest to northeast, and paleocurrents and channel measurements indicate flow occurred predominantly along the axis of the valley (Table 1). These currents generated transgressive tidal ravinement within the estuary that reworked lowstand fluvial deposits and modified the subaerial unconformity, redefining the geometry and time significance of the valley bottom and walls. Additionally, there is evidence for reworking by meandering tidally-influenced fluvial channels and/or a tidally modified bayhead delta deposits, which deposited inclined heterolithic strata (Fig. 6F). These deposits erode into the “B” shoreface, modifying the basal unconformity (Boyd et al., 2006).

A second phase of tidal reworking and erosion occurs along the eastern (seaward) flank of the incised valley (Fig. 14). This surface occurs at the base of 20–38 m (westward thinning) of coarsening-upward packages of lagoon, flood-tidal delta, and tidal inlet facies (Figs. 8, 11, 12). The underlying shoreface is locally scoured, however, it does not contain high-relief incisions, indicating that fluvial incision was limited to the western part of the study area (Figs. 8, 9). The transgressive ravinement surface (tRs; Table 2) at the base of these deposits “climbs” over fluvial terrace deposits to the west where it merges with the base of carbonaceous shales containing thin coals (Figs. 8, 12). The resulting surface represents a composite subaerial unconformity (SU), maximum regressive surface (mRs), and tidal ravinement surface (tRs) that formed over multiple stages of the relative sea-level cycle.

Transgressive reworking of lowstand fluvial deposits that make up valley floor deposits is documented in both modern (Allen and Posamentier, 1993) and ancient (e.g., Willis, 1997; Bhattacharya and Willis, 2001) estuarine incised valley fills. Tidal ravinement generates a diachronous surface that becomes younger in an up-valley direction (Zaitlin et al., 1994). This is a result of tidal energy progressively reaching further landward as relative sea-level rises. Additionally, because sufficient tidal currents may not be present outside of the estuary, ravinement is likely to be limited to the valley and thus not regionally mappable (Allen and Posamentier, 1993). At Main Canyon, there are two distinct phases of tidal ravinement that are interpreted to have occurred at separate stages of the relative sea-level rise. These surfaces merge in a basinward direction and diverge landward (Figs 8, 12).

At Main Canyon, fluvially-derived terrace deposits are preserved along the eastern margin of the incised valley and are bounded at their base a subaerial unconformity (SU) and their tops and margins by combined maximum regressive (mRs) and tidal ravinement surfaces (tRs) (Figs. 8, 12). The presence of these terraces suggests the incising rivers were not one hundred percent efficient at sediment removal (Holbrook and Bhattacharya, 2012; Li and Bhattacharya, 2013). Estimating the magnitude of erosion resulting from tidal ravinement within R-T cycle 1 is complicated by the composite nature of the basal erosional surface. Upwards of 22 m of local relief occurs along the eastern margins of the incised valley (Fig. 4A), representing a maximum estimate erosion as fluvial incision occurred prior to tidal modification of the incised valley dimensions. Using the base of the preserved fluvial terrace as a reference (Fig. 8), ravinement associated with the maximum regressive surface (mRs) and the landward migrating tidal inlet is estimated to be between 5 and 10 m.

R-T cycle 1 (“D” Interval): Flanking lagoons and barrier islands migrate landward. While barrier islands can occur along both regressive and transgressive shorelines (Nummedal and Swift, 1987; Simms et al., 2006; Boyd, 2010), barrier-island and lagoonal facies within the John Henry Member occur as transgressive deposits (Allen and Johnson, 2011). Multiple lines of evidence support this interpretation: 1) their occurrence between underlying tidal ravinement surfaces and capping wave ravinement surface (Fig. 11), which itself is evidence for a transgressive period; 2) marine influence (e.g., shell lags and trace fossils) within lagoonal mudstones; 2) tidal sedimentary structures, body fossils, and trace fossils within sandstones; 3) their overall geometry, architecture, and relationship with surrounding facies are all indicative of a transgressive back-barrier lagoon system; 4) southwest-directed paleocurrents and inclined laminations within washover fans (Fig. 7D) indicate landward sediment transport.

Landward migration of the barrier island system of R-T cycle 1 is apparent from the coarsening upward transition from muddy lagoon deposits with interbedded washover fans into gravely flood-tidal delta lobes and the capping inlet facies (Fig. 11). Additionally, the landward pinchout of these deposits is observed ~2.5 km from the mouth of Main Canyon (Fig. 12). These deposits occur adjacent to one another within a barrier island system (e.g., Fig. 15) and form a vertical succession that conforms to Walther's law when the barrier migrates landward. Tidal inlet scouring during rising relative sea-level results in tidal ravinement and formation of relatively coarse-grained sediment delivered via longshore drift. Further landward, carbonaceous shales (Fig. 7A) occur above estuarine sand-dominated facies and record the transition to a quiet lagoonal setting.

At Pamlico Sound (Fig. 15A), a series of incised valleys that formed during the last glacio-eustatic lowstand are currently occupied by estuaries. A narrow, landward migrating, microtidal barrier-island chain is dissected by tidal inlets with well-developed sandy flood-tidal deltas. These deltas build into low-energy sheltered lagoons that occupy the interfluvial areas between the estuaries (Boyd, 2010). Due to relatively high wave energy, ebb-tidal delta deposits are reworked and have low preservation potential in this system. This is analogous to the John Henry Member, where ebb-tidal deltas are not observed due to wave reworking and ravinement during relative sea-level rise. Flood-tidal deltas occupy a protected position behind the barrier island and consequently have a much higher preservation potential. Tidal delta deposits within the John Henry Member (Fig. 8) scale very well to those that occupy the landward positions of inlets surrounding Pamlico Sound, with sandy delta deposits being continuous for 4 to 5 km along the coast and 2 to 3 km landward of the inlet mouth. Longshore drift occurs from north to south along the barrier islands and causes the inlets to migrate to the south.

The Neuse River empties into a low energy, protected estuary at its basinward reach (Fig. 16A). Approximately 35 km from the coast, the estuary makes a sharp turn and runs subparallel to the shoreline and drains into back-barrier lagoons. A subaerial interfluvial zone exists east of the estuary that is less than 2 m above sea level; this interfluvial zone is, in turn, bordered to the east by back-barrier lagoons. As sea-level continues to rise and the barrier islands migrate landward, this interfluvial area will be drowned by the retreating lagoon. When the barrier islands migrate far enough landward, tidal inlet migration and tidal channels will produce a ravinement surface, modifying the subaerial unconformity. This situation is comparable to R-T cycle 1 within the John Henry Member, where lagoonal deposits overrode and modified the shore-parallel incised valley and estuary (Figs. 12, 14).

<u>R-T cycle 2 (“E” Interval): Wave ravinement and renewed shoreface deposition.</u> Within R-T cycle 1 of the John Henry Member, retreat of the shoreline kept pace with infilling of the estuary by bayhead delta and estuarine sediments, as is evidenced by capping carbonaceous lagoonal mudstones (Fig. 14). Back-barrier and carbonaceous lagoonal deposits are truncated by the retreating shoreface, producing a ravinement surface (Nummedal and Swift, 1987). The preservation of transgressive strata below this wave ravinement surface (wRs; Table 2) requires high sediment supply and a high subsidence rate (Catuneanu, 2006) in order to first deposit and then protect them from subsequent erosion (Allen and Johnson, 2011).

Following incised valley infilling and landward migration of the shoreline and associated barrier islands within R-T cycle 1, the shoreline prograded to the northeast (Fig. 14). This led to deposition of the "E" shoreface across the northern Kaiparowits Plateau which thickens to the northeast, supporting the change in depositional dip. The landward pinch out of the "E" shoreface occurs approximately 1.5 km to the east of the Dutton monocline (5 km southwest of Main Canyon) (Fig. 3) in Upper Valley (Hettinger et al., 1993). Shoreface strata are truncated by tidal channels in the western study area (Figs. 9, 14) and form a tidal ravinement surface (tRs). To the east, the "E" shoreface is overlain by a tidal sheet (Fig. 3A), across a conformable contact recording a process change (pCt) from wave-dominated to tide-dominated deposition (Table 2).

R-T Cycle 2 (Transgressive interval): Sand-rich back barrier with landward tidal channels and flats. Tide-dominated transgressive deposits of R-T cycle 2 display geometries, architecture, and facies distributions that are consistent with deposition along a tide-dominated, sand-rich, back-barrier platform (Fig. 15B). Littoral drift and flood currents transport large quantities of sediment into lagoons, and channel migration causes sheet-like geometries in the rock record. Similar nonchannelized tidal sandstones occur in the Hosta Sandstone (Cretaceous, New Mexico) and are interpreted to record migration of barforms and dunes on the landward side of a barrier island on a shallow back-barrier platform (Sixsmith et al., 2008). Shallow water depths between 1.4 and 3.7 m were estimated using cross-set heights measurements, constant with deposition on a shallow back-barrier platform. R-T cycle 2 at Main Canyon, tidal sheet deposits pinch out near the mouth of the canyon, and thicken to >20 m northeast near the North Creek Reservoir. The western part of Main Canyon contains large (>30 m thick) tidal channels with bidirectional paleocurrent indicators that show dominant flow within these channels was to the northeast (Fig. 8). Water depths within these channels were estimated to be between 2.8 and 7.5 m, indicating slight landward-deepening within the back-barrier. Finer-grained tidal-flat facies and carbonaceous shales separate channels (Fig. 8). The down-dip relationship with tidal sheets suggests that tidal currents were funneled through progressively narrower channels in a landward direction. This cone-shaped planform geometry is common in tidal channels due to the progressive landward decrease in tidal energy (Hughes, 2012).

The Frisian Islands (Fig. 15B) contain large areas of low-sinuosity, blind tidal channels, disconnected from a fluvial feeder system (Sixsmith et al., 2008). Sediment is supplied to the back-barrier thorough tidal inlets via wind-generated, eastward longshore drift (FitzGerald and Penland, 1987). Strong mesotidal currents redistribute sediment within the back-barrier and form migrating dunes and barforms, which if preserved in the rock record would form a sheet-like geometry containing pervasive tidal indicators. Tidal creeks dissect the tidal flats and marshes that occur on the landward flank of the lagoon. This is analogous to the John Henry Member, where tidal channels and creeks occur landward of a tidal sheet and dissect the adjacent tidal flats and marsh deposits (Fig. 14).

R-T cycle 3 (“F” Interval): Mouth bars and coastal plain deposits. Within the lower portion of R-T cycle 3, distributary channels (LF 2.1), mouth bars (LF 2.4), and interdistributary rooted carbonaceous shales (LF 2.2) record the shoreline turnaround indicating basinward progradation of the coastal plain into a back-barrier lagoon (Allen and Johnson, 2011). The rate of relative sea-level rise outpaced terrestrial sediment supply into the landward side of the back-barrier long enough for substantial (>30 m) lagoonal deposits to accumulate landward of the barrier island. However, once the rate of sea-level rise was no longer able to keep pace with terrestrial sediment input, the coastal plain advanced basinward (Fig. 14).

Two scenarios are considered to explain how the rate of sediment supply became sufficient enough to drive progradation into the back-barrier. The first, is that the rate of relative sea-level rise was no longer able to keep pace with distributary channels that supplied sediment into the back-barrier. The second possibility, is that throughout the transgressive phase of R-T cycle 2, distributary channels were cut off from the back-barrier, and consequently, no sediment was supplied to the landward flanks of the lagoon. Avulsion of a distributary channel may have diverted flow into the lagoon and resulted in increased sediment supply to the landward flank. The outcome of either scenario is the same: accommodation present within the back-barrier was subsequently filled with regressive coastal plain facies.

Facies association 2 (coastal plain) dominate the upper intervals of the John Henry Member near Main Canyon. Multistory, fluvial channel complexes >30 m thick are present within the section (Fig. 8), recording aggradation of stationary channel belts through time, and/or the continuous reoccupation of preexisting topographic lows through avulsions (Morozova and Smith, 2000; Slingerland and Smith, 2004; Aslan et al., 2005; Miall, 2014). Water depths were calculated from cross-set measurements to be between 2.4 and 6.2 m. Multistory, fluvial channel complexes (Fig. 8) within the John Henry Member at Main Canyon were deposited within 10–20 km of the adjacent shoreline (Fig. 16). Rough estimates of backwater lengths in fluvial sections at Bull Canyon, 60 km southwest of Main Canyon (Johnson et al., 2013; Turner et al., in review), indicate that Main Canyon should have been well within the range of backwater effects during this time interval. Flow deceleration near the upstream extent of the backwater zone causes streams to lose their sediment transport capacity and drives deposition, shortening channel-fill timescales. This leads to an increase in avulsion frequency (Chatanantavet et al., 2012), thus also favoring the formation of amalgamated channel belts as observed within R-T cycles 3 at Main Canyon (Fig. 12).

Alternative Interpretations for Incised Valleys (R-T cycle 1)

At Main Canyon, R-T cycle 1 of the John Henry Member contains deep northeast-trending incisions that truncate the underlying shoreface in the western and central parts of the study area. The favored interpretation (discussed above) for this high-relief surface, is a compound surface of erosion that was first generated by fluvial incision in response to a fall in relative sea-level, which produced an incised valley. This valley was later modified by tidal ravinement during the following transgression. Incisions have >20 m of relief locally and are mappable for > 6 km southwest of Main Canyon (Fig. 3), representing a minimum width of the initial incised valley system. These dimensions are consistent with the both modern (Boyd, 2006) and ancient (Willis, 1997; Gibling, 2006) examples of incised valleys, supporting the incised valley interpretation. Extensive lowstand fluvial channel deposits and/or paleosols that would provide definitive evidence for subaerial exposure are not present above this boundary (we believe because they were removed erosive tidal currents), three alternative interpretations of this boundary will be briefly considered: (1) incision via tidal inlet migration; (2) incision of distributary channels during a normal regression, abandonment related to upstream avulsion, followed by tidal modification; (3) autogenic scouring at confluences. It is important to note that each of these hypotheses are presented as end-member cases, but they are not mutually exclusive.

The first alternative hypothesis suggests that high-energy tidal currents within southward migrating tidal inlets are responsible for generating the erosional surfaces preserved at Main Canyon. Modern tidal inlets are known to erode into underlying shoreface strata significantly with tidal channels that occupy modern inlets commonly 5–10 m deep (Hayes and FitzGerald, 2013) and reaching depths in excess of 20–30 m (Allen and Posamentier, 1993). This is comparable to the maximum erosion of 22 m documented at Main Canyon. However, inlets that reach depths in excess of 25 m are commonly located near the mouths of former fluvial valleys (Hayes and FitzGerald, 2013). This is the case along the Gironde Estuary of France where the estuary mouth is constricted by coastal barriers which focus the tidal currents, forming a deep tidal channel that is 20 to 30 m deep along the thalweg (Allen and Posamentier, 1993). Facies interpreted as tidal inlet fill within the John Henry Member are associated with only 2 to 3 m of erosion. Therefore, it is unlikely that the large-scale (>20 m) incisions at Main Canyon were generated exclusively through autogenic inlet migration.

Even within well-understood settings, the differentiation between incised valleys and distributary channel incisions is not always clear-cut. Distributary channels branch off from large prograding delta systems many tens of kilometers upstream of the shoreline, often at a position near the upstream extent of the backwater effects (Abdel-Fattah et al., 2004; Jerolmack and Mohrig, 2007). Channels often incise at the same scale of an incised valley (Chidsey et al., 2004; Willis and Gabel, 2003; Hampson and Howell, 2005). However, Olariu and Bhattacharya (2006) argue that during normal regressions, distributary channels rarely incise and are more commonly shallowly scoured (1–3 m) and more likely to avulse to another location rather than incise (Li and Bhattacharya, 2013). If it is accepted that prograding distributary channels are capable of incising during a normal regression, the incisions at Main Canyon may represent an abandoned distributary channel that was later modified by tidal processes.

Best and Ashworth (1997) demonstrate that channel scour up to five times greater than the mean channel depth can occur along bends, confluences, and control points. Autogenic processes, independent of base-level fluctuations, generate these incisions. Within R-T cycle 1 of the John Henry Member at Main Canyon, channel depth estimates calculated from terrace deposits indicate flow depths between 2.5 and 6.5 m. The preserved valley relief is at least 22 m near these terrace deposits, which is between 3.4 and 8.8 times the inferred flow depth of the associated channels. The erosional boundary is laterally extensive throughout the study area, and its expression is observed many km away along Fifty Mile Mountain, underscoring that it is regional. Additionally, incisions are typically greater than five times the estimated mean channel depths. Therefore, it is unlikely that erosion into the shoreface was generated solely as a result of autogenic scouring.

Controls on Preservation: Shoreline Trajectory

The preservation of transgressive deposits is regulated predominantly by the shoreline trajectory of the overlying bounding surface (Allen and Johnson, 2011). Helland-Hansen and Gjelberg (1994, p. 670) define shoreline trajectory as “the cross sectional path of the shoreline as it migrates.” Thick accumulations of transgressive strata in Cretaceous deposits of the Western Interior Seaway have been associated with steep, accretionary shoreline trajectories (Cattaneo and Steel, 2003; Sixsmith et al., 2008; Allen and Johnson, 2011). An accretionary shoreline trajectory requires that the rates of sediment supply and accommodation are balanced (Helland-Hansen and Martinsen, 1996), which causes the overlying bounding surface to diverge from the underlying topography leading to the preservation of transgressive deposits. Consequently, steeper the shoreline trajectories facilitate the preservation of thicker transgressive deposits (Thorne and Swift, 1991; Allen and Johnson, 2011).

Within estuaries, transgressive deposits are commonly well-preserved as a result of their position within paleovalleys (Dalrymple et al., 1992; Allen and Posamentier, 1993; Zaitlin et al., 1994). This is because it is easier to get an upward trajectory relative to a valley bottom than to a topographically higher interfluve (Cattaneo and Steel, 2003). Estuaries that contain a fluvial sediment source are influenced by significant wave energy, and are filled from all sides. If the rate of sediment supplied to the head of the estuary exceeds the rate of relative sea-level rise, the estuary will become overfilled, a delta will form, and the location of the shoreline will remain fixed (Simms et al., 2006). Alternatively, if the rate of relative sea-level rise keeps pace with or exceeds terrestrial sediment supply, the valley will flood and the shoreline will retreat.

Within the John Henry Member, we recognize evidence for both transgressive estuarine, and transgressive barrier island deposits occurring along the flanking interfluve. The accumulation and subsequent preservation of such thick (>38 m) transgressive deposits along the interfluve require a combination of factors to be in place to generate a shoreline trajectory that is sufficiently steep. Allen and Johnson (2011) ruled out autogenic topographic changes (e.g., a steeply dipping shoreline gradient) because no evidence for elevation change within barrier systems to the south was observed. At Main Canyon, however, there is evidence for stratigraphic thinning landward onto underlying topography (Figs. 8, 11, 12). Thick accumulations of transgressive deposits can develop during transgressions occurring across high-gradient (>0.001) topography because the shoreface retreats slowly and allowing more time for sediment accumulation behind the barrier (Cattaneo and Steel, 2003). Estimates on the shoreline gradient (Table 3) near Main Canyon indicate steep (>0.01) profile existed during deposition of the John Henry Member. Inherent topography, generated by a steep depositional profile, combined with balanced high-sedimentation rates and subsidence led to the preservation of thick transgressive barrier island deposits observed at the mouth of Main Canyon.

Regional Stratigraphic Trends and Paleogeography

Relatively little research has been conducted on John Henry Member exposures in the northern Kaiparowits Plateau (Hettinger, et al., 1993), in contrast to coeval fluvial and tidal deposits (Shanley et al., 1992; Gallin et al., 2010; Gooley, 2010; Pettinga, 2013; Turner et al., in review) along the southern margin of the plateau, and shoreface and marginal marine strata along Fifty-Mile Mountain (e.g., Peterson, 1969b; Shanley and McCabe, 1991; Allen and Johnson, 2010, 2011; Dooling, 2013). The following discussion relates stratigraphic trends observed at Main Canyon to the regional stratigraphy and depositional system within the Late Cretaceous Kaiparowits Basin.

Correlations across the northern Kaiparowits Plateau. The compacted thickness of the John Henry Member increases by >200 m from south to north in the northern plateau (Fig. 13). Although there are more coals to the south (Left Hand Collet), the overall decompacted distributions still show a significant thickening north of Escalante (Fig. 1), toward the Henry Basin (Fig. 4 of Peterson et al., 1980). The >500 m thick John Henry Member section at Buck Hollow is a focus of our ongoing studies (Mulhern et al., 2014); nevertheless, a preliminary correlation is presented here, along with an illustrative paleogeographic reconstruction for the lower section (Figs. 13, 16). More detailed paleogeographic maps focused on the northern Kaiparowits Plateau are provided in Appendix A.

Based on this correlation, much of the thickening occurs in the “A-B” interval, where offshore mudstones above the Calico bed are over 160 m thick (Fig. 13). This indicates a deep basin to the north and northerly pinch outs of the lower shorefaces. The basinward shift in depositional facies that occurs within R-T cycle 1 (lower John Henry Member sequence boundary) at Main Canyon generated a shore-parallel incised valley system that correlates down depositional dip to the “C” sandstone interval (Fig. 13). That down-dip expression at Buck Hollow is a sharp-based 50 m thick package of shoreface sandstone (Fig. 13), which records sediment bypass, and during falling relative sea level.

These thick (>50 m) packages of shoreface strata (within the “C” interval) that occur at Buck Hollow internally contain mouth bars and channel forms (Mulhern et al., 2014). Mouth bars represent the distal deposits of terminal distributary channels which were modified into wave-dominated shoreface strands by wave energy and longshore drift (Olariu and Bhattacharya, 2006). Therefore the “C” interval at Buck Hollow is interpreted to represent a wave-modified lowstand delta that formed detached from the previous “A” and “B” shorelines (Fig. 13) (Zhu et al., 2012).

Backfilling of the Main Canyon incised valley network and landward migration of barrier islands (Fig. 14) took place during relative sea level rise associated with back-stepping of the shoreline during the “D” interval, and is recorded at Buck Hollow as a 70 m-thick package of carbonaceous lagoonal shales, tide-dominated channel fills, washover fans, and barrier island sandstones (Mulhern et al. 2014). These deposits are capped by a flooding surface and renewed shoreface deposition (the “E” shoreface), which can be correlated from Buck Hollow to Main Canyon via air photos (Fig. 13).

The “E” shoreface is overlain by transgressive lagoonal and bayhead delta deposits at Buck Hollow comprising the “F” sandstone interval at this location. A similar turnaround from a regressive to transgressive shoreline trajectory is observed at Main Canyon where the “E” shoreface is overlain by sand-rich back-barrier sheets, lagoonal fines, and tidal channels. Above this interval, distributary channels and northeastward prograding coastal plain facies record the infilling of the back-barrier system, marking the regressive turnaround at Main Canyon. These coastal plain deposits are >100 m thick at White Mountain (Fig. 13). A final flooding surface occurs within the “G” interval at Buck Hollow and places laterally extensive offshore deposits on top of the “F” interval. We correlate this flooding surface to the base of >40 m of tide-dominated lagoon fill preserved at White Mountain, which were deposited during rising sea-level. The overlying coastal plain and fluvial channels become progressively more amalgamated up section and transition into the highly amalgamated channel belt complexes of the Drip Tank Member that caps the John Henry Member (Fig. 13) and record the final retreat of the Western Interior Seaway across the Kaiparowits Basin.

The John Henry Member increases in compacted thickness by 47% (>160 m) over 14 km from Main Canyon to Buck Hollow (Figs. 3, 13), indicating an average depositional slope of ~0.011 (Table 3). Such dramatic variation in thickness over a relatively short distance is not readily explained through autogenic processes or as a result of fluctuations in eustatic sea-level, which were between 15 and 30 m on the 10^6-year scale in the Late Cretaceous (Miller et al., 2005). Active faulting within the Cretaceous Western Interior foreland basin is known to create localized zones of increased and decreased accommodation that controlled sedimentation patterns and sand body distributions (e.g., Jennette et al., 1991; Hart and Plint, 1993; Taylor and Lovell, 1995; Van Wagoner, 1995; Bhattacharya and Willis, 2001; Lawton and Bradford, 2011). It is hypothesized here that the foredeep was actively deforming and acted as a primary control on deposition. Possible faulting mechanisms include subsurface propagation of blind thrust faults, early displacement along Laramide-style basement uplifts (c.f., Tindall et al., 2010; Lawton and Bradford, 2011), and/or local subsidence related to strike-slip faulting. Additionally, local changes in sea-floor bathymetry can enhance tidal currents and lead to erosion (Harris, 1994; Baker et al., 1995; Hori et al., 2002; Willis and Gabel, 2003), which may have driven the extensive tidal ravinement (Fig. 10) observed at Main Canyon. Dynamic subsidence may also have influenced more regional depositional patterns (Liu and Nummedal, 2004; Liu et al., 2008; Aschoff and Steel, 2011).

Table 2

Descriptions of key bounding surfaces in the John Henry Member at Main Canyon

Surface	Description	Key Characteristics	Erosional?
A surfaces: Separate transgressive from underlying regressive units			
Max regressive surface (mRs)	Unconformable erosional boundary at the base of transgressive units; Marks the onset of relative sea-level rise; Transgressive surface at the base of incised valley fill; Forms a compund surface with the SU and tRs	Truncates regressive shorefaces; overlain by fluvial and/or tide-dominated facies	Yes - 5 to 10 m of relief; Up to 22 m of relief when forming a compound surface with SU
Process change to tide-dominated (pCt)	Conformable contact between transgressive units and underlying shoreface deposits; Also used to describe a conformable boundary separating two transgressive units	Occasional shell lag or coal rich interval	Conformable
Tidal ravinement surface (tRs)	Erosional contact marking a process change from a wave-to tide-dominated coastline separating underlying shoreface sand bodies from overlying tidal channels; Forms a compound surface of erosion with mRs and SU	Tidal incision into shoreface strata; Locally developed firm ground bored by *Gastrochaenolites*	Yes - 5 to 10 m of relief; Up to 22 m of relief when forming a compound surface with SU
B surfaces: Separate regressive from underlying transgressive units			
Wave ravinement surface (wRs)	Separates estuarine, lagoonal, tidal, and/or coastal plain facies from overlying shoreface facies	Well-developed pebble/cobble lag overlain by offshore deposits	Minor relief on the order of 10 cm; total erosion likely on the order of 10 m
Flooding surface (FS)	Separates two regressive shoreface parasequences	Deepening of facies; Thin <10 cm siltstone, shell lag, or stratified pebble lag	No
Tide- to fluvial-dominated process change (pCf)	Gradational boundary between lagoonal and/or tide-dominated facies and overlying distributary mouth bars, channels, and/or coastal plain facies	Placed at the last sign of marine influence at the top of transgressive units	Yes - up to 2 m from channel scour; Relatively conformable
Subaerial Unconformity (SU)	Records fluvial incision and bypass across an erosional contact; Heavily modified by tidal currents associated with the mRs	Highly undulatory with southwest-northeast trending incisions; Overlain by tide-dominated deposits; Locally preserved fluvial deposits	Yes - over 22 m of local relief

Figure 8. Correlation of strata in the Main Canyon study area. The lower to middle John Henry Member records the west to east progradation of shoreface parasequences, and the development of a shore-parallel incised valley backfilled with a complex assemblage of high-energy tide-dominated estuarine deposits. Fluvial terrace deposits and debris flows record incision and collapse of the valley wall, respectively. During the late stages of valley infilling, a landward migrating back-barrier platform overrode the valley, forming flood-tidal delta and inlet deposits that thin onto the valley flank. Tidal channels and lagoonal deposits are observed stratigraphically above the “E” shoreface in the western part of the study area, whereas sand-rich back-barrier deposits are recorded to the east. Landward progradation of the coastal plain into the back-barrier marks the base of R-T cycle 3. Bounding surfaces wRs (1) and wRs (2) refer to successive wave ravinement surfaces in the section. Lithofacies numbers are displayed next to the corresponding pattern.

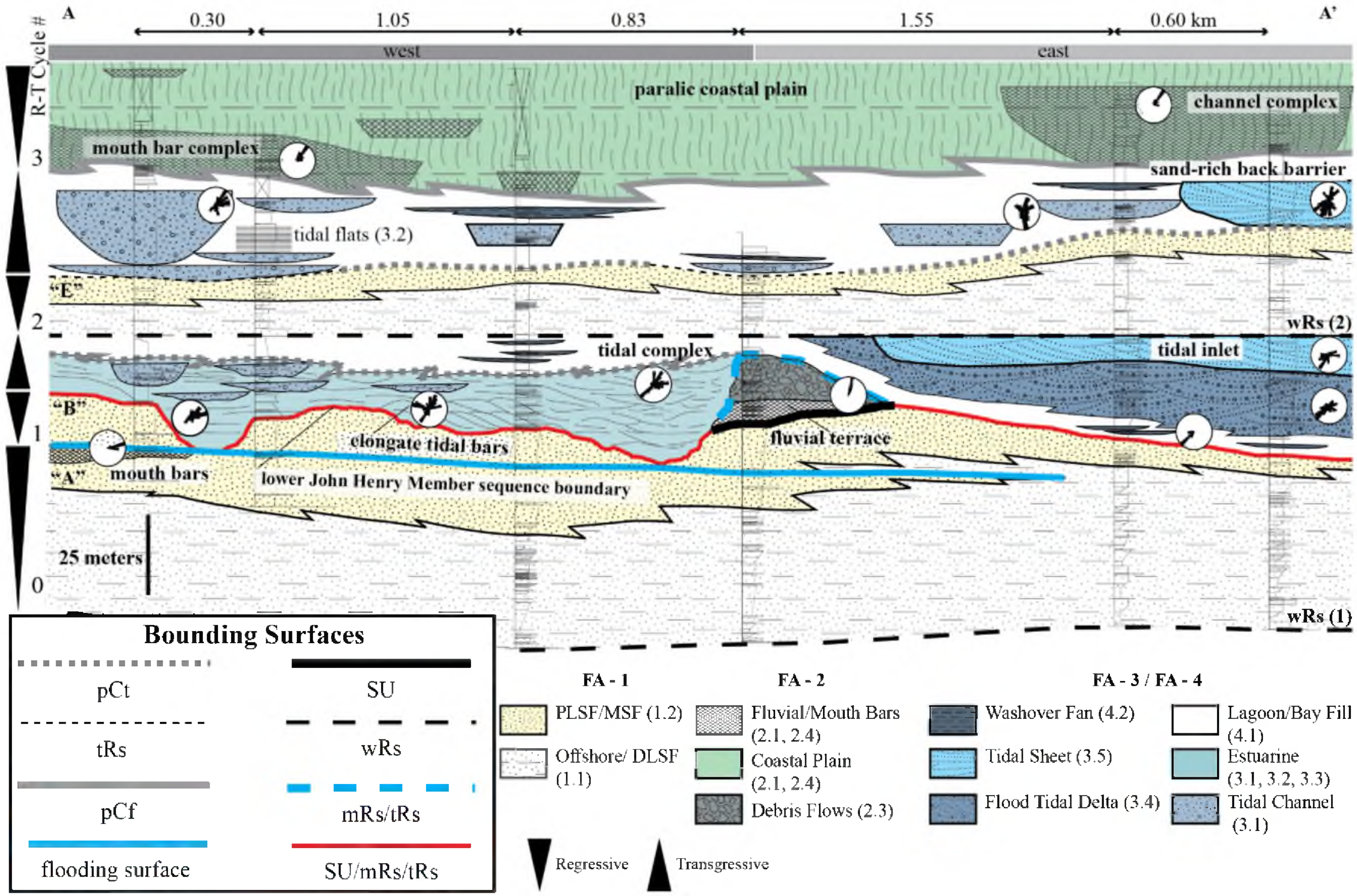

A
A'
0.30
1.05
0.83
1.55
0.60 km
west
east
R-T Cycle #
3
2
1
0
paralic coastal plain
channel complex
mouth bar complex
sand-rich back barrier
tidal flats (3.2)
"E"
wRs (2)
tidal complex
tidal inlet
"B"
elongate tidal bars
fluvial terrace
"A"
mouth bars
lower John Henry Member sequence boundary
25 meters
wRs (1)
Bounding Surfaces
pCt
SU
tRs
wRs
pCf
mRs/tRs
flooding surface
SU/mRs/tRs
FA - 1
FA - 2
FA - 3 / FA - 4
PLSF/MSF (1.2)
Offshore/ DLSF (1.1)
Fluvial/Mouth Bars (2.1, 2.4)
Coastal Plain (2.1, 2.4)
Debris Flows (2.3)
Washover Fan (4.2)
Tidal Sheet (3.5)
Flood Tidal Delta (3.4)
Lagoon/Bay Fill (4.1)
Estuarine (3.1, 3.2, 3.3)
Tidal Channel (3.1)
Regressive
Transgressive

Figure 9. Representative measured sections from the western part of Main Canyon with uninterpreted and interpreted photomosaics. Shoreface strata in R-T cycle 1 and R-T cycle 2 amalgamate to form cliffs upwards of 30 m thick that are truncated by an erosional surface with >16 m of local relief.

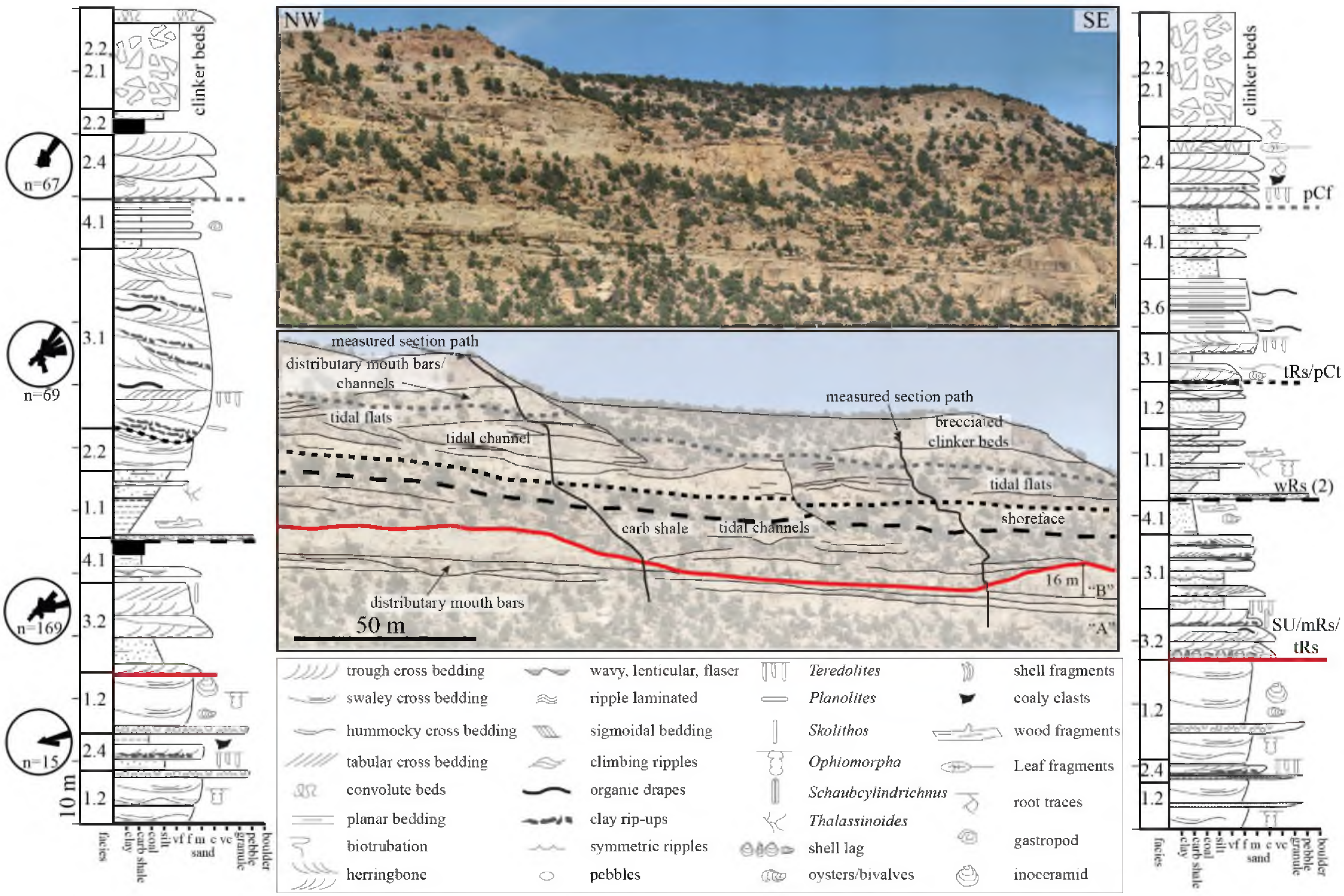
NW
SE
measured section path
distributary mouth bars/
channels
tidal flats
tidal channel
measured section path
brecciated
clinker beds
tidal flats
shoreface
carb shale
tidal channels
16 m
"B"
"A"
distributary mouth bars
50 m
clinker beds
n=67
n=69
n=169
n=15
10 m
facies
clay
carb shale
coal
silt
vf f m c vc
sand
granule
pebble
boulder
pCf
tRs/pCt
wRs (2)
SU/mRs/
tRs
trough cross bedding
swaley cross bedding
hummocky cross bedding
tabular cross bedding
convolute beds
planar bedding
biotrubation
herringbone
wavy, lenticular, flaser
ripple laminated
sigmoidal bedding
climbing ripples
organic drapes
clay rip-ups
symmetric ripples
pebbles
Teredolites
Planolites
Skolithos
Ophiomorpha
Schaubcylindrichnus
Thalassinoides
shell lag
oysters/bivalves
shell fragments
coaly clasts
wood fragments
Leaf fragments
root traces
gastropod
inoceramid

Figure 10. Evidence for tidal ravinement at Main Canyon. A-C) Tidal ravinement into the “B” shoreface. Elongate tidal bars (LF 3.1) accrete to the southeast (arrows) and downlap onto the ravinement surface. Relief along this surface can reach 22 m. Individual bars can be in excess of 15 m in height; D) Heterolithic tidal complex (LF 3.1) with compound internal channel architecture, which rests unconformably on the “B” shoreface; E) Internal architecture of the tidal complex; F) 30 m-thick tidal channel overlies the “E” shoreface with up to 5 m of erosional relief. Channel deposits (LF 3.1) are composed of accreting barforms and laterally transition into tidal flat (LF 3.6) and bay-fill fines. Down depositional dip to the northeast, this channel correlates to tidal sheet deposits of lithofacies (Fig. 6A).

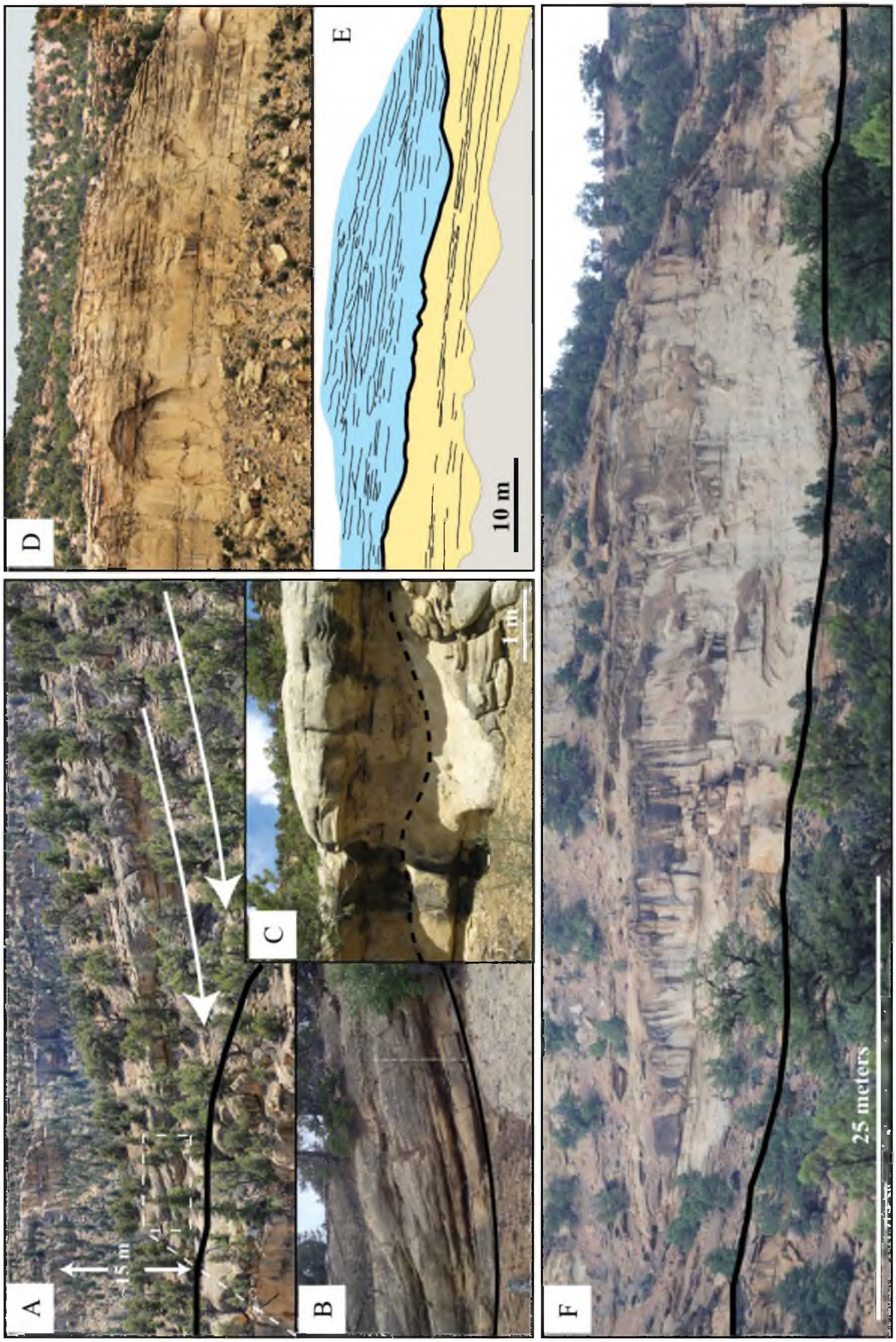
A
15 m
B
C
1 m
D
E
10 m
F
25 meters

Figure 11. Representative measured section and uninterpreted and interpreted field photo from the eastern part of Main Canyon. The section begins on a wave ravinement surface (wRs (1)) and ends in fluvial channels in R-T cycle 3. See Table 2 for bounding surface information. Abbreviations: PLSF – proximal lower shoreface; DLSF – distal lower shoreface. See Figure 9 for legend of stratigraphic symbols.

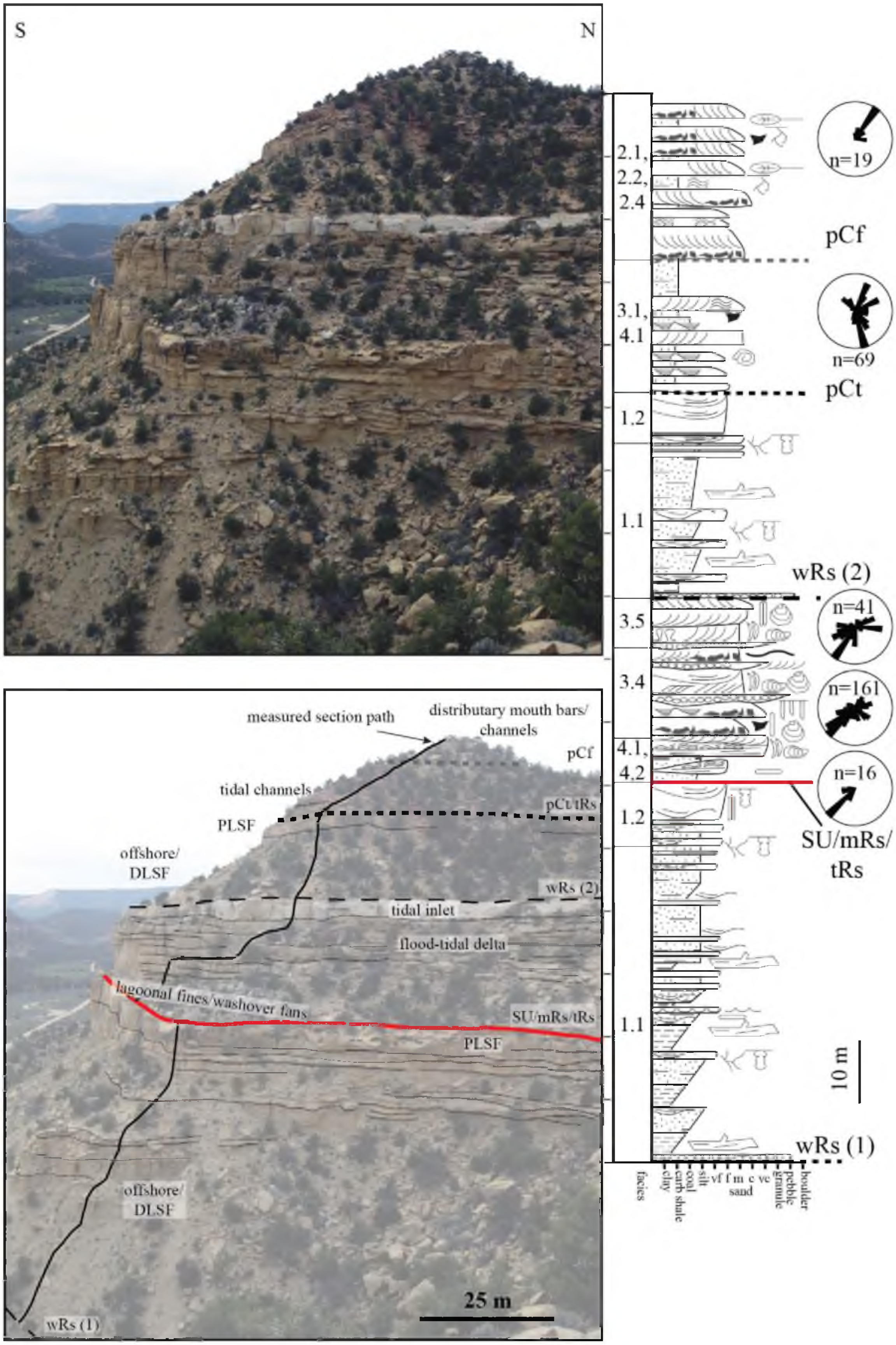
S
N
2.1,
2.2,
2.4
pCf
n=19
3.1,
4.1
n=69
pCt
1.2
1.1
wRs (2)
3.5
n=41
3.4
n=161
4.1,
4.2
n=16
SU/mRs/tRs
1.2
1.1
10 m
wRs (1)
facies
clay
carb shale
coal
silt
vf f m c vc
sand
granule
pebble
boulder
measured section path
distributary mouth bars/ channels
pCf
tidal channels
pCt/tRs
PLSF
offshore/ DLSF
wRs (2)
tidal inlet
flood-tidal delta
lagoonal fines/washover fans
SU/mRs/tRs
PLSF
offshore/ DLSF
25 m
wRs (1)

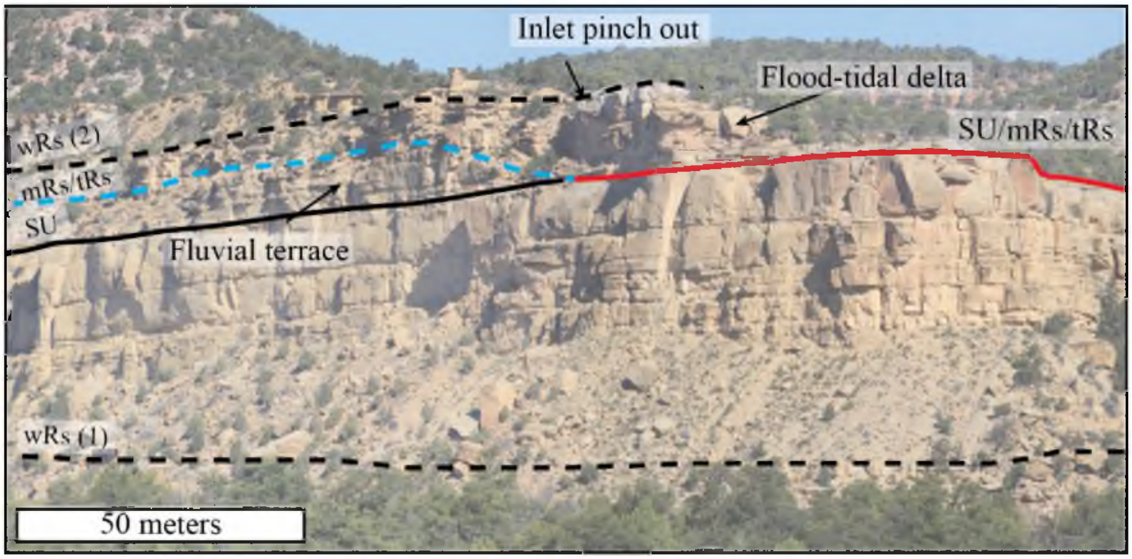

Figure 12. Facies relationships between regressive and transgressive deposits at the boundary between the central and eastern zone of R-T cycle 1. The lower John Henry Member sequence boundary within R-T cycle 1 is heavily modified by tidal ravinement forming a compound surface of erosion (SU/mRs/tRs). East of this location this boundary is relatively flat lying with only minor erosional scour relief occurring locally. The landward pinch out of tidal inlet and flood tidal delta deposits is observed and transitions landward into lagoonal/bay-fill fines. The transgressive interval is capped by wave ravinement (wRs (2)) and overlain by offshore and distal lower shoreface deposits of lithofacies 1.1.

Figure 13. Preliminary southeast to northwest regional correlation (Fig.1) of the Straight Cliffs Formation illustrating thickness trends and stratigraphic relationships. Correlation of measured sections collected at Main Canyon and White Mountain indicate the John Henry Member is ~ 350 m thick R-T cycles. Note this model predicts the “C” shoreface at Buck Hollow is detached from the older shoreface sands observed at Main Canyon. Abbreviations: TCM - Tibbet Canyon Member; SHM - Smoky Hollow Member; JHM - John Henry Member; DTM – Drip Tank Member; DLSF - distal lower shoreface; pCf - process change from tide- to fluvial-dominated processes; tRs - tidal ravinement surface; wRs - wave ravinement surface; FS - flooding surface; SU/mRs/tRs - combined subaerial unconformity, maximum regressive surface, and tidal ravinement surface; LJHMSB - lower John Henry Member sequence boundary.

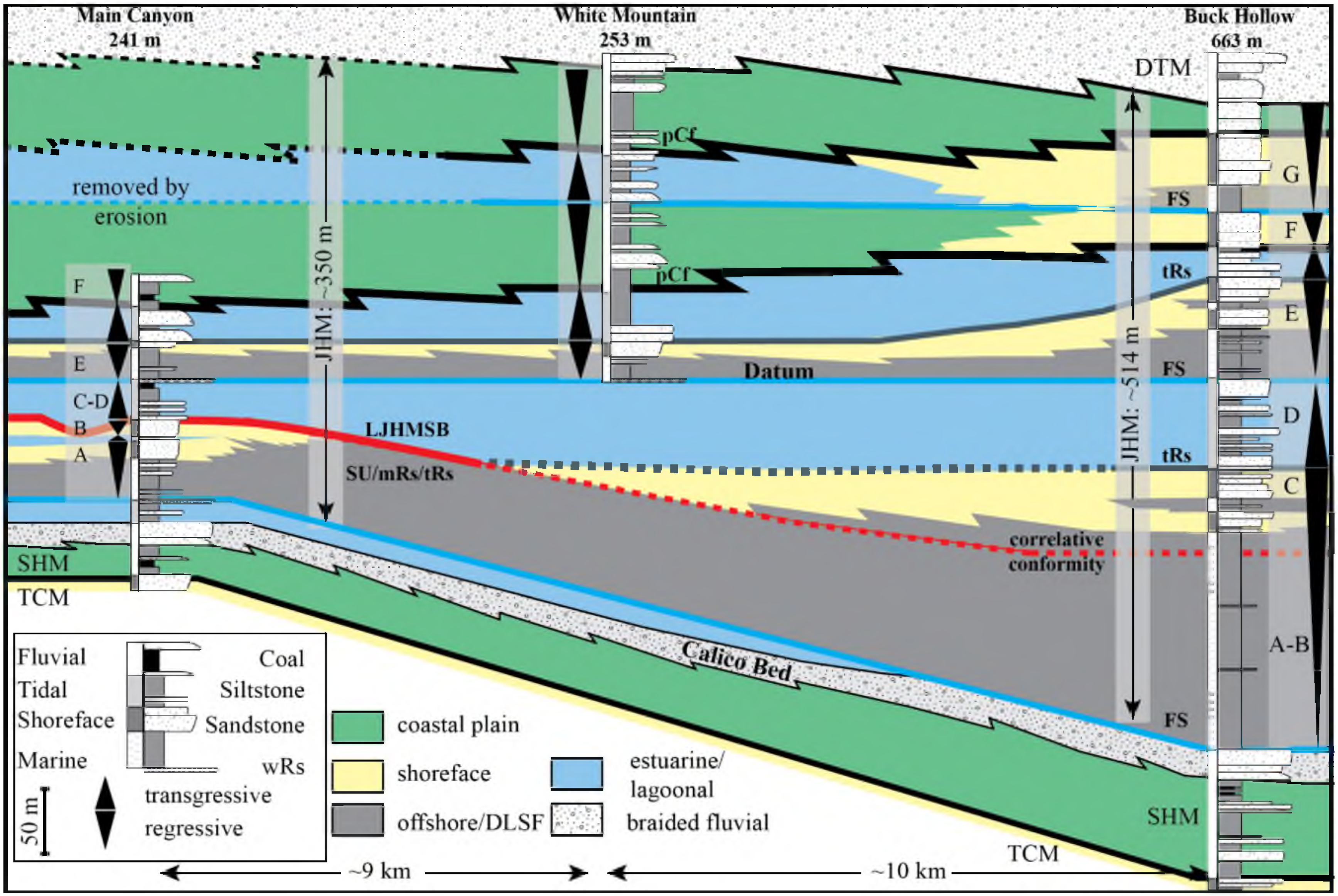
Main Canyon
241 m
White Mountain
253 m
Buck Hollow
663 m
DTM
removed by
erosion
pCf
pCf
JHM: ~350 m
JHM: ~514 m
FS
tRs
FS
tRs
FS
G
F
E
D
C
A-B
F
E
C-D
B
A
Datum
LJHMSB
SU/mRs/tRs
correlative
conformity
Calico Bed
SHM
TCM
SHM
TCM
Fluvial
Tidal
Shoreface
Marine
Coal
Siltstone
Sandstone
wRs
50 m
transgressive
regressive
coastal plain
shoreface
offshore/DLSF
estuarine/
lagoonal
braided fluvial
~9 km
~10 km

Figure 14. Conceptual depositional model for the development Main Canyon stratigraphy focused on preservation of shore-parallel valleys and back-barrier lagoons from oldest (A, deposition of the “A” and “B” shorefaces) to youngest (J, deposition of “F” interval). A relative sea-level curve was generated based on shoreline movements and facies relationships.

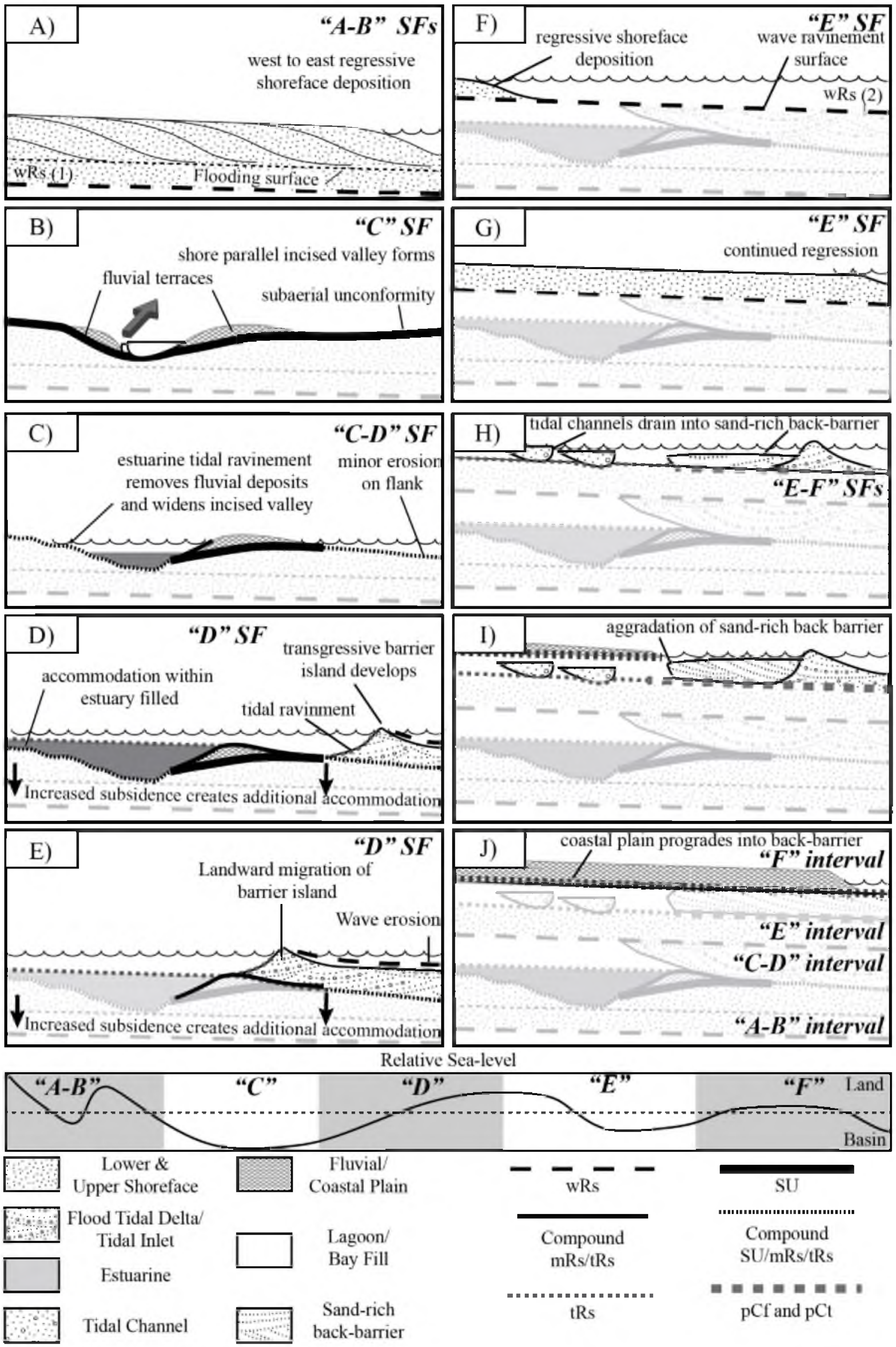

A)
"A-B" SFs
west to east regressive shoreface deposition
wRs (1)
Flooding surface
B)
"C" SF
shore parallel incised valley forms
fluvial terraces
subaerial unconformity
C)
"C-D" SF
estuarine tidal ravinement removes fluvial deposits and widens incised valley
minor erosion on flank
D)
"D" SF
transgressive barrier island develops
accommodation within estuary filled
tidal ravinment
Increased subsidence creates additional accommodation
E)
"D" SF
Landward migration of barrier island
Wave erosion
Increased subsidence creates additional accommodation
F)
"E" SF
regressive shoreface deposition
wave ravinement surface
wRs (2)
G)
"E" SF
continued regression
H)
tidal channels drain into sand-rich back-barrier
"E-F" SFs
I)
aggradation of sand-rich back barrier
J)
coastal plain progrades into back-barrier
"F" interval
"E" interval
"C-D" interval
"A-B" interval
Relative Sea-level
"A-B"
"C"
"D"
"E"
"F"
Land
Basin
Lower & Upper Shoreface
Flood Tidal Delta/ Tidal Inlet
Estuarine
Tidal Channel
Fluvial/ Coastal Plain
Lagoon/ Bay Fill
Sand-rich back-barrier
wRs
Compound mRs/tRs
tRs
SU
Compound SU/mRs/tRs
pCf and pCt

Table 3

Depositional gradient estimates for the John Henry Member

Interval/Surface	**Thickness Change (m)**	**Distance (km)**	**Slope**	**°**
"A" FS (min)	17	2.8	0.0061	0.348
"A" FS (max)	38	2.9	0.0131	0.751
East Flank IV	18	2.5	0.0072	0.413
JHM from MC to BH	164	14.5	0.0113	0.648
JHM from LHC to MC	95	40	0.0024	0.1361

Estimates on the depositional slope of the John Henry Member (JHM). Flooding surfaces (FS) within the "A" shoreface were estimated using Figure 2 of Hettinger et al. (1993); Eastern flank of the incised valley (IV) within R-T cycle 1 (Fig. 8); Average slope for the JHM estimated using the thickness difference between Main Canyon (MC) and Buck Hollow (BH) (Fig. 13); The JHM is 255 m thick at Left Hand Collet (LHC) and ~350 m thick at Main Canyon. These estimates indicate a steep depositional profile was present during deposition of the JHM.

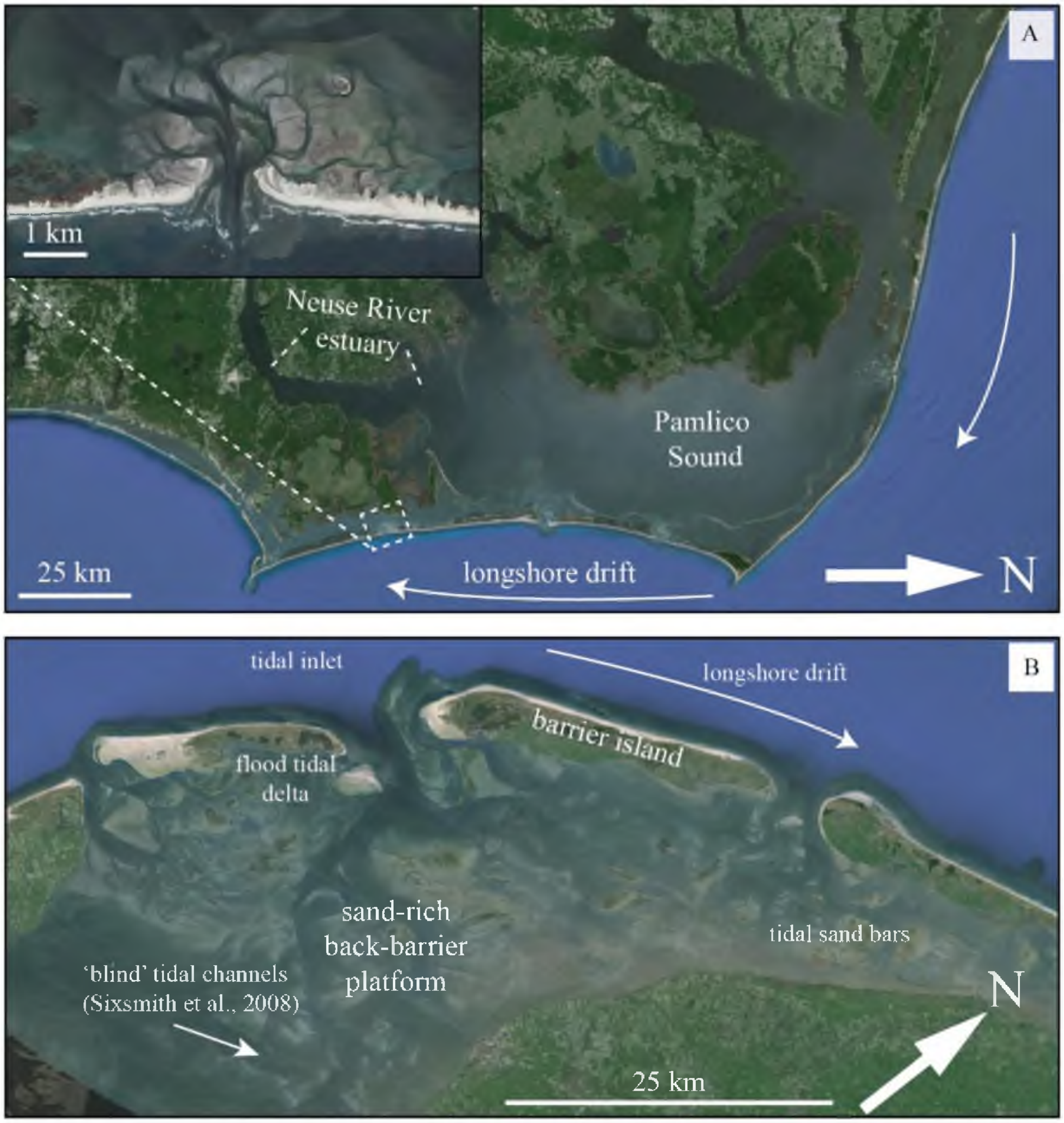

Figure 15. Satellite images of two modern coastlines that display snapshots of modern shorelines with geometries and depositional processes analogous to the John Henry Member at Main Canyon. A) Incised valleys at Pamlico Sound, North Carolina, are flanked by lagoons. Insert) Detailed image of a sand-rich flood-tidal delta that occupies the seaward flank of a shore-parallel portion of an estuary. Sand is supplied from north to south directed longshore drift. B) Sand-rich back-barrier deposits along the Friesian Islands, Netherlands are analogous to tidal strata deposited within R-T cycle 3 of the John Henry Member. Map data: Google, Landsat, Terrametrics, and DigitalGlobe.

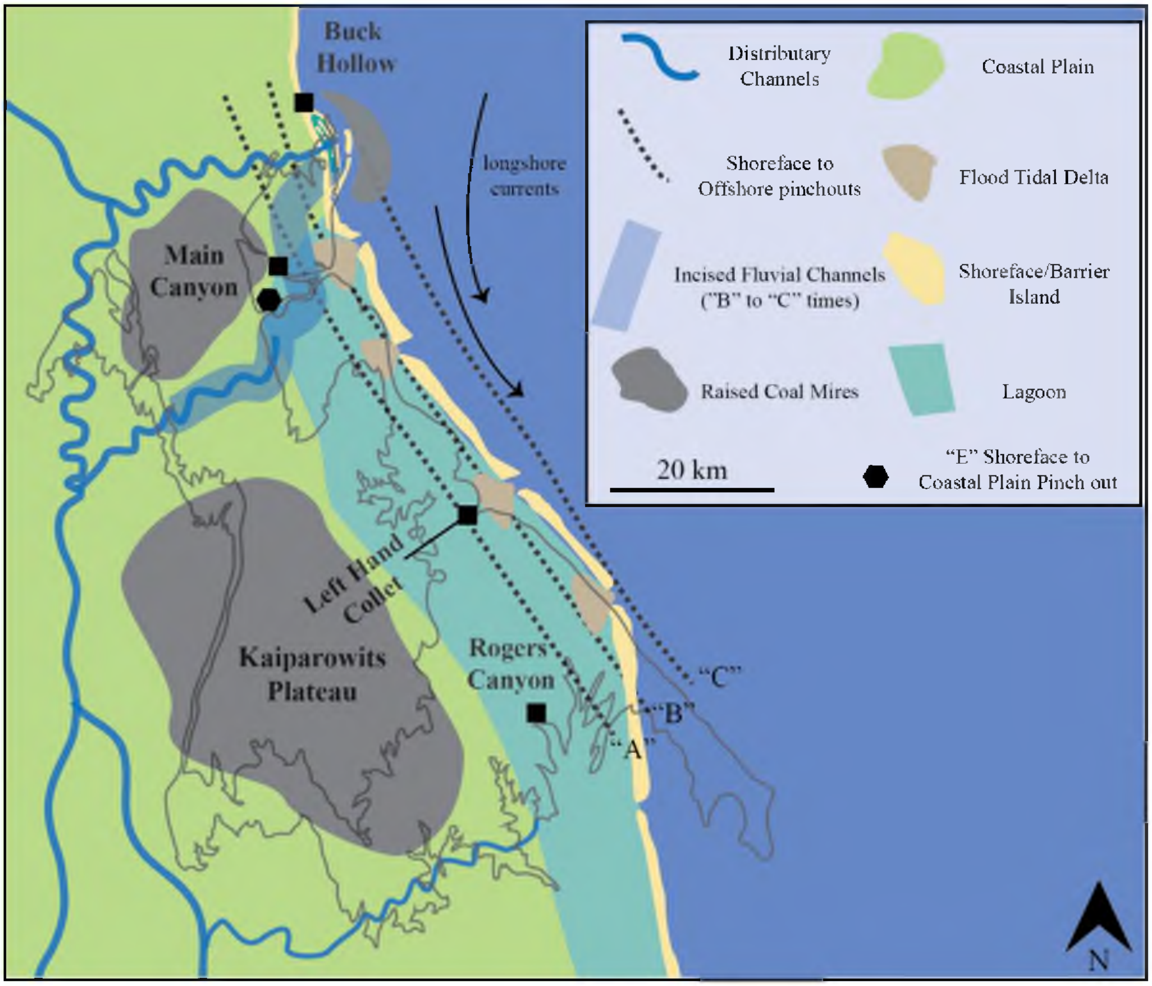

Figure 16. Paleogeographic sketch of the Kaiparowits Plateau during deposition of the transgressive deposits of R-T cycle 1 of Main Canyon. The downdip shoreface pinchouts into offshore mudstones of the "A," "B," and "C" shorefaces are shown. Facies belts throughout the plateau tend to trend northwest-southeast and parallel the shoreline. Raised coal mires in the center of the plateau deflected fluvial systems to the north.

IMPLICATIONS

This study demonstrates the influence of antecedent topography generated by fluvial incision during a forced regression on the distribution of transgressive tidal deposits within high-frequency (fourth- and fifth- order) relative sea-level cycles. Our findings have implications for reservoir distribution in analogous subsurface settings. Incised valleys formed during forced regressions have proven to be prolific subsurface petroleum reservoirs (e.g., Van Wagoner et al., 1990; Boyd et al., 2006). They form natural containers occupied by sand-rich transgressive facies with high porosity, and high permeability that are commonly overlain by offshore mudstones of an overlying high-stand, which provide an effective seal. Most models predict the interdistributary zones separating incised valleys along-strike to contain little to no accumulations of reservoir quality sands. Consequently, these zones may be overlooked in shallow marine petroleum systems, with the focus of drilling the incised valley container. However, this study demonstrates that within high accommodation, high sediment supply settings, the flanks of shore-parallel and/or shore-oblique incised valleys may host significant volumes of high-quality transgressive reservoir facies.

At Main Canyon, sand-rich flood-tidal delta deposits are limited to the eastern flank of the shore-parallel incised valley developed in R-T cycle 1, and comprise over 38 m thick sands and gravels at the mouth of the canyon, that thin to <20 m over only 2.25 km to the west (Fig. 8). These sand-rich facies then pinch out into fine-grained carbonaceous bay-fill. This stratigraphic relationship, in conjunction with the overlying offshore mudstones of the next R-T cycle, would provide an effective sealing mechanism, and permit hydrocarbon accumulation. The thin zone of bay-fill fines that underlie the sandy flood-tidal delta deposits (Fig. 8) separate it from the underlying shoreface. These clay-rich deposits have potential to act as a barrier to fluid flow, and consequently compartmentalize the reservoir. Landward, tidal channels and washover fans occur within carbonaceous shales and likely form disconnected sand bodies. As a result, the flood-tidal delta succession may not be connected to any other sandy facies, and act as a separate flow unit in the subsurface. This study documents the potential for partitioning of facies within transgressive reservoirs highlights the importance of understanding the distribution of sand-rich facies in predicting any potential compartmentalization. Results may help improve reservoir management techniques within analogous subsurface reservoirs.

CONCLUSIONS

Four facies associations are preserved within the lower to middle John Henry Member at Main Canyon: wave-dominated shorefaces, coastal plain and fluvial facies, sand-rich tide-influenced coastal margin, and low-energy bay deposits. Tide-dominated sandstones and low-energy bay-fill record deposition in back-barrier lagoons and estuaries during transgressions. Wave-dominated shoreface and coastal plain facies record regression of the shoreline and infilling of bays and lagoons. Depositional units are organized into transgressive-regressive cycles bound by wave ravinement surfaces. The surface of maximum regression (mRs) is associated with estuarine tidal ravinement that removed most of the falling stage and low stand fluvial deposited from the incised valley, and also modified the pre-existing valley dimensions. Consequently, the preserved valley system at Main Canyon represents a stratigraphic valley, rather than a preserved geomorphic valley.

Regional stratigraphic relationships indicate a stepped forced regression occurred during the "A-B-C" sandstone intervals, with the largest basinward shift (~14 km) occurring at the transition between the "B" and "C" sandstones. This is in contrast with previous interpretations that placed a sequence boundary at the top of the "A" shoreface. The "C" shoreface in the northern Kaiparowits Plateau was deposited as a wave-modified lowstand delta detached from older shoreface deposits. We propose the "lower John Henry Member sequence boundary" be placed at the "B" to "C" shoreface transition throughout the Kaiparowits Plateau. Overlying R-T cycles are not associated with valley incision, but instead preserve sand-rich back-barrier and tidal channel deposits which are overlain distributary mouth bars, fluvial channels and coastal plain fines, which record infilling of the back-barrier. The preservation of >30 m thick accumulations of transgressive back-barrier deposits indicate an accretionary shoreline trajectory with balanced rates of high sediment supply and accommodation.

APPENDIX A

PALEOGEOGRAPHIC SKETCHES OF THE NORTHERN KAIPAROWITS PLATEAU

Paleogeographic sketches illustrate the major facies bands and pinchouts throughout the northern Kaiparowits Plateau.

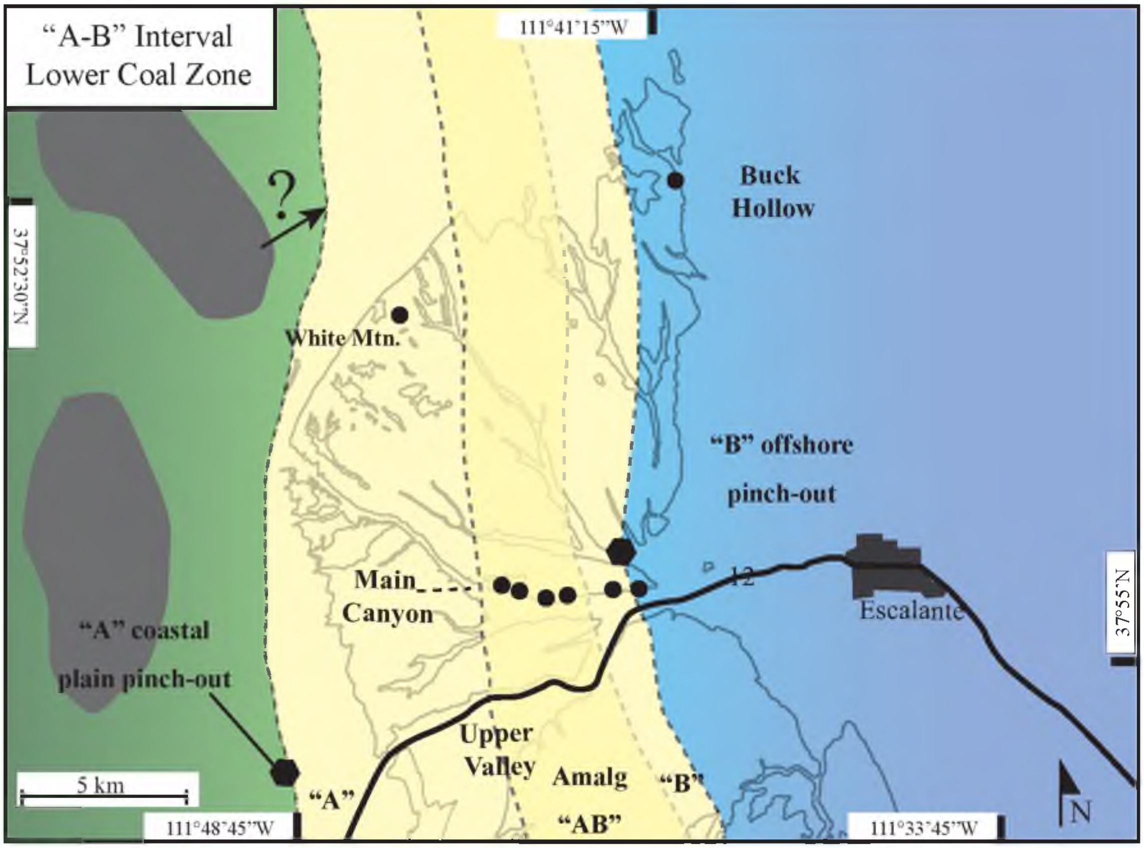

The "A" and "B" shorefaces stack progradationally from W-E in the Northern Kaiparowits Plateau. The "A" shoreface pinches out into coal bearing coastal plain deposits ~4.5 km west of Upper Valley (Hettinger et al., 1993). The "B" shoreface pinches out into offshore mudstones at the mouth of Main Canyon. These units amalgamate in the central portion of Main Canyon forming cliffs in excess of 50 m. At Buck Hollow no shoreface sandstones are observed within the "A-B" intervals. Rather ~ 160 m of mudstones and siltstone record offshore sedimentation.

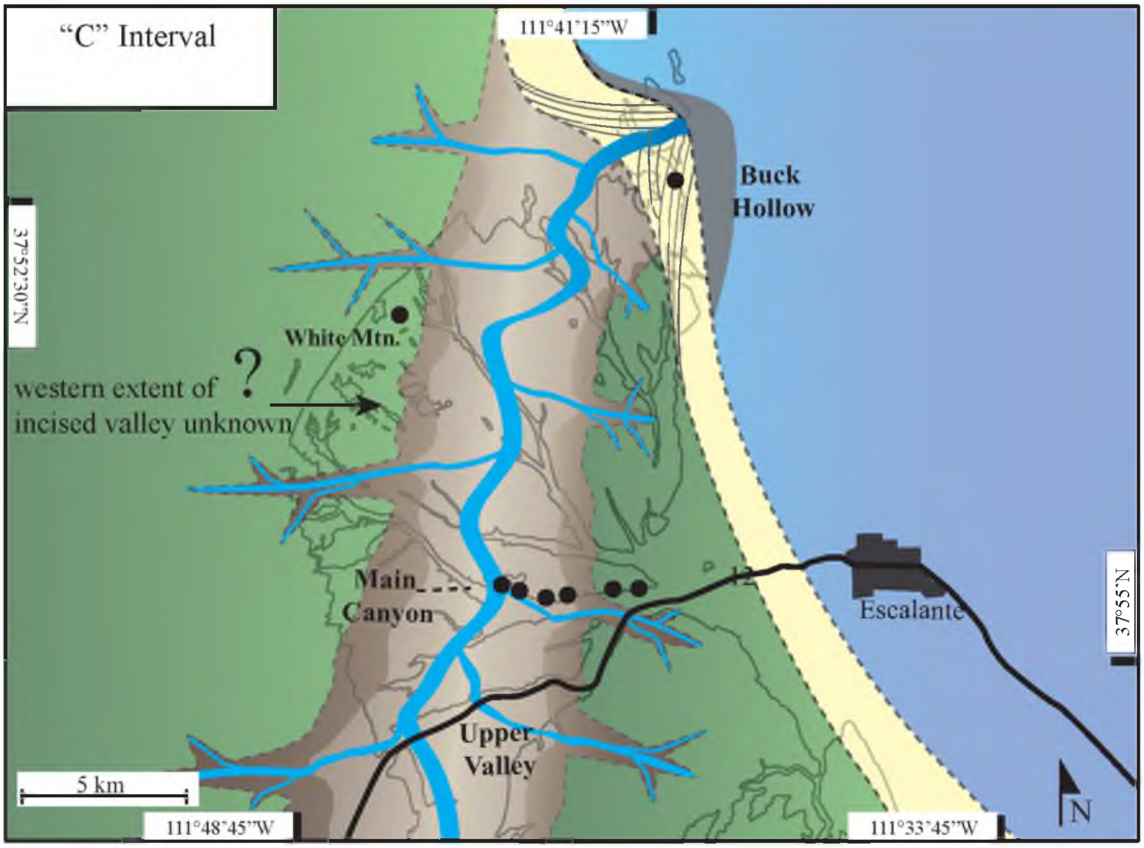

A southwest to northeast trending incised valley is observed at Main Canyon. The lowstand shoreline is preserved 14 km northeast at Buck Hollow as a delta influenced shoreface. Preliminary scouting suggests that southwest of Escalante, at Alvey wash, the shoreline was disconnected from the older "A" and "B" shoreface sandstones. Smaller tributary streams and their associated valleys may have been responsible for local scours within the larger valley system. During the C Interval two thick delta-influenced shorefaces progradationally stack from W-E at Buck Hollow. These large sands are stacked, amalgamated, delta lobes evidenced by sharp based packages with channelized internal architecture.

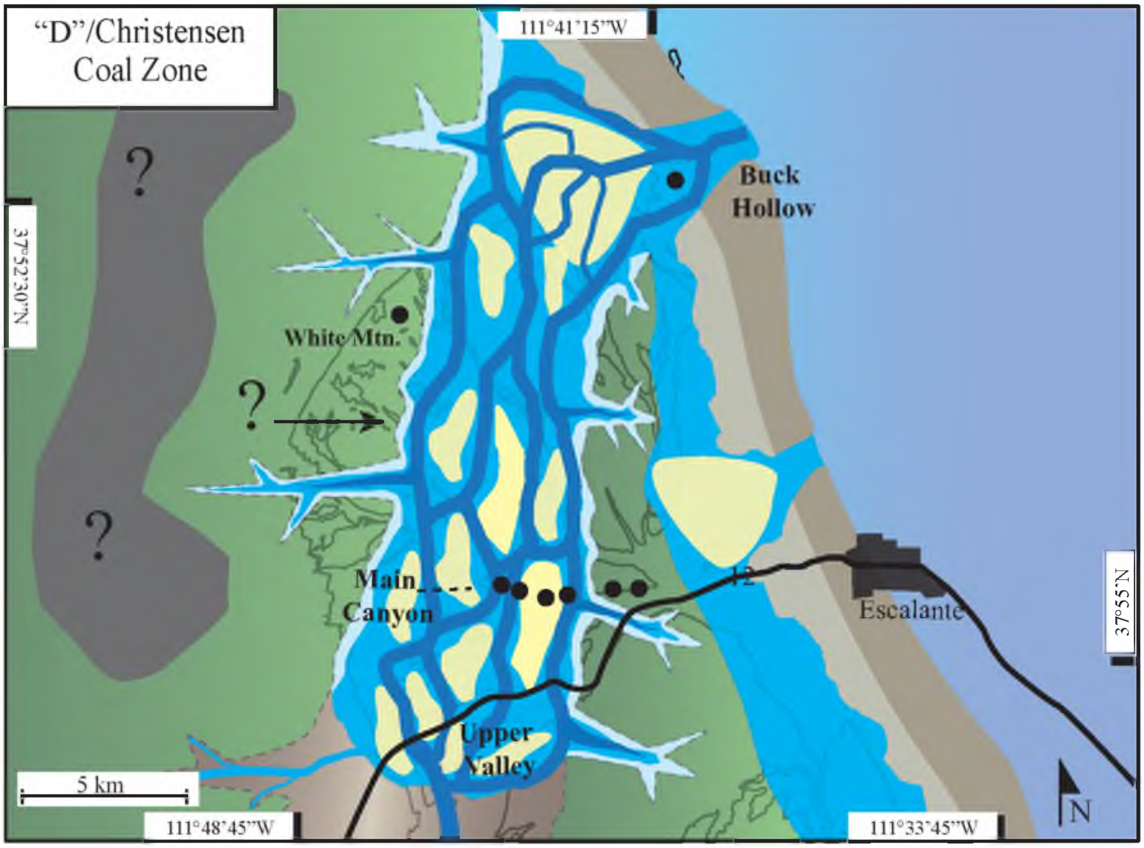

High energy tidal deposits at Main Canyon were deposited within a mixed tide- and wave-dominated estuary. Tidal channels were mostly oriented SW-NE, however, local meanders and bends were likely common throughout the estuary. The majority of lowstand fluvial deposits were reworked during the early stages of flooding as a result of the high basinal tidal energy. The eastern flank of the valley would have acted as a paleo-topographic high, that controlled the distribution of barrier island and lagoonal sediments that are preserved to the east. Between the "C" and "D" intervals the system turns around from regressive to transgressive. The "D" interval is a thick transgressive package at Buck Hollow. During the early "D" a tidal ravinement surface is overlain with isolated packages of channelized tidal sands. Moving upward, the section contains washover fans, shell hash beds and thick lagoonal carbonaceous shales and coals.

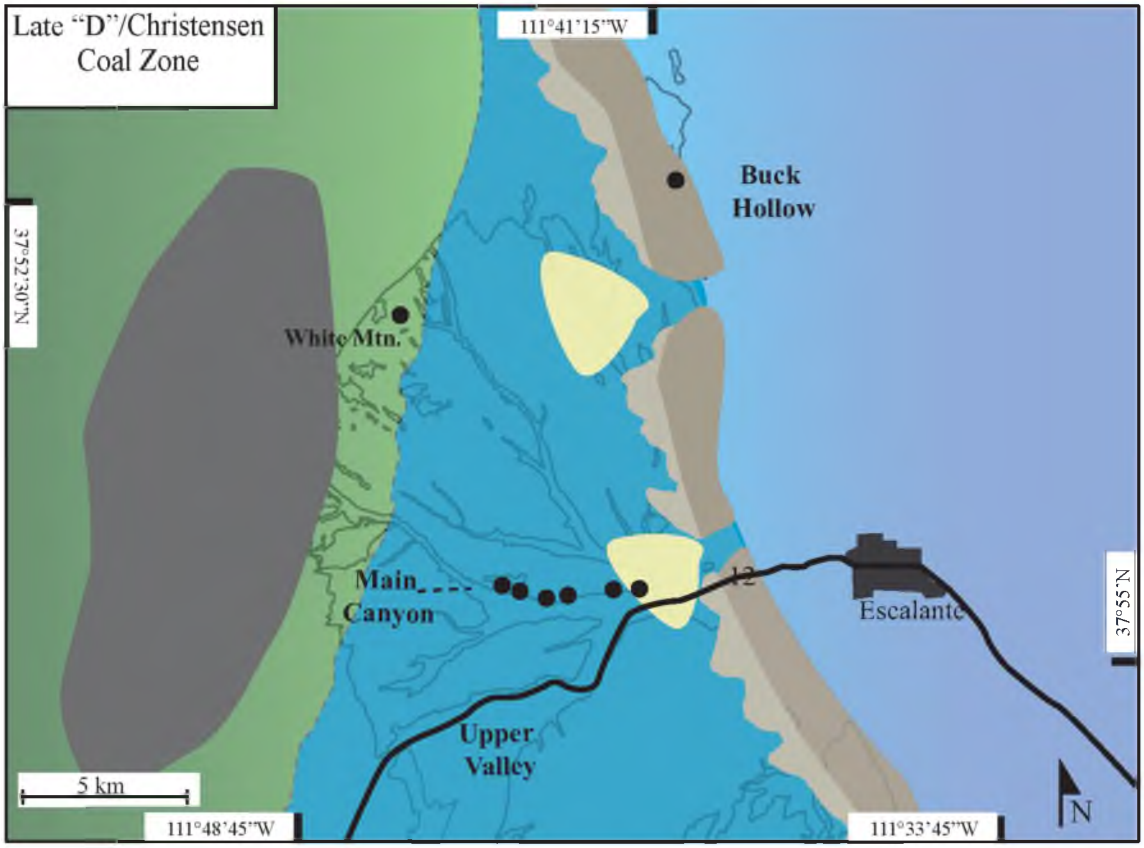

Flood-tidal delta deposits are excellently preserved in the eastern portion of Main Canyon and record the continual landward migration of the barrier island system during transgression. The western study area preserves thick packages of carbonaceous shales dissected by thin washover fans and tidal channels representing deposition within the sheltered portions of the lagoon. As transgression continues from E-W in the northeast Kaiparowits region a transgressive shoreface, likely a barrier island, is preserved at Buck Hollow. Lagoonal/estuarine carbonaceous shales and coals are directly overlain by a sharp-based, thick-bedded, laterally continuous shoreface cliff band.

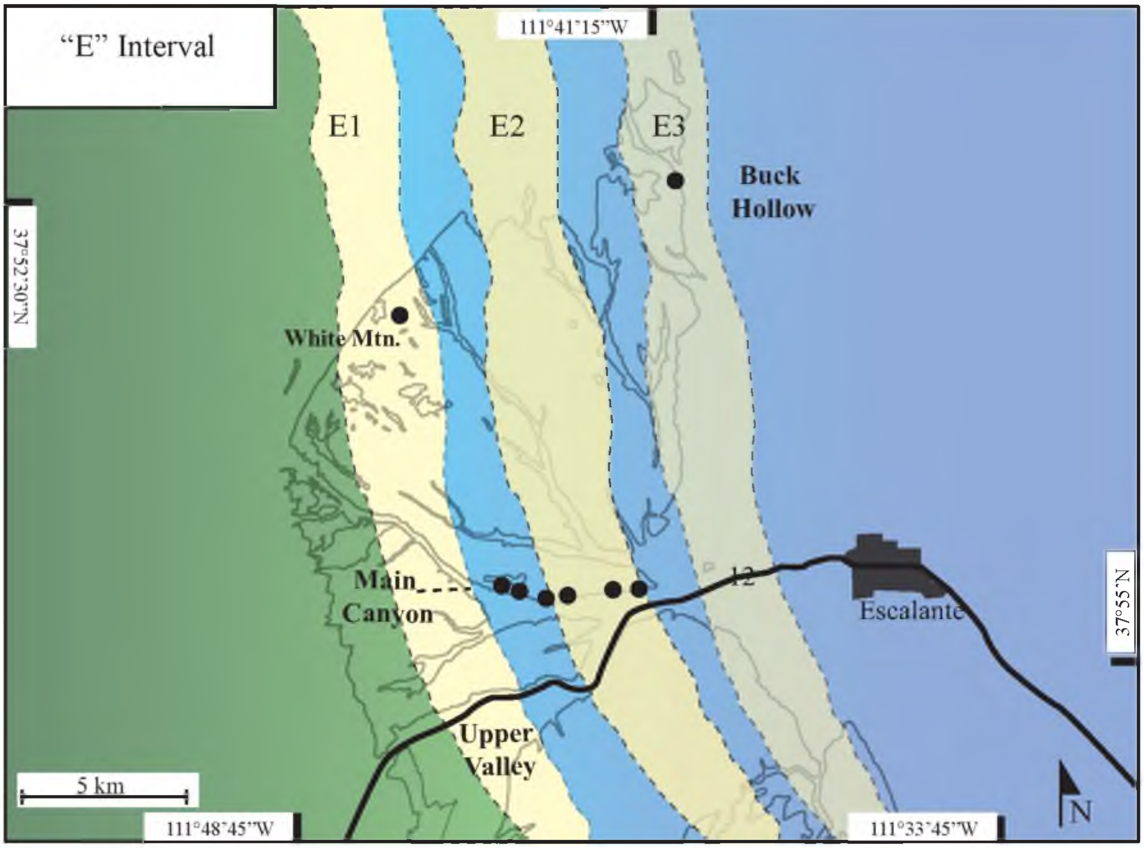

The "E" shoreface is relatively thin at Main Canyon and records progradation of the shoreline to the northeast. Three shoreface parasequences make up the "E" Interval at Buck Hollow. These coarsening upwards packages reflect a prograding wave-dominated shoreline moving from W-E across the North Kaiparowits region.

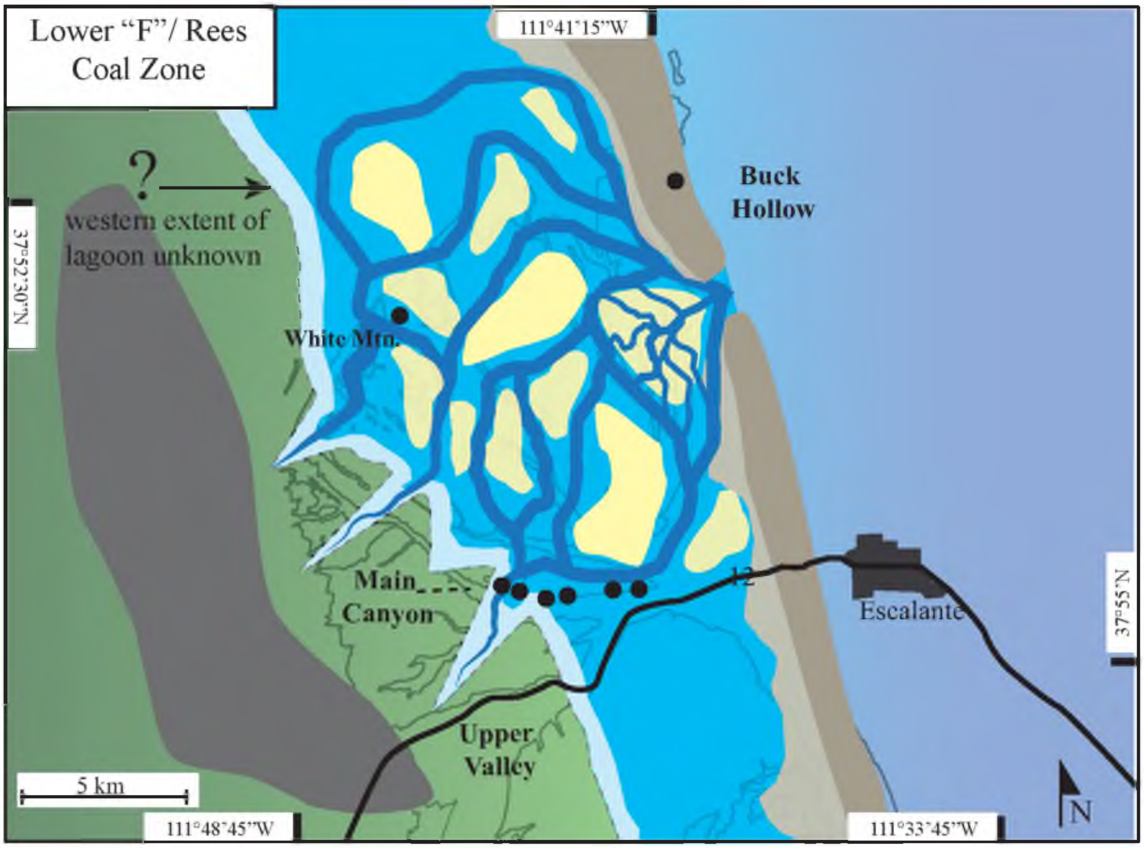

A slight pause and/or rise in relative sea-level results in the development of a sand-rich back-barrier platform. These deposits are preserved as tidal sheets in the eastern portion of Main Canyon and northeast between Buck Hollow and Main Canyon. Tidal channels preserved in the western portion of Main Canyon were likely funnel shaped as a result of decreasing tidal energy in the landward direction. During the earliest "F" interval the system aggrades and a barrier island at or near Buck Hollow shelters a tidal inlet systems. Only small, sporadic shoreface deposits are preserved during this time as subsequent tidal ravinement prevents preservation in this interval.

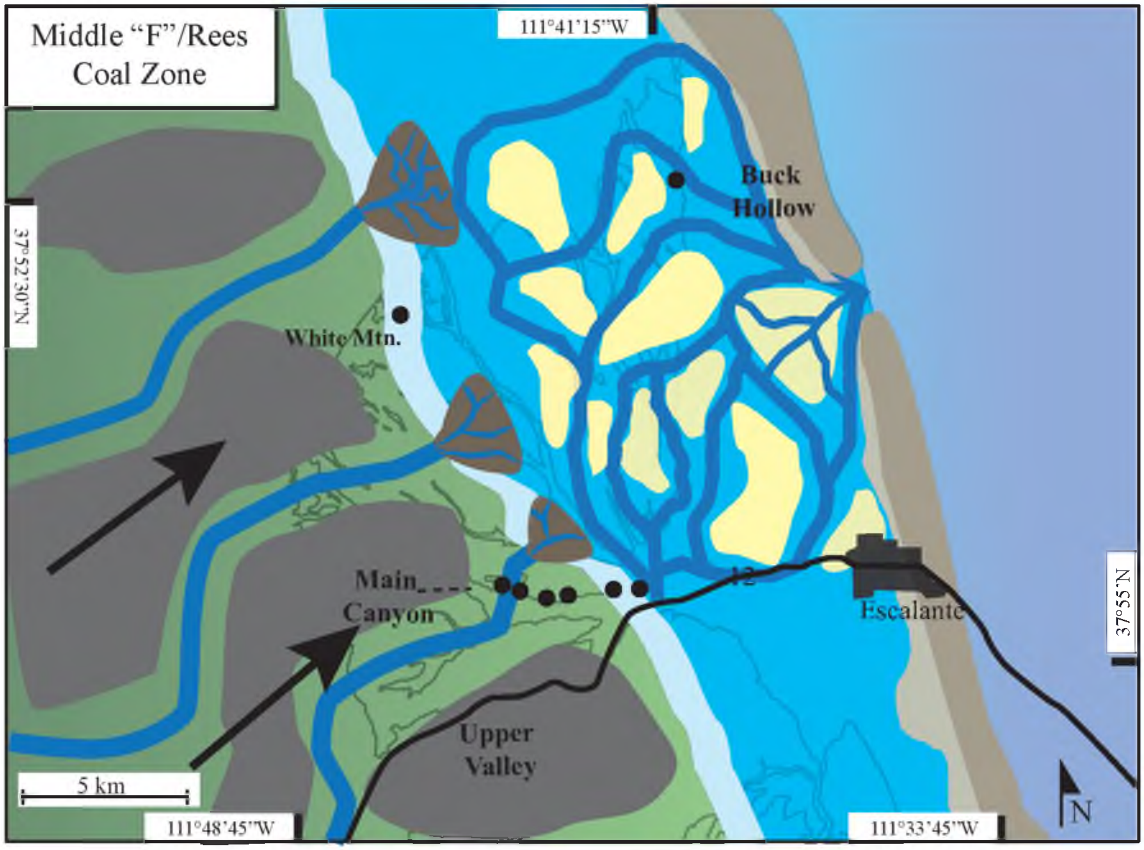

Terrestrial sediments supply front the southwest outpaced available accommodation within the sand-rich back-barrier. Consequently, the coastal plain progrades to the northeast and the lagoon is infilled with distributary mouth bars, bay-head deltas, distributary channels, and coastal plain mudstones and siltstone which record the shoreline turnaround. During the Middle F Interval channelized tidal deposits are dominant in Buck Hollow. Ravinement erodes underlying shoreface deposits and stacked tidal channel deposits are preserved.

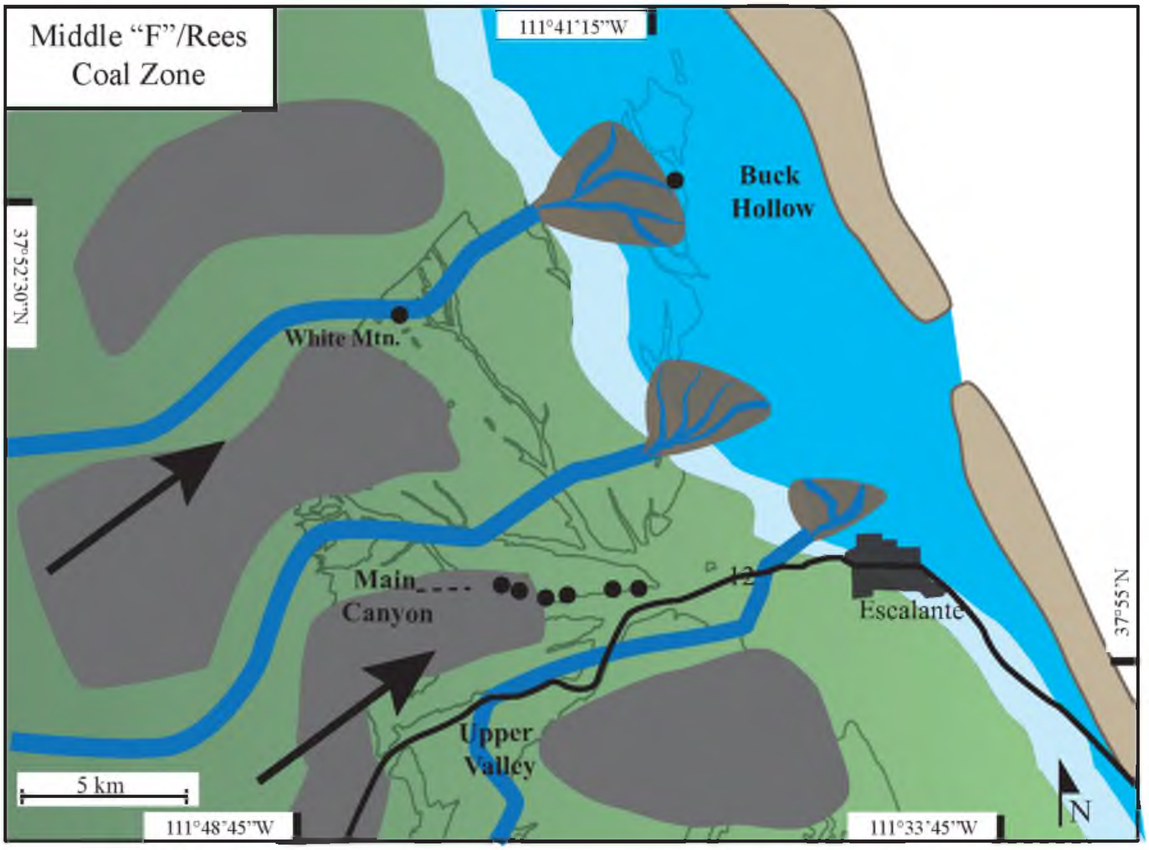

Channel complexes and coastal plain siltstone and mudstones are preserved at Main Canyon and White Mountain as the lagoon is infilled with sediment from the southwest. As the back-barrier system continues to in fill a bayhead delta progrades into Buck Hollow. Isolated sandy bayhead delta deposits and muddier bay fill are preserved.

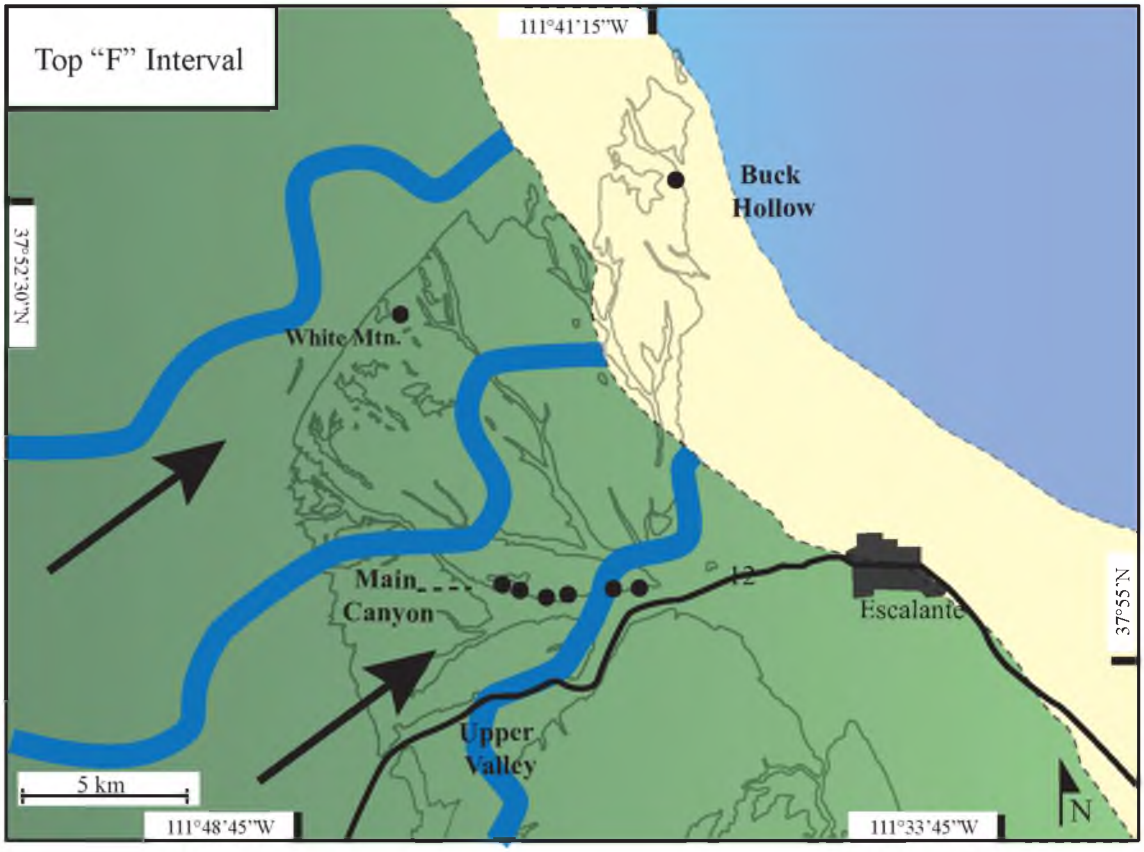

Coastal plain and fluvial facies comprise the John Henry Member at White Mountain. These deposits are no longer preserved at Main Canyon. As the back-barrier system continues to infill a small flooding surface leads to the deposition of a laterally continuous shoreface at Buck Hollow. This fine to medium grained sand interval contains alternating laminated and bioturbated packages.

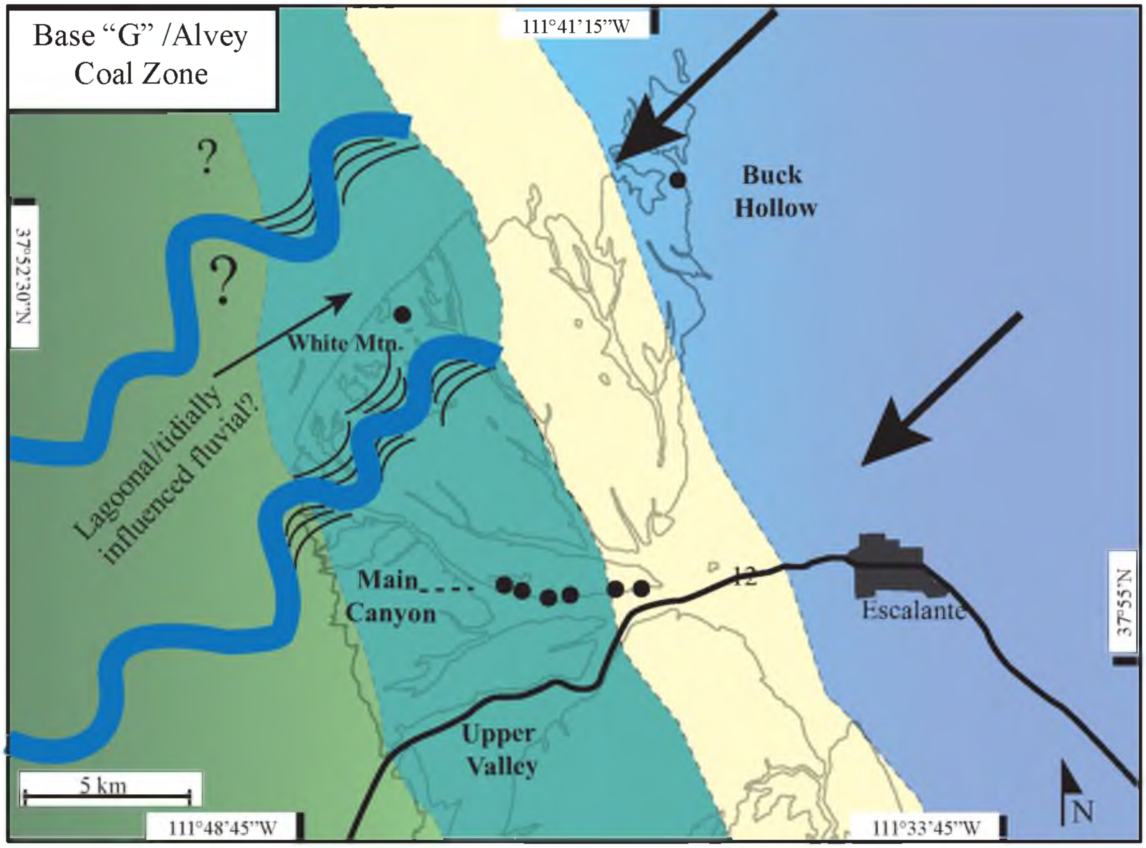

Tidally-influenced sandstones and carbonaceous mudstones are preserved at White Mountain and represent deposition within either tidally influenced fluvial channels and/or back-barrier lagoons with tidal channels. Further research is needed to determine the exact nature of these deposits. A significant flooding surface separates the "F" and the "G" Intervals. The basal part of the "G" at Buck Hollow contains offshore mudstone deposits.

At White Mountain distributary channels become continuously more amalgamated up section. These channels supplied sediment to the "G" shoreline at Buck Hollow. During the upper part of the "G" interval wave-dominated shoreface deposits range from distal lower shoreface to upper shoreface, beach, and fluvial deposits.

APPENDIX B

MEASURED SECTIONS

Nine measured sections are provided in Appendix B. GPS locations for the base of each section are provided in Table 4 The location of the six sections measured through Main Canyon and the section collected near White Mountain are shown on Figure 3. Two detailed sections of tidal and estuarine deposits of R-T cycle illustrate the differences between the western and eastern parts of Main Canyon within this interval.

Table 4

GPS locations for measured sections

Section ID	Latitude	Longitude	Elevation (m)
MC-MS-1	37.767978°	-111.739674°	2091
MC-MS-2	37.767729°	-111.692312°	1918
MC-MS-3	37.765201°	-111.725160°	1990
MC-MS-4	37.765137°	-111.716385°	1905
MC-MS-5	37.766890°	-111.698189°	1930
MC-MS-6	37.767490°	-111.736690°	2104
Flood-Tidal Delta	37.767339°	-111.698691°	1988
Estuarine Bars	37.767030°	-111.726380°	2078

Legend of Stratigraphic Symbols

- *Ophiomorpha*
- 2-D symmetrical ripples
- shell fragments
- sigmoidal bedding
- ripple laminated
- interference ripples
- climbing ripples
- shell lag
- trough cross bedding
- swaley cross bedding
- hummocky cross bedding
- tabular cross bedding
- gently inclined laminations
- planar bedding
- biotrubation
- herringbone
- wavy, lenticular, flaser
- convolute beds
- clay rip-ups
- organic drapes
- barform accretion sets
- *Teredolites*

clay cs coal s vfs fs ms cs vcs g p b

cs = carbonaceous shale
s = siltstone
vfs= very fine grained sandstone
fs = fine grained sandstone
ms = medium grained sandstone
cs = coarse grained sandstone
vcs = very coarse grained sandstone
g = granule
p = pebble
b = boulder

- mudstone
- interbedded sand/silt/mud
- sandstone
- conglomerate

coal	esturaine
fluvial	tidal
coastal plain	lagoon/ bay fill
shoreface	offshore/ DLSF

- *Thalassinoides*
- pebble lag
- inoceramid
- oysters/bivales
- root traces
- wood fragments
- leaf fragments
- coaly clasts
- shale clasts with preserved bedding
- skattered pebbles

Schaubcylindrichnus

reactivation surfaces

MC-MS-1

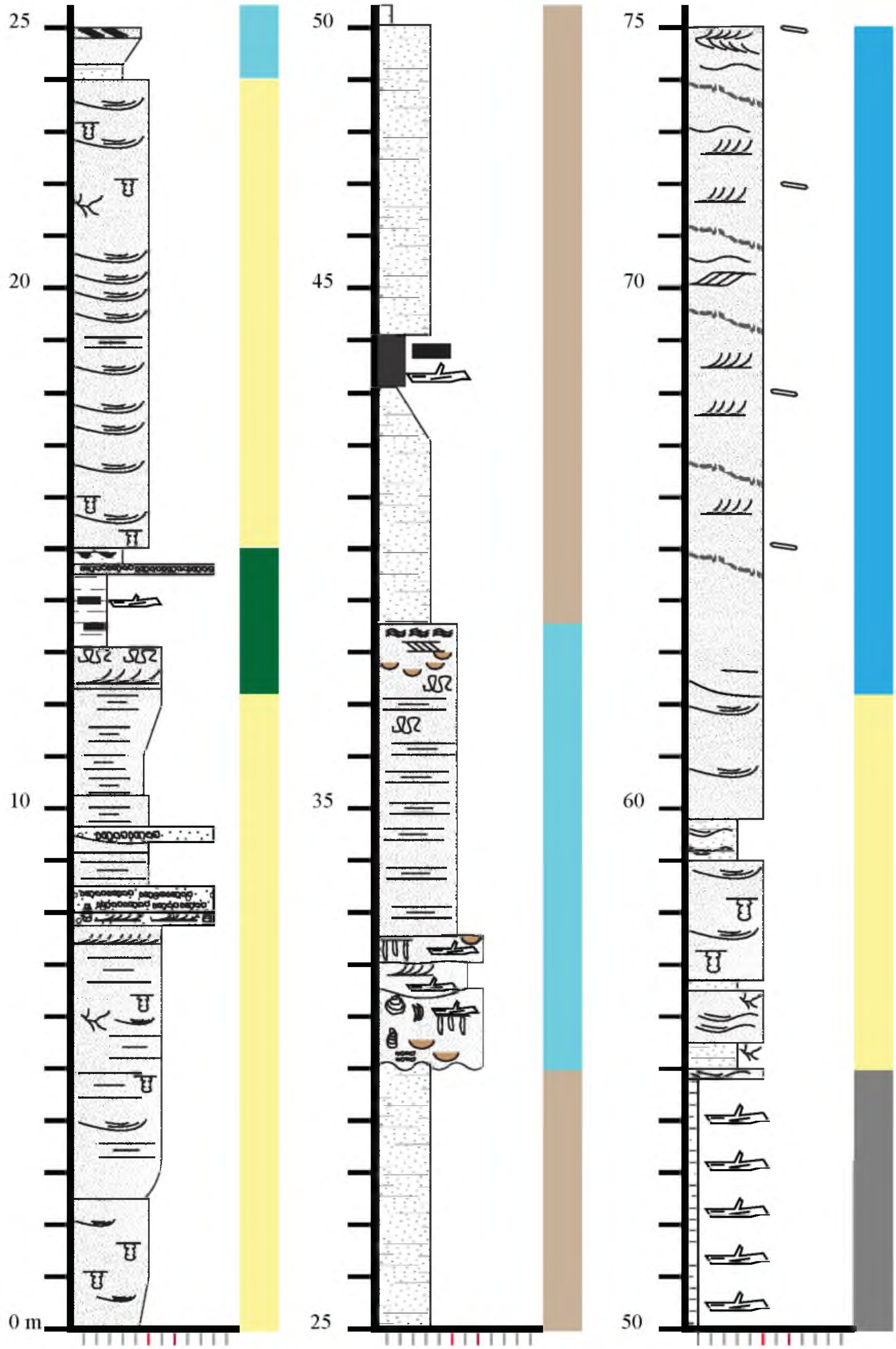

MC-MS-1

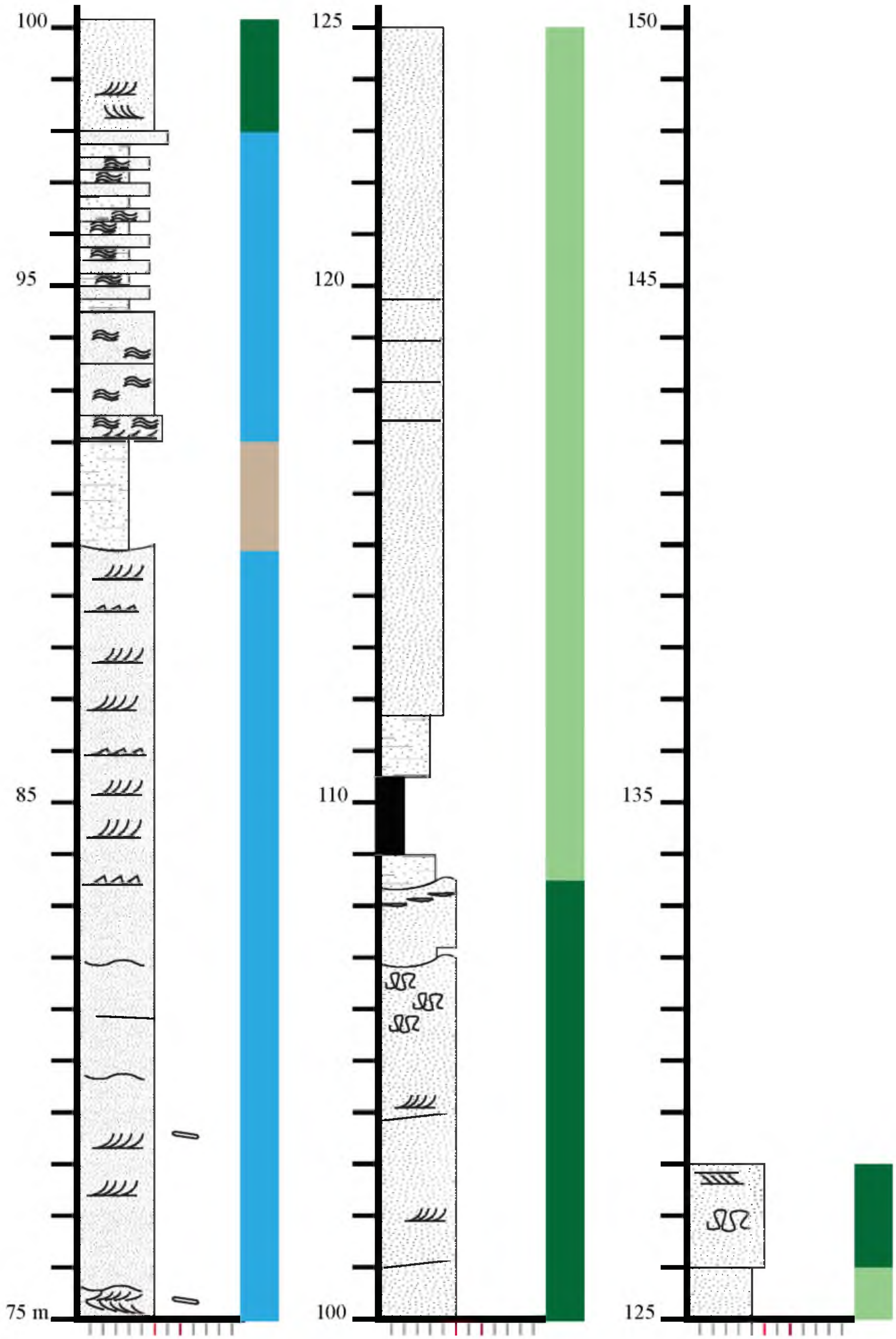

MC-MS-2

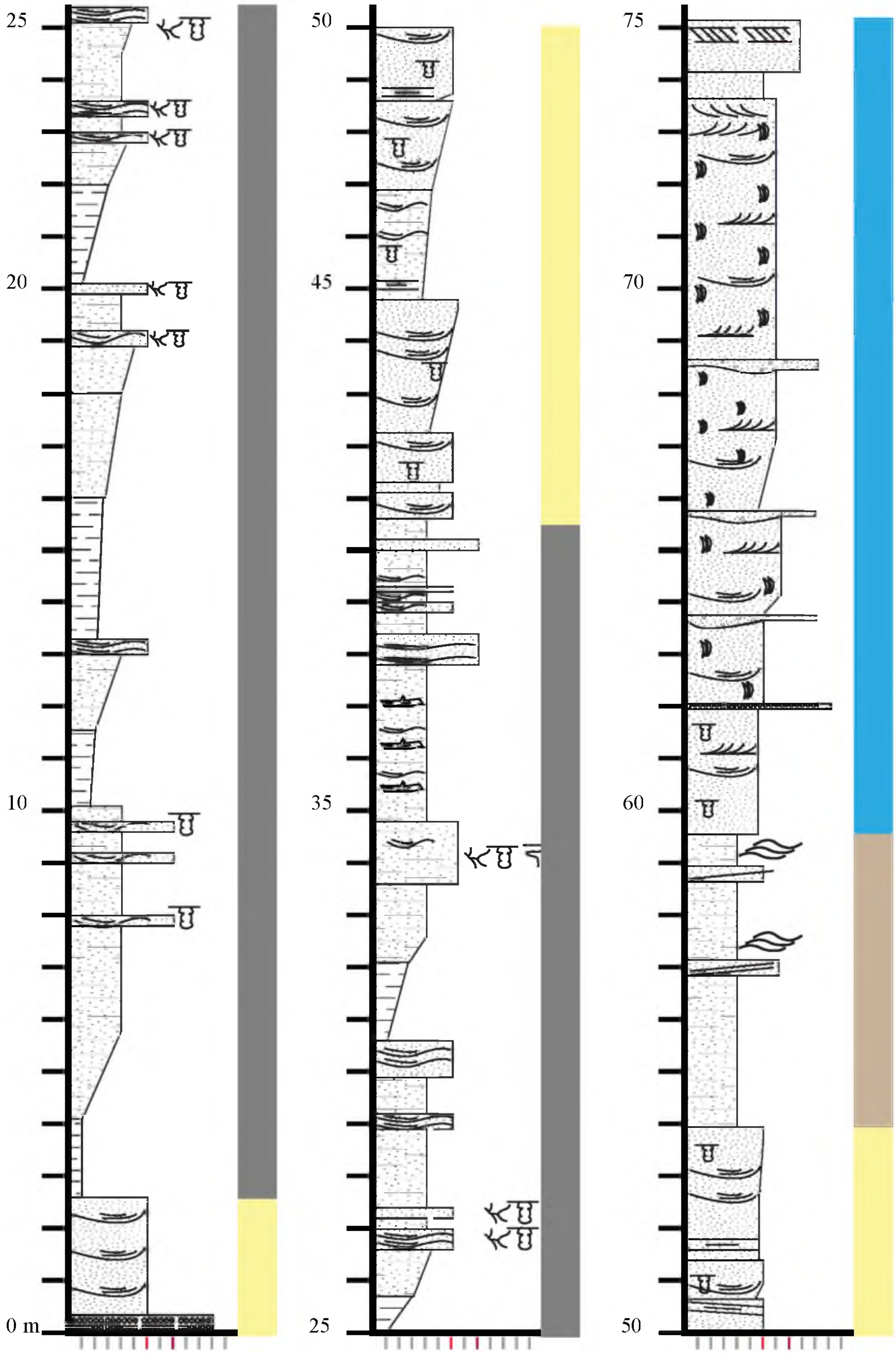

MC-MS-2

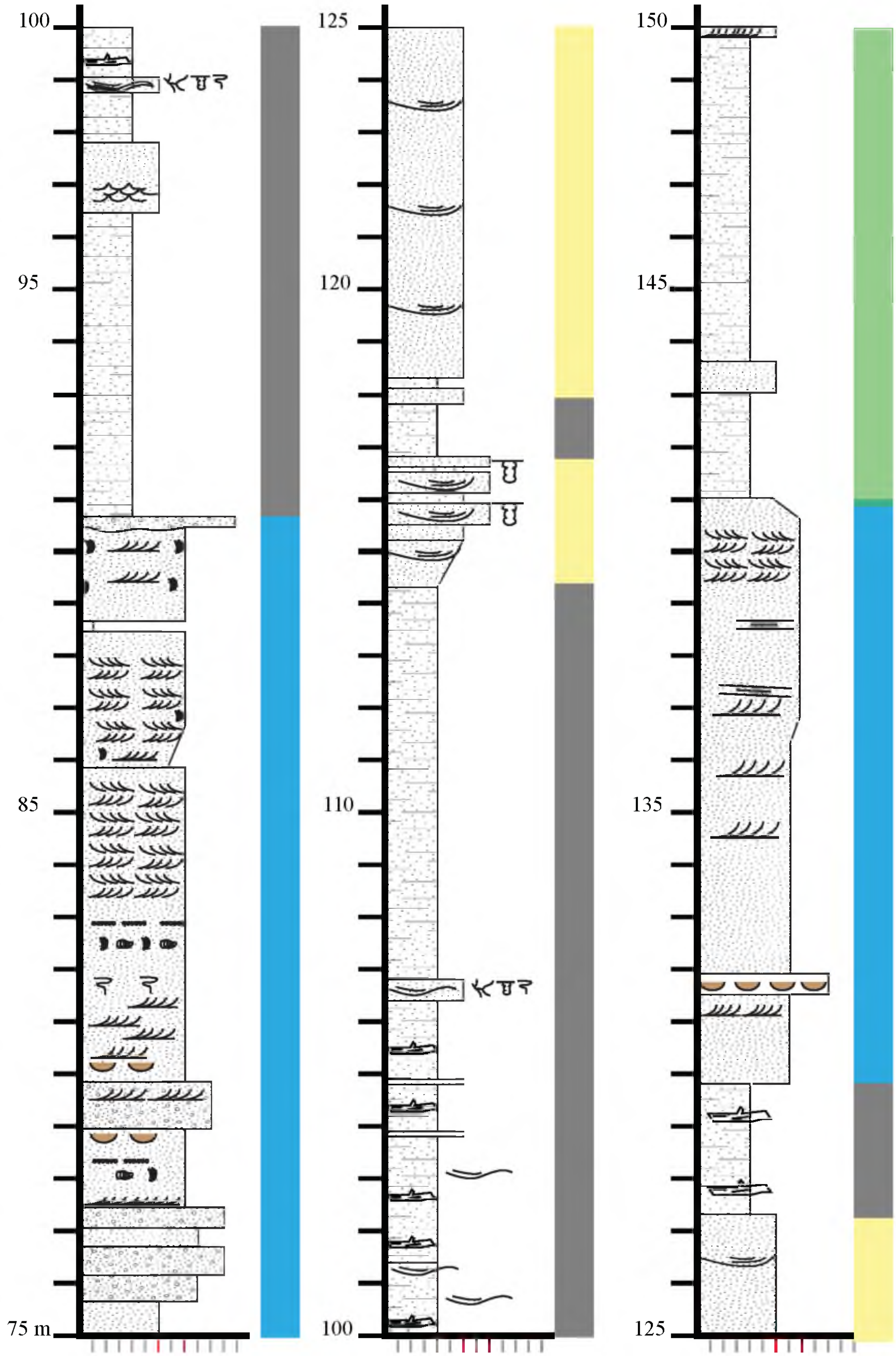

MC-MS-2

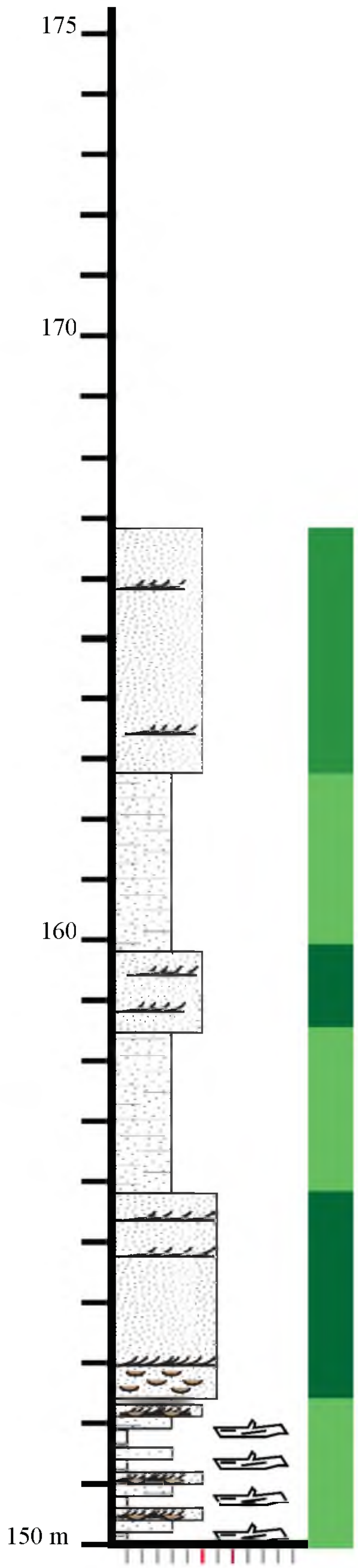

MC-MS-3

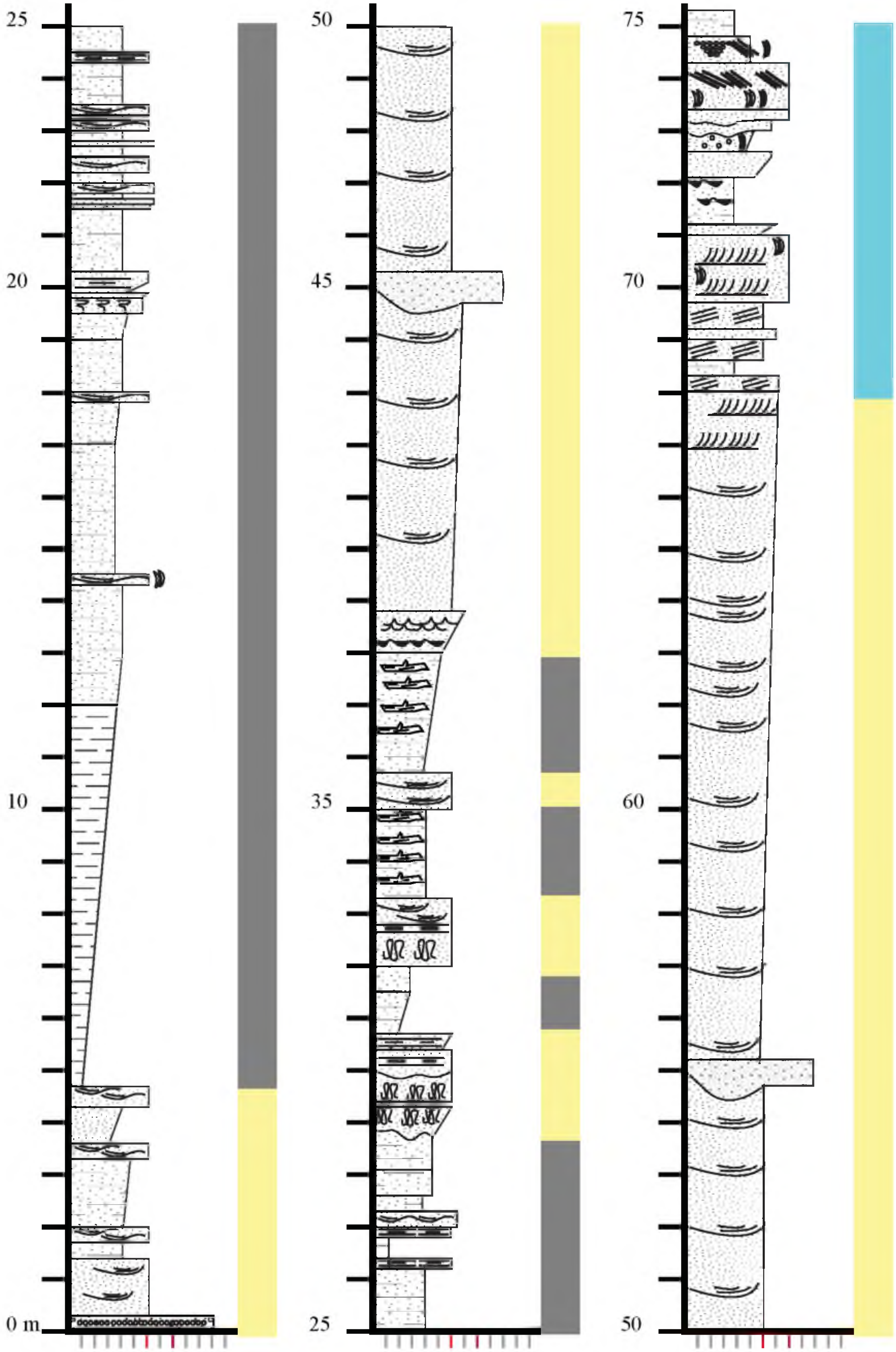

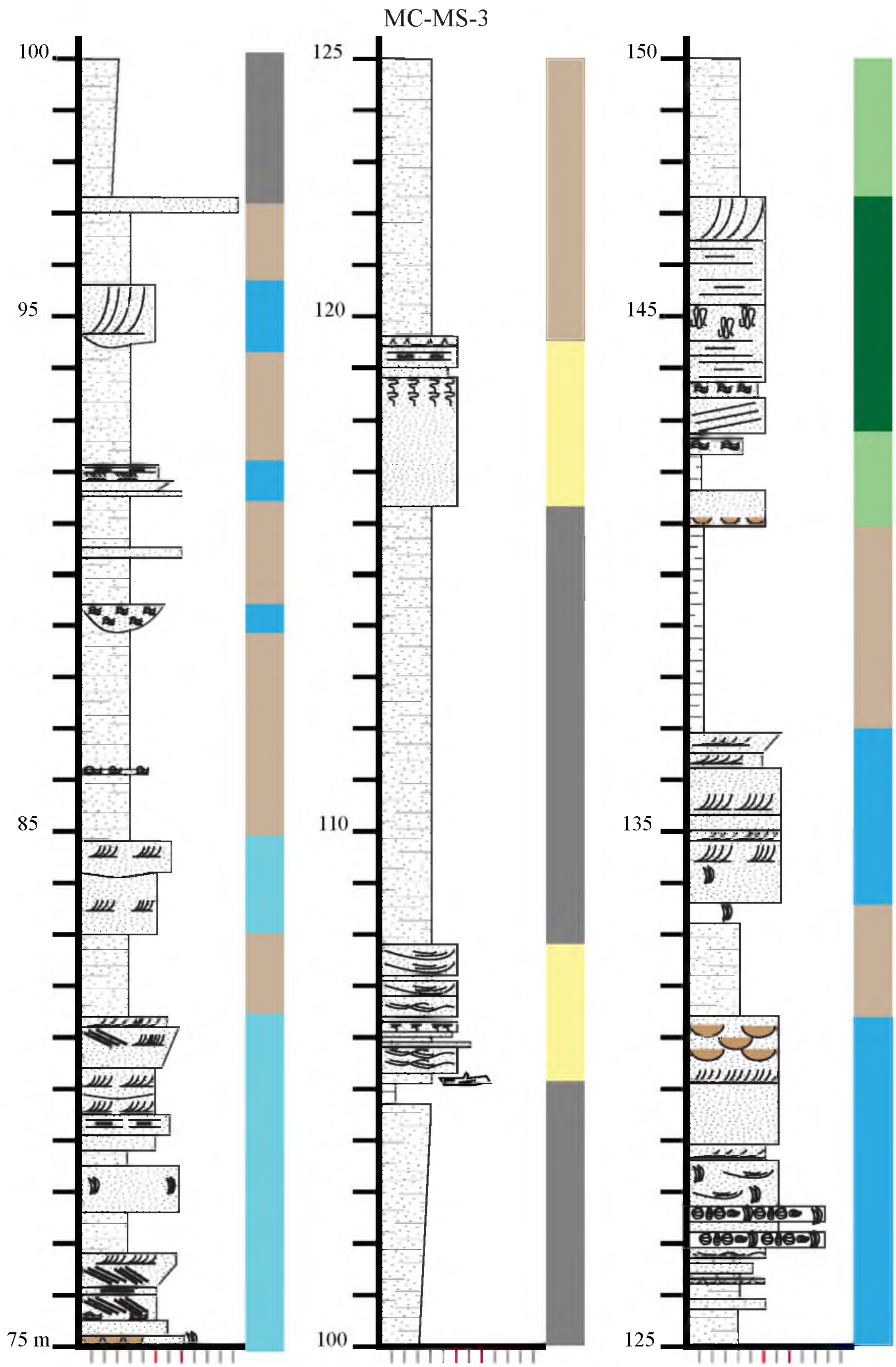
MC-MS-3
100
95
85
75 m
125
120
110
100
150
145
135
125

MC-MS-3

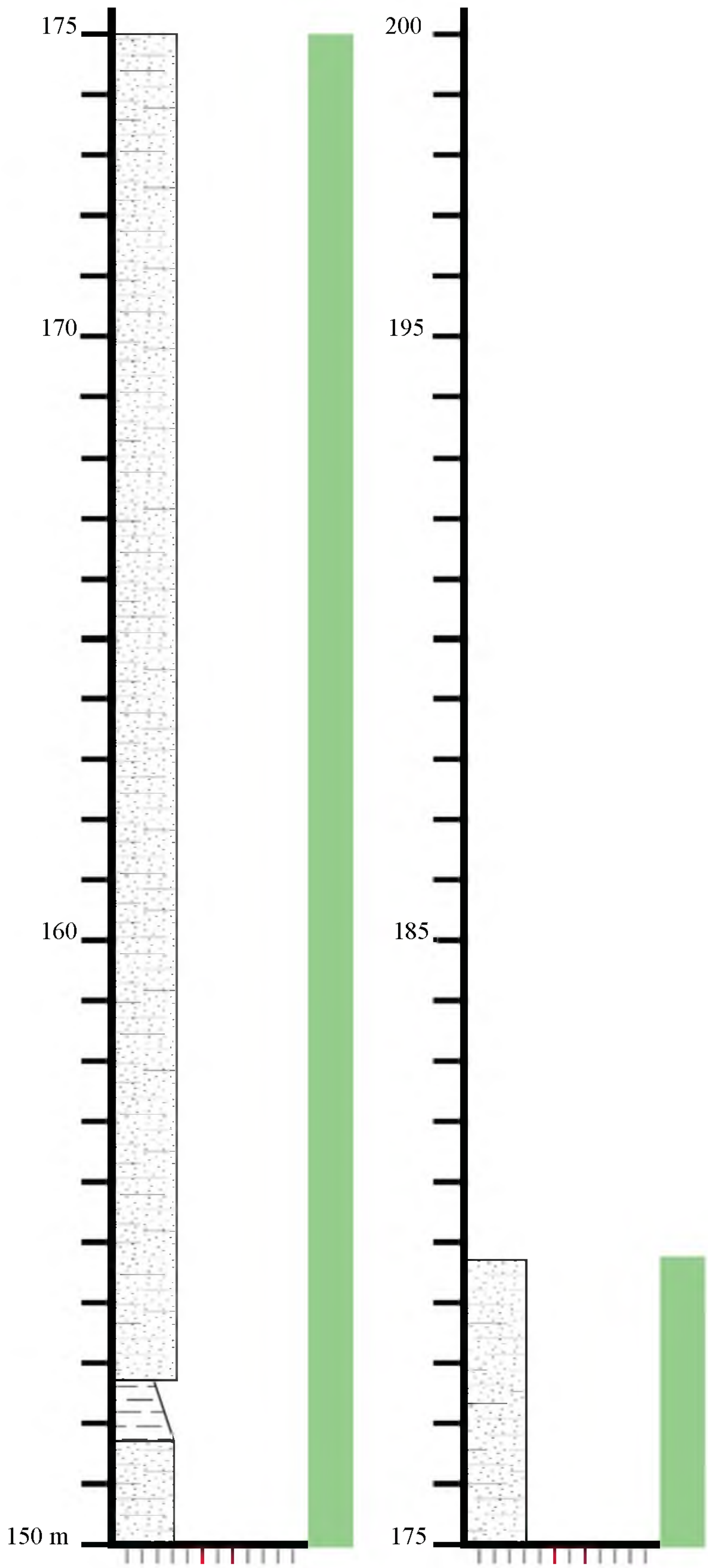

MC-MS-4

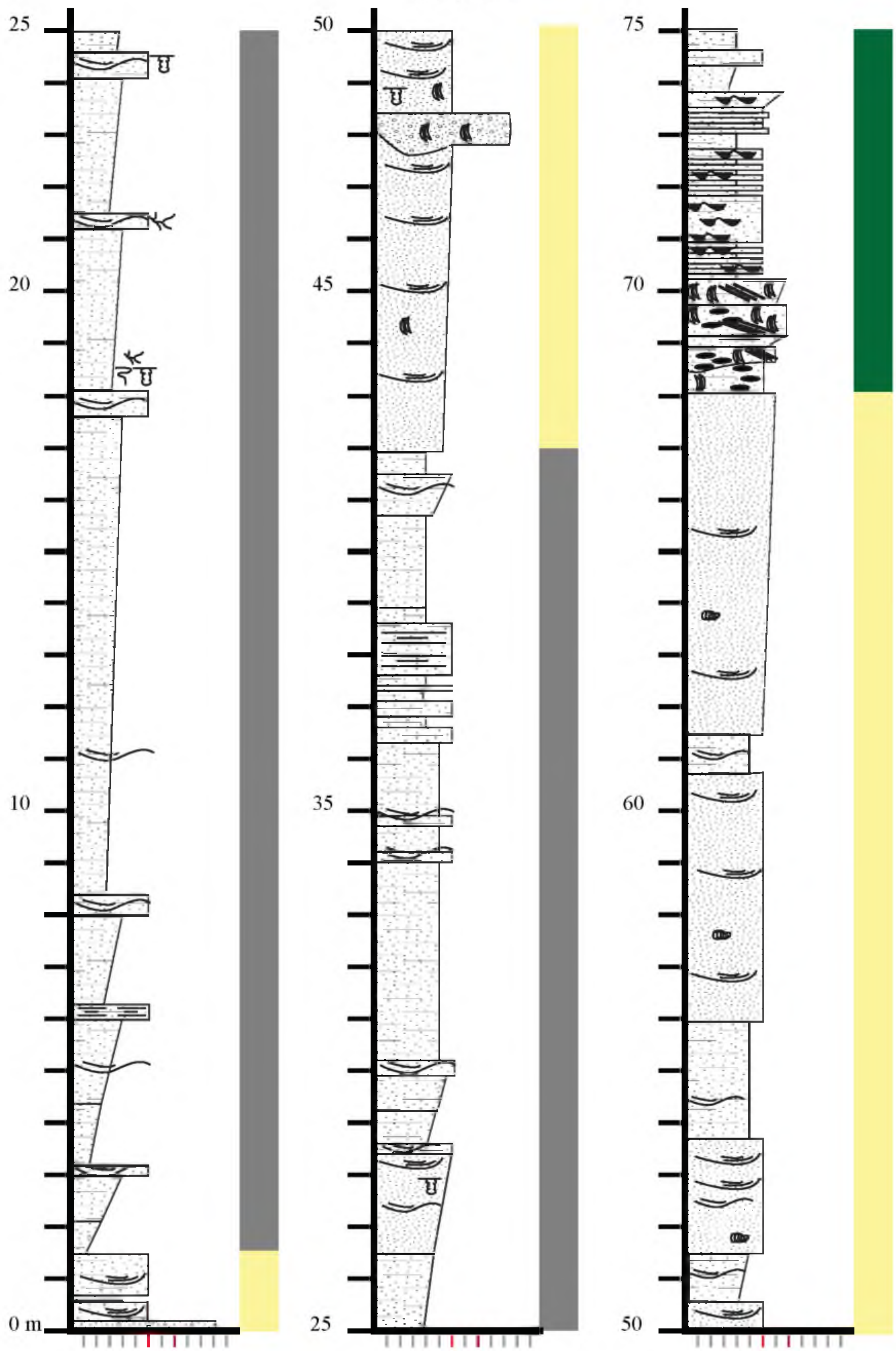

MC-MS-4

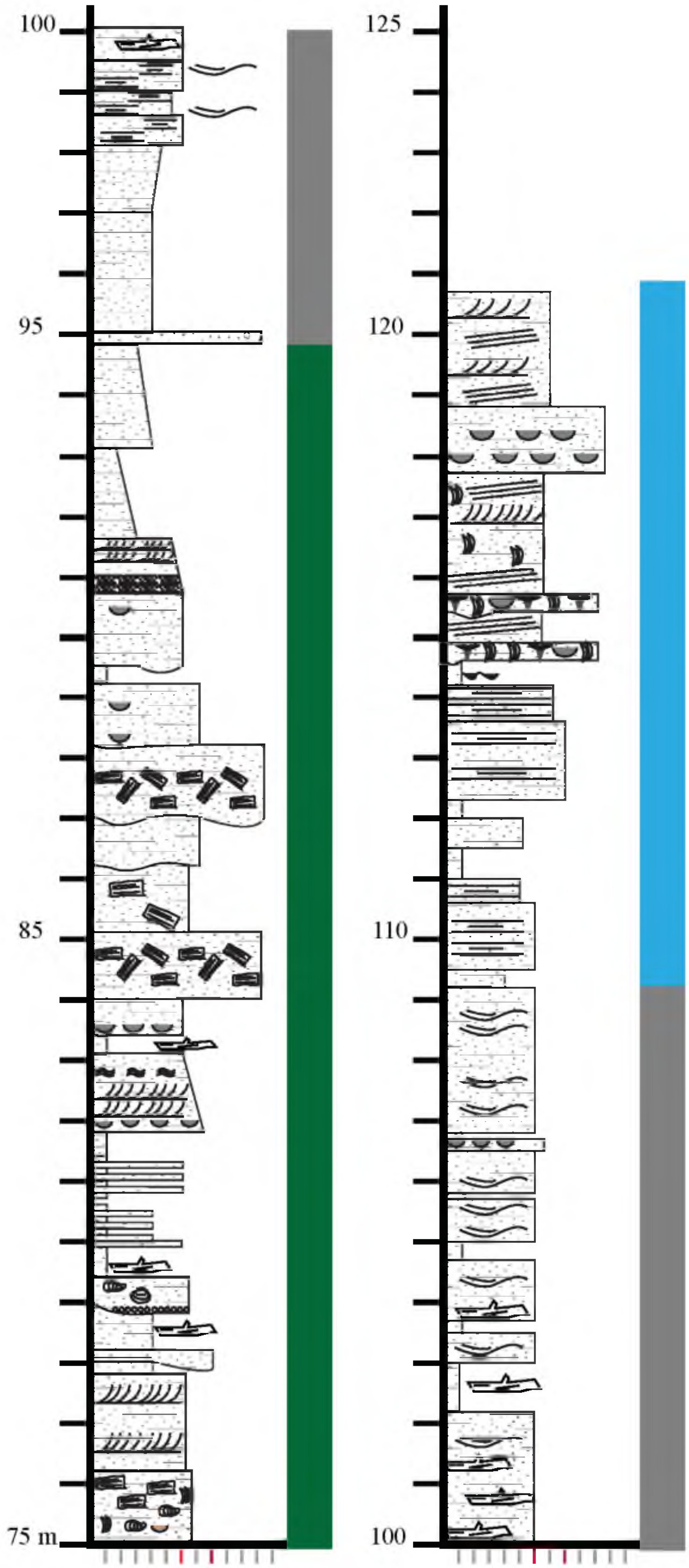

MC-MS-5

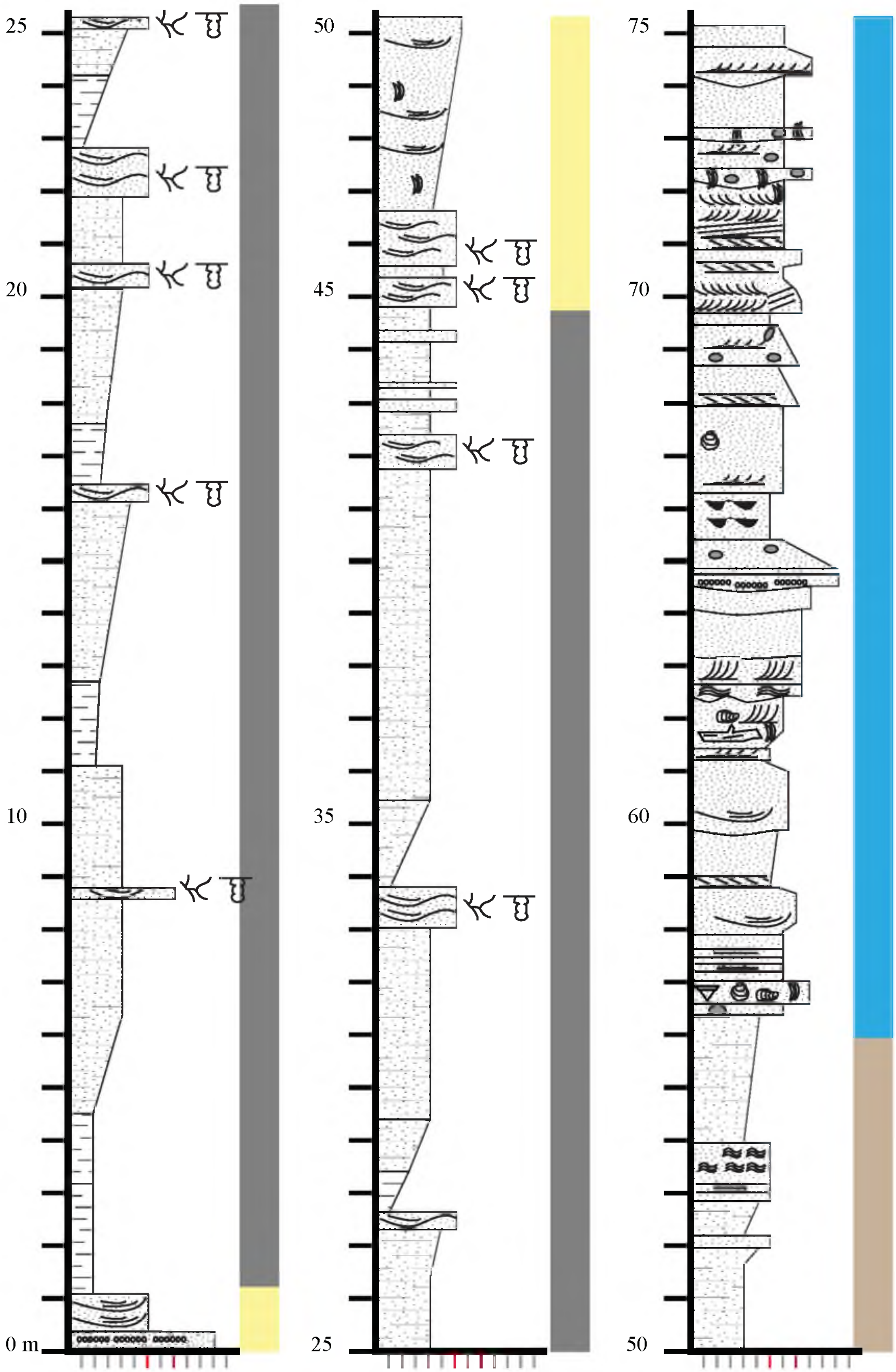

MC-MS-5

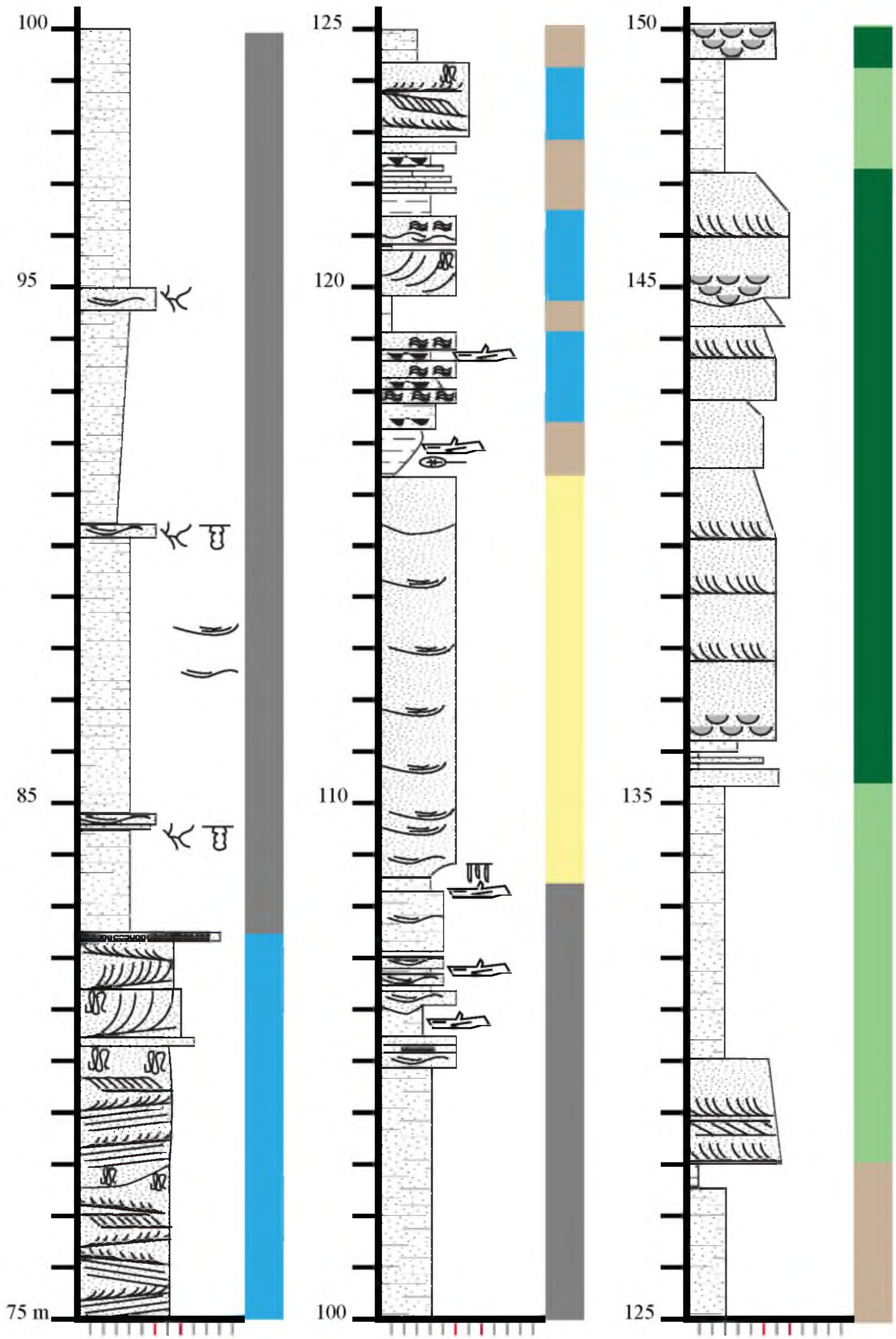

MC-MS-5

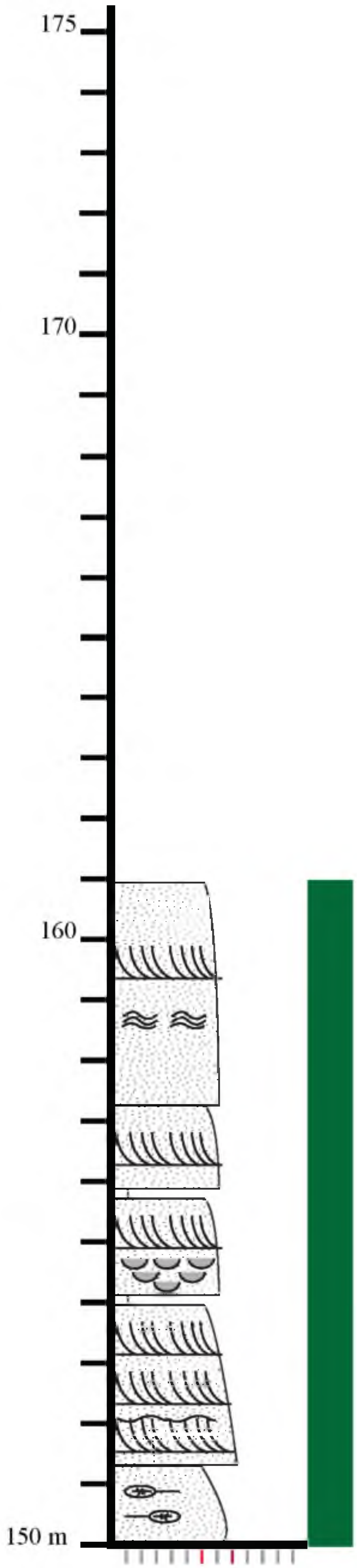

MC -MS - 6

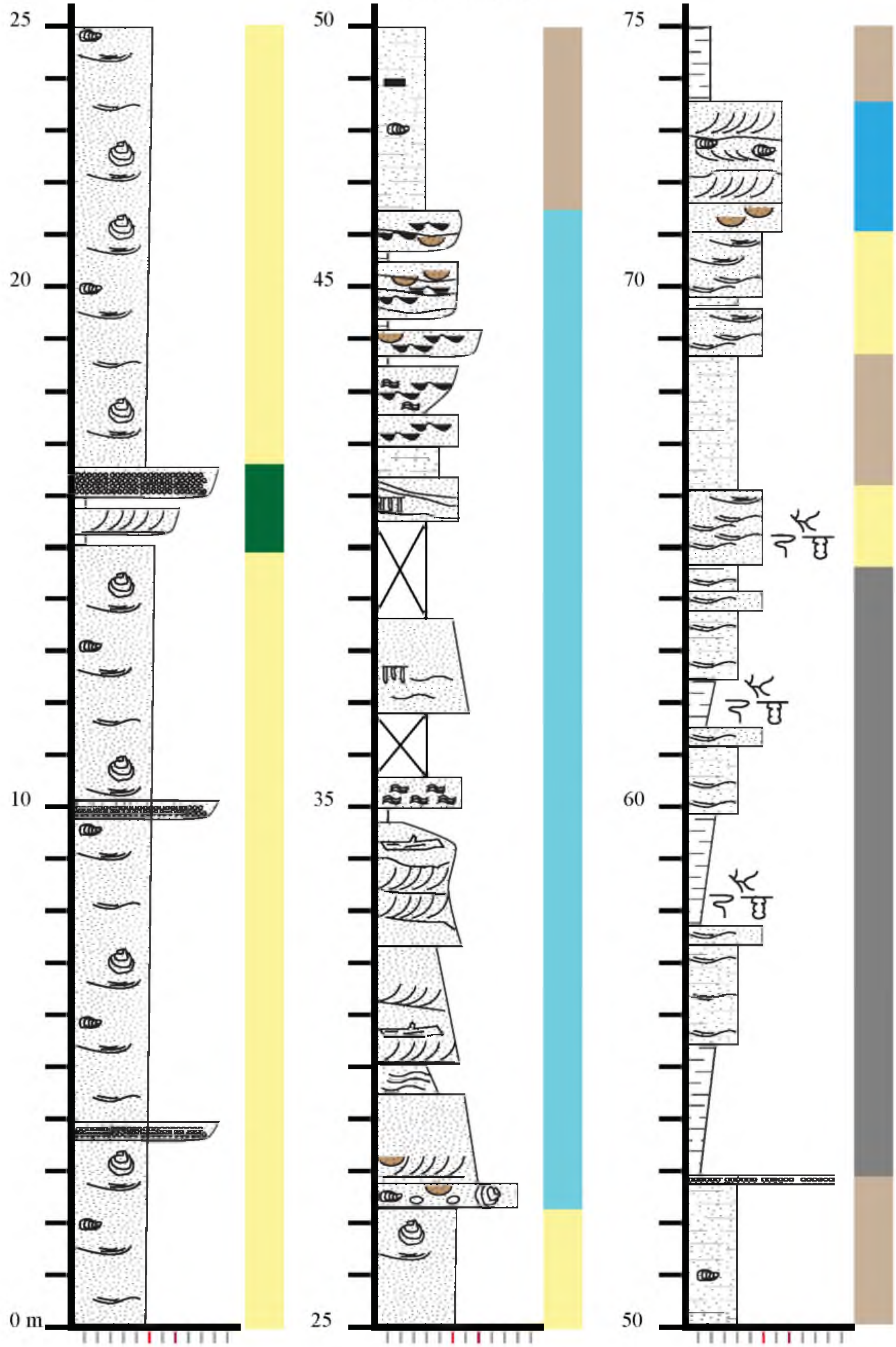

MC -MS - 6

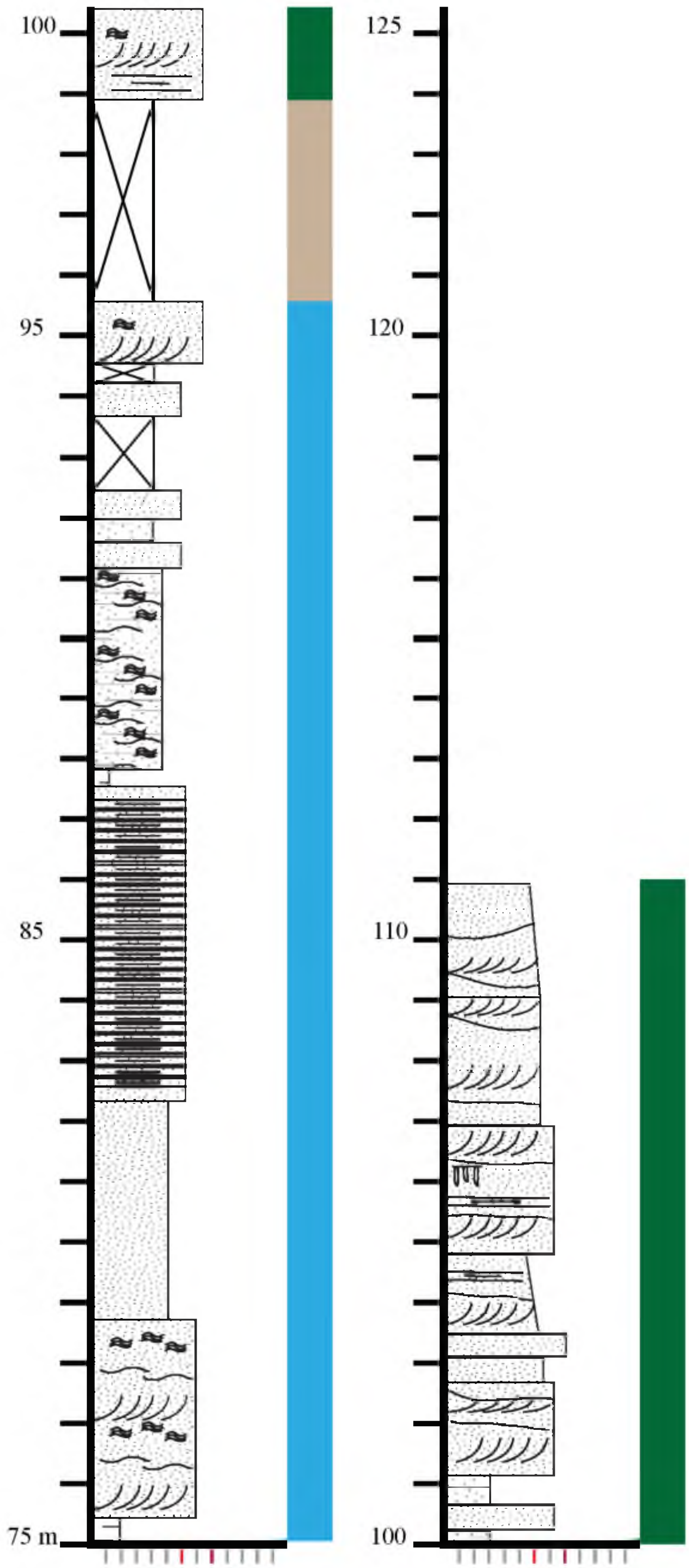

MS -7 - White Mountain

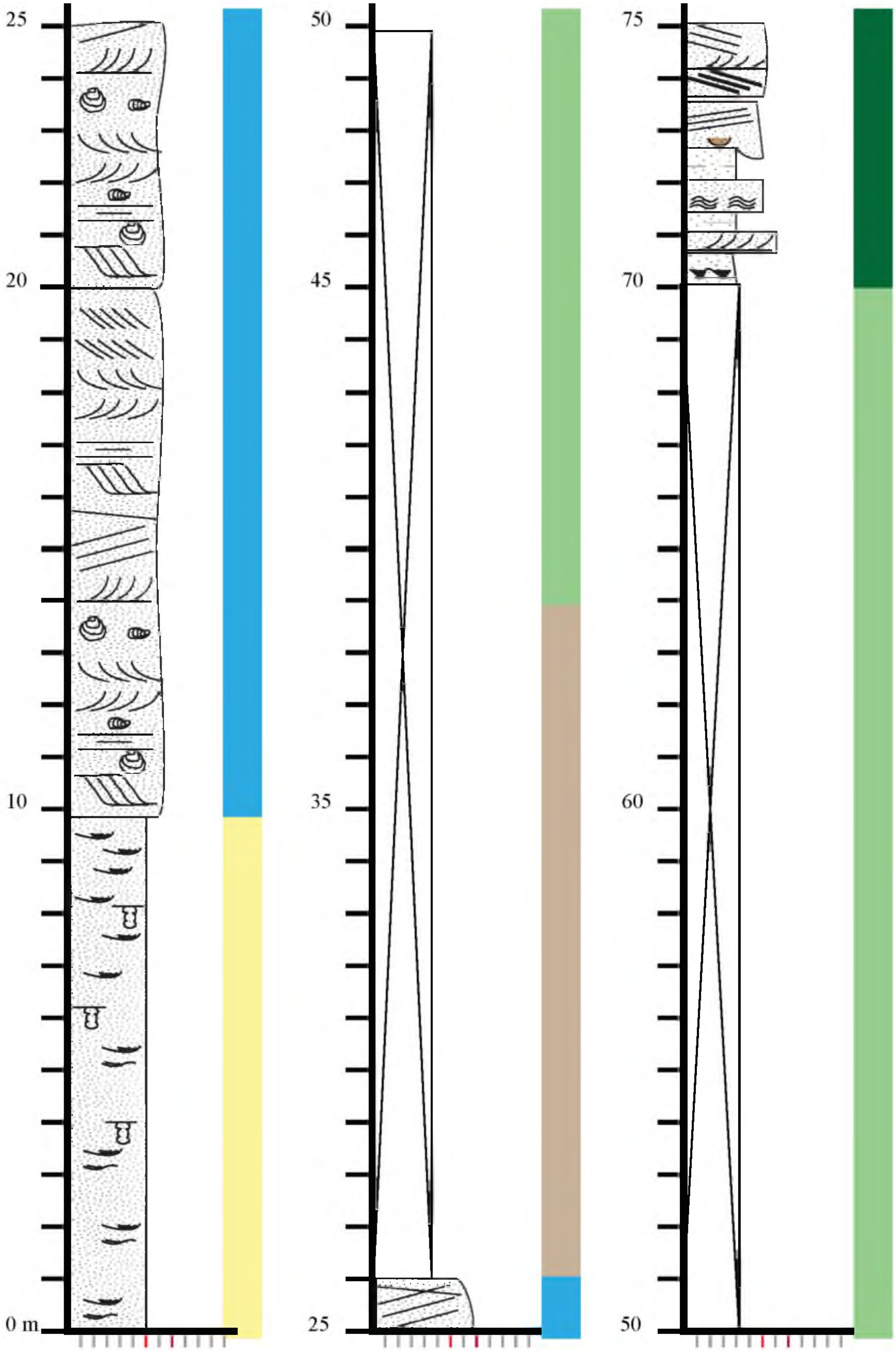

MS -7 - White Mountain

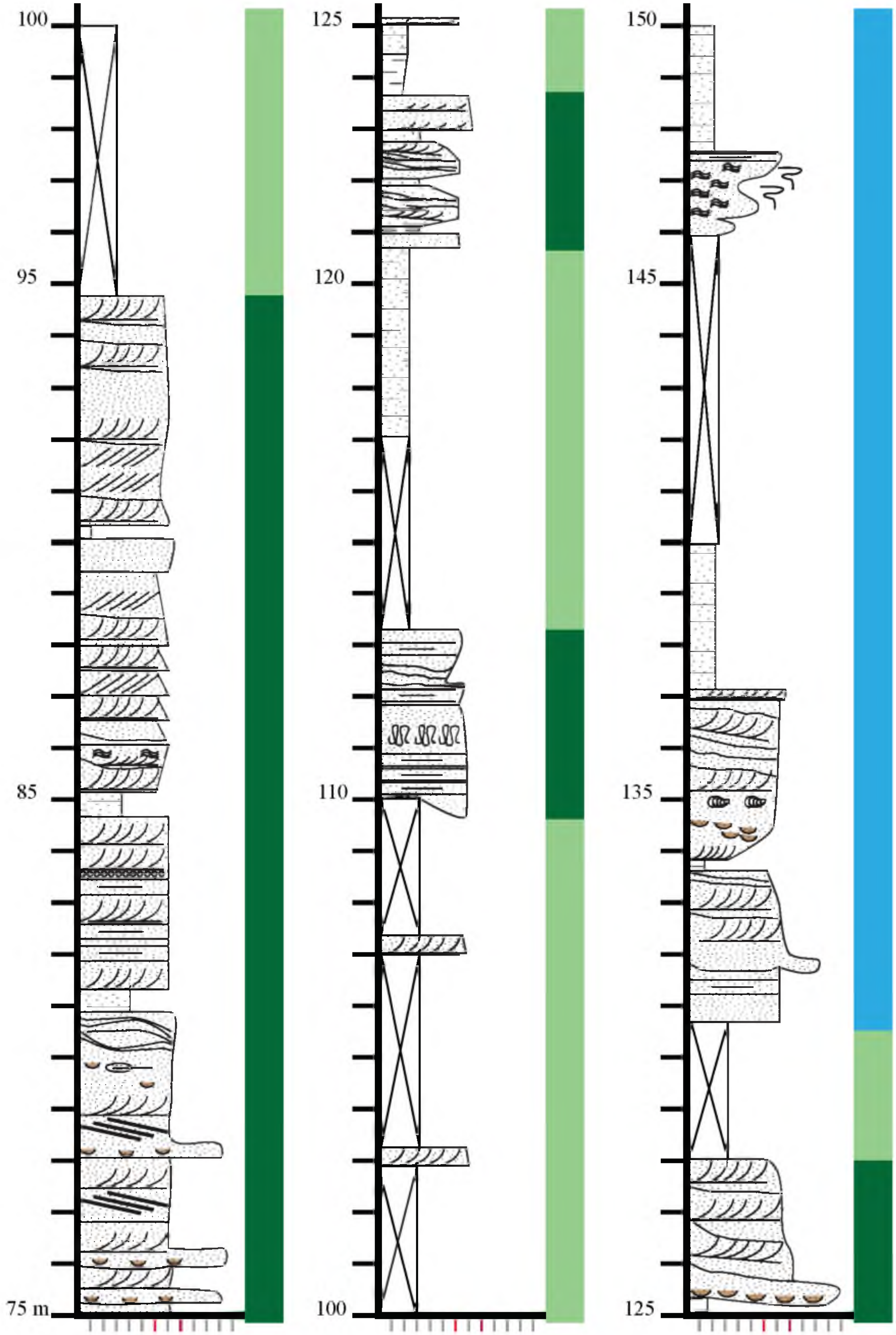

MS -7 - White Mountain

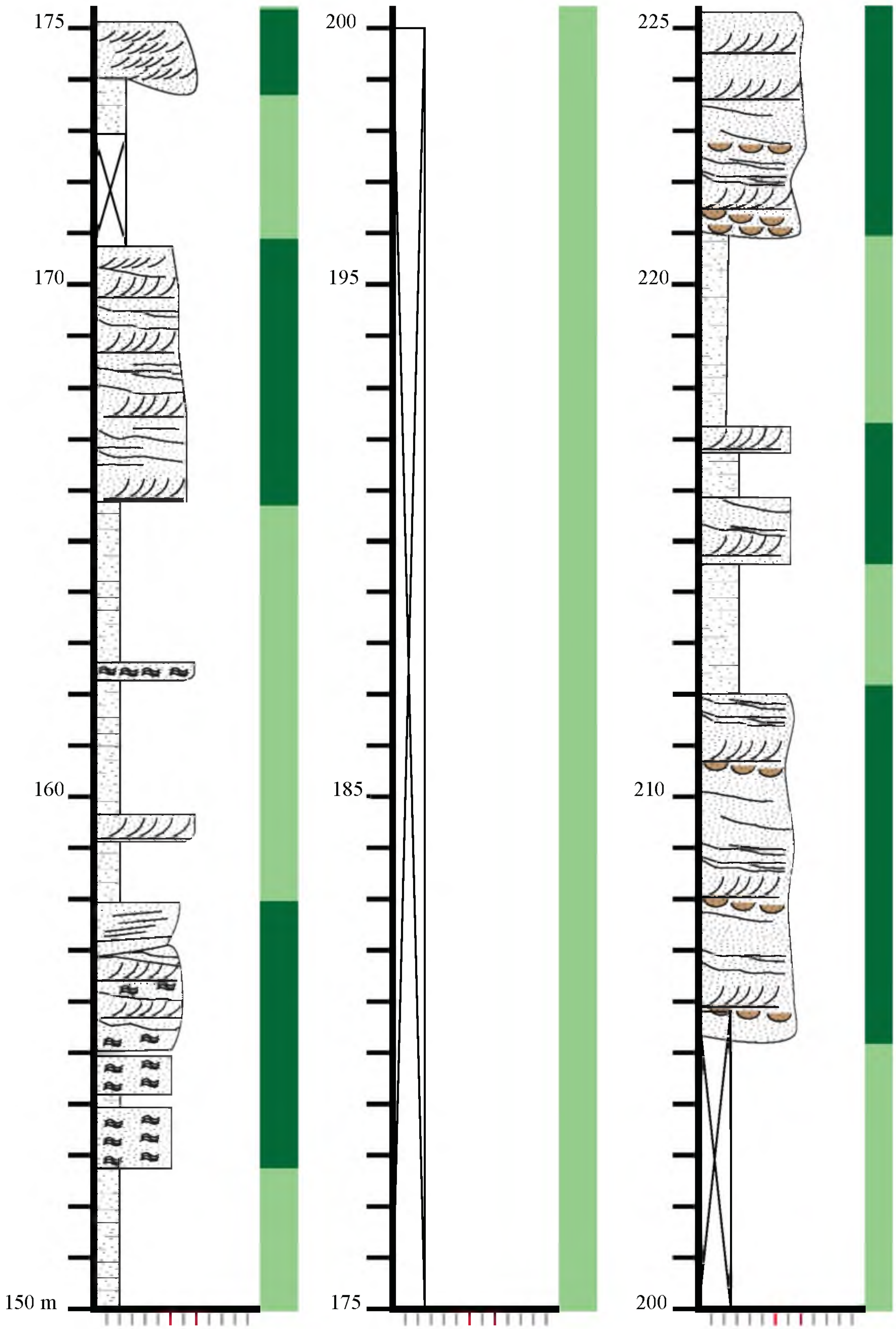

MS -7 - White Mountain

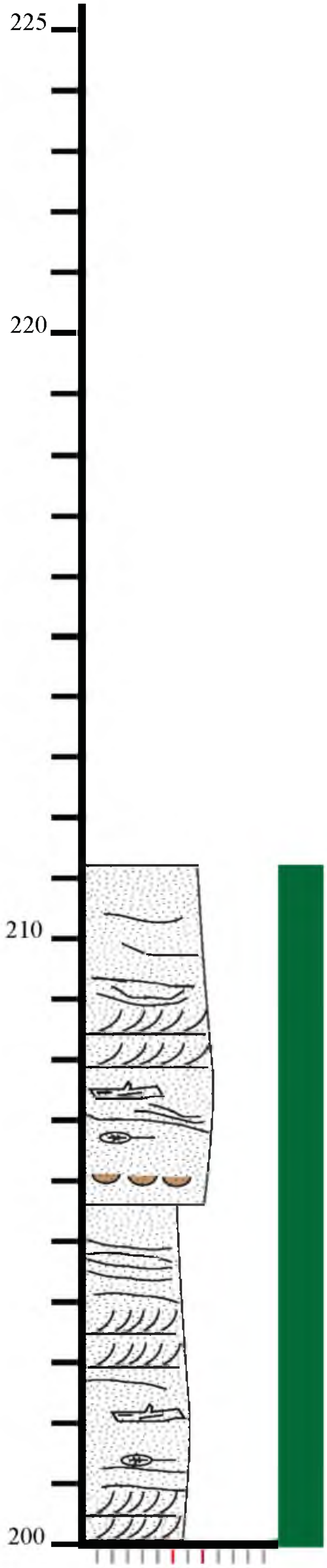

Flood-Tidal Delta (Tidal Gulch)

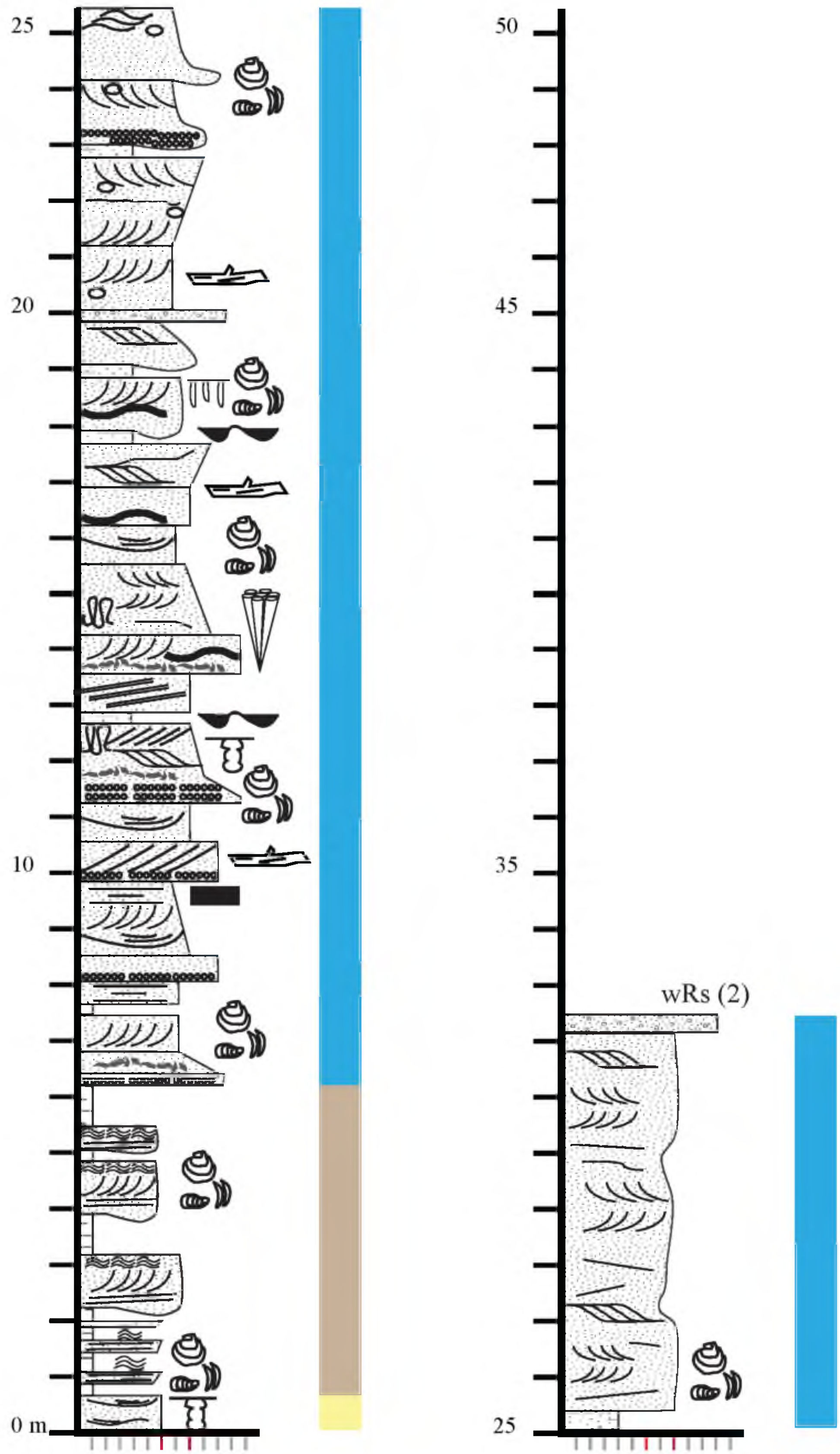

Estuarine Tidal (Sunman Canyon)

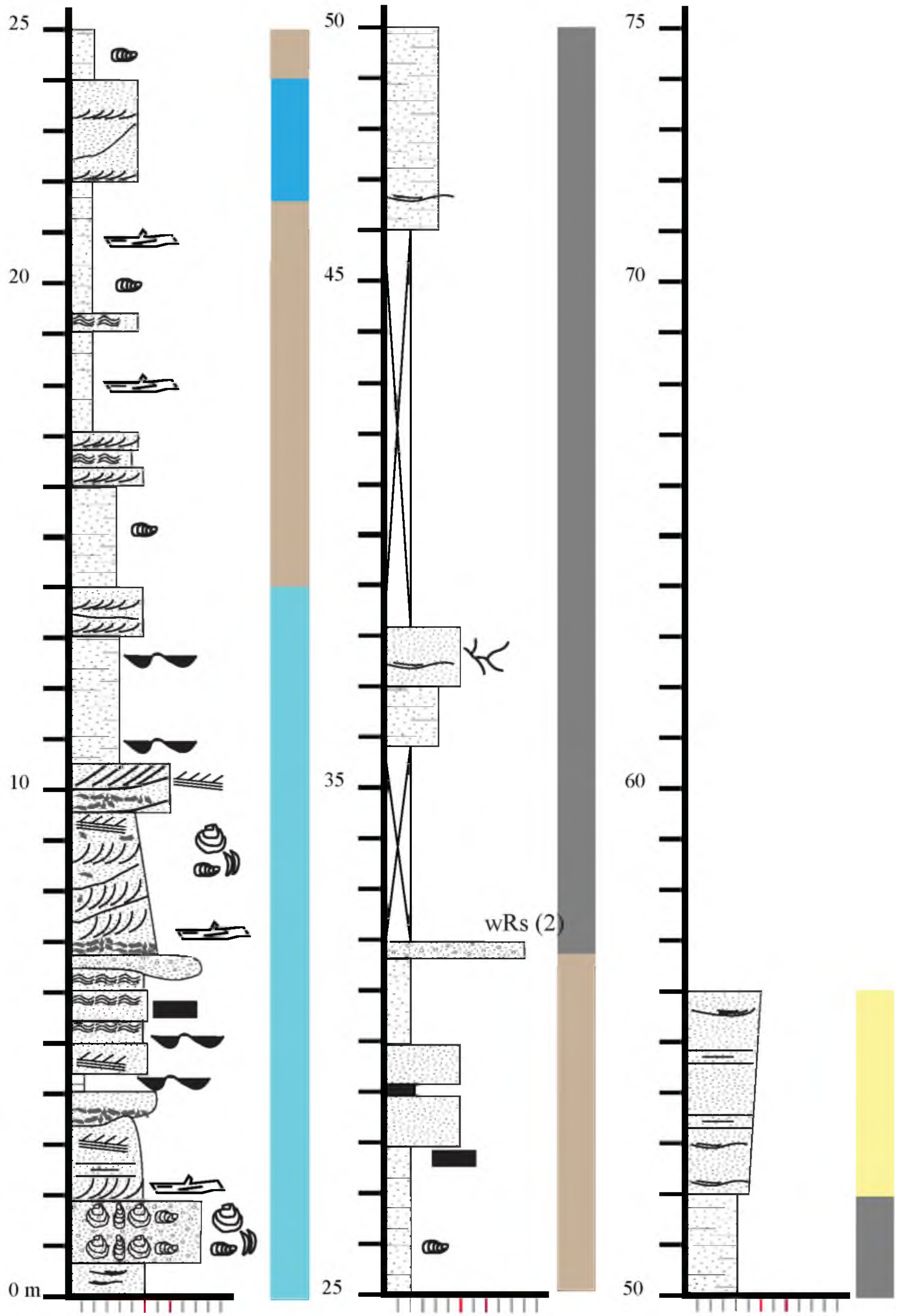

APPENDIX C

DIFFERENTIAL GPS DATA

Bounding surfaces were mapped using a differential GPS paired with a laser range finder. Data are presented in Table 5. All units are referenced to: MENTOR:UTM83-12:NAD83 UTM, Zone 12 North, Meter. Surface abbreviations are as follows: wRs (1)-wave ravinement surface that overlies the Calico Bed or estuarine tidal deposits of the Calico Sequence, marks the base of the John Henry Member; Top “A”-flooding surface separating the “A” and “B” shoreface; LJHMSB- lower John Henry Member sequence boundary, truncates the “B” shoreface throughout Main Canyon; wRs (2)- regional surface that truncates tidal and estuarine deposits of R-T cycle 1 throughout Main Canyon, marks base of “E” shoreface; Top CB- top of the Calico Bed.

Evidence for Syntectonic Sedimentation

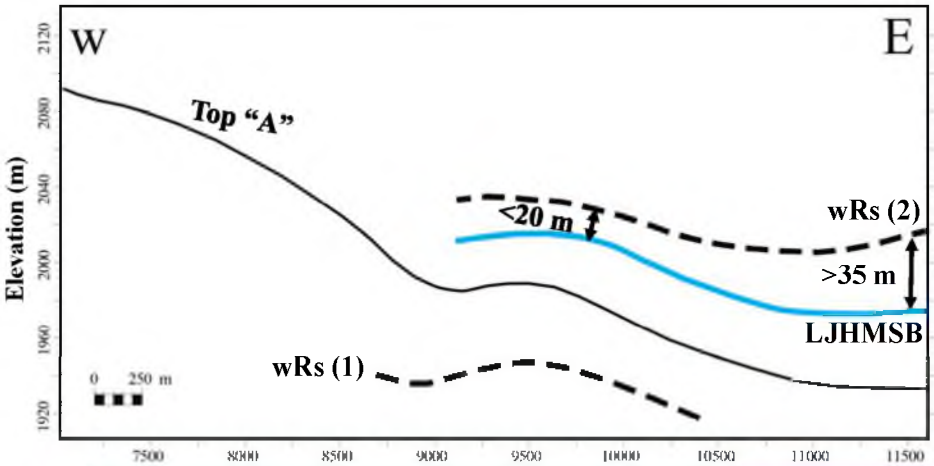

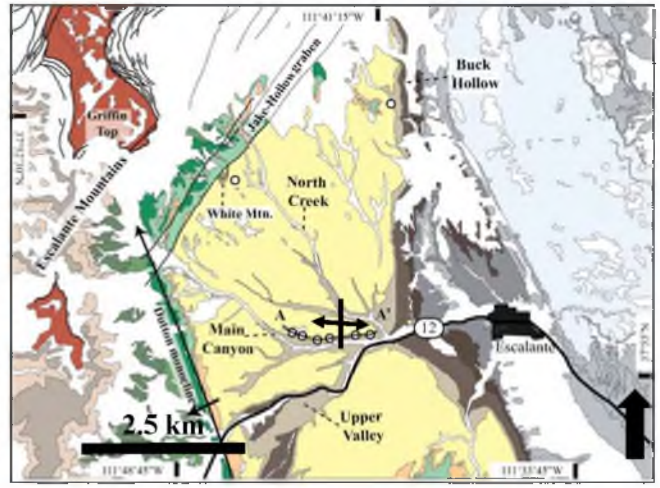

Table 5
Bounding surface differential GPS data

Surface	X	Y	Depth	Surface	X	Y	Depth	Surface	X	Y	Depth
wRs (1)	436987.23	4180066.74	1937.89	wRs (1)	436665.43	4179448.51	1984.92	wRs (1)	436296.84	4179416.74	1996.31
wRs (1)	436804.10	4179927.29	1951.70	wRs (1)	436692.02	4179439.31	1978.42	wRs (1)	436292.48	4179410.74	1996.24
wRs (1)	436816.78	4179936.45	1949.27	wRs (1)	436679.32	4179459.23	1973.35	wRs (1)	436286.68	4179409.68	1995.74
wRs (1)	436817.60	4179938.24	1949.04	wRs (1)	436729.05	4179420.27	1977.29	wRs (1)	436277.37	4179412.62	1996.50
wRs (1)	436824.88	4179945.43	1947.28	wRs (1)	436733.15	4179422.60	1977.05	wRs (1)	436267.62	4179412.49	1995.84
wRs (1)	436851.42	4179961.17	1944.88	wRs (1)	436774.45	4179410.96	1976.78	wRs (1)	436263.21	4179413.12	1995.66
wRs (1)	436851.96	4179972.23	1944.07	wRs (1)	436785.82	4179411.10	1976.23	wRs (1)	436259.40	4179411.97	1996.31
wRs (1)	436851.94	4179979.25	1944.37	wRs (1)	436803.89	4179409.82	1972.99	wRs (1)	436254.80	4179406.44	1995.27
wRs (1)	436852.93	4179982.26	1944.10	wRs (1)	436814.32	4179403.33	1973.90	wRs (1)	436240.95	4179397.33	1996.85
wRs (1)	436863.02	4179990.34	1942.73	wRs (1)	436561.58	4179446.23	1985.50	wRs (1)	436232.26	4179396.43	1996.52
wRs (1)	436867.13	4179993.77	1942.07	wRs (1)	435423.92	4179267.61	2019.06	wRs (1)	436226.14	4179396.72	1996.51
wRs (1)	436872.89	4179995.91	1941.36	wRs (1)	435404.47	4179266.18	2020.17	wRs (1)	436216.05	4179392.46	1996.83
wRs (1)	436882.17	4179994.80	1941.84	wRs (1)	435395.45	4179264.26	2020.79	wRs (1)	436208.09	4179391.41	1997.72
wRs (1)	436886.87	4180008.36	1941.77	wRs (1)	435381.82	4179257.94	2021.46	wRs (1)	436199.32	4179385.52	1998.39
wRs (1)	436896.36	4180019.14	1942.07	wRs (1)	435345.76	4179246.82	2021.06	wRs (1)	436189.79	4179380.68	1997.24
wRs (1)	436908.02	4180030.20	1940.62	wRs (1)	435334.19	4179240.98	2020.78	wRs (1)	436153.07	4179373.00	2000.48
wRs (1)	436908.71	4180032.14	1940.87	wRs (1)	435304.80	4179239.80	2023.29	wRs (1)	436141.93	4179370.08	2000.89
wRs (1)	436912.61	4180035.38	1941.00	wRs (1)	435291.38	4179245.92	2021.98	wRs (1)	436123.49	4179369.07	2001.44
wRs (1)	436915.27	4180036.66	1940.68	wRs (1)	435292.26	4179225.69	2023.68	wRs (1)	436106.67	4179369.11	2000.60
wRs (1)	436924.56	4180043.86	1940.31	wRs (1)	435182.82	4179185.77	2027.75	wRs (1)	435983.75	4179328.01	2001.85
wRs (1)	436930.95	4180048.13	1940.52	wRs (1)	436464.15	4179471.38	1987.36	wRs (1)	436005.28	4179336.31	2001.68
wRs (1)	436935.83	4180052.50	1941.17	wRs (1)	436463.03	4179464.79	1988.47	wRs (1)	436010.81	4179333.95	2002.26
wRs (1)	436942.39	4180058.50	1940.57	wRs (1)	436455.77	4179456.52	1988.60	wRs (1)	436026.01	4179330.47	2003.06
wRs (1)	436947.47	4180060.20	1940.60	wRs (1)	436451.16	4179455.11	1988.87	wRs (1)	435423.92	4179267.61	2019.06
wRs (1)	436985.82	4180067.81	1937.95	wRs (1)	436447.18	4179453.00	1989.28	wRs (1)	435404.47	4179266.18	2020.17
wRs (1)	436988.25	4180066.42	1937.68	wRs (1)	436444.63	4179440.55	1990.43	wRs (1)	435395.45	4179264.26	2020.79
wRs (1)	436994.34	4180064.80	1937.48	wRs (1)	436437.78	4179433.88	1990.55	wRs (1)	435381.82	4179257.94	2021.46
wRs (1)	437029.27	4180035.70	1937.86	wRs (1)	436435.95	4179425.01	1990.85	wRs (1)	435345.76	4179246.82	2021.06
wRs (1)	437023.53	4180036.72	1937.35	wRs (1)	436433.49	4179419.57	1991.27	wRs (1)	435334.19	4179240.98	2020.78
wRs (1)	437018.73	4180056.82	1938.23	wRs (1)	436427.90	4179414.50	1991.42	wRs (1)	435304.80	4179239.80	2023.29
wRs (1)	437100.83	4180033.27	1938.90	wRs (1)	436418.93	4179396.95	1992.20	wRs (1)	435291.38	4179245.92	2021.98

Table 5 (continued)

Surface	X	Y	Depth
wRs (1)	437106.67	4180031.11	1939.05
wRs (1)	437120.04	4180032.14	1939.09
wRs (1)	436560.19	4179446.60	1984.71
wRs (1)	436580.16	4179439.02	1984.88
wRs (1)	436616.13	4179447.43	1983.98
wRs (1)	436635.03	4179460.99	1981.66
wRs (1)	436447.18	4179453.00	1989.28
wRs (1)	436444.63	4179440.55	1990.43
wRs (1)	436437.78	4179433.88	1990.55
wRs (1)	436435.95	4179425.01	1990.85
wRs (1)	436433.49	4179419.57	1991.27
wRs (1)	436427.90	4179414.50	1991.42
wRs (1)	436418.93	4179396.95	1992.20
wRs (1)	436414.50	4179380.45	1992.62
wRs (1)	436370.73	4179389.13	1991.28
wRs (1)	436358.11	4179385.55	1993.99
wRs (1)	436348.15	4179391.74	1994.83
wRs (1)	436308.96	4179416.11	1995.40
wRs (1)	436302.79	4179416.80	1995.52
wRs (1)	436296.84	4179416.74	1996.31
wRs (1)	436292.48	4179410.74	1996.24
wRs (1)	436286.68	4179409.68	1995.74
wRs (1)	436277.37	4179412.62	1996.50
wRs (1)	436267.62	4179412.49	1995.84
wRs (1)	436263.21	4179413.12	1995.66
wRs (1)	436259.40	4179411.97	1996.31
wRs (1)	436254.80	4179406.44	1995.27
wRs (1)	436240.95	4179397.33	1996.85
wRs (1)	436232.26	4179396.43	1996.52
wRs (1)	436226.14	4179396.72	1996.51
wRs (1)	436216.05	4179392.46	1996.83

Surface	X	Y
wRs (1)	436414.50	4179380.45
wRs (1)	436370.73	4179389.13
wRs (1)	436358.11	4179385.55
wRs (1)	436348.15	4179391.74
wRs (1)	436308.96	4179416.11
wRs (1)	436302.79	4179416.80
wRs (1)	436839.40	4179895.93
wRs (1)	436861.69	4179920.50
wRs (1)	436857.34	4179933.77
wRs (1)	436886.49	4179956.37
wRs (1)	436886.31	4179962.29
wRs (1)	437621.78	4180281.49
wRs (1)	437591.30	4180260.22
wRs (1)	437632.18	4180276.21
wRs (1)	437696.27	4180221.80
wRs (1)	437699.22	4180222.61
wRs (1)	437748.41	4180185.90
wRs (1)	437723.89	4180185.43
wRs (1)	437769.96	4180187.82
wRs (1)	437772.45	4180186.54
wRs (1)	437786.62	4180172.82
wRs (1)	437791.18	4180170.94
wRs (1)	437798.37	4180165.39
wRs (1)	437808.22	4180150.36
wRs (1)	437819.78	4180133.76
wRs (1)	437830.10	4180128.23
wRs (1)	437869.75	4180108.50
wRs (1)	437879.75	4180100.26
wRs (1)	437896.36	4180097.47
wRs (1)	437918.98	4180089.85
wRs (1)	437944.10	4180082.32

Depth	Surface	X	Y	Depth
1992.62	wRs (1)	435292.26	4179225.69	2023.68
1991.28	wRs (1)	435182.82	4179185.77	2027.75
1993.99	wRs (1)	436464.15	4179471.38	1987.36
1994.83	wRs (1)	436463.03	4179464.79	1988.47
1995.40	wRs (1)	436455.77	4179456.52	1988.60
1995.52	wRs (1)	436451.16	4179455.11	1988.87
1946.35	wRs (1)	438927.45	4180245.21	1919.46
1944.71	wRs (1)	438963.74	4180240.11	1917.53
1944.48	wRs (1)	439009.36	4180240.19	1916.81
1940.42	wRs (1)	439026.98	4180252.34	1917.50
1940.83	wRs (1)	439051.97	4180257.97	1916.82
1948.68	wRs (1)	439071.43	4180275.06	1918.05
1947.96	wRs (1)	439099.54	4180274.31	1918.05
1947.97	wRs (1)	439129.40	4180251.23	1916.40
1948.74	wRs (1)	439156.53	4180252.08	1915.43
1948.29	wRs (1)	439199.42	4180253.18	1917.06
1945.78	wRs (1)	439242.63	4180262.28	1919.06
1945.83	wRs (1)	439289.18	4180280.93	1921.71
1945.47	wRs (1)	439330.17	4180287.41	1922.55
1946.38	wRs (1)	438962.35	4180238.45	1917.40
1945.19	wRs (1)	438927.45	4180245.21	1919.46
1945.67	wRs (1)	438963.74	4180240.11	1917.53
1945.45	wRs (1)	439009.36	4180240.19	1916.81
1944.63	wRs (1)	439026.98	4180252.34	1917.50
1942.94	wRs (1)	439051.97	4180257.97	1916.82
1942.41	wRs (1)	439071.43	4180275.06	1918.05
1941.82	wRs (1)	439099.54	4180274.31	1918.05
1938.52	wRs (1)	439129.40	4180251.23	1916.40
1938.74	wRs (1)	439156.53	4180252.08	1915.43
1938.28	wRs (1)	439199.42	4180253.18	1917.06
1938.12	wRs (1)	439242.63	4180262.28	1919.06

Table 5 (continued)

Surface	X	Y	Depth
wRs (1)	436208.09	4179391.41	1997.72
wRs (1)	436199.32	4179385.52	1998.39
wRs (1)	436189.79	4179380.68	1997.24
wRs (1)	436153.07	4179373.00	2000.48
wRs (1)	436141.93	4179370.08	2000.89
wRs (1)	436123.49	4179369.07	2001.44
wRs (1)	436106.67	4179369.11	2000.60
wRs (1)	435983.75	4179328.01	2001.85
wRs (1)	436005.28	4179336.31	2001.68
wRs (1)	436010.81	4179333.95	2002.26
wRs (1)	436026.01	4179330.47	2003.06
wRs (1)	436824.51	4179879.89	1949.58
Top "A"	436777.03	4179973.70	1998.64
Top "A"	436788.64	4179983.33	1997.43
Top "A"	436791.61	4179988.22	1997.29
Top "A"	436800.39	4179998.94	1996.77
Top "A"	436803.70	4180005.95	1995.38
Top "A"	436814.04	4180017.57	1993.76
Top "A"	436823.90	4180029.42	1993.58
Top "A"	436832.16	4180037.75	1993.77
Top "A"	436840.58	4180042.43	1992.20
Top "A"	436844.98	4180051.90	1990.91
Top "A"	436848.88	4180059.09	1990.46
Top "A"	436859.71	4180069.92	1989.70
Top "A"	436868.37	4180079.71	1989.87
Top "A"	436872.92	4180088.03	1991.83
Top "A"	436885.16	4180088.04	1987.78
Top "A"	436894.49	4180094.51	1987.64
Top "A"	436898.83	4180102.01	1990.02
Top "A"	436906.29	4180109.55	1989.77
Top "A"	436914.71	4180115.02	1988.36

Surface	X	Y
wRs (1)	437962.66	4180079.01
wRs (1)	437949.12	4180078.68
wRs (1)	438516.80	4180242.37
wRs (1)	438546.55	4180219.76
wRs (1)	438619.22	4180194.40
wRs (1)	438615.77	4180194.78
wRs (1)	438630.54	4180181.69
wRs (1)	438635.31	4180176.58
wRs (1)	438713.95	4180131.34
wRs (1)	438727.06	4180119.97
wRs (1)	438747.07	4180113.21
wRs (1)	438734.72	4180118.89
Top "A"	437081.20	4180104.94
Top "A"	437086.75	4180104.49
Top "A"	437091.20	4180105.56
Top "A"	437095.79	4180104.98
Top "A"	437099.03	4180101.58
Top "A"	437108.18	4180099.37
Top "A"	437120.68	4180100.95
Top "A"	437127.59	4180103.79
Top "A"	437139.24	4180104.53
Top "A"	437158.58	4180105.70
Top "A"	437169.21	4180112.36
Top "A"	437178.51	4180113.65
Top "A"	437206.41	4180119.43
Top "A"	437234.84	4180127.95
Top "A"	437260.71	4180135.48
Top "A"	437292.20	4180137.55
Top "A"	437313.35	4180139.04
Top "A"	437338.64	4180141.58
Top "A"	437350.69	4180142.89

Depth		Surface	X	Y	Depth
1936.21		wRs (1)	439289.18	4180280.93	1921.71
1936.63		wRs (1)	439330.17	4180287.41	1922.55
1924.09		wRs (1)	438962.35	4180238.45	1917.40
1920.17		Top "A"	436674.94	4179901.98	2012.18
1919.24		Top "A"	436685.01	4179910.56	2011.40
1919.87		Top "A"	436704.52	4179917.39	2008.97
1920.17		Top "A"	436715.87	4179925.88	2007.84
1918.86		Top "A"	436731.93	4179941.06	2005.53
1916.41		Top "A"	436741.85	4179946.18	2004.08
1916.24		Top "A"	436745.15	4179951.56	2004.65
1917.09		Top "A"	436755.70	4179958.67	2001.40
1916.87		Top "A"	436771.69	4179970.62	1999.50
1984.86		Top "A"	436706.20	4179373.02	2028.61
1985.60		Top "A"	436719.08	4179372.16	2027.23
1985.06		Top "A"	436727.34	4179368.72	2028.09
1985.97		Top "A"	436732.26	4179368.10	2028.28
1985.35		Top "A"	436738.37	4179363.34	2027.69
1986.20		Top "A"	436744.05	4179363.86	2027.69
1986.17		Top "A"	436749.41	4179360.15	2026.86
1986.17		Top "A"	436758.27	4179356.12	2027.04
1987.52		Top "A"	436765.80	4179362.28	2026.85
1988.13		Top "A"	436777.75	4179365.84	2024.79
1987.80		Top "A"	436788.85	4179369.09	2025.42
1988.78		Top "A"	436798.77	4179366.01	2025.58
1991.04		Top "A"	436801.70	4179364.29	2024.31
1990.74		Top "A"	436811.72	4179358.40	2025.01
1992.19		Top "A"	436819.63	4179354.97	2024.27
1990.69		Top "A"	436834.24	4179350.63	2024.92
1992.00		Top "A"	436841.80	4179352.69	2024.04
1991.65		Top "A"	436850.33	4179351.76	2021.98
1990.83		Top "A"	436856.66	4179346.56	2023.26

Table 5 (continued)

Surface	X	Y	Depth
Top "A"	436924.14	4180117.12	1986.07
Top "A"	436944.98	4180130.44	1985.69
Top "A"	436950.49	4180129.63	1984.64
Top "A"	436959.07	4180133.81	1985.12
Top "A"	436971.12	4180139.08	1986.48
Top "A"	436982.67	4180136.99	1985.62
Top "A"	436993.24	4180137.30	1986.34
Top "A"	436996.70	4180136.67	1985.49
Top "A"	437006.85	4180129.47	1984.31
Top "A"	437021.28	4180117.68	1984.00
Top "A"	437027.52	4180122.14	1987.57
Top "A"	437033.21	4180116.16	1986.94
Top "A"	437039.19	4180114.28	1986.00
Top "A"	437046.84	4180112.39	1986.14
Top "A"	437050.02	4180110.69	1985.67
Top "A"	437056.48	4180104.30	1984.48
Top "A"	437064.26	4180108.53	1987.20
Top "A"	437073.23	4180107.20	1985.68
Top "A"	437189.10	4179267.25	2010.30
Top "A"	437196.79	4179270.04	2010.86
Top "A"	437205.84	4179274.46	2009.98
Top "A"	437219.44	4179279.14	2007.76
Top "A"	437240.22	4179288.68	2008.23
Top "A"	437254.77	4179286.95	2007.09
Top "A"	437267.57	4179291.82	2006.17
Top "A"	437279.01	4179296.18	2006.50
Top "A"	437279.03	4179296.18	2006.52
Top "A"	437287.90	4179295.74	2006.51
Top "A"	437299.22	4179304.07	2004.04
Top "A"	437312.35	4179304.86	2003.87
Top "A"	437325.45	4179305.09	2004.97
Top "A"	437356.93	4180141.08	1992.50
Top "A"	436518.35	4179353.00	2038.06
Top "A"	436531.87	4179361.98	2037.09
Top "A"	436542.91	4179367.70	2036.05
Top "A"	436553.23	4179375.02	2035.57
Top "A"	436565.69	4179376.16	2033.67
Top "A"	436593.21	4179388.78	2027.79
Top "A"	436608.87	4179390.43	2031.65
Top "A"	436623.05	4179394.50	2033.41
Top "A"	436633.60	4179397.38	2030.73
Top "A"	436639.40	4179394.61	2031.20
Top "A"	436641.67	4179394.33	2031.20
Top "A"	436660.53	4179390.04	2030.12
Top "A"	436667.44	4179389.53	2030.11
Top "A"	436671.93	4179387.32	2030.54
Top "A"	436682.39	4179375.61	2030.60
Top "A"	436686.26	4179371.24	2029.84
Top "A"	436696.67	4179367.85	2028.87
Top "A"	436498.07	4179903.15	2027.34
Top "A"	436489.46	4179904.25	2028.09
Top "A"	436483.26	4179903.36	2028.75
Top "A"	436475.59	4179905.93	2029.57
Top "A"	436469.79	4179903.40	2029.82
Top "A"	436462.00	4179906.99	2030.43
Top "A"	436447.82	4179910.51	2030.46
Top "A"	436446.99	4179903.55	2030.67
Top "A"	436445.97	4179905.41	2030.56
Top "A"	436446.03	4179911.12	2031.38
Top "A"	436436.83	4179911.40	2030.92
Top "A"	436432.13	4179912.15	2031.93
Top "A"	436422.60	4179912.98	2032.20
Top "A"	436866.61	4179342.33	2022.70
Top "A"	436876.54	4179341.53	2022.48
Top "A"	436877.10	4179342.62	2021.41
Top "A"	436886.92	4179339.85	2021.55
Top "A"	436897.49	4179340.70	2021.15
Top "A"	436901.06	4179344.13	2019.90
Top "A"	436909.58	4179342.97	2017.80
Top "A"	436925.23	4179340.11	2018.32
Top "A"	436940.38	4179334.99	2018.17
Top "A"	436951.03	4179333.19	2016.19
Top "A"	436963.83	4179331.92	2016.28
Top "A"	436982.24	4179329.49	2016.93
Top "A"	436996.89	4179328.53	2016.09
Top "A"	437004.10	4179330.42	2015.35
Top "A"	437135.64	4179263.32	2012.71
Top "A"	437159.42	4179264.45	2011.68
Top "A"	437173.10	4179265.61	2012.28
Top "A"	437182.58	4179264.68	2012.10
Top "A"	436246.49	4180009.87	2036.61
Top "A"	436230.00	4180034.84	2036.80
Top "A"	436221.99	4180045.30	2038.09
Top "A"	436213.78	4180052.64	2038.44
Top "A"	436202.89	4180065.53	2038.84
Top "A"	436194.43	4180081.13	2039.47
Top "A"	436168.90	4180122.65	2043.60
Top "A"	436149.37	4180133.10	2043.86
Top "A"	436126.33	4180140.16	2045.42
Top "A"	436115.89	4180140.16	2045.42
Top "A"	436097.84	4180149.76	2046.18
Top "A"	436092.89	4180149.59	2046.62
Top "A"	436078.26	4180154.36	2048.95

Table 5 (continued)

Surface	X	Y	Depth
Top "A"	437338.29	4179312.17	2002.83
Top "A"	437338.25	4179313.16	2002.67
Top "A"	437366.13	4179315.80	2002.52
Top "A"	437374.53	4179318.37	2001.12
Top "A"	437389.81	4179326.02	2000.22
Top "A"	437400.13	4179336.51	1999.93
Top "A"	437417.06	4179343.17	1999.34
Top "A"	437425.75	4179347.59	1997.86
Top "A"	437439.34	4179353.35	1997.42
Top "A"	437456.51	4179365.43	1996.24
Top "A"	437470.19	4179373.12	1995.63
Top "A"	437474.49	4179376.40	1995.31
Top "A"	437479.59	4179383.92	1993.42
Top "A"	437494.10	4179387.60	1994.55
Top "A"	437498.51	4179393.23	1993.97
Top "A"	437511.43	4179395.38	1992.27
Top "A"	437520.54	4179396.67	1992.51
Top "A"	437523.30	4179397.74	1992.50
Top "A"	437543.42	4179388.50	1992.75
Top "A"	437574.82	4179319.56	2000.16
Top "A"	436571.58	4179939.72	2022.00
Top "A"	436510.47	4179878.55	2005.17
Top "A"	436537.43	4179920.23	2023.77
Top "A"	436515.21	4179919.19	2026.58
Top "A"	435066.36	4179080.04	2085.20
Top "A"	435059.48	4179067.43	2085.00
Top "A"	435044.42	4179069.03	2084.31
Top "A"	435025.63	4179065.59	2084.48
Top "A"	434982.69	4179045.72	2083.91
Top "A"	434969.00	4179040.30	2084.80
Top "A"	434957.38	4179043.26	2085.39

Surface	X	Y	Depth
Top "A"	436416.36	4179912.02	2033.43
Top "A"	436407.55	4179908.85	2032.97
Top "A"	436404.31	4179910.01	2033.43
Top "A"	436398.38	4179912.57	2034.09
Top "A"	436393.38	4179913.90	2034.93
Top "A"	436387.03	4179915.08	2034.13
Top "A"	436379.32	4179916.08	2034.16
Top "A"	436360.16	4179917.74	2034.63
Top "A"	436356.18	4179919.55	2035.10
Top "A"	436350.29	4179923.49	2035.36
Top "A"	436344.16	4179926.63	2034.81
Top "A"	436331.05	4179933.13	2036.00
Top "A"	436327.14	4179935.24	2035.23
Top "A"	436313.19	4179943.07	2036.67
Top "A"	436307.60	4179944.96	2036.39
Top "A"	436305.21	4179946.54	2037.05
Top "A"	436302.64	4179950.78	2036.02
Top "A"	436297.39	4179957.72	2035.98
Top "A"	436290.36	4179964.82	2035.96
Top "A"	436284.06	4179971.49	2036.27
Top "A"	436274.02	4179976.44	2036.67
Top "A"	436268.15	4179983.15	2036.26
Top "A"	436264.96	4179989.11	2035.97
Top "A"	436255.98	4179998.05	2036.24
Top "A"	436394.57	4179277.03	2044.51
Top "A"	436363.81	4179278.69	2044.32
Top "A"	436344.89	4179314.31	2041.60
Top "A"	436340.45	4179315.20	2045.45
Top "A"	436319.38	4179347.69	2046.41
Top "A"	436309.59	4179347.00	2047.34
Top "A"	436294.69	4179351.74	2047.76

Surface	X	Y	Depth
Top "A"	436044.75	4180168.72	2049.98
Top "A"	435370.48	4179203.93	2073.05
Top "A"	435357.22	4179191.37	2070.95
Top "A"	435349.15	4179181.20	2070.25
Top "A"	435335.66	4179180.23	2071.42
Top "A"	435315.17	4179172.01	2077.54
Top "A"	435297.80	4179167.84	2077.64
Top "A"	435288.02	4179168.81	2077.86
Top "A"	435273.50	4179167.31	2079.00
Top "A"	435259.60	4179167.41	2078.81
Top "A"	435248.66	4179158.16	2080.43
Top "A"	435241.62	4179157.51	2078.82
Top "A"	435232.83	4179148.55	2079.54
Top "A"	435224.37	4179143.50	2080.81
Top "A"	435215.02	4179137.78	2079.87
Top "A"	435204.02	4179127.47	2080.76
Top "A"	435190.85	4179121.90	2080.78
Top "A"	435171.02	4179118.38	2080.07
Top "A"	435162.63	4179112.64	2082.79
Top "A"	435143.64	4179107.26	2082.59
Top "A"	435128.51	4179108.18	2083.86
Top "A"	435114.32	4179102.36	2085.36
Top "A"	435098.31	4179094.24	2086.07
Top "A"	435080.10	4179084.72	2084.78
Top "A"	435177.99	4180225.73	2084.72
Top "A"	435174.01	4180227.48	2085.18
Top "A"	435168.46	4180230.41	2084.44
Top "A"	435164.27	4180233.24	2084.14
Top "A"	435157.64	4180234.67	2084.10
Top "A"	435155.32	4180237.47	2084.28
Top "A"	435149.95	4180239.75	2084.96

Table 5 (continued)

Surface	X	Y	Depth
Top "A"	434945.75	4179037.58	2087.64
Top "A"	434913.60	4179026.00	2085.09
Top "A"	434893.68	4179029.95	2082.17
Top "A"	436581.93	4179430.38	2032.43
Top "A"	436577.21	4179427.47	2032.02
Top "A"	436564.05	4179425.86	2032.41
Top "A"	436556.39	4179424.80	2032.79
Top "A"	436543.30	4179426.74	2032.56
Top "A"	436528.56	4179420.57	2035.36
Top "A"	436510.60	4179414.52	2036.91
Top "A"	436508.68	4179412.64	2036.93
Top "A"	436494.62	4179411.24	2038.33
Top "A"	436485.53	4179404.75	2038.72
Top "A"	436484.03	4179394.21	2039.06
Top "A"	436483.72	4179386.12	2039.07
Top "A"	436479.20	4179378.70	2039.11
Top "A"	436476.27	4179370.04	2038.93
Top "A"	436472.82	4179367.75	2039.61
Top "A"	436472.91	4179362.85	2039.85
Top "A"	436469.56	4179359.13	2039.39
Top "A"	436465.56	4179357.59	2039.15
Top "A"	436465.22	4179345.32	2040.02
Top "A"	436458.49	4179339.92	2040.23
Top "A"	436448.05	4179333.69	2040.24
Top "A"	436441.90	4179327.06	2041.64
Top "A"	436439.88	4179315.45	2041.48
Top "A"	436431.35	4179307.81	2042.14
Top "A"	436423.65	4179299.79	2043.04
Top "A"	436417.48	4179291.51	2043.39
Top "A"	436402.10	4179283.02	2043.85
Top "A"	434884.64	4180332.45	2097.88

Surface	X	Y	Depth
Top "A"	436276.87	4179350.66	2048.08
Top "A"	436262.63	4179350.35	2047.20
Top "A"	436241.94	4179349.20	2048.66
Top "A"	436230.63	4179347.54	2049.24
Top "A"	436224.57	4179345.54	2048.64
Top "A"	436225.51	4179340.54	2049.47
Top "A"	436216.40	4179341.17	2049.47
Top "A"	436212.83	4179335.35	2049.93
Top "A"	436206.75	4179330.57	2049.53
Top "A"	436192.35	4179322.86	2049.46
Top "A"	436174.72	4179319.70	2050.45
Top "A"	436163.23	4179319.26	2051.90
Top "A"	436148.57	4179320.58	2051.77
Top "A"	436140.01	4179314.50	2052.57
Top "A"	436124.86	4179292.18	2053.49
Top "A"	436108.22	4179281.00	2052.80
Top "A"	436088.39	4179270.69	2053.59
Top "A"	436084.66	4179269.77	2053.27
Top "A"	436069.20	4179265.02	2054.01
Top "A"	436019.95	4179272.82	2055.59
Top "A"	436009.71	4179276.49	2052.49
Top "A"	435943.50	4179238.16	2057.91
Top "A"	435214.99	4180205.90	2084.96
Top "A"	435209.80	4180208.44	2085.01
Top "A"	435206.81	4180211.20	2085.17
Top "A"	435199.15	4180213.45	2084.15
Top "A"	435195.58	4180217.59	2084.68
Top "A"	435190.97	4180222.89	2084.48
Top "A"	435185.71	4180224.05	2084.76
Top "A"	435181.85	4180225.98	2084.22
Top "A"	434606.48	4180408.07	2096.59

Surface	X	Y	Depth
Top "A"	435145.64	4180244.49	2085.09
Top "A"	435141.03	4180247.05	2085.29
Top "A"	435135.90	4180249.02	2084.81
Top "A"	435127.63	4180252.54	2085.38
Top "A"	435126.88	4180253.49	2085.07
Top "A"	435115.79	4180258.18	2086.02
Top "A"	435110.98	4180259.15	2085.92
Top "A"	435105.10	4180261.80	2086.21
Top "A"	435098.92	4180262.94	2086.19
Top "A"	435095.00	4180264.15	2086.67
Top "A"	435088.86	4180266.61	2086.33
Top "A"	435081.07	4180266.13	2086.74
Top "A"	435055.99	4180272.02	2086.55
Top "A"	435046.85	4180277.89	2087.68
Top "A"	435064.55	4180266.54	2087.36
Top "A"	435051.82	4180269.12	2086.98
Top "A"	435045.22	4180275.07	2087.31
Top "A"	435037.91	4180276.08	2088.09
Top "A"	435027.51	4180280.26	2087.74
Top "A"	435021.22	4180281.38	2089.14
Top "A"	435015.26	4180283.01	2088.60
Top "A"	435002.32	4180287.50	2089.12
Top "A"	434990.50	4180287.71	2089.55
Top "A"	434982.68	4180290.09	2089.95
Top "A"	434977.97	4180289.80	2088.92
Top "A"	434954.42	4180299.96	2088.98
Top "A"	434945.74	4180300.90	2091.48
Top "A"	434934.38	4180302.68	2092.09
Top "A"	434914.61	4180317.83	2094.58
Top "A"	434891.45	4180330.64	2095.20
Top "A"	434969.00	4179040.30	2084.80

Table 5 (continued)

Surface	X	Y	Depth
Top "A"	434873.48	4180331.22	2098.01
Top "A"	434866.31	4180334.42	2098.24
Top "A"	434851.84	4180339.12	2099.42
Top "A"	434835.10	4180342.97	2100.72
Top "A"	434825.57	4180345.18	2101.03
Top "A"	434848.34	4180367.28	2091.92
Top "A"	434840.64	4180369.26	2091.18
Top "A"	434819.04	4180368.85	2089.98
Top "A"	434809.34	4180372.01	2090.48
Top "A"	434804.18	4180374.30	2091.45
Top "A"	434794.76	4180375.19	2091.30
Top "A"	434789.15	4180376.59	2090.40
Top "A"	434783.18	4180379.29	2090.49
Top "A"	434777.78	4180383.77	2091.32
Top "A"	434770.91	4180379.32	2089.54
Top "A"	434760.28	4180384.39	2092.36
Top "A"	434755.72	4180381.47	2092.18
Top "A"	434750.54	4180384.85	2093.40
Top "A"	434742.33	4180382.11	2094.40
Top "A"	434735.54	4180383.87	2094.35
Top "A"	434731.95	4180384.33	2094.42
Top "A"	434723.16	4180386.56	2094.32
Top "A"	434718.19	4180387.96	2094.85
Top "A"	434703.00	4180393.71	2095.74
Top "A"	434697.94	4180395.59	2096.07
Top "A"	434693.25	4180397.38	2096.08
Top "A"	434679.59	4180399.19	2095.96
Top "A"	434676.35	4180402.28	2096.44
Top "A"	434664.16	4180399.69	2096.71
Top "A"	434658.81	4180401.65	2096.93
Top "A"	434646.19	4180402.69	2095.69

Surface	X	Y	Depth
Top "A"	434602.99	4180406.85	2096.39
Top "A"	434596.99	4180408.27	2097.24
Top "A"	434592.13	4180406.63	2096.66
Top "A"	434586.40	4180409.74	2096.83
Top "A"	434578.41	4180410.05	2096.87
Top "A"	434574.37	4180410.95	2096.11
Top "A"	434534.14	4180410.88	2097.66
Top "A"	434528.70	4180411.28	2097.38
Top "A"	435370.48	4179203.93	2073.05
Top "A"	435357.22	4179191.37	2070.95
Top "A"	435349.15	4179181.20	2070.25
Top "A"	435335.66	4179180.23	2071.42
Top "A"	435315.17	4179172.01	2077.54
Top "A"	435297.80	4179167.84	2077.64
Top "A"	435288.02	4179168.81	2077.86
Top "A"	435273.50	4179167.31	2079.00
Top "A"	435259.60	4179167.41	2078.81
Top "A"	435248.66	4179158.16	2080.43
Top "A"	435241.62	4179157.51	2078.82
Top "A"	435232.83	4179148.55	2079.54
Top "A"	435224.37	4179143.50	2080.81
Top "A"	435215.02	4179137.78	2079.87
Top "A"	435204.02	4179127.47	2080.76
Top "A"	435190.85	4179121.90	2080.78
Top "A"	435171.02	4179118.38	2080.07
Top "A"	435162.63	4179112.64	2082.79
Top "A"	435143.64	4179107.26	2082.59
Top "A"	435128.51	4179108.18	2083.86
Top "A"	435114.32	4179102.36	2085.36
Top "A"	435098.31	4179094.24	2086.07
Top "A"	435080.10	4179084.72	2084.78

Surface	X	Y	Depth
Top "A"	434957.38	4179043.26	2085.39
Top "A"	434945.75	4179037.58	2087.64
Top "A"	434913.60	4179026.00	2085.09
Top "A"	434893.68	4179029.95	2082.17
Top "A"	436581.93	4179430.38	2032.43
Top "A"	436577.21	4179427.47	2032.02
Top "A"	436564.05	4179425.86	2032.41
Top "A"	436556.39	4179424.80	2032.79
Top "A"	436543.30	4179426.74	2032.56
Top "A"	436528.56	4179420.57	2035.36
Top "A"	436510.60	4179414.52	2036.91
Top "A"	436508.68	4179412.64	2036.93
Top "A"	436494.62	4179411.24	2038.33
Top "A"	436485.53	4179404.75	2038.72
Top "A"	436484.03	4179394.21	2039.06
Top "A"	436483.72	4179386.12	2039.07
Top "A"	436479.20	4179378.70	2039.11
Top "A"	436476.27	4179370.04	2038.93
Top "A"	436472.82	4179367.75	2039.61
Top "A"	436472.91	4179362.85	2039.85
Top "A"	436469.56	4179359.13	2039.39
Top "A"	436465.56	4179357.59	2039.15
Top "A"	436465.22	4179345.32	2040.02
Top "A"	436458.49	4179339.92	2040.23
Top "A"	436448.05	4179333.69	2040.24
Top "A"	436441.90	4179327.06	2041.64
Top "A"	436439.88	4179315.45	2041.48
Top "A"	436431.35	4179307.81	2042.14
Top "A"	436423.65	4179299.79	2043.04
Top "A"	436417.48	4179291.51	2043.39
Top "A"	436402.10	4179283.02	2043.85

Table 5 (continued)

Surface	X	Y	Depth
Top "A"	434639.49	4180402.35	2094.78
Top "A"	434631.14	4180403.51	2094.61
Top "A"	434625.53	4180408.81	2095.00
Top "A"	434617.38	4180405.40	2096.19
Top "A"	434611.20	4180407.48	2096.39
Top "A"	436309.59	4179347.00	2047.34
Top "A"	436294.69	4179351.74	2047.76
Top "A"	436276.87	4179350.66	2048.08
Top "A"	436262.63	4179350.35	2047.20
Top "A"	436241.94	4179349.20	2048.66
Top "A"	436230.63	4179347.54	2049.24
Top "A"	436224.57	4179345.54	2048.64
Top "A"	436225.51	4179340.54	2049.47
Top "A"	436216.40	4179341.17	2049.47
Top "A"	436212.83	4179335.35	2049.93
Top "A"	436206.75	4179330.57	2049.53
Top "A"	436192.35	4179322.86	2049.46
Top "A"	436174.72	4179319.70	2050.45
Top "A"	436163.23	4179319.26	2051.90
Top "A"	436148.57	4179320.58	2051.77
Top "A"	436140.01	4179314.50	2052.57
Top "A"	436124.86	4179292.18	2053.49
Top "A"	436108.22	4179281.00	2052.80
Top "A"	436088.39	4179270.69	2053.59
Top "A"	436084.66	4179269.77	2053.27
Top "A"	436069.20	4179265.02	2054.01
Top "A"	436019.95	4179272.82	2055.59
Top "A"	436009.71	4179276.49	2052.49
Top "A"	435943.50	4179238.16	2057.91
Top "A"	435214.99	4180205.90	2084.96
Top "A"	435209.80	4180208.44	2085.01
Top "A"	435066.36	4179080.04	2085.20
Top "A"	435059.48	4179067.43	2085.00
Top "A"	435044.42	4179069.03	2084.31
Top "A"	435025.63	4179065.59	2084.48
Top "A"	434982.69	4179045.72	2083.91
Top "A"	435155.32	4180237.47	2084.28
Top "A"	435149.95	4180239.75	2084.96
Top "A"	435145.64	4180244.49	2085.09
Top "A"	435141.03	4180247.05	2085.29
Top "A"	435135.90	4180249.02	2084.81
Top "A"	435127.63	4180252.54	2085.38
Top "A"	435126.88	4180253.49	2085.07
Top "A"	435115.79	4180258.18	2086.02
Top "A"	435110.98	4180259.15	2085.92
Top "A"	435105.10	4180261.80	2086.21
Top "A"	435098.92	4180262.94	2086.19
Top "A"	435095.00	4180264.15	2086.67
Top "A"	435088.86	4180266.61	2086.33
Top "A"	435081.07	4180266.13	2086.74
Top "A"	435055.99	4180272.02	2086.55
Top "A"	435046.85	4180277.89	2087.68
Top "A"	435064.55	4180266.54	2087.36
Top "A"	435051.82	4180269.12	2086.98
Top "A"	435045.22	4180275.07	2087.31
Top "A"	435037.91	4180276.08	2088.09
Top "A"	435027.51	4180280.26	2087.74
Top "A"	435021.22	4180281.38	2089.14
Top "A"	435015.26	4180283.01	2088.60
Top "A"	435002.32	4180287.50	2089.12
Top "A"	434990.50	4180287.71	2089.55
Top "A"	434982.68	4180290.09	2089.95
Top "A"	436394.57	4179277.03	2044.51
Top "A"	436363.81	4179278.69	2044.32
Top "A"	436344.89	4179314.31	2041.60
Top "A"	436340.45	4179315.20	2045.45
Top "A"	436319.38	4179347.69	2046.41
Top "A"	434825.57	4180345.18	2101.03
Top "A"	434848.34	4180367.28	2091.92
Top "A"	434840.64	4180369.26	2091.18
Top "A"	434819.04	4180368.85	2089.98
Top "A"	434809.34	4180372.01	2090.48
Top "A"	434804.18	4180374.30	2091.45
Top "A"	434794.76	4180375.19	2091.30
Top "A"	434789.15	4180376.59	2090.40
Top "A"	434783.18	4180379.29	2090.49
Top "A"	434777.78	4180383.77	2091.32
Top "A"	434770.91	4180379.32	2089.54
Top "A"	434760.28	4180384.39	2092.36
Top "A"	434755.72	4180381.47	2092.18
Top "A"	434750.54	4180384.85	2093.40
Top "A"	434742.33	4180382.11	2094.40
Top "A"	434735.54	4180383.87	2094.35
Top "A"	434731.95	4180384.33	2094.42
Top "A"	434723.16	4180386.56	2094.32
Top "A"	434718.19	4180387.96	2094.85
Top "A"	434703.00	4180393.71	2095.74
Top "A"	434697.94	4180395.59	2096.07
Top "A"	434693.25	4180397.38	2096.08
Top "A"	434679.59	4180399.19	2095.96
Top "A"	434676.35	4180402.28	2096.44
Top "A"	434664.16	4180399.69	2096.71
Top "A"	434658.81	4180401.65	2096.93

Table 5 (continued)

Surface	X	Y	Depth
Top "A"	435206.81	4180211.20	2085.17
Top "A"	435199.15	4180213.45	2084.15
Top "A"	435195.58	4180217.59	2084.68
Top "A"	435190.97	4180222.89	2084.48
Top "A"	435185.71	4180224.05	2084.76
Top "A"	435181.85	4180225.98	2084.22
Top "A"	435177.99	4180225.73	2084.72
Top "A"	435174.01	4180227.48	2085.18
Top "A"	435168.46	4180230.41	2084.44
Top "A"	435164.27	4180233.24	2084.14
Top "A"	435157.64	4180234.67	2084.10
Top "A"	434578.41	4180410.05	2096.87
Top "A"	434574.37	4180410.95	2096.11
Top "A"	434534.14	4180410.88	2097.66
Top "A"	434528.70	4180411.28	2097.38
Top "A"	434420.58	4180461.31	2096.26
Top "A"	434397.87	4180459.07	2095.25
Top "A"	434385.50	4180461.10	2094.83
Top "A"	434381.52	4180461.76	2095.17
Top "A"	434380.15	4180463.85	2095.96
Top "A"	434374.85	4180460.59	2094.92
Top "A"	434369.34	4180458.86	2095.91
Top "A"	434362.34	4180453.93	2095.54
Top "A"	434357.70	4180455.49	2095.68
Top "A"	434355.67	4180455.30	2095.67
Top "A"	434348.94	4180451.97	2096.92
Top "A"	434346.69	4180445.30	2098.32
Top "A"	434343.15	4180445.21	2097.72
Top "A"	434339.56	4180447.39	2097.99
Top "A"	434334.01	4180446.23	2097.07
Top "A"	434330.32	4180447.12	2097.26

Surface	X	Y	Depth
Top "A"	434977.97	4180289.80	2088.92
Top "A"	434954.42	4180299.96	2088.98
Top "A"	434945.74	4180300.90	2091.48
Top "A"	434934.38	4180302.68	2092.09
Top "A"	434914.61	4180317.83	2094.58
Top "A"	434891.45	4180330.64	2095.20
Top "A"	434884.64	4180332.45	2097.88
Top "A"	434873.48	4180331.22	2098.01
Top "A"	434866.31	4180334.42	2098.24
Top "A"	434851.84	4180339.12	2099.42
Top "A"	434835.10	4180342.97	2100.72
Top "A"	434140.73	4180513.75	2092.86
Top "A"	434136.05	4180513.37	2092.88
Top "A"	434167.19	4180489.23	2091.43
Top "A"	434157.61	4180502.73	2093.84
Top "A"	434149.09	4180501.16	2093.36
Top "A"	434143.92	4180504.09	2093.24
Top "A"	434137.31	4180507.57	2093.38
Top "A"	434131.88	4180508.13	2092.62
Top "A"	434129.38	4180507.89	2092.84
Top "A"	434121.23	4180510.28	2092.85
Top "A"	434113.80	4180511.83	2092.58
Top "A"	434107.72	4180515.65	2092.61
Top "A"	434101.44	4180516.43	2092.48
Top "A"	434091.50	4180518.01	2091.35
Top "A"	434081.34	4180523.25	2093.19
Top "A"	434071.66	4180523.12	2092.73
Top "A"	434064.42	4180525.84	2091.86
Top "A"	434054.56	4180524.14	2090.47
Top "A"	434040.74	4180529.90	2089.61
Top "A"	434029.75	4180535.10	2088.73

Surface	X	Y	Depth
Top "A"	434646.19	4180402.69	2095.69
Top "A"	434639.49	4180402.35	2094.78
Top "A"	434631.14	4180403.51	2094.61
Top "A"	434625.53	4180408.81	2095.00
Top "A"	434617.38	4180405.40	2096.19
Top "A"	434611.20	4180407.48	2096.39
Top "A"	434606.48	4180408.07	2096.59
Top "A"	434602.99	4180406.85	2096.39
Top "A"	434596.99	4180408.27	2097.24
Top "A"	434592.13	4180406.63	2096.66
Top "A"	434586.40	4180409.74	2096.83
Top "A"	435375.42	4180154.72	2078.65
Top "A"	435364.94	4180155.98	2078.30
Top "A"	435358.76	4180163.44	2079.68
Top "A"	435350.15	4180164.02	2078.55
Top "A"	435341.60	4180169.00	2078.77
Top "A"	435337.86	4180172.66	2079.43
Top "A"	435331.70	4180171.84	2079.44
Top "A"	435323.27	4180171.92	2079.35
Top "A"	435320.90	4180173.23	2079.72
Top "A"	435312.26	4180175.50	2080.96
Top "A"	435301.51	4180176.23	2082.16
Top "A"	435294.87	4180179.77	2081.27
Top "A"	435287.53	4180182.87	2082.14
Top "A"	435280.65	4180184.72	2081.89
Top "A"	435274.30	4180185.35	2080.52
Top "A"	435267.93	4180183.07	2081.27
Top "A"	435262.40	4180182.79	2081.18
Top "A"	435256.19	4180187.40	2083.25
Top "A"	435253.85	4180196.83	2082.68
Top "A"	435246.47	4180198.63	2083.11

Table 5 (continued)

Surface	X	Y	Depth
Top "A"	434326.78	4180447.35	2096.87
Top "A"	434321.96	4180450.87	2097.67
Top "A"	434315.64	4180451.55	2098.75
Top "A"	434307.29	4180452.91	2099.29
Top "A"	434303.18	4180453.01	2099.39
Top "A"	434295.76	4180453.91	2099.25
Top "A"	434289.49	4180456.91	2099.10
Top "A"	434281.83	4180460.90	2098.28
Top "A"	434274.51	4180464.48	2098.12
Top "A"	434268.59	4180468.75	2099.06
Top "A"	434263.32	4180466.93	2097.26
Top "A"	434256.52	4180464.76	2094.32
Top "A"	434200.45	4180480.69	2090.45
Top "A"	434192.45	4180487.01	2090.18
Top "A"	434165.15	4180505.88	2093.82
Top "A"	434153.84	4180510.77	2093.52
Top "A"	434145.60	4180513.65	2092.24
Top "A"	434346.69	4180445.30	2098.32
Top "A"	434343.15	4180445.21	2097.72
Top "A"	434339.56	4180447.39	2097.99
Top "A"	434334.01	4180446.23	2097.07
Top "A"	434330.32	4180447.12	2097.26
Top "A"	434326.78	4180447.35	2096.87
Top "A"	434321.96	4180450.87	2097.67
Top "A"	434315.64	4180451.55	2098.75
Top "A"	434307.29	4180452.91	2099.29
Top "A"	434303.18	4180453.01	2099.39
Top "A"	434295.76	4180453.91	2099.25
Top "A"	434289.49	4180456.91	2099.10
Top "A"	434281.83	4180460.90	2098.28
Top "A"	434274.51	4180464.48	2098.12
Top "A"	434016.14	4180537.05	2088.82
Top "A"	433998.77	4180548.32	2091.34
Top "A"	433988.50	4180545.84	2086.07
Top "A"	433955.82	4180560.94	2091.90
Top "A"	433940.38	4180558.62	2090.48
Top "A"	433923.43	4180559.98	2089.55
Top "A"	433921.77	4180549.22	2088.60
Top "A"	433892.04	4180564.41	2094.64
Top "A"	433875.50	4180568.47	2093.68
Top "A"	434244.18	4180267.13	2019.93
Top "A"	435427.77	4180149.59	2078.58
Top "A"	435418.75	4180154.04	2078.28
Top "A"	435410.71	4180147.72	2078.38
Top "A"	435401.06	4180145.99	2079.31
Top "A"	435392.55	4180147.67	2079.24
Top "A"	435388.03	4180153.70	2079.44
Top "A"	435379.12	4180150.91	2079.66
Top "A"	434071.66	4180523.12	2092.73
Top "A"	434064.42	4180525.84	2091.86
Top "A"	434054.56	4180524.14	2090.47
Top "A"	434040.74	4180529.90	2089.61
Top "A"	434029.75	4180535.10	2088.73
Top "A"	434016.14	4180537.05	2088.82
Top "A"	433998.77	4180548.32	2091.34
Top "A"	433988.50	4180545.84	2086.07
Top "A"	433955.82	4180560.94	2091.90
Top "A"	433940.38	4180558.62	2090.48
Top "A"	433923.43	4180559.98	2089.55
Top "A"	433921.77	4180549.22	2088.60
Top "A"	433892.04	4180564.41	2094.64
Top "A"	433875.50	4180568.47	2093.68
Top "A"	435239.99	4180198.27	2084.03
Top "A"	435234.76	4180199.29	2083.50
Top "A"	435225.63	4180201.21	2083.56
Top "A"	435216.80	4180205.59	2083.91
Top "A"	435206.41	4180210.56	2083.97
Top "A"	435201.53	4180212.86	2083.98
Top "A"	434420.58	4180461.31	2096.26
Top "A"	434397.87	4180459.07	2095.25
Top "A"	434385.50	4180461.10	2094.83
Top "A"	434381.52	4180461.76	2095.17
Top "A"	434380.15	4180463.85	2095.96
Top "A"	434374.85	4180460.59	2094.92
Top "A"	434369.34	4180458.86	2095.91
Top "A"	434362.34	4180453.93	2095.54
Top "A"	434357.70	4180455.49	2095.68
Top "A"	434355.67	4180455.30	2095.67
Top "A"	434348.94	4180451.97	2096.92
Top "A"	435267.93	4180183.07	2081.27
Top "A"	435262.40	4180182.79	2081.18
Top "A"	435256.19	4180187.40	2083.25
Top "A"	435253.85	4180196.83	2082.68
Top "A"	435246.47	4180198.63	2083.11
Top "A"	435239.99	4180198.27	2084.03
Top "A"	435234.76	4180199.29	2083.50
Top "A"	435225.63	4180201.21	2083.56
Top "A"	435216.80	4180205.59	2083.91
Top "A"	435206.41	4180210.56	2083.97
Top "A"	435201.53	4180212.86	2083.98
LJHMSB	436637.90	4179884.45	2026.17
LJHMSB	436646.52	4179892.82	2024.85
LJHMSB	436664.94	4179898.53	2022.22

Table 5 (continued)

Surface	X	Y	Depth	Surface	X	Y	Depth	Surface	X	Y	Depth
Top "A"	434268.59	4180468.75	2099.06	Top "A"	434244.18	4180267.13	2019.93	LJHMSB	436684.50	4179910.98	2019.56
Top "A"	434263.32	4180466.93	2097.26	Top "A"	435427.77	4180149.59	2078.58	LJHMSB	436704.48	4179918.33	2015.37
Top "A"	434256.52	4180464.76	2094.32	Top "A"	435418.75	4180154.04	2078.28	LJHMSB	436717.85	4179929.78	2011.55
Top "A"	434200.45	4180480.69	2090.45	Top "A"	435410.71	4180147.72	2078.38	LJHMSB	436722.44	4179934.70	2010.70
Top "A"	434192.45	4180487.01	2090.18	Top "A"	435401.06	4180145.99	2079.31	LJHMSB	436724.64	4179935.31	2009.85
Top "A"	434165.15	4180505.88	2093.82	Top "A"	435392.55	4180147.67	2079.24	LJHMSB	436725.96	4179937.19	2010.30
Top "A"	434153.84	4180510.77	2093.52	Top "A"	435388.03	4180153.70	2079.44	LJHMSB	436728.12	4179939.95	2012.42
Top "A"	434145.60	4180513.65	2092.24	Top "A"	435379.12	4180150.91	2079.66	LJHMSB	436732.01	4179942.34	2014.35
Top "A"	434140.73	4180513.75	2092.86	Top "A"	435375.42	4180154.72	2078.65	LJHMSB	436738.94	4179948.54	2013.34
Top "A"	434136.05	4180513.37	2092.88	Top "A"	435364.94	4180155.98	2078.30	LJHMSB	436746.54	4179955.17	2012.50
Top "A"	434167.19	4180489.23	2091.43	Top "A"	435358.76	4180163.44	2079.68	LJHMSB	436752.19	4179959.49	2013.88
Top "A"	434157.61	4180502.73	2093.84	Top "A"	435350.15	4180164.02	2078.55	LJHMSB	436765.55	4179967.73	2013.48
Top "A"	434149.09	4180501.16	2093.36	Top "A"	435341.60	4180169.00	2078.77	LJHMSB	436781.18	4179977.49	2010.81
Top "A"	434143.92	4180504.09	2093.24	Top "A"	435337.86	4180172.66	2079.43	LJHMSB	436791.54	4179990.28	2010.43
Top "A"	434137.31	4180507.57	2093.38	Top "A"	435331.70	4180171.84	2079.44	LJHMSB	436797.30	4179994.75	2008.03
Top "A"	434131.88	4180508.13	2092.62	Top "A"	435323.27	4180171.92	2079.35	LJHMSB	436808.73	4180012.94	2007.30
Top "A"	434129.38	4180507.89	2092.84	Top "A"	435320.90	4180173.23	2079.72	LJHMSB	436822.76	4180028.67	2009.02
Top "A"	434121.23	4180510.28	2092.85	Top "A"	435312.26	4180175.50	2080.96	LJHMSB	436825.81	4180036.23	2006.29
Top "A"	434113.80	4180511.83	2092.58	Top "A"	435301.51	4180176.23	2082.16	LJHMSB	436832.37	4180041.43	2004.95
Top "A"	434107.72	4180515.65	2092.61	Top "A"	435294.87	4180179.77	2081.27	LJHMSB	436839.00	4180053.02	2008.08
Top "A"	434101.44	4180516.43	2092.48	Top "A"	435287.53	4180182.87	2082.14	LJHMSB	436840.24	4180057.64	2008.25
Top "A"	434091.50	4180518.01	2091.35	Top "A"	435280.65	4180184.72	2081.89	LJHMSB	436844.79	4180062.84	2006.86
Top "A"	434081.34	4180523.25	2093.19	Top "A"	435274.30	4180185.35	2080.52	LJHMSB	436848.40	4180068.81	2006.71
LJHMSB	436852.35	4180078.88	2006.86	LJHMSB	437179.69	4180104.87	2014.46	LJHMSB	436797.57	4179364.45	2024.98
LJHMSB	436855.58	4180083.96	2007.60	LJHMSB	437184.62	4180102.45	2012.37	LJHMSB	436801.23	4179359.42	2027.01
LJHMSB	436861.20	4180086.97	2007.58	LJHMSB	437197.58	4180106.53	2012.12	LJHMSB	436810.45	4179356.99	2025.24
LJHMSB	436868.76	4180089.88	2006.17	LJHMSB	437210.08	4180104.62	2012.83	LJHMSB	436819.31	4179353.12	2026.36
LJHMSB	436874.64	4180095.71	2006.35	LJHMSB	437231.87	4180110.05	2012.35	LJHMSB	436833.24	4179351.30	2024.74
LJHMSB	436883.16	4180099.91	2004.85	LJHMSB	437256.43	4180116.52	2014.86	LJHMSB	436843.55	4179353.17	2024.04
LJHMSB	436891.89	4180105.94	2005.56	LJHMSB	437269.46	4180117.37	2014.14	LJHMSB	436850.08	4179349.90	2024.09
LJHMSB	436896.33	4180111.92	2006.03	LJHMSB	437276.97	4180117.47	2012.93	LJHMSB	436853.45	4179348.06	2025.53

Table 5 (continued)

Surface	X	Y	Depth	Surface	X	Y	Depth	Surface	X	Y	Depth
LJHMSB	436903.18	4180116.28	2004.97	LJHMSB	437295.21	4180118.88	2012.44	LJHMSB	436856.40	4179344.72	2025.40
LJHMSB	436912.58	4180122.95	2003.87	LJHMSB	437308.55	4180117.10	2013.43	LJHMSB	436861.20	4179344.42	2026.66
LJHMSB	436922.45	4180127.26	2002.29	LJHMSB	437329.89	4180115.54	2013.43	LJHMSB	436867.96	4179341.37	2026.68
LJHMSB	436925.80	4180128.11	2000.27	LJHMSB	437344.18	4180118.99	2013.43	LJHMSB	436870.91	4179341.19	2025.96
LJHMSB	436930.94	4180130.98	1999.73	LJHMSB	437364.95	4180122.65	2013.88	LJHMSB	436872.80	4179338.57	2025.61
LJHMSB	436943.26	4180134.40	2003.14	LJHMSB	437371.37	4180121.38	2012.83	LJHMSB	436878.59	4179341.23	2028.37
LJHMSB	436950.25	4180135.14	2004.10	LJHMSB	437379.50	4180119.09	2015.16	LJHMSB	436881.05	4179339.85	2027.82
LJHMSB	436954.85	4180136.89	2005.04	LJHMSB	436530.96	4179356.65	2049.33	LJHMSB	436887.72	4179340.31	2028.18
LJHMSB	436963.98	4180139.54	2004.70	LJHMSB	436546.10	4179357.95	2048.81	LJHMSB	436892.60	4179340.51	2030.40
LJHMSB	436966.84	4180140.68	2005.97	LJHMSB	436556.71	4179363.24	2048.64	LJHMSB	436898.91	4179339.69	2030.06
LJHMSB	436975.97	4180140.73	2004.20	LJHMSB	436573.01	4179371.35	2048.28	LJHMSB	436901.30	4179343.59	2033.36
LJHMSB	436991.06	4180137.83	2004.22	LJHMSB	436594.88	4179381.53	2047.07	LJHMSB	436904.53	4179343.04	2034.64
LJHMSB	437000.98	4180134.64	2003.92	LJHMSB	436619.45	4179395.74	2039.84	LJHMSB	436912.43	4179341.13	2035.62
LJHMSB	437021.74	4180131.69	2005.13	LJHMSB	436633.11	4179393.33	2039.06	LJHMSB	436919.75	4179338.57	2039.60
LJHMSB	437027.26	4180125.57	2004.39	LJHMSB	436648.33	4179390.80	2036.76	LJHMSB	436921.09	4179337.90	2038.84
LJHMSB	437034.93	4180117.40	2007.36	LJHMSB	436661.36	4179389.18	2035.21	LJHMSB	436927.11	4179336.15	2038.67
LJHMSB	437043.17	4180116.90	2008.65	LJHMSB	436668.92	4179386.13	2033.34	LJHMSB	436929.33	4179335.88	2037.94
LJHMSB	437050.15	4180117.57	2010.08	LJHMSB	436676.25	4179376.78	2034.60	LJHMSB	436935.53	4179336.23	2036.44
LJHMSB	437063.32	4180111.86	2008.84	LJHMSB	436718.46	4179372.17	2032.28	LJHMSB	436944.11	4179334.08	2038.55
LJHMSB	437063.63	4180111.80	2009.70	LJHMSB	436723.44	4179368.95	2030.53	LJHMSB	436938.56	4179334.41	2037.01
LJHMSB	437077.33	4180108.82	2009.62	LJHMSB	436732.16	4179371.04	2032.73	LJHMSB	436947.75	4179333.28	2036.99
LJHMSB	437083.45	4180109.86	2010.62	LJHMSB	436746.03	4179362.12	2033.27	LJHMSB	436966.67	4179328.82	2034.27
LJHMSB	437092.56	4180107.81	2010.84	LJHMSB	436755.10	4179355.56	2031.46	LJHMSB	436980.40	4179326.70	2037.93
LJHMSB	437096.70	4180103.93	2010.14	LJHMSB	436760.80	4179363.19	2029.99	LJHMSB	436989.67	4179322.73	2038.40
LJHMSB	437114.20	4180103.86	2011.92	LJHMSB	436760.94	4179362.22	2030.19	LJHMSB	436999.85	4179321.62	2038.47
LJHMSB	437136.80	4180106.92	2011.80	LJHMSB	436775.01	4179357.88	2028.93	LJHMSB	437007.33	4179321.31	2038.13
LJHMSB	437140.55	4180103.55	2011.99	LJHMSB	436774.95	4179358.84	2028.69	LJHMSB	437016.76	4179319.96	2038.17
LJHMSB	437147.67	4180098.46	2011.93	LJHMSB	436783.97	4179369.37	2026.87	LJHMSB	437024.49	4179317.66	2038.16
LJHMSB	437158.69	4180101.40	2011.69	LJHMSB	436793.32	4179364.54	2024.77	LJHMSB	437538.16	4179373.94	2015.89
LJHMSB	437530.95	4179378.04	2017.93	LJHMSB	437122.60	4179248.32	2038.19	LJHMSB	436332.64	4179937.43	2047.40
LJHMSB	437517.27	4179382.32	2016.28	LJHMSB	437108.67	4179244.99	2038.21	LJHMSB	436316.84	4179950.48	2053.51

Table 5 (continued)

Surface	X	Y	Depth	Surface	X	Y	Depth	Surface	X	Y	Depth
LJHMSB	437518.84	4179381.03	2017.65	LJHMSB	437094.50	4179245.86	2036.22	LJHMSB	436310.15	4179953.03	2052.40
LJHMSB	437506.64	4179381.86	2016.78	LJHMSB	437083.71	4179245.30	2036.91	LJHMSB	436299.79	4179958.14	2046.81
LJHMSB	437501.53	4179381.15	2016.59	LJHMSB	437069.26	4179246.18	2037.60	LJHMSB	436290.42	4179963.96	2046.57
LJHMSB	437490.32	4179379.75	2017.22	LJHMSB	437054.46	4179243.01	2037.73	LJHMSB	436280.66	4179973.64	2046.61
LJHMSB	437482.67	4179380.68	2017.68	LJHMSB	437037.30	4179234.66	2038.88	LJHMSB	436274.92	4179981.03	2047.85
LJHMSB	437474.32	4179376.99	2016.83	LJHMSB	437032.15	4179239.35	2041.17	LJHMSB	436265.58	4179995.27	2049.22
LJHMSB	437464.70	4179366.20	2018.34	LJHMSB	436615.13	4179946.51	2029.93	LJHMSB	436250.88	4180008.81	2049.02
LJHMSB	437449.74	4179358.64	2020.13	LJHMSB	436607.56	4179948.04	2031.78	LJHMSB	436236.15	4180036.47	2050.12
LJHMSB	437427.16	4179345.82	2021.62	LJHMSB	436593.56	4179948.86	2032.99	LJHMSB	436231.03	4180038.62	2049.73
LJHMSB	437416.95	4179343.96	2021.62	LJHMSB	436567.80	4179953.55	2033.37	LJHMSB	436215.68	4180050.71	2050.20
LJHMSB	437410.47	4179331.75	2022.61	LJHMSB	436566.80	4179942.16	2032.30	LJHMSB	436206.06	4180057.18	2048.41
LJHMSB	437401.83	4179332.42	2022.28	LJHMSB	436558.03	4179941.03	2034.46	LJHMSB	436197.73	4180063.11	2049.24
LJHMSB	437386.49	4179318.34	2023.42	LJHMSB	436546.42	4179938.20	2036.26	LJHMSB	436175.31	4180105.90	2049.42
LJHMSB	437372.68	4179315.93	2023.58	LJHMSB	436538.63	4179937.44	2037.80	LJHMSB	436130.41	4180139.27	2051.36
LJHMSB	437357.55	4179315.89	2024.50	LJHMSB	436529.57	4179932.19	2039.21	LJHMSB	436105.50	4180145.93	2053.25
LJHMSB	437347.08	4179310.37	2025.42	LJHMSB	436516.83	4179926.47	2038.88	LJHMSB	436086.24	4180150.67	2052.32
LJHMSB	437338.48	4179308.05	2025.80	LJHMSB	436503.16	4179917.08	2038.91	LJHMSB	436044.86	4180164.49	2053.29
LJHMSB	437327.71	4179302.64	2025.62	LJHMSB	436488.77	4179914.30	2039.68	LJHMSB	435975.21	4180203.65	2056.82
LJHMSB	437312.35	4179298.82	2027.45	LJHMSB	436479.27	4179913.03	2040.12	LJHMSB	435401.47	4179189.26	2085.75
LJHMSB	437300.09	4179294.10	2028.38	LJHMSB	436470.33	4179910.29	2039.62	LJHMSB	435375.18	4179198.39	2083.86
LJHMSB	437281.00	4179290.91	2029.16	LJHMSB	436454.76	4179907.79	2041.55	LJHMSB	435368.64	4179190.01	2087.87
LJHMSB	437275.37	4179290.27	2029.32	LJHMSB	436441.34	4179910.25	2044.53	LJHMSB	435359.38	4179188.65	2085.79
LJHMSB	437263.15	4179278.12	2030.61	LJHMSB	436430.37	4179911.70	2042.99	LJHMSB	435351.81	4179175.82	2083.23
LJHMSB	437255.11	4179277.83	2030.78	LJHMSB	436423.81	4179913.55	2043.05	LJHMSB	435337.98	4179169.29	2082.69
LJHMSB	437243.40	4179276.05	2031.35	LJHMSB	436417.92	4179912.30	2043.65	LJHMSB	435318.17	4179167.65	2082.06
LJHMSB	437229.86	4179278.66	2031.18	LJHMSB	436407.67	4179910.33	2044.26	LJHMSB	435290.98	4179166.10	2084.22
LJHMSB	437223.66	4179275.75	2033.07	LJHMSB	436404.69	4179912.22	2045.10	LJHMSB	435256.73	4179149.98	2091.59
LJHMSB	437216.82	4179268.92	2029.68	LJHMSB	436391.79	4179918.89	2047.64	LJHMSB	435245.05	4179143.71	2091.59
LJHMSB	437203.60	4179268.03	2030.26	LJHMSB	436386.73	4179918.71	2046.39	LJHMSB	435238.52	4179139.49	2092.91
LJHMSB	437193.82	4179266.76	2030.79	LJHMSB	436377.37	4179920.61	2047.68	LJHMSB	435230.13	4179133.96	2091.99
LJHMSB	437176.96	4179260.83	2031.16	LJHMSB	436365.29	4179919.79	2045.58	LJHMSB	435214.48	4179128.16	2094.01

Table 5 (continued)

Surface	X	Y	Depth
LJHMSB	437167.26	4179261.14	2032.69
LJHMSB	437152.09	4179259.63	2033.57
LJHMSB	437139.70	4179255.10	2037.42
LJHMSB	437133.65	4179246.52	2039.28
LJHMSB	435159.78	4179103.75	2092.20
LJHMSB	435140.65	4179097.95	2094.43
LJHMSB	435128.02	4179097.69	2096.05
LJHMSB	435108.38	4179085.28	2097.47
LJHMSB	435089.01	4179079.94	2098.78
LJHMSB	435077.38	4179075.52	2099.19
LJHMSB	435060.58	4179060.53	2096.89
LJHMSB	435041.18	4179059.01	2098.96
LJHMSB	435018.09	4179038.30	2101.41
LJHMSB	434989.65	4179023.37	2104.04
LJHMSB	434969.32	4179025.76	2099.71
LJHMSB	434917.24	4179004.57	2102.74
LJHMSB	436551.35	4179411.94	2048.17
LJHMSB	436537.67	4179411.91	2047.15
LJHMSB	436532.40	4179411.10	2047.81
LJHMSB	436524.58	4179408.04	2049.17
LJHMSB	436518.67	4179405.17	2049.35
LJHMSB	436511.73	4179405.46	2048.76
LJHMSB	436502.84	4179406.09	2049.89
LJHMSB	436494.20	4179402.73	2050.42
LJHMSB	436485.91	4179398.16	2049.90
LJHMSB	436479.13	4179368.39	2051.51
LJHMSB	436467.78	4179350.32	2055.27
LJHMSB	436467.11	4179340.90	2054.21
LJHMSB	436458.57	4179338.27	2051.31
LJHMSB	436449.18	4179331.55	2051.56
LJHMSB	436442.89	4179329.52	2052.75
LJHMSB	436360.34	4179923.68	2046.39
LJHMSB	436351.77	4179924.81	2046.82
LJHMSB	436346.77	4179930.44	2048.02
LJHMSB	436339.61	4179934.50	2047.93
LJHMSB	436262.74	4179346.80	2058.79
LJHMSB	436243.64	4179338.66	2061.33
LJHMSB	436233.26	4179339.21	2062.54
LJHMSB	436217.32	4179338.67	2061.64
LJHMSB	436206.58	4179303.35	2066.94
LJHMSB	436188.76	4179307.50	2063.37
LJHMSB	436180.10	4179308.61	2062.70
LJHMSB	436136.68	4179280.53	2073.08
LJHMSB	436108.54	4179257.07	2065.21
LJHMSB	436094.89	4179248.64	2065.83
LJHMSB	436069.76	4179251.20	2065.69
LJHMSB	436049.44	4179249.92	2070.71
LJHMSB	436041.81	4179259.27	2067.53
LJHMSB	435971.89	4179213.52	2068.19
LJHMSB	435805.91	4179085.13	2064.26
LJHMSB	434820.16	4180351.05	2108.14
LJHMSB	434836.95	4180343.66	2105.34
LJHMSB	434848.71	4180339.97	2101.71
LJHMSB	434857.25	4180339.69	2099.86
LJHMSB	434874.74	4180332.44	2097.13
LJHMSB	434887.25	4180333.25	2097.72
LJHMSB	434906.57	4180319.17	2095.59
LJHMSB	434921.38	4180314.07	2094.22
LJHMSB	434943.34	4180300.54	2090.92
LJHMSB	434953.27	4180299.15	2088.98
LJHMSB	434964.90	4180293.40	2089.28
LJHMSB	434976.87	4180287.75	2089.47
LJHMSB	435202.96	4179115.69	2090.74
LJHMSB	435196.58	4179116.45	2091.29
LJHMSB	435181.11	4179110.21	2095.95
LJHMSB	435168.35	4179106.24	2094.64
LJHMSB	435083.58	4180267.71	2093.00
LJHMSB	435086.52	4180266.19	2094.28
LJHMSB	435086.31	4180264.97	2094.60
LJHMSB	435093.08	4180262.58	2095.43
LJHMSB	435101.00	4180263.87	2099.40
LJHMSB	435112.30	4180256.09	2099.70
LJHMSB	435116.86	4180253.46	2101.67
LJHMSB	435128.12	4180244.61	2100.39
LJHMSB	435137.43	4180243.26	2100.11
LJHMSB	435145.73	4180240.49	2100.08
LJHMSB	435152.19	4180238.37	2099.23
LJHMSB	435156.27	4180233.87	2098.36
LJHMSB	435163.47	4180231.70	2097.53
LJHMSB	435167.94	4180231.51	2095.78
LJHMSB	435174.47	4180229.14	2094.48
LJHMSB	435182.36	4180225.56	2093.43
LJHMSB	435186.24	4180222.78	2092.59
LJHMSB	435193.22	4180213.96	2090.64
LJHMSB	435188.44	4179950.19	2016.96
LJHMSB	435200.55	4180212.65	2090.82
LJHMSB	435211.79	4180204.87	2089.83
LJHMSB	435215.10	4180202.22	2090.59
LJHMSB	435215.74	4180204.09	2091.14
LJHMSB	435219.63	4180202.93	2089.98
LJHMSB	435225.79	4180199.04	2089.60
LJHMSB	435236.75	4180200.21	2089.97
LJHMSB	434830.53	4180378.72	2107.07

Table 5 (continued)

Surface	X	Y	Depth	Surface	X	Y	Depth	Surface	X	Y	Depth
LJHMSB	436430.54	4179302.41	2053.55	LJHMSB	434991.48	4180291.65	2090.14	LJHMSB	434817.97	4180382.45	2108.97
LJHMSB	436421.28	4179293.79	2054.50	LJHMSB	435003.59	4180288.15	2089.17	LJHMSB	434804.22	4180383.54	2109.27
LJHMSB	436406.53	4179277.64	2055.17	LJHMSB	435011.71	4180284.29	2089.85	LJHMSB	434798.54	4180385.25	2108.17
LJHMSB	436387.87	4179267.82	2056.67	LJHMSB	435019.13	4180281.36	2089.35	LJHMSB	434790.95	4180387.95	2109.71
LJHMSB	436366.04	4179267.81	2054.20	LJHMSB	435026.51	4180279.56	2088.40	LJHMSB	434784.46	4180390.35	2109.58
LJHMSB	436314.41	4179343.95	2055.19	LJHMSB	435037.95	4180276.19	2087.49	LJHMSB	434775.88	4180391.97	2108.59
LJHMSB	436305.59	4179344.38	2055.22	LJHMSB	435053.98	4180271.97	2088.00	LJHMSB	434771.17	4180394.11	2109.18
LJHMSB	436297.08	4179347.40	2055.83	LJHMSB	435065.04	4180270.33	2090.60	LJHMSB	434766.70	4180394.40	2109.47
LJHMSB	436289.14	4179347.60	2056.73	LJHMSB	435072.31	4180269.64	2091.17	LJHMSB	434760.53	4180394.99	2110.01
LJHMSB	436274.07	4179347.45	2058.24	LJHMSB	435073.99	4180272.04	2092.77	LJHMSB	434751.93	4180392.45	2107.38
LJHMSB	434744.92	4180391.09	2106.55	LJHMSB	436423.81	4179913.55	2043.05	LJHMSB	435337.98	4179169.29	2082.69
LJHMSB	434740.71	4180391.65	2107.75	LJHMSB	436417.92	4179912.30	2043.65	LJHMSB	435318.17	4179167.65	2082.06
LJHMSB	434734.48	4180394.76	2107.61	LJHMSB	436407.67	4179910.33	2044.26	LJHMSB	435290.98	4179166.10	2084.22
LJHMSB	434724.93	4180393.91	2106.22	LJHMSB	436404.69	4179912.22	2045.10	LJHMSB	435256.73	4179149.98	2091.59
LJHMSB	434719.86	4180395.48	2106.37	LJHMSB	436391.79	4179918.89	2047.64	LJHMSB	435245.05	4179143.71	2091.59
LJHMSB	434716.24	4180395.70	2106.81	LJHMSB	436386.73	4179918.71	2046.39	LJHMSB	435238.52	4179139.49	2092.91
LJHMSB	434710.88	4180396.43	2106.79	LJHMSB	436377.37	4179920.61	2047.68	LJHMSB	435230.13	4179133.96	2091.99
LJHMSB	434708.84	4180397.31	2106.40	LJHMSB	436365.29	4179919.79	2045.58	LJHMSB	435214.48	4179128.16	2094.01
LJHMSB	434704.27	4180397.83	2106.43	LJHMSB	436360.34	4179923.68	2046.39	LJHMSB	435202.96	4179115.69	2090.74
LJHMSB	434696.46	4180401.08	2104.95	LJHMSB	436351.77	4179924.81	2046.82	LJHMSB	435196.58	4179116.45	2091.29
LJHMSB	434700.28	4180399.72	2106.14	LJHMSB	436346.77	4179930.44	2048.02	LJHMSB	435181.11	4179110.21	2095.95
LJHMSB	434696.74	4180402.89	2105.40	LJHMSB	436339.61	4179934.50	2047.93	LJHMSB	435168.35	4179106.24	2094.64
LJHMSB	434693.12	4180403.71	2106.09	LJHMSB	436332.64	4179937.43	2047.40	LJHMSB	435159.78	4179103.75	2092.20
LJHMSB	434688.99	4180404.13	2105.48	LJHMSB	436316.84	4179950.48	2053.51	LJHMSB	435140.65	4179097.95	2094.43
LJHMSB	434682.30	4180404.81	2105.13	LJHMSB	436310.15	4179953.03	2052.40	LJHMSB	435128.02	4179097.69	2096.05
LJHMSB	434680.53	4180406.71	2103.91	LJHMSB	436299.79	4179958.14	2046.81	LJHMSB	435108.38	4179085.28	2097.47
LJHMSB	434672.13	4180407.99	2102.92	LJHMSB	436290.42	4179963.96	2046.57	LJHMSB	435089.01	4179079.94	2098.78
LJHMSB	434668.00	4180407.88	2102.67	LJHMSB	436280.66	4179973.64	2046.61	LJHMSB	435077.38	4179075.52	2099.19
LJHMSB	434661.87	4180408.83	2103.41	LJHMSB	436274.92	4179981.03	2047.85	LJHMSB	435060.58	4179060.53	2096.89
LJHMSB	434655.84	4180410.68	2104.00	LJHMSB	436265.58	4179995.27	2049.22	LJHMSB	435041.18	4179059.01	2098.96
LJHMSB	434651.78	4180410.73	2103.87	LJHMSB	436250.88	4180008.81	2049.02	LJHMSB	435018.09	4179038.30	2101.41

Table 5 (continued)

Surface	X	Y	Depth	Surface	X	Y	Depth	Surface	X	Y	Depth
LJHMSB	434649.54	4180410.51	2103.36	LJHMSB	436236.15	4180036.47	2050.12	LJHMSB	434989.65	4179023.37	2104.04
LJHMSB	434645.68	4180412.37	2104.14	LJHMSB	436231.03	4180038.62	2049.73	LJHMSB	434969.32	4179025.76	2099.71
LJHMSB	434637.99	4180412.87	2104.11	LJHMSB	436215.68	4180050.71	2050.20	LJHMSB	434917.24	4179004.57	2102.74
LJHMSB	434634.68	4180412.85	2104.82	LJHMSB	436206.06	4180057.18	2048.41	LJHMSB	436551.35	4179411.94	2048.17
LJHMSB	436558.03	4179941.03	2034.46	LJHMSB	436197.73	4180063.11	2049.24	LJHMSB	436537.67	4179411.91	2047.15
LJHMSB	436546.42	4179938.20	2036.26	LJHMSB	436175.31	4180105.90	2049.42	LJHMSB	436532.40	4179411.10	2047.81
LJHMSB	436538.63	4179937.44	2037.80	LJHMSB	436130.41	4180139.27	2051.36	LJHMSB	436524.58	4179408.04	2049.17
LJHMSB	436529.57	4179932.19	2039.21	LJHMSB	436105.50	4180145.93	2053.25	LJHMSB	436518.67	4179405.17	2049.35
LJHMSB	436516.83	4179926.47	2038.88	LJHMSB	436086.24	4180150.67	2052.32	LJHMSB	436511.73	4179405.46	2048.76
LJHMSB	436503.16	4179917.08	2038.91	LJHMSB	436044.86	4180164.49	2053.29	LJHMSB	436502.84	4179406.09	2049.89
LJHMSB	436488.77	4179914.30	2039.68	LJHMSB	435975.21	4180203.65	2056.82	LJHMSB	436494.20	4179402.73	2050.42
LJHMSB	436479.27	4179913.03	2040.12	LJHMSB	435401.47	4179189.26	2085.75	LJHMSB	436485.91	4179398.16	2049.90
LJHMSB	436470.33	4179910.29	2039.62	LJHMSB	435375.18	4179198.39	2083.86	LJHMSB	436479.13	4179368.39	2051.51
LJHMSB	436454.76	4179907.79	2041.55	LJHMSB	435368.64	4179190.01	2087.87	LJHMSB	436467.78	4179350.32	2055.27
LJHMSB	436441.34	4179910.25	2044.53	LJHMSB	435359.38	4179188.65	2085.79	LJHMSB	436467.11	4179340.90	2054.21
LJHMSB	436430.37	4179911.70	2042.99	LJHMSB	435351.81	4179175.82	2083.23	LJHMSB	436458.57	4179338.27	2051.31
LJHMSB	436449.18	4179331.55	2051.56	LJHMSB	434964.90	4180293.40	2089.28	LJHMSB	435236.75	4180200.21	2089.97
LJHMSB	436442.89	4179329.52	2052.75	LJHMSB	434976.87	4180287.75	2089.47	LJHMSB	434830.53	4180378.72	2107.07
LJHMSB	436430.54	4179302.41	2053.55	LJHMSB	434991.48	4180291.65	2090.14	LJHMSB	434817.97	4180382.45	2108.97
LJHMSB	436421.28	4179293.79	2054.50	LJHMSB	435003.59	4180288.15	2089.17	LJHMSB	434804.22	4180383.54	2109.27
LJHMSB	436406.53	4179277.64	2055.17	LJHMSB	435011.71	4180284.29	2089.85	LJHMSB	434798.54	4180385.25	2108.17
LJHMSB	436387.87	4179267.82	2056.67	LJHMSB	435019.13	4180281.36	2089.35	LJHMSB	434790.95	4180387.95	2109.71
LJHMSB	436366.04	4179267.81	2054.20	LJHMSB	435026.51	4180279.56	2088.40	LJHMSB	434784.46	4180390.35	2109.58
LJHMSB	436314.41	4179343.95	2055.19	LJHMSB	435037.95	4180276.19	2087.49	LJHMSB	434775.88	4180391.97	2108.59
LJHMSB	436305.59	4179344.38	2055.22	LJHMSB	435053.98	4180271.97	2088.00	LJHMSB	434771.17	4180394.11	2109.18
LJHMSB	436297.08	4179347.40	2055.83	LJHMSB	435065.04	4180270.33	2090.60	LJHMSB	434766.70	4180394.40	2109.47
LJHMSB	436289.14	4179347.60	2056.73	LJHMSB	435072.31	4180269.64	2091.17	LJHMSB	434760.53	4180394.99	2110.01
LJHMSB	436274.07	4179347.45	2058.24	LJHMSB	435073.99	4180272.04	2092.77	LJHMSB	434751.93	4180392.45	2107.38
LJHMSB	436262.74	4179346.80	2058.79	LJHMSB	435083.58	4180267.71	2093.00	LJHMSB	434744.92	4180391.09	2106.55
LJHMSB	436243.64	4179338.66	2061.33	LJHMSB	435086.52	4180266.19	2094.28	LJHMSB	434740.71	4180391.65	2107.75
LJHMSB	436233.26	4179339.21	2062.54	LJHMSB	435086.31	4180264.97	2094.60	LJHMSB	434734.48	4180394.76	2107.61

Table 5 (continued)

Surface	X	Y	Depth	Surface	X	Y	Depth	Surface	X	Y	Depth
LJHMSB	436217.32	4179338.67	2061.64	LJHMSB	435093.08	4180262.58	2095.43	LJHMSB	434724.93	4180393.91	2106.22
LJHMSB	436206.58	4179303.35	2066.94	LJHMSB	435101.00	4180263.87	2099.40	LJHMSB	434719.86	4180395.48	2106.37
LJHMSB	436188.76	4179307.50	2063.37	LJHMSB	435112.30	4180256.09	2099.70	LJHMSB	434716.24	4180395.70	2106.81
LJHMSB	436180.10	4179308.61	2062.70	LJHMSB	435116.86	4180253.46	2101.67	LJHMSB	434710.88	4180396.43	2106.79
LJHMSB	436136.68	4179280.53	2073.08	LJHMSB	435128.12	4180244.61	2100.39	LJHMSB	434708.84	4180397.31	2106.40
LJHMSB	436108.54	4179257.07	2065.21	LJHMSB	435137.43	4180243.26	2100.11	LJHMSB	434704.27	4180397.83	2106.43
LJHMSB	436094.89	4179248.64	2065.83	LJHMSB	435145.73	4180240.49	2100.08	LJHMSB	434696.46	4180401.08	2104.95
LJHMSB	436069.76	4179251.20	2065.69	LJHMSB	435152.19	4180238.37	2099.23	LJHMSB	434700.28	4180399.72	2106.14
LJHMSB	436049.44	4179249.92	2070.71	LJHMSB	435156.27	4180233.87	2098.36	LJHMSB	434696.74	4180402.89	2105.40
LJHMSB	436041.81	4179259.27	2067.53	LJHMSB	435163.47	4180231.70	2097.53	LJHMSB	434693.12	4180403.71	2106.09
LJHMSB	435971.89	4179213.52	2068.19	LJHMSB	435167.94	4180231.51	2095.78	LJHMSB	434688.99	4180404.13	2105.48
LJHMSB	435805.91	4179085.13	2064.26	LJHMSB	435174.47	4180229.14	2094.48	LJHMSB	434682.30	4180404.81	2105.13
LJHMSB	434820.16	4180351.05	2108.14	LJHMSB	435182.36	4180225.56	2093.43	LJHMSB	434680.53	4180406.71	2103.91
LJHMSB	434836.95	4180343.66	2105.34	LJHMSB	435186.24	4180222.78	2092.59	LJHMSB	434672.13	4180407.99	2102.92
LJHMSB	434848.71	4180339.97	2101.71	LJHMSB	435193.22	4180213.96	2090.64	LJHMSB	434668.00	4180407.88	2102.67
LJHMSB	434857.25	4180339.69	2099.86	LJHMSB	435188.44	4179950.19	2016.96	LJHMSB	434661.87	4180408.83	2103.41
LJHMSB	434874.74	4180332.44	2097.13	LJHMSB	435200.55	4180212.65	2090.82	LJHMSB	434655.84	4180410.68	2104.00
LJHMSB	434887.25	4180333.25	2097.72	LJHMSB	435211.79	4180204.87	2089.83	LJHMSB	434651.78	4180410.73	2103.87
LJHMSB	434906.57	4180319.17	2095.59	LJHMSB	435215.10	4180202.22	2090.59	LJHMSB	434649.54	4180410.51	2103.36
LJHMSB	434921.38	4180314.07	2094.22	LJHMSB	435215.74	4180204.09	2091.14	LJHMSB	434645.68	4180412.37	2104.14
LJHMSB	434943.34	4180300.54	2090.92	LJHMSB	435219.63	4180202.93	2089.98	LJHMSB	434637.99	4180412.87	2104.11
LJHMSB	434953.27	4180299.15	2088.98	LJHMSB	435225.79	4180199.04	2089.60	LJHMSB	434634.68	4180412.85	2104.82
LJHMSB	434629.55	4180413.00	2105.60	LJHMSB	434382.18	4180479.42	2116.97	LJHMSB	434126.02	4180519.83	2110.01
LJHMSB	434621.05	4180415.96	2105.99	LJHMSB	434364.02	4180472.94	2114.26	LJHMSB	434183.07	4180488.46	2110.74
LJHMSB	434614.39	4180415.22	2105.48	LJHMSB	434361.59	4180474.91	2115.03	LJHMSB	434172.97	4180500.05	2113.24
LJHMSB	434607.99	4180415.96	2105.80	LJHMSB	434340.34	4180454.74	2109.95	LJHMSB	434169.57	4180496.67	2110.46
LJHMSB	434604.96	4180416.31	2106.76	LJHMSB	434335.70	4180452.75	2109.13	LJHMSB	434158.70	4180511.63	2114.45
LJHMSB	434599.97	4180417.01	2106.29	LJHMSB	434331.57	4180456.75	2109.83	LJHMSB	434152.04	4180503.57	2111.06
LJHMSB	434594.31	4180419.29	2107.07	LJHMSB	434326.84	4180458.19	2111.41	LJHMSB	434143.35	4180512.60	2111.00
LJHMSB	434581.47	4180421.12	2106.89	LJHMSB	434322.58	4180457.73	2111.43	LJHMSB	434139.64	4180510.50	2109.25
LJHMSB	434578.39	4180420.67	2106.11	LJHMSB	434317.56	4180456.70	2114.29	LJHMSB	434136.19	4180512.44	2109.26

Table 5 (continued)

Surface	X	Y	Depth	Surface	X	Y	Depth	Surface	X	Y	Depth
LJHMSB	434572.59	4180421.52	2105.81	LJHMSB	434307.94	4180454.82	2114.30	LJHMSB	434129.75	4180516.09	2110.16
LJHMSB	434565.04	4180420.77	2106.94	LJHMSB	434300.94	4180455.08	2113.00	LJHMSB	434124.67	4180512.14	2109.74
LJHMSB	434561.71	4180415.36	2107.55	LJHMSB	434293.38	4180455.39	2113.00	LJHMSB	434119.59	4180514.62	2110.15
LJHMSB	434555.91	4180419.46	2108.17	LJHMSB	434289.34	4180455.75	2112.53	LJHMSB	434105.60	4180524.83	2110.63
LJHMSB	434549.33	4180420.19	2109.31	LJHMSB	434287.23	4180456.69	2113.28	LJHMSB	434101.80	4180524.18	2109.88
LJHMSB	434545.16	4180416.40	2109.18	LJHMSB	434281.58	4180456.78	2112.35	LJHMSB	434095.53	4180527.74	2113.52
LJHMSB	434540.65	4180416.97	2109.31	LJHMSB	434277.31	4180460.87	2113.90	LJHMSB	434088.52	4180530.11	2112.28
LJHMSB	434536.13	4180420.56	2109.32	LJHMSB	434278.99	4180462.30	2114.27	LJHMSB	434082.47	4180525.47	2111.42
LJHMSB	434530.99	4180419.98	2107.90	LJHMSB	434275.47	4180463.80	2114.14	LJHMSB	434076.91	4180526.07	2110.10
LJHMSB	434525.94	4180421.05	2107.31	LJHMSB	434273.21	4180465.93	2113.95	LJHMSB	434064.20	4180530.06	2110.08
LJHMSB	434520.26	4180423.22	2108.36	LJHMSB	434268.22	4180469.95	2113.86	LJHMSB	434057.91	4180533.11	2110.53
LJHMSB	434515.25	4180423.71	2108.09	LJHMSB	434259.46	4180470.15	2109.61	LJHMSB	434048.31	4180536.48	2110.30
LJHMSB	434510.43	4180427.48	2108.92	LJHMSB	434255.65	4180467.01	2109.11	LJHMSB	434041.06	4180535.26	2109.29
LJHMSB	434494.24	4180424.58	2107.78	LJHMSB	434250.12	4180471.69	2109.03	LJHMSB	434032.82	4180538.03	2109.27
LJHMSB	434481.06	4180429.34	2107.77	LJHMSB	434243.77	4180475.22	2110.95	LJHMSB	434024.01	4180544.20	2109.29
LJHMSB	434472.57	4180431.04	2108.06	LJHMSB	434239.00	4180476.37	2110.50	LJHMSB	434019.16	4180544.22	2109.41
LJHMSB	434462.69	4180434.24	2107.71	LJHMSB	434233.91	4180476.74	2109.35	LJHMSB	434007.96	4180548.68	2108.61
LJHMSB	434456.55	4180436.00	2108.21	LJHMSB	434228.87	4180478.43	2111.35	LJHMSB	433999.79	4180551.16	2108.18
LJHMSB	434451.48	4180434.42	2109.08	LJHMSB	434219.41	4180483.70	2111.88	LJHMSB	433994.51	4180547.12	2106.19
LJHMSB	434445.87	4180431.73	2108.20	LJHMSB	434209.44	4180488.69	2110.07	LJHMSB	433984.43	4180550.23	2106.86
LJHMSB	434441.59	4180428.14	2108.67	LJHMSB	434201.22	4180486.56	2108.91	LJHMSB	433983.60	4180548.14	2106.63
LJHMSB	434424.38	4180435.62	2108.67	LJHMSB	434193.90	4180490.91	2109.21	LJHMSB	433958.28	4180564.64	2107.89
LJHMSB	434421.08	4180433.71	2107.75	LJHMSB	434182.74	4180499.61	2109.08	LJHMSB	433943.34	4180566.09	2106.44
LJHMSB	434462.69	4180469.76	2119.16	LJHMSB	434172.43	4180511.11	2108.38	LJHMSB	433932.41	4180565.13	2106.31
LJHMSB	434452.68	4180469.50	2121.29	LJHMSB	434165.62	4180507.89	2110.74	LJHMSB	433928.86	4180563.24	2104.96
LJHMSB	434430.82	4180459.89	2119.46	LJHMSB	434153.84	4180515.78	2110.87	LJHMSB	433925.95	4180561.77	2104.39
LJHMSB	434402.37	4180467.69	2119.59	LJHMSB	434147.09	4180516.70	2109.07	LJHMSB	433917.53	4180560.04	2104.57
LJHMSB	434392.28	4180481.48	2118.80	LJHMSB	434271.39	4180277.41	2022.49	LJHMSB	433895.11	4180572.45	2106.85
LJHMSB	433879.33	4180569.61	2106.98	LJHMSB	435240.87	4180202.26	2091.54	LJHMSB	434494.24	4180424.58	2107.78
LJHMSB	435432.72	4180155.43	2083.69	LJHMSB	435236.62	4180199.35	2090.01	LJHMSB	434481.06	4180429.34	2107.77
LJHMSB	435424.88	4180156.79	2083.77	LJHMSB	435230.68	4180201.32	2090.73	LJHMSB	434472.57	4180431.04	2108.06

Table 5 (continued)

Surface	X	Y	Depth
LJHMSB	435421.79	4180157.02	2084.45
LJHMSB	435413.73	4180157.83	2086.10
LJHMSB	435416.80	4180167.34	2092.74
LJHMSB	435395.90	4180152.63	2090.93
LJHMSB	435389.09	4180156.59	2090.93
LJHMSB	435383.73	4180161.95	2090.44
LJHMSB	435381.51	4180164.00	2090.44
LJHMSB	435369.13	4180164.30	2089.47
LJHMSB	435362.23	4180165.86	2090.26
LJHMSB	435358.58	4180167.54	2090.07
LJHMSB	435356.15	4180170.71	2090.26
LJHMSB	435350.71	4180169.19	2091.60
LJHMSB	435345.13	4180172.12	2091.31
LJHMSB	435341.34	4180175.74	2092.12
LJHMSB	435331.10	4180175.70	2089.01
LJHMSB	435327.33	4180175.00	2086.80
LJHMSB	435320.52	4180172.71	2085.83
LJHMSB	435315.44	4180175.71	2085.86
LJHMSB	435310.58	4180177.22	2086.03
LJHMSB	435305.48	4180177.25	2084.86
LJHMSB	435299.73	4180177.79	2084.72
LJHMSB	435295.21	4180179.69	2084.64
LJHMSB	435291.16	4180182.51	2085.38
LJHMSB	435290.75	4180183.90	2085.13
LJHMSB	435284.17	4180185.57	2085.32
LJHMSB	435280.74	4180185.35	2085.84
LJHMSB	435276.38	4180186.28	2086.09
LJHMSB	435271.46	4180188.24	2085.66
LJHMSB	435262.75	4180192.85	2087.54
LJHMSB	435254.34	4180187.73	2087.83
LJHMSB	435186.26	4179950.52	2017.67
LJHMSB	435226.28	4180199.15	2089.91
LJHMSB	435222.09	4180200.94	2090.23
LJHMSB	435219.54	4180201.93	2090.88
LJHMSB	435214.81	4180203.49	2091.15
LJHMSB	435209.42	4180208.15	2091.37
LJHMSB	435204.62	4180210.61	2090.97
LJHMSB	435199.77	4180213.78	2092.25
LJHMSB	435195.96	4180213.26	2089.98
LJHMSB	435190.66	4180224.27	2091.96
LJHMSB	435188.76	4180225.26	2092.25
LJHMSB	435183.49	4180226.47	2093.11
LJHMSB	435181.53	4180229.10	2093.34
LJHMSB	434629.55	4180413.00	2105.60
LJHMSB	434621.05	4180415.96	2105.99
LJHMSB	434614.39	4180415.22	2105.48
LJHMSB	434607.99	4180415.96	2105.80
LJHMSB	434604.96	4180416.31	2106.76
LJHMSB	434599.97	4180417.01	2106.29
LJHMSB	434594.31	4180419.29	2107.07
LJHMSB	434581.47	4180421.12	2106.89
LJHMSB	434578.39	4180420.67	2106.11
LJHMSB	434572.59	4180421.52	2105.81
LJHMSB	434565.04	4180420.77	2106.94
LJHMSB	434561.71	4180415.36	2107.55
LJHMSB	434555.91	4180419.46	2108.17
LJHMSB	434549.33	4180420.19	2109.31
LJHMSB	434545.16	4180416.40	2109.18
LJHMSB	434540.65	4180416.97	2109.31
LJHMSB	434536.13	4180420.56	2109.32
LJHMSB	434530.99	4180419.98	2107.90
LJHMSB	434525.94	4180421.05	2107.31
LJHMSB	434462.69	4180434.24	2107.71
LJHMSB	434456.55	4180436.00	2108.21
LJHMSB	434451.48	4180434.42	2109.08
LJHMSB	434445.87	4180431.73	2108.20
LJHMSB	434441.59	4180428.14	2108.67
LJHMSB	434424.38	4180435.62	2108.67
LJHMSB	434421.08	4180433.71	2107.75
LJHMSB	434462.69	4180469.76	2119.16
LJHMSB	434452.68	4180469.50	2121.29
LJHMSB	434430.82	4180459.89	2119.46
LJHMSB	434402.37	4180467.69	2119.59
LJHMSB	434392.28	4180481.48	2118.80
LJHMSB	434382.18	4180479.42	2116.97
LJHMSB	434364.02	4180472.94	2114.26
LJHMSB	434361.59	4180474.91	2115.03
LJHMSB	434340.34	4180454.74	2109.95
LJHMSB	434335.70	4180452.75	2109.13
LJHMSB	434331.57	4180456.75	2109.83
LJHMSB	434326.84	4180458.19	2111.41
LJHMSB	434322.58	4180457.73	2111.43
LJHMSB	434317.56	4180456.70	2114.29
LJHMSB	434307.94	4180454.82	2114.30
LJHMSB	434300.94	4180455.08	2113.00
LJHMSB	434293.38	4180455.39	2113.00
LJHMSB	434289.34	4180455.75	2112.53
LJHMSB	434287.23	4180456.69	2113.28
LJHMSB	434281.58	4180456.78	2112.35
LJHMSB	434277.31	4180460.87	2113.90
LJHMSB	434278.99	4180462.30	2114.27
LJHMSB	434275.47	4180463.80	2114.14
LJHMSB	434273.21	4180465.93	2113.95

Table 5 (continued)

Surface	X	Y	Depth	Surface	X	Y	Depth	Surface	X	Y	Depth
LJHMSB	435254.17	4180198.09	2090.81	LJHMSB	434520.26	4180423.22	2108.36	LJHMSB	434268.22	4180469.95	2113.86
LJHMSB	435248.46	4180199.34	2091.71	LJHMSB	434515.25	4180423.71	2108.09	LJHMSB	434259.46	4180470.15	2109.61
LJHMSB	435243.90	4180201.44	2091.97	LJHMSB	434510.43	4180427.48	2108.92	LJHMSB	434255.65	4180467.01	2109.11
LJHMSB	434250.12	4180471.69	2109.03	LJHMSB	434032.82	4180538.03	2109.27	LJHMSB	435305.48	4180177.25	2084.86
LJHMSB	434243.77	4180475.22	2110.95	LJHMSB	434024.01	4180544.20	2109.29	LJHMSB	435299.73	4180177.79	2084.72
LJHMSB	434239.00	4180476.37	2110.50	LJHMSB	434019.16	4180544.22	2109.41	LJHMSB	435295.21	4180179.69	2084.64
LJHMSB	434233.91	4180476.74	2109.35	LJHMSB	434007.96	4180548.68	2108.61	LJHMSB	435291.16	4180182.51	2085.38
LJHMSB	434228.87	4180478.43	2111.35	LJHMSB	433999.79	4180551.16	2108.18	LJHMSB	435290.75	4180183.90	2085.13
LJHMSB	434219.41	4180483.70	2111.88	LJHMSB	433994.51	4180547.12	2106.19	LJHMSB	435284.17	4180185.57	2085.32
LJHMSB	434209.44	4180488.69	2110.07	LJHMSB	433984.43	4180550.23	2106.86	LJHMSB	435280.74	4180185.35	2085.84
LJHMSB	434201.22	4180486.56	2108.91	LJHMSB	433983.60	4180548.14	2106.63	LJHMSB	435276.38	4180186.28	2086.09
LJHMSB	434193.90	4180490.91	2109.21	LJHMSB	433958.28	4180564.64	2107.89	LJHMSB	435271.46	4180188.24	2085.66
LJHMSB	434182.74	4180499.61	2109.08	LJHMSB	433943.34	4180566.09	2106.44	LJHMSB	435262.75	4180192.85	2087.54
LJHMSB	434172.43	4180511.11	2108.38	LJHMSB	433932.41	4180565.13	2106.31	LJHMSB	435254.34	4180187.73	2087.83
LJHMSB	434165.62	4180507.89	2110.74	LJHMSB	433928.86	4180563.24	2104.96	LJHMSB	435186.26	4179950.52	2017.67
LJHMSB	434153.84	4180515.78	2110.87	LJHMSB	433925.95	4180561.77	2104.39	LJHMSB	435254.17	4180198.09	2090.81
LJHMSB	434147.09	4180516.70	2109.07	LJHMSB	433917.53	4180560.04	2104.57	LJHMSB	435248.46	4180199.34	2091.71
LJHMSB	434271.39	4180277.41	2022.49	LJHMSB	433895.11	4180572.45	2106.85	LJHMSB	435243.90	4180201.44	2091.97
LJHMSB	434126.02	4180519.83	2110.01	LJHMSB	433879.33	4180569.61	2106.98	LJHMSB	435240.87	4180202.26	2091.54
LJHMSB	434183.07	4180488.46	2110.74	LJHMSB	435432.72	4180155.43	2083.69	LJHMSB	435236.62	4180199.35	2090.01
LJHMSB	434172.97	4180500.05	2113.24	LJHMSB	435424.88	4180156.79	2083.77	LJHMSB	435230.68	4180201.32	2090.73
LJHMSB	434169.57	4180496.67	2110.46	LJHMSB	435421.79	4180157.02	2084.45	LJHMSB	435226.28	4180199.15	2089.91
LJHMSB	434158.70	4180511.63	2114.45	LJHMSB	435413.73	4180157.83	2086.10	LJHMSB	435222.09	4180200.94	2090.23
LJHMSB	434152.04	4180503.57	2111.06	LJHMSB	435416.80	4180167.34	2092.74	LJHMSB	435219.54	4180201.93	2090.88
LJHMSB	434143.35	4180512.60	2111.00	LJHMSB	435395.90	4180152.63	2090.93	LJHMSB	435214.81	4180203.49	2091.15
LJHMSB	434139.64	4180510.50	2109.25	LJHMSB	435389.09	4180156.59	2090.93	LJHMSB	435209.42	4180208.15	2091.37
LJHMSB	434136.19	4180512.44	2109.26	LJHMSB	435383.73	4180161.95	2090.44	LJHMSB	435204.62	4180210.61	2090.97
LJHMSB	434129.75	4180516.09	2110.16	LJHMSB	435381.51	4180164.00	2090.44	LJHMSB	435199.77	4180213.78	2092.25
LJHMSB	434124.67	4180512.14	2109.74	LJHMSB	435369.13	4180164.30	2089.47	LJHMSB	435195.96	4180213.26	2089.98
LJHMSB	434119.59	4180514.62	2110.15	LJHMSB	435362.23	4180165.86	2090.26	LJHMSB	435190.66	4180224.27	2091.96
LJHMSB	434105.60	4180524.83	2110.63	LJHMSB	435358.58	4180167.54	2090.07	LJHMSB	435188.76	4180225.26	2092.25

Table 5 (continued)

Surface	X	Y	Depth	Surface	X	Y	Depth	Surface	X	Y	Depth
LJHMSB	434101.80	4180524.18	2109.88	LJHMSB	435356.15	4180170.71	2090.26	LJHMSB	435183.49	4180226.47	2093.11
LJHMSB	434095.53	4180527.74	2113.52	LJHMSB	435350.71	4180169.19	2091.60	LJHMSB	435181.53	4180229.10	2093.34
LJHMSB	434088.52	4180530.11	2112.28	LJHMSB	435345.13	4180172.12	2091.31	LJHMSB	436785.33	4179946.68	2011.49
LJHMSB	434082.47	4180525.47	2111.42	LJHMSB	435341.34	4180175.74	2092.12	LJHMSB	436793.74	4179959.65	2010.77
LJHMSB	434076.91	4180526.07	2110.10	LJHMSB	435331.10	4180175.70	2089.01	LJHMSB	436805.14	4179973.63	2007.96
LJHMSB	434064.20	4180530.06	2110.08	LJHMSB	435327.33	4180175.00	2086.80	LJHMSB	436808.23	4179978.65	2007.67
LJHMSB	434057.91	4180533.11	2110.53	LJHMSB	435320.52	4180172.71	2085.83	LJHMSB	436812.62	4179989.63	2007.07
LJHMSB	434048.31	4180536.48	2110.30	LJHMSB	435315.44	4180175.71	2085.86	LJHMSB	436818.10	4179995.31	2006.74
LJHMSB	434041.06	4180535.26	2109.29	LJHMSB	435310.58	4180177.22	2086.03	LJHMSB	436823.67	4180009.96	2006.66
LJHMSB	436832.82	4180022.02	2006.70	LJHMSB	437136.24	4180118.88	2012.41	LJHMSB	437913.39	4180179.61	2004.82
LJHMSB	436833.62	4180030.92	2007.53	LJHMSB	437142.89	4180118.89	2012.76	LJHMSB	437925.54	4180168.50	2003.45
LJHMSB	436839.36	4180043.04	2007.13	LJHMSB	437151.21	4180122.57	2013.66	LJHMSB	437943.13	4180139.87	2004.85
LJHMSB	436843.22	4180052.73	2007.87	LJHMSB	437156.86	4180124.11	2013.01	LJHMSB	437955.69	4180137.33	2003.00
LJHMSB	436850.73	4180063.33	2007.66	LJHMSB	437166.09	4180128.03	2013.25	LJHMSB	437965.02	4180136.65	2003.14
LJHMSB	436860.61	4180073.75	2006.30	LJHMSB	437174.23	4180128.06	2012.25	LJHMSB	437980.56	4180134.16	2000.42
LJHMSB	436870.45	4180080.47	2007.36	LJHMSB	437183.16	4180131.45	2012.29	LJHMSB	438050.23	4180151.76	1993.89
LJHMSB	436874.97	4180090.72	2007.36	LJHMSB	437190.32	4180135.46	2012.74	LJHMSB	438060.60	4180145.27	1995.48
LJHMSB	436884.78	4180099.92	2005.77	LJHMSB	437204.97	4180143.66	2014.74	LJHMSB	438075.89	4180140.16	1996.53
LJHMSB	436890.53	4180106.58	2005.13	LJHMSB	437216.23	4180151.74	2014.69	LJHMSB	438085.19	4180131.45	1995.04
LJHMSB	436894.45	4180111.47	2004.81	LJHMSB	437228.00	4180156.66	2014.26	LJHMSB	438094.26	4180124.38	1994.39
LJHMSB	436899.22	4180117.43	2004.47	LJHMSB	437240.35	4180160.97	2012.53	LJHMSB	438099.66	4180113.44	1995.29
LJHMSB	436914.43	4180121.28	2004.45	LJHMSB	437249.84	4180166.74	2013.68	LJHMSB	438102.91	4180104.39	1995.92
LJHMSB	436925.96	4180125.67	2005.56	LJHMSB	437262.42	4180170.32	2016.03	LJHMSB	438402.84	4180061.79	1981.86
LJHMSB	436936.42	4180133.02	2006.71	LJHMSB	437272.67	4180172.38	2014.26	LJHMSB	438401.75	4180069.72	1981.85
LJHMSB	436944.00	4180133.94	2006.23	LJHMSB	437558.28	4180386.90	2015.01	LJHMSB	438398.45	4180078.39	1981.60
LJHMSB	436954.95	4180133.14	2004.32	LJHMSB	437586.92	4180361.53	2014.82	LJHMSB	438377.85	4180084.04	1983.63
LJHMSB	436978.90	4180133.39	2005.38	LJHMSB	437616.23	4180346.49	2015.43	LJHMSB	438336.90	4180088.53	1984.73
LJHMSB	436982.02	4180139.67	2011.98	LJHMSB	437631.97	4180345.20	2016.48	LJHMSB	438306.16	4180093.64	1983.58
LJHMSB	436993.07	4180133.19	2009.66	LJHMSB	437641.81	4180336.73	2015.31	LJHMSB	438387.58	4180404.60	1987.33
LJHMSB	437011.37	4180123.39	2008.61	LJHMSB	437650.26	4180345.31	2017.05	LJHMSB	438412.59	4180405.27	1988.11
LJHMSB	437018.74	4180121.82	2008.16	LJHMSB	437659.57	4180349.31	2016.00	LJHMSB	438446.42	4180377.28	1983.91

Table 5 (continued)

Surface	X	Y	Depth
LJHMSB	437040.59	4180123.92	2011.95
LJHMSB	437047.89	4180123.83	2012.67
LJHMSB	437052.21	4180122.57	2012.04
LJHMSB	437059.78	4180123.62	2013.80
LJHMSB	437070.60	4180120.53	2011.39
LJHMSB	437080.86	4180113.47	2009.82
LJHMSB	437086.82	4180114.30	2011.01
LJHMSB	437093.85	4180116.89	2011.81
LJHMSB	437092.07	4180116.50	2010.35
LJHMSB	437099.19	4180116.42	2010.72
LJHMSB	437104.84	4180118.20	2012.33
LJHMSB	437112.12	4180124.86	2015.37
LJHMSB	437119.66	4180119.15	2014.50
LJHMSB	437126.85	4180114.40	2013.62
LJHMSB	437129.58	4180115.91	2012.82
LJHMSB	438727.29	4180331.34	1974.95
LJHMSB	438732.56	4180321.27	1974.37
LJHMSB	438737.48	4180308.77	1973.82
LJHMSB	438747.63	4180301.13	1973.87
LJHMSB	438755.79	4180287.18	1972.91
LJHMSB	438767.11	4180265.75	1974.31
LJHMSB	438765.82	4180243.81	1973.37
LJHMSB	438772.47	4180222.49	1975.97
LJHMSB	438775.58	4180205.70	1975.20
LJHMSB	438785.35	4180200.35	1975.22
LJHMSB	438792.16	4180197.69	1975.23
LJHMSB	438808.09	4180196.24	1973.42
LJHMSB	438820.21	4180196.42	1973.02
LJHMSB	438883.52	4180353.26	1974.11
LJHMSB	438902.79	4180350.14	1974.47
LJHMSB	438925.14	4180344.66	1973.29

Surface	X	Y	Depth
LJHMSB	437766.26	4180252.82	2012.43
LJHMSB	437778.53	4180249.76	2011.99
LJHMSB	437788.21	4180234.67	2010.47
LJHMSB	437790.04	4180231.29	2010.72
LJHMSB	437800.11	4180229.32	2010.52
LJHMSB	437802.12	4180230.57	2010.68
LJHMSB	437820.45	4180219.39	2008.73
LJHMSB	437829.09	4180217.89	2011.72
LJHMSB	437835.94	4180203.09	2008.91
LJHMSB	437849.89	4180195.53	2007.99
LJHMSB	437859.11	4180190.96	2007.81
LJHMSB	437860.19	4180191.36	2007.19
LJHMSB	437875.75	4180195.76	2006.47
LJHMSB	437888.33	4180185.72	2006.52
LJHMSB	437899.00	4180182.26	2003.73
LJHMSB	439466.76	4180399.45	1980.05
LJHMSB	438772.47	4180222.49	1975.97
LJHMSB	438775.58	4180205.70	1975.20
LJHMSB	438785.35	4180200.35	1975.22
LJHMSB	438792.16	4180197.69	1975.23
LJHMSB	438808.09	4180196.24	1973.42
LJHMSB	438820.21	4180196.42	1973.02
LJHMSB	438883.52	4180353.26	1974.11
LJHMSB	438902.79	4180350.14	1974.47
LJHMSB	438925.14	4180344.66	1973.29
LJHMSB	438960.20	4180347.62	1973.85
LJHMSB	438977.97	4180348.67	1973.53
LJHMSB	439004.39	4180362.09	1973.89
LJHMSB	439015.89	4180371.54	1973.53
LJHMSB	439028.25	4180378.21	1974.70
LJHMSB	439093.85	4180387.12	1974.71

Surface	X	Y	Depth
LJHMSB	438474.99	4180356.82	1984.72
LJHMSB	438493.42	4180345.64	1983.55
LJHMSB	438523.73	4180294.88	1981.81
LJHMSB	438535.74	4180293.67	1980.55
LJHMSB	438551.94	4180288.92	1980.77
LJHMSB	438576.16	4180287.41	1979.95
LJHMSB	438586.78	4180279.42	1979.67
LJHMSB	438595.92	4180274.18	1978.85
LJHMSB	438606.89	4180268.62	1979.01
LJHMSB	438614.87	4180273.39	1978.92
LJHMSB	438623.50	4180269.63	1977.91
LJHMSB	438630.51	4180265.17	1978.68
LJHMSB	438637.83	4180263.47	1977.01
LJHMSB	438644.20	4180265.93	1976.82
LJHMSB	438721.37	4180339.16	1971.69
wRs (2)	436899.84	4180141.72	2029.28
wRs (2)	436883.34	4180129.33	2029.02
wRs (2)	436869.78	4180124.35	2030.80
wRs (2)	436862.78	4180118.05	2031.38
wRs (2)	437230.30	4179272.25	2051.85
wRs (2)	437255.67	4179284.60	2051.52
wRs (2)	437275.11	4179293.00	2048.12
wRs (2)	437299.39	4179300.98	2048.96
wRs (2)	437342.18	4179318.00	2045.59
wRs (2)	437399.44	4179345.87	2049.43
wRs (2)	437425.63	4179349.14	2050.99
wRs (2)	437466.57	4179369.82	2048.57
wRs (2)	437489.40	4179392.47	2042.06
wRs (2)	437506.31	4179401.53	2044.83
wRs (2)	437520.19	4179421.22	2040.74
wRs (2)	437675.59	4179555.80	2034.19

Table 5 (continued)

Surface	X	Y	Depth
LJHMSB	438960.20	4180347.62	1973.85
LJHMSB	438977.97	4180348.67	1973.53
LJHMSB	439004.39	4180362.09	1973.89
LJHMSB	439015.89	4180371.54	1973.53
LJHMSB	439028.25	4180378.21	1974.70
LJHMSB	439093.85	4180387.12	1974.71
LJHMSB	439114.19	4180376.67	1974.00
LJHMSB	439138.46	4180370.90	1972.61
LJHMSB	439153.37	4180368.44	1971.92
LJHMSB	439181.95	4180368.96	1972.86
LJHMSB	439202.82	4180365.30	1971.21
LJHMSB	439226.90	4180369.13	1973.93
LJHMSB	439270.07	4180366.54	1975.07
LJHMSB	439303.80	4180363.15	1975.64
LJHMSB	439361.02	4180373.72	1978.39
LJHMSB	439368.61	4180369.78	1976.90
LJHMSB	439367.23	4180369.39	1977.53
LJHMSB	439385.37	4180377.59	1976.61
LJHMSB	439404.51	4180383.07	1977.00
LJHMSB	439427.15	4180391.50	1979.09
LJHMSB	439460.25	4180401.21	1980.51
wRs (2)	437579.79	4180371.57	2033.63
wRs (2)	437583.50	4180368.80	2033.20
wRs (2)	437591.46	4180372.99	2030.95
wRs (2)	438360.59	4180422.57	2008.66
wRs (2)	438378.66	4180426.75	2011.70
wRs (2)	438403.87	4180426.02	2012.78
wRs (2)	438454.05	4180392.01	2007.76
wRs (2)	438502.16	4180350.18	2010.12
wRs (2)	438529.08	4180303.29	2008.74
wRs (2)	438542.16	4180303.10	2010.00

Surface	X	Y	Depth
LJHMSB	439114.19	4180376.67	1974.00
LJHMSB	439138.46	4180370.90	1972.61
LJHMSB	439153.37	4180368.44	1971.92
LJHMSB	439181.95	4180368.96	1972.86
LJHMSB	439202.82	4180365.30	1971.21
LJHMSB	439226.90	4180369.13	1973.93
LJHMSB	439270.07	4180366.54	1975.07
LJHMSB	439303.80	4180363.15	1975.64
LJHMSB	439361.02	4180373.72	1978.39
LJHMSB	439368.61	4180369.78	1976.90
LJHMSB	439367.23	4180369.39	1977.53
LJHMSB	439385.37	4180377.59	1976.61
LJHMSB	439404.51	4180383.07	1977.00
LJHMSB	439427.15	4180391.50	1979.09
LJHMSB	439460.25	4180401.21	1980.51
LJHMSB	439466.76	4180399.45	1980.05
wRs (2)	437294.42	4180188.61	2033.99
wRs (2)	437285.71	4180186.42	2032.53
wRs (2)	437284.00	4180188.79	2032.95
wRs (2)	437247.50	4180166.64	2034.69
wRs (2)	437226.27	4180157.09	2035.60
wRs (2)	438946.45	4180235.30	2005.54
wRs (2)	438901.06	4180242.58	2006.21
wRs (2)	439367.16	4180400.30	2014.64
wRs (2)	439347.01	4180393.80	2014.78
wRs (2)	439340.52	4180404.52	2017.27
wRs (2)	439311.81	4180396.13	2013.82
wRs (2)	439288.69	4180400.07	2014.33
wRs (2)	439268.81	4180407.69	2012.97
wRs (2)	439256.78	4180410.58	2013.21
wRs (2)	439234.60	4180406.69	2010.64

Surface	X	Y	Depth
wRs (2)	437694.07	4179585.32	2030.10
wRs (2)	437724.69	4179601.46	2026.70
wRs (2)	438410.75	4180073.21	2007.73
wRs (2)	438415.55	4180079.75	2009.86
wRs (2)	438413.06	4180082.87	2009.54
wRs (2)	438410.76	4180090.70	2009.37
wRs (2)	438410.73	4180095.43	2010.69
wRs (2)	438373.81	4180099.94	2010.47
wRs (2)	438356.27	4180105.21	2009.84
wRs (2)	438113.17	4180129.71	2013.87
wRs (2)	438110.24	4180133.56	2014.25
wRs (2)	438107.44	4180137.46	2013.96
wRs (2)	438104.71	4180145.07	2014.92
wRs (2)	438087.25	4180159.20	2017.25
wRs (2)	438083.88	4180167.11	2017.55
wRs (2)	438079.23	4180170.45	2018.28
wRs (2)	437942.17	4180145.38	2021.31
wRs (2)	437899.64	4180194.33	2024.29
wRs (2)	437947.97	4180175.15	2024.60
wRs (2)	437891.46	4180204.45	2024.65
wRs (2)	437820.67	4180225.79	2026.45
wRs (2)	438596.27	4180296.61	2007.20
wRs (2)	438613.40	4180295.61	2007.69
wRs (2)	438622.23	4180290.67	2007.08
wRs (2)	438633.92	4180290.48	2006.51
wRs (2)	438641.65	4180306.92	2006.16
wRs (2)	438728.05	4180406.56	2005.46
wRs (2)	438734.53	4180393.10	2005.53
wRs (2)	438750.93	4180364.57	2006.18
wRs (2)	438759.67	4180352.08	2006.73
wRs (2)	438774.11	4180335.03	2006.23

Surface	X	Y	Depth	Surface
wRs (2)	438550.94	4180302.83	2008.73	wRs (2)
wRs (2)	438558.89	4180304.79	2009.11	wRs (2)
wRs (2)	438572.99	4180307.41	2008.49	wRs (2)
wRs (2)	438596.27	4180296.61	2007.20	wRs (2)
wRs (2)	438613.40	4180295.61	2007.69	wRs (2)
wRs (2)	438622.23	4180290.67	2007.08	wRs (2)
wRs (2)	438633.92	4180290.48	2006.51	wRs (2)
wRs (2)	438641.65	4180306.92	2006.16	wRs (2)
wRs (2)	438728.05	4180406.56	2005.46	wRs (2)
wRs (2)	438734.53	4180393.10	2005.53	wRs (2)
wRs (2)	438750.93	4180364.57	2006.18	wRs (2)
wRs (2)	438759.67	4180352.08	2006.73	wRs (2)
wRs (2)	438774.11	4180335.03	2006.23	wRs (2)
wRs (2)	438783.29	4180323.06	2007.21	wRs (2)
wRs (2)	438794.40	4180313.57	2006.56	wRs (2)
wRs (2)	438789.56	4180310.89	2005.61	wRs (2)
wRs (2)	438801.45	4180297.75	2007.74	wRs (2)
wRs (2)	438806.06	4180283.84	2006.95	wRs (2)
wRs (2)	438800.33	4180249.51	2004.52	wRs (2)
wRs (2)	438806.10	4180237.38	2006.35	wRs (2)
wRs (2)	438809.31	4180232.96	2004.75	wRs (2)
wRs (2)	438861.70	4180250.06	2005.63	wRs (2)
wRs (2)	438866.26	4180246.50	2005.34	wRs (2)
wRs (2)	438884.28	4180244.72	2004.56	wRs (2)
wRs (2)	438909.55	4180246.24	2007.49	wRs (2)
wRs (2)	438921.24	4180235.94	2005.62	wRs (2)
wRs (2)	438932.90	4180231.87	2004.80	wRs (2)
wRs (2)	439152.73	4180412.80	2010.23	wRs (2)
wRs (2)	439133.19	4180410.42	2006.98	wRs (2)
wRs (2)	439108.83	4180407.86	2006.29	wRs (2)
wRs (2)	439086.89	4180426.56	2006.55	wRs (2)

Table 5 (continued)

X	Y	Depth
439225.29	4180408.76	2011.15
439199.55	4180416.09	2013.51
439171.44	4180409.10	2010.23
439152.73	4180412.80	2010.23
439133.19	4180410.42	2006.98
439108.83	4180407.86	2006.29
439086.89	4180426.56	2006.55
439051.64	4180432.13	2006.68
439036.90	4180420.70	2006.23
439020.41	4180422.23	2005.51
439001.18	4180415.43	2004.40
438949.34	4180381.60	2006.48
438938.20	4180375.79	2005.89
438887.19	4180392.34	2012.23
438836.74	4180386.15	2006.98
438810.37	4180388.92	2007.83
438793.67	4180370.01	2007.11
438360.59	4180422.57	2008.66
438378.66	4180426.75	2011.70
438403.87	4180426.02	2012.78
438454.05	4180392.01	2007.76
438502.16	4180350.18	2010.12
438529.08	4180303.29	2008.74
438542.16	4180303.10	2010.00
438550.94	4180302.83	2008.73
438558.89	4180304.79	2009.11
438572.99	4180307.41	2008.49
439152.73	4180412.80	2010.23
439133.19	4180410.42	2006.98
439108.83	4180407.86	2006.29
439086.89	4180426.56	2006.55

Surface	X	Y	Depth
wRs (2)	438783.29	4180323.06	2007.21
wRs (2)	438794.40	4180313.57	2006.56
wRs (2)	438789.56	4180310.89	2005.61
wRs (2)	438801.45	4180297.75	2007.74
wRs (2)	438806.06	4180283.84	2006.95
wRs (2)	438800.33	4180249.51	2004.52
wRs (2)	438806.10	4180237.38	2006.35
wRs (2)	438809.31	4180232.96	2004.75
wRs (2)	438861.70	4180250.06	2005.63
wRs (2)	438866.26	4180246.50	2005.34
wRs (2)	438884.28	4180244.72	2004.56
wRs (2)	438909.55	4180246.24	2007.49
wRs (2)	438921.24	4180235.94	2005.62
wRs (2)	438932.90	4180231.87	2004.80
wRs (2)	438946.45	4180235.30	2005.54
wRs (2)	438901.06	4180242.58	2006.21
wRs (2)	439367.16	4180400.30	2014.64
wRs (2)	439347.01	4180393.80	2014.78
wRs (2)	439340.52	4180404.52	2017.27
wRs (2)	439311.81	4180396.13	2013.82
wRs (2)	439288.69	4180400.07	2014.33
wRs (2)	439268.81	4180407.69	2012.97
wRs (2)	439256.78	4180410.58	2013.21
wRs (2)	439234.60	4180406.69	2010.64
wRs (2)	439225.29	4180408.76	2011.15
wRs (2)	439199.55	4180416.09	2013.51
wRs (2)	439171.44	4180409.10	2010.23
Top CB	436620.21	4179466.73	1972.69
Top CB	436626.62	4179472.44	1971.24
Top CB	436632.69	4179477.35	1970.56
Top CB	436641.17	4179478.93	1970.22

Surface	X	Y	Depth
wRs (2)	439051.64	4180432.13	2006.68
wRs (2)	439036.90	4180420.70	2006.23
wRs (2)	439020.41	4180422.23	2005.51
wRs (2)	439001.18	4180415.43	2004.40
wRs (2)	438949.34	4180381.60	2006.48
wRs (2)	438938.20	4180375.79	2005.89
wRs (2)	438887.19	4180392.34	2008.34
wRs (2)	438836.74	4180386.15	2006.98
wRs (2)	438810.37	4180388.92	2007.83
wRs (2)	438793.67	4180370.01	2007.11
Top "E"	439275.41	4180443.78	2039.67
Top "E"	439234.95	4180447.18	2038.87
Top "E"	439160.27	4180456.17	2036.57
Top "E"	438999.17	4180476.91	2037.30
Top "E"	438980.97	4180469.81	2036.08
Top "E"	438928.91	4180431.55	2034.88
Top "E"	438866.03	4180429.59	2036.34
Top "E"	438824.48	4180425.84	2035.61
Top "E"	438812.17	4180420.33	2034.13
Top "E"	438470.20	4180412.12	2039.74
Top "E"	438493.70	4180414.13	2037.17
Top "E"	438501.79	4180419.11	2039.06
Top "E"	438505.10	4180442.35	2041.67
wRs (2)	439347.01	4180393.80	2014.78
wRs (2)	439340.52	4180404.52	2017.27
wRs (2)	439311.81	4180396.13	2013.82
wRs (2)	439288.69	4180400.07	2014.33
wRs (2)	439268.81	4180407.69	2012.97
wRs (2)	439256.78	4180410.58	2013.21
wRs (2)	439234.60	4180406.69	2010.64
wRs (2)	439225.29	4180408.76	2011.15

Surface
wRs (2)
wRs (2)
wRs (2)
wRs (2)
wRs (2)
wRs (2)
wRs (2)
wRs (2)
wRs (2)
wRs (2)
Top "E"
Top "E"
Top "E"
Top "E"
Top "E"
Top "E"
Top "E"
Top "E"
Top "E"
Top "E"
Top "E"
Top "E"
Top "E"
Top CB
Top CB
Top CB
Top CB
Top CB
Top CB
Top CB
Top CB

Table 5 (continued)

X	Y	Depth
439051.64	4180432.13	2006.68
439036.90	4180420.70	2006.23
439020.41	4180422.23	2005.51
439001.18	4180415.43	2004.40
438949.34	4180381.60	2006.48
438938.20	4180375.79	2005.89
438887.19	4180392.34	2008.34
438836.74	4180386.15	2006.98
438810.37	4180388.92	2007.83
438793.67	4180370.01	2007.11
439275.41	4180443.78	2039.67
439234.95	4180447.18	2038.87
439160.27	4180456.17	2036.57
438999.17	4180476.91	2037.30
438980.97	4180469.81	2036.08
438928.91	4180431.55	2034.88
438866.03	4180429.59	2036.34
438824.48	4180425.84	2035.61
438812.17	4180420.33	2034.13
438470.20	4180412.12	2039.74
438493.70	4180414.13	2037.17
438501.79	4180419.11	2039.06
438505.10	4180442.35	2041.67
436554.85	4179464.21	1972.30
436563.21	4179459.11	1973.93
436561.89	4179459.51	1973.25
436567.07	4179461.79	1972.15
436576.99	4179463.60	1970.94
436585.04	4179466.91	1966.97
436591.89	4179469.09	1967.23
436604.19	4179466.89	1968.44

Surface	X	Y	Depth
Top CB	436648.05	4179478.83	1969.50
Top CB	436649.28	4179478.66	1969.48
Top CB	436668.10	4179473.49	1968.55
Top CB	436673.21	4179474.97	1967.10
Top CB	436680.47	4179470.58	1967.52
Top CB	436691.07	4179466.02	1965.39
Top CB	436713.03	4179457.99	1962.28
Top CB	436723.32	4179450.55	1962.32
Top CB	436731.82	4179445.11	1961.45
Top CB	436739.67	4179447.68	1958.59
Top CB	436760.56	4179440.55	1960.03
Top CB	436504.55	4179809.97	1972.19
Top CB	436493.45	4179815.97	1974.08
Top CB	436475.26	4179810.46	1970.51
Top CB	436458.51	4179806.89	1969.21
Top CB	436470.68	4179824.32	1977.63
Top CB	436443.27	4179817.65	1975.04
Top CB	436417.86	4179818.03	1976.59
Top CB	436398.97	4179814.91	1975.10
Top CB	436391.03	4179815.85	1975.15
Top CB	436375.03	4179806.61	1970.80
Top CB	436369.98	4179811.67	1972.30
Top CB	436359.06	4179804.68	1970.52
Top CB	436351.95	4179812.93	1971.66
Top CB	436347.61	4179812.27	1970.95
Top CB	436343.08	4179819.17	1971.47
Top CB	436337.36	4179817.57	1969.50
Top CB	436333.45	4179822.04	1971.04
Top CB	436327.71	4179826.03	1971.64
Top CB	436316.14	4179832.70	1973.57
Top CB	436300.48	4179841.27	1972.72

Table 5 (continued)

Surface	X	Y	Depth
wRs (2)	439199.55	4180416.09	2013.51
wRs (2)	439171.44	4180409.10	2010.23
Top CB	436288.28	4179852.20	1971.85
Top CB	436281.16	4179858.09	1972.05
Top CB	436275.07	4179858.97	1971.83
Top CB	436270.76	4179864.14	1971.71
Top CB	436263.31	4179881.61	1975.06
Top CB	436250.44	4179882.15	1974.75
Top CB	436242.63	4179886.20	1974.78
Top CB	436228.58	4179891.96	1970.52
Top CB	436209.59	4179915.04	1973.71
Top CB	436209.21	4179914.79	1974.14
Top CB	436599.76	4179502.83	1970.19
Top CB	436591.92	4179503.00	1970.42
Top CB	436586.38	4179501.36	1971.52
Top CB	436575.90	4179497.14	1972.40
Top CB	436553.81	4179502.58	1968.94
Top CB	436514.13	4179507.77	1972.24
Top CB	436505.94	4179506.54	1972.85
Top CB	436498.95	4179502.00	1973.14
Top CB	436484.26	4179503.53	1968.80
Top CB	436464.19	4179497.05	1973.55
Top CB	436459.68	4179494.94	1973.36
Top CB	436456.25	4179492.58	1972.75
Top CB	436455.26	4179484.43	1974.27
Top CB	436436.73	4179478.75	1972.85
Top CB	436435.60	4179464.77	1976.42
Top CB	436430.49	4179457.98	1977.17
Top CB	436427.89	4179452.04	1976.98
Top CB	436425.96	4179441.44	1974.49
Top CB	436423.76	4179436.20	1975.32

Surface	X	Y	Depth
Top CB	436609.96	4179465.69	1970.43
Top CB	436614.69	4179465.83	1972.29
Top CB	436358.75	4179439.37	1979.63
Top CB	436351.58	4179444.89	1979.07
Top CB	436346.92	4179443.94	1978.96
Top CB	436343.05	4179442.37	1978.95
Top CB	436336.52	4179439.95	1979.85
Top CB	436329.32	4179439.52	1980.06
Top CB	436323.18	4179437.55	1980.54
Top CB	436315.68	4179435.36	1980.98
Top CB	436302.27	4179432.15	1982.81
Top CB	436282.00	4179434.12	1980.61
Top CB	436269.13	4179436.34	1979.18
Top CB	436262.74	4179432.84	1980.03
Top CB	436254.70	4179432.36	1980.02
Top CB	436245.81	4179429.09	1979.98
Top CB	436240.75	4179421.21	1981.53
Top CB	436235.56	4179419.30	1981.34
Top CB	436228.89	4179417.59	1981.61
Top CB	436218.45	4179412.41	1982.89
Top CB	436209.21	4179408.55	1984.55
Top CB	436202.72	4179408.43	1984.68
Top CB	436198.08	4179404.34	1986.91
Top CB	436192.80	4179400.56	1989.66
Top CB	436183.39	4179395.32	1990.72
Top CB	436154.15	4179392.40	1991.69
Top CB	436140.24	4179390.17	1989.28
Top CB	436117.14	4179404.67	1981.40
Top CB	436110.67	4179402.29	1983.08
Top CB	436096.17	4179401.77	1985.05
Top CB	436076.39	4179400.13	1986.42

Surface	X	Y	Depth
Top CB	436291.06	4179848.29	1972.77
Top CB	436291.31	4179850.57	1972.01
Top CB	435958.15	4179371.31	1988.95
Top CB	435938.86	4179366.06	1990.70
Top CB	435921.08	4179364.66	1987.25
Top CB	436599.76	4179502.83	1970.19
Top CB	436591.92	4179503.00	1970.42
Top CB	436586.38	4179501.36	1971.52
Top CB	436575.90	4179497.14	1972.40
Top CB	436553.81	4179502.58	1968.94
Top CB	436514.13	4179507.77	1972.24
Top CB	436505.94	4179506.54	1972.85
Top CB	436498.95	4179502.00	1973.14
Top CB	436484.26	4179503.53	1968.80
Top CB	436464.19	4179497.05	1973.55
Top CB	436459.68	4179494.94	1973.36
Top CB	436456.25	4179492.58	1972.75
Top CB	436455.26	4179484.43	1974.27
Top CB	436436.73	4179478.75	1972.85
Top CB	436435.60	4179464.77	1976.42
Top CB	436430.49	4179457.98	1977.17
Top CB	436427.89	4179452.04	1976.98
Top CB	436425.96	4179441.44	1974.49
Top CB	436423.76	4179436.20	1975.32
Top CB	436423.59	4179428.85	1976.48
Top CB	436417.92	4179426.41	1978.04
Top CB	436411.00	4179420.89	1979.24
Top CB	436404.92	4179417.08	1978.69
Top CB	436404.61	4179401.90	1979.51
Top CB	436394.69	4179402.20	1979.57
Top CB	436386.78	4179401.59	1980.35

Table 5 (continued)

Surface	X	Y	Depth	Surface	X	Y	Depth	Surface	X	Y	Depth
Top CB	436423.59	4179428.85	1976.48	Top CB	436240.75	4179421.21	1981.53	-	-	-	-
Top CB	436417.92	4179426.41	1978.04	Top CB	436235.56	4179419.30	1981.34	-	-	-	-
Top CB	436411.00	4179420.89	1979.24	Top CB	436228.89	4179417.59	1981.61	-	-	-	-
Top CB	436404.92	4179417.08	1978.69	Top CB	436218.45	4179412.41	1982.89	-	-	-	-
Top CB	436404.61	4179401.90	1979.51	Top CB	436209.21	4179408.55	1984.55	-	-	-	-
Top CB	436394.69	4179402.20	1979.57	Top CB	436202.72	4179408.43	1984.68	-	-	-	-
Top CB	436386.78	4179401.59	1980.35	Top CB	436198.08	4179404.34	1986.91	-	-	-	-
Top CB	436368.40	4179429.33	1978.74	Top CB	436192.80	4179400.56	1989.66	-	-	-	-
Top CB	436063.93	4179402.11	1988.80	Top CB	436183.39	4179395.32	1990.72	-	-	-	-
Top CB	436050.64	4179402.47	1989.69	Top CB	436154.15	4179392.40	1991.69	-	-	-	-
Top CB	436046.81	4179400.07	1989.01	Top CB	436140.24	4179390.17	1989.28	-	-	-	-
Top CB	436021.38	4179373.45	1988.12	Top CB	436117.14	4179404.67	1981.40	-	-	-	-
Top CB	436007.84	4179377.83	1984.49	Top CB	436110.67	4179402.29	1983.08	-	-	-	-
Top CB	435996.11	4179380.60	1984.32	Top CB	436096.17	4179401.77	1985.05	-	-	-	-
Top CB	435989.36	4179381.09	1985.41	Top CB	436076.39	4179400.13	1986.42	-	-	-	-
Top CB	435979.95	4179379.70	1984.69	Top CB	436063.93	4179402.11	1988.80	-	-	-	-
Top CB	436368.40	4179429.33	1978.74	Top CB	436050.64	4179402.47	1989.69	-	-	-	-
Top CB	436358.75	4179439.37	1979.63	Top CB	436046.81	4179400.07	1989.01	-	-	-	-
Top CB	436351.58	4179444.89	1979.07	Top CB	436021.38	4179373.45	1988.12	-	-	-	-
Top CB	436346.92	4179443.94	1978.96	Top CB	436007.84	4179377.83	1984.49	-	-	-	-
Top CB	436343.05	4179442.37	1978.95	Top CB	435996.11	4179380.60	1984.32	-	-	-	-
Top CB	436336.52	4179439.95	1979.85	Top CB	435989.36	4179381.09	1985.41	-	-	-	-
Top CB	436329.32	4179439.52	1980.06	Top CB	435979.95	4179379.70	1984.69	-	-	-	-
Top CB	436323.18	4179437.55	1980.54	Top CB	435958.15	4179371.31	1988.95	-	-	-	-
Top CB	436315.68	4179435.36	1980.98	Top CB	435938.86	4179366.06	1990.70	-	-	-	-
Top CB	436302.27	4179432.15	1982.81	Top CB	435921.08	4179364.66	1987.25	-	-	-	-
Top CB	436282.00	4179434.12	1980.61	-	-	-	-	-	-	-	-
Top CB	436269.13	4179436.34	1979.18	-	-	-	-	-	-	-	-
Top CB	436262.74	4179432.84	1980.03	-	-	-	-	-	-	-	-
Top CB	436254.70	4179432.36	1980.02	-	-	-	-	-	-	-	-
Top CB	436245.81	4179429.09	1979.98	-	-	-	-	-	-	-	-

APPENDIX D

PALEOCURRENT DATA AND WATER DEPTH ESIMATES

Over 1000 paleocurrent and accretion set measurements were collected from the Smokey Hollow through upper John Henry Member and are organized in Table 6. Measurements are grouped by stratigraphic position. ID numbers are as follows: 1 - thin Smoky Hollow Member (SHM) channels; 2 - thick SHM channels/transition Zone; 3 - lower Calico Bed; 4 - upper Calico Bed; 5 - estuarine SMH above Calico Bed; 6 - distributary mouthbars above the "A" shoreface (R-T cycle 0); 7 - washover fans overlying the "B" shoreface between sections 5 and 6 at the mouth of Main Canyon (R-T cycle 1); 8 - flood tidal delta deposits underlying white tidal sheet at the mouth of Main Canyon between sections 5 and 6; 9 - white tidal inlet, forms capping unit of flood tidal delta succession at mouth of Main Canyon; 10 - fluvial terrace located along eastern margin of incised valley (R-T cycle 1); 11 - heterolithic tidal complex (R-T cycle 1); 12 - sigmoidal shaped estuarine tidal bars (R-T cycle 1); 13 - tidal bars at 36 m on MS 1; 14 - tidal bars at 32 m on MS 1; 15 - amalgamated ebb-dominated tidal bars overlying the "B" shoreface west of MS 1; 16 - tidal channels/bars at 92 m on MS 2; 17 - tidal channels/bars at 63 m on MS 5; 18 - tidal channels/bars at 67 m on MS 5; 19 - tidal channels/bars at 86 meters on MS 2; 20 - tidal channels/bars at 92 m on MS 1; 21 - upper tidal channels between MS 3 and MS 6; 22 - white sand-rich tidal sheet, measurments taken near the North Creek Reservoir; 23 - bayhead delta/distributary mouth bars at the upper reaches of MS 6; 24 - multistory fluvial channel complex and associated channels near the mouth of Main Canyon. Feature abbreviations are as follows: TrAxis-trough axis; Acc-accretion surface; PCS-planar cross stratification; HB-Lower-herringbone lower cross bed; HB-Upper-herringbone upper cross bed. All measurements are presented in trend and plunge format.

Table 6

Main Canyon paleocurrent data

ID	Trend	Plunge	Feature	Height	Qual	ID	Trend	Plunge	Feature	Height	Qual
1	40	23	TrAxis	5	2	2	70	11	TrAxis	20	2
1	35		TrAxis	10	2	2	100	22	TrAxis	15	2
1	10	18	TrAxis	5	2	2	95	10	TrAxis	10	2
1	15	5	PCS	5	2	3	350	18	PCS	5	2
1	140	5	TrAxis	3	2	3	20	13	TrAxis	16	2
1	120		TrAxis	15	2	3	340	20	TrAxis	10	2
1	60	4	TrAxis	30	2	3	18	7	TrAxis	25	2
1	50	13	TrAxis	10	2	3	30	20	TrAxis	8	2
1	90	7	TrAxis	15	2	3	52	5	TrAxis	35	2
1	100	12	TrAxis	10	2	3	0	6	TrAxis	20	2
1	85	8	TrAxis	5	2	3	25	25	TrAxis	20	2
1	115	8	TrAxis	10	2	3	90	15	TrAxis	20	2
1	110	18	TrAxis	15	2	3	65	0	TrAxis	15	2
1	120		TrAxis	50	2	3	35	25	TrAxis	18	2
1	80	23	TrAxis	10	2	3	25	13	PCS	25	2
2	100	21	TrAxis	20	2	3	80	15	TrAxis	5	2
2	80	15	TrAxis	10	1	3	105	29	Acc	30	2
2	95	12	TrAxis	20	1	3	12	12	Acc	35	2
2	60	24	TrAxis	15	1	4	20	15	TrAxis	7	2
2	70	22	TrAxis	30	2	4	1	10	TrAxis	5	2
2	80	8	TrAxis	25	2	4	20	18	TrAxis	20	2
2	110	12	TrAxis	10	2	4	27	14	TrAxis	22	2
2	130	15	TrAxis	15	2	4	30	18	TrAxis	30	2
2	115	17	Acc	25	2	4	18	16	TrAxis	22	2
2	70	16	Acc	30	2	4	350	17	Acc	40	2
2	90	7	TrAxis	3	2	4	355	18	TrAxis	35	2
2	50	21	TrAxis	3	2	4	340	20	TrAxis	20	2
2	90	20	PCS	20	2	4	10	15	TrAxis	43	2
2	100	9	TrAxis	10	2	4	70	13	TrAxis	7	2

Table 6 (continued)

ID	Trend	Plunge	Feature	Height	Qual	ID
4	345	16	TrAxis	8	2	5
4	85	18	Acc	50	2	5
4	10	20	TrAxis	15	2	5
4	40	13	TrAxis	22	2	5
4	350	16	Acc	20	2	5
4	352	14	TrAxis	18	2	5
4	28	16	TrAxis	10	2	5
4	13	6	TrAxis	19	2	5
4	46	10	TrAxis	10	2	5
5	82	28	TrAxis	10	2	5
5	210	15	TrAxis	12	2	5
5	195	25	TrAxis	10	2	5
5	110	7	TrAxis	20	2	5
5	95	12	TrAxis	25	2	5
5	85	25	TrAxis	16	2	5
5	265	12	TrAxis	7	2	5
5	100	15	TrAxis	7	2	5
5	235	5	TrAxis	15	2	5
5	75	26	TrAxis	20	2	5
5	75	17	TrAxis	10	2	5
5	255	26	TrAxis	30	2	5
5	78	18	TrAxis	15	2	5
5	238	10	TrAxis	15	2	5
5	65	15	TrAxis	20	2	5
5	75	35	TrAxis	30	2	5
5	130	15	PCS	20	2	5
5	90	5	TrAxis	10	2	5
5	52	34	TrAxis	5	2	5
5	50	10	TrAxis	30	2	5

Trend	Plunge	Feature	Height	Qual
20	10	TrAxis	5	2
45	25	TrAxis	15	2
230	10	TrAxis	17	2
155	24	TrAxis	30	2
65	35	PCS	80	2
80	15	PCS	30	2
195	12	TrAxis	50	2
200	28	TrAxis	30	2
45	18	TrAxis	30	2
28	24	TrAxis	5	2
190	28	TrAxis	30	2
203	16	TrAxis	30	2
75	17	TrAxis	35	2
65	25	TrAxis	20	2
155	24	TrAxis	25	2
75	25	TrAxis	25	2
91	25	TrAxis	20	2
207	25	TrAxis	25	2
90	20	TrAxis	26	2
35	19	TrAxis	18	2
235	19	TrAxis	17	2
237	18	TrAxis	20	2
202	20	TrAxis	18	2
215	21	TrAxis	20	2
92	12	TrAxis	30	2
65	10	TrAxis	20	2
65	7	TrAxis	10	2
0	25	TrAxis	5	2
78	12	TrAxis	35	2

Table 6 (continued)

ID	Trend	Plunge	Feature	Height	Qual	ID
5	65	15	TrAxis	70	2	7
6	19	25	Acc	14	2	7
6	22	30	PCS	18	2	7
6	16	40	PCS	3	2	7
6	24	40	PCS	12	2	8
6	18	35	PCS	8	2	8
6	14	45	PCs	20	2	8
6	17	32	PCS	18	2	8
6	18	40	PCS	40	1	8
6	13	45	TrAxis	10	2	8
6	17	55	TrAxis	80	1	8
6	11	42	TrAxis	50	1	8
6	30	35	TrAxis	20	2	8
6	24	80	TrAxis	30	2	8
6	18	62	TrAxis	10	2	8
6	7	25	TrAxis	12	2	8
7	235	30	Ripple	2	2	8
7	223	30	Ripple	2.5	2	8
7	220	15	TrAxis	10	2	8
7	210	20	Ripple	3	2	8
7	253	18	Ripple	3	2	8
7	230	10	Ripple	3	2	8
7	200	5	Ripple	4	2	8
7	225	10	Ripple	1.5	2	8
7	240	5	Ripple	1.5	2	8
7	260	7	Ripple	2	2	8
7	270	5	Ripple	1.5	2	8
7	221	10	Ripple	2	2	8
7	227	10	Ripple	2	2	8

Trend	Plunge	Feature	Height	Qual
220	10	Ripple	1.5	2
250	5	Ripple	3	2
202	5	Ripple	6	2
260	7	Ripple	2	2
20	15	PCS	40	2
32	22	PCS	40	2
35	22	PCS	30	1
45	28	PCS	40	2
20	14	PCS	50	2
30	20	PCS	30	2
72	20	PCS	40	2
71	23	PCS	50	2
22	15	PCS	20	2
29	15	PCS	40	2
320	25	PCS	25	1
311	15	PCS	10	2
305	20	PCS	50	2
38	14	PCS	100	2
291	21	PCS	20	2
310	12	PCS	40	2
20	5	PCS	15	2
160	15	PCS	10	2
340	28	PCS	10	2
205	10	PCS	10	2
240	10	PCS	5	3
230	10	PCS	30	3
195	5	PCS	30	2
180	13	PCS	20	2
180	14	PCS	5	2

Table 6 (continued)

ID	Trend	Plunge	Feature	Height	Qual	ID
8	175	2	PCS	1	2	8
8	175	16	PCS	5	3	8
8	220	13	PCS	20	2	8
8	88	10	PCS	15	2	8
8	260	12	PCS	5	2	8
8	305	20	PCS	100	2	8
8	290	26	PCS	10	2	8
8	130	30	PCS	40	2	8
8	215	25	PCS	20	2	8
8	125	12	PCS	30	2	8
8	135	16	PCS	30	2	8
8	30	8	PCS	30	2	8
8	250	20	PCS	20	2	8
8	160	17	PCS	20	2	8
8	270	12	TrAxis	5	2	8
8	190	30	TrAxis	50	1	8
8	125	25	TrAxis	30	1	8
8	165	20	TrAxis	30	1	8
8	45	20	TrAxis	40	1	8
8	240	15	TrAxis	15	2	8
8	225	5	TrAxis	30	2	8
8	245	5	TrAxis	30	2	8
8	230	20	TrAxis	30	2	8
8	230	10	TrAxis	30	2	8
8	233	15	TrAxis	30	2	8
8	233	22	TrAxis	30	2	8
8	250	15	TrAxis	30	2	8
8	78	22	TrAxis	30	2	8
8	220	13	TrAxis	20	2	8

Trend	Plunge	Feature	Height	Qual
230	16	TrAxis	18	2
210	15	TrAxis	16	2
221	15	TrAxis	19	2
120	18	TrAxis	18	2
140	20	TrAxis	25	2
230	25	TrAxis	30	2
180	25	TrAxis	30	2
120	3	TrAxis	15	2
75	35	TrAxis	5	2
85	20	TrAxis	15	2
90	20	TrAxis	5	2
120	5	TrAxis	9	2
220	6	TrAxis	10	2
200	9	TrAxis	9	2
230	10	TrAxis	8	2
230	11	TrAxis	8	2
115	7	TrAxis	7	2
55	5	TrAxis	7	2
135	10	TrAxis	27	2
60	20	TrAxis	9	2
230	15	TrAxis	8	2
135	15	TrAxis	10	2
80	10	TrAxis	10	2
90	10	TrAxis	10	2
240	15	PCS	40	2
226	15	PCS	15	2
180	20	PCS	20	2
230	20	PCS	20	2
210	15	PCS	35	2

Table 6 (continued)

ID	Trend	Plunge	Feature	Height	Qual	ID
8	187	20	PCS	35	2	8
8	190	21	PCS	20	2	8
8	250	21	PCS	35	2	8
8	252	10	PCS	20	2	8
8	255	11	PCS	20	2	8
8	115	10	TrAxis	18	2	8
8	123	5	TrAxis	17	2	8
8	253	15	TrAxis	22	2	8
8	210	15	TrAxis	1	2	8
8	65	14	TrAxis	10	2	8
8	75	10	TrAxis	30	2	8
8	210	12	TrAxis	30	2	8
8	60	9	TrAxis	15	2	8
8	92	16	TrAxis	23	2	8
8	210	15	TrAxis	7	2	8
8	110	23	TrAxis	28	2	8
8	200	15	TrAxis	5	2	8
8	135	10	TrAxis	40	2	8
8	82	17	HBU	7	2	8
8	240	20	HBL	7	2	8
8	290	16	PCS			8
8	220	13	PCS	20	2	8
8	88	10	PCS	15	2	8
8	270	12	TrAxis	5	2	8
8	260	12	PCS	5	2	8
8	305	20	Acc	100	2	8
8	290	26	PCS	10	2	8
8	190	30	TrAxis	50	1	8
8	130	30	PCS	40	2	8

Trend	Plunge	Feature	Height	Qual
125	25	TrAxis	30	1
165	20	TrAxis	30	1
215	25	Acc	20	2
45	20	TrAxis	40	1
240	14	TrAxis	15	2
225	10	TrAxis	20	2
125	12	PCS	30	2
135	16	PCS	30	2
30	8	PCS	30	2
250	20	PCS	20	2
160	17	PCS	20	2
220	15	Bar Acc	150	2
210	14	Bar Acc	150	2
225	20	Bar Acc	150	2
60	17	TrAxis	40	1
75	16	TrAxis	30	1
265	10	TrAxis	10	3
237	5	TrAxis	20	3
165	30	TrAxis	40	2
50	18	TrAxis	5	1
73	15	TrAxis	5	1
235	18	PCS	10	2
78	10	TrAxis	5	1
58	10	TrAxis	5	1
215	8	PCS	10	2
51	15	TrAxis	20	2
40	25	HB-Lower	10	1
240	30	HB-Upper	10	1
85	18	TrAxis	10	1

Table 6 (continued)

ID	Trend	Plunge	Feature	Height	Qual	ID
8	220	10	TrAxis	10	2	9
8	55	20	Sig Acc	15	2	9
8	230	20	PCS	30	2	9
8	220	20	PCS	30	2	9
9	240	10	Acc	100	1	9
9	210	32	Pl Acc	15	1	9
9	90	10	TrAxis	5	1	9
9	125	15	TrAxis	10	1	9
9	250	15	PCS	20	1	9
9	214	18	Acc	50	1	9
9	215	15	PCS	15	1	9
9	218	10	PCS	15	1	9
9	2	25	PCS	5	1	9
9	210	36	PCS	5	1	9
9	180	10	PCS	10	2	9
9	65	18	TrAxis	15	1	9
9	240	16	Acc	15	1	10
9	65	9	TrAxis	15	1	10
9	242	15	PCS	5	2	10
9	230	15	PCS	5	1	10
9	187	38	TrAxis	20	1	10
9	210	35	Sig Acc	25	2	10
9	250	25	Bar Acc	50	1	10
9	221	15	PCS	20	1	10
9	221	12	PCS	22	2	10
9	245	15	TrAxis	15	2	10
9	62	24	TrAxis	15	2	10
9	243	35	TrAxis	20	2	10
9	232	38	TrAxis	20	2	10

Trend	Plunge	Feature	Height	Qual
190	16	TrAxis	15	2
90	17	TrAxis	15	1
90	9	TrAxis	15	2
270	6	TrAxis	15	2
272	5	TrAxis	15	2
90	20	PCS	15	2
187	10	PCS	13	2
250	5	TrAxis	15	2
291	3	TrAxis	25	2
50	3	TrAxis	20	2
50	3	TrAxis	10	2
275	5	TrAxis	12	2
200	25	TrAxis	12	2
235	25	TrAxis	15	2
15	13	TrAxis	12	2
35	15	TrAxis	12	2
341	14	TrAxis	30	1
337	20	TrAxis	15	1
330	6	TrAxis	20	1
358	7	TrAxis	15	1
341	14	TrAxis	30	1
350	13	PCS	35	1
320	13	TrAxis	10	2
10	13	Acc	50	2
335	20	TrAxis	15	2
40	20	PCS	10	1
41	18	PCS	15	1
31	18	TrAxis	10	1
330	5	PCS	25	1

Table 6 (continued)

ID	Trend	Plunge	Feature	Height	Qual	ID
10	15	25	TrAxis	25	1	11
10	18	10	Ripple	5	1	11
10	18	5	TrAxis	20	1	11
10	55	15	TrAxis	20	1	11
10	28	25	PCS	40	1	11
10	345	14	TrAxis	40	1	11
10	15	-	Ripple	5	2	11
10	15	32	PCS	10	2	11
10	10	20	TrAxis	15	2	11
10	0	10	TrAxis	20	2	11
10	10	12	TrAxis	25	2	11
10	355	13	TrAxis	15	2	11
10	15	25	TrAxis	20	2	11
10	25	16	TrAxis	20	2	11
10	3	15	TrAxis	20	1	11
10	56	15	TrAxis	15	2	11
10	45	13	TrAxis	10	2	11
10	2	13	TrAxis	10	1	11
10	335	20	PCS	10	1	11
10	200	18	PCS	15	1	11
11	15	15	Acc	20	2	11
11	25	20	Acc	25	2	11
11	30	25	Acc	10	2	11
11	45	30	Acc	30	2	11
11	90	25	Acc	10	2	11
11	5	15	Acc	20	1	11
11	355	15	Acc	5	3	11
11	220	15	Acc	5	3	11
11	225	10	Acc	50	2	11

Trend	Plunge	Feature	Height	Qual
220	5	Acc	10	2
225	5	Acc	13	2
220	10	Acc	35	2
10	25	Acc	15	1
227	13	TrAxis	5	2
216	10	TrAxis	5	3
150	10	TrAxis	30	3
145	5	TrAxis	10	3
142	10	TrAxis	20	2
125	5	TrAxis	50	3
30	10	TrAxis	13	1
190	12	PCS	20	2
200	10	TrAxis	15	2
315	15	TrAxis	10	2
300	17	TrAxis	10	2
62	18	PCS	10	2
0	20	TrAxis	5	2
50	17	TrAxis	5	2
35	12	TrAxis	5	2
260	13	TrAxis	10	2
280	3	TrAxis	15	2
65	18	PCS	15	2
7	20	PCS	12	2
0	15	TrAxis	12	2
1	12	PCS	18	2
217	12	PCS	20	2
220	15	TrAxis	20	2
120	-	Acc	15	2
100	-	PCS	10	2

Table 6 (continued)

ID	Trend	Plunge	Feature	Height	Qual	ID
11	105	-	PCs	20	2	12
11	122	-	PCS	15	2	12
11	103.5	-	PCS	15	2	12
11	10	-	TrAxis	5	2	12
11	87	-	TrAxis	20	2	12
11	75	-	TrAxis	40	2	12
11	92	-	TrAxis	20	2	12
11	89	-	TrAxis	5	2	12
11	100	-	PCS	10	2	12
11	87	-	PCS	3	2	12
11	70	-	PCS	10	2	12
11	87	-	PCS	25	2	12
11	74	-	TrAxis	15	2	12
11	138	-	PCS	5	2	12
11	70	-	TrAxis	5	2	12
11	85	-	TrAxis	7	2	12
11	80	-	TrAxis	10	2	12
12	45	20	TrAxis	15	2	12
12	285	20	TrAxis	15	2	12
12	300	20	TrAxis	15	2	12
12	40	15	TrAxis	10	2	12
12	290	10	TrAxis	10	2	12
12	15	15	TrAxis	10	2	12
12	23	15	TrAxis	15	3	12
12	62	12	TrAxis	1	2	12
12	200	15	TrAxis	1	2	12
12	215	15	TrAxis	1	2	12
12	215	15	PCS	1	2	12
12	225	15	PCS	1	2	12

Trend	Plunge	Feature	Height	Qual
245	40	PCS	50	2
232	15	TrAxis	1	2
230	15	TrAxis	1	2
215	15	PCS	1	2
25	13	TrAxis	15	2
281	40	PCS	3	2
278	31	PCS	3	2
280	29	PCS	3	2
268	33	PCS	3	2
295	19	PCS	3	2
290	20	PCS	3	2
283	41	PCS	3	2
281	25	PCS	3	2
285	35	PCS	3	2
271	38	PCS	3	2
185	12	TrAxis	5	2
269	16	TrAxis	5	2
200	35	TrAxis	3	2
290	12	TrAxis	5	2
290	8	TrAxis	5	2
20	10	TrAxis	15	1
39	19	PCS	20	1
11	42	PCS	20	2
20	20	PCS	20	2
30	20	PCS	20	2
25	10	PCS	20	2
31	15	PCS	20	2
10	10	PCS	20	2
20	10	PCS	20	2

Table 6 (continued)

ID	Trend	Plunge	Feature	Height	Qual	ID
12	50	10	PCS	20	2	13
12	55	11	PCS	30	2	13
12	70	19	Acc	100	2	13
12	150	32	Acc	100	1	13
12	157	33	Acc	100	1	13
12	162	36	Acc	100	1	13
12	5	25	PCS	20	1	13
12	30	39	PCS	30	2	13
12	70	29	PCS	30	2	13
12	75	35	PCS	20	2	13
12	45	20	PCS	20	2	13
12	70	21	TrAxis	20	2	13
12	205	15	TrAxis	20	2	13
12	216	16	TrAxis	15	2	13
12	225	15	TrAxis	20	2	13
12	218	15	TrAxis	20	2	13
12	45	16	TrAxis	15	2	13
12	18	11	TrAxis	20	2	13
12	225	5	TrAxis	20	2	13
12	220	15	TrAxis	20	2	13
13	60	10	Ripples	1	2	13
13	69	10	Ripples	1	2	13
13	70	10	Ripples	1	2	13
13	10	10	Ripples	1	2	13
13	19	10	Ripples	1	2	13
13	40	45	PCS	50	2	13
13	10	15	PCS	30	2	13
13	50	10	Ripples	3	2	13
13	45	20	PCS	15	2	13

Trend	Plunge	Feature	Height	Qual
45	20	PCS	15	2
47	20	PCS	15	2
40	15	PCS	10	2
32	10	PCS	10	2
15	20	PCS	10	2
23	15	TrAxis	15	3
62	12	TrAxis	1	2
75	15	TrAxis	1	2
71	15	TrAxis	1	2
18	15	TrAxis	1	2
22	15	TrAxis	1	2
50	40	PCS	50	2
12	17	PCS	30	2
52	9	PCS	3	2
46	18	PCS	15	2
45	18	TrAxis	15	2
47	17	TrAxis	15	2
41	13	TrAxis	10	2
30	12	TrAxis	10	2
25	20	TrAxis	10	2
19	15	TrAxis	15	3
227	16	TrAxis	15	2
227	17	TrAxis	17	2
227	23	TrAxis	15	2
230	18	TrAxis	15	2
246	10	TrAxis	23	2
227	12	TrAxis	15	2
230	23	TrAxis	15	2
235	12	TrAxis	18	2

Table 6 (continued)

ID	Trend	Plunge	Feature	Height	Qual	ID
13	242	10	TrAxis	10	2	15
13	237	10	TrAxis	15	2	15
13	228	11	TrAxis	15	2	15
13	228	15	TrAxis	18	2	15
13	225	23	TrAxis	10	2	15
13	223	18	TrAxis	9	2	15
13	225	17	TrAxis	9	2	15
13	230	23	TrAxis	15	2	15
14	20	40	TrAxis	10	1	15
14	30	15	TrAxis	10	1	15
14	0	20	TrAxis	10	1	15
14	25	20	TrAxis	2	1	15
14	25	23	TrAxis	10	1	15
14	11	5	TrAxis	5	1	15
14	80	45	TrAxis	5	1	15
14	70	15	TrAxis	25	1	15
14	345	15	TrAxis	5	1	15
14	343	50	TrAxis	3	1	15
14	35	20	TrAxis	10	1	15
14	23	15	TrAxis	15	1	15
14	30	23	TrAxis	10	1	15
14	35	23	TrAxis	15	1	15
15	21	15	Acc	50	2	15
15	88	26	PCS	25	2	15
15	79	23	PCS	25	2	15
15	75	16	PCS	25	2	15
15	90	20	PCS	23	2	15
15	75	23	PCs	25	2	15
15	70	18	PCS	30	2	15

Trend	Plunge	Feature	Height	Qual
80	20	PCS	15	2
75	15	TrAxis	15	1
65	32	TrAxis	30	2
65	18	TrAxis	15	2
72	28	TrAxis	15	2
50	15	TrAxis	10	2
48	14	TrAxis	15	2
65	20	TrAxis	20	2
72	17	TrAxis	20	2
83	6	TrAxis	40	2
60	12	TrAxis	10	2
85	19	TrAxis	20	2
70	8	TrAxis	50	1
50	11	TrAxis	20	2
70	22	TrAxis	20	2
45	20	TrAxis	15	2
25	10	TrAxis	15	2
75	25	TrAxis	5	2
65	20	TrAxis	25	2
45	14	TrAxis	25	2
55	13	TrAxis	20	2
70	8	TrAxis	25	2
80	11	TrAxis	20	2
65	22	TrAxis	20	2
45	8	TrAxis	20	2
56	22	TrAxis	20	2
70	8	TrAxis	20	2
0	9	TrAxis	20	2
330	5	Acc	25	1

Table 6 (continued)

ID	Trend	Plunge	Feature	Height	Qual	ID
15	14	13	TrAxis	20	1	15
15	124	21	PCS	25	1	15
15	216	19	TrAxis	10	2	15
15	133	16	PCS	30	1	15
15	136	19	PCS	10	1	15
15	142	18	PCS	20	2	15
15	161	6	PCS	5	2	15
15	3	9	PCS	5	2	15
15	146	29	PCS	50	1	15
15	127	17	PCS	10	2	15
15	146	5	PCS	13	1	15
15	142	15	PCS	35	2	15
15	172	14	PCS	15	2	15
15	29	8	TrAxis	5	1	15
15	227	10	TrAxis	5	2	15
15	125	30	PCS	30	2	15
15	216	20	TrAxis	10	2	15
15	142	20	PCS	20	2	15
15	150	20	PCS	50	1	15
15	145	5	PCS	13	1	15
15	300	10	TrAxis	30	2	15
15	120	10	TrAxis	10	2	15
15	70	12	TrAxis	15	2	15
15	290	18	TrAxis	20	2	15
15	75	12	TrAxis	18	2	15
15	270	7	TrAxis	30	2	15
15	120	25	PCS	50	2	15
15	310	12	PCS	15	2	15
15	315	18	PCS	10	2	15

Trend	Plunge	Feature	Height	Qual
65	23	TrAxis	7	2
110	12	PCS	15	2
75	28	PCS	15	2
70	16	TrAxis	12	2
80	10	TrAxis	3	2
55	7	PCS	15	2
230	10	TrAxis	10	2
110	16	TrAxis	5	2
275	25	TrAxis	10	2
150	16	TrAxis	15	2
160	10	TrAxis	25	2
40	-	TrAxis	15	2
195	21	TrAxis	40	2
272	10	TrAxis	10	2
170	15	TrAxis	10	2
80	15	TrAxis	20	2
65	12	Ripple	3	2
40	14	TrAxis	20	2
45	-	TrAxis	30	2
75	-	TrAxis	10	2
60	-	TrAxis	40	2
40	-	TrAxis	20	2
60	-	TrAxis	10	2
30	-	TrAxis	15	2
70	-	TrAxis	25	2
50	-	TrAxis	40	2
73	-	TrAxis	40	2
60	-	TrAxis	20	2
80	-	TrAxis	7	2

Table 6 (continued)

ID	Trend	Plunge	Feature	Height	Qual	ID
15	75	-	TrAxis	10	2	17
15	40	-	TrAxis	15	2	17
15	82	-	TrAxis	20	2	17
15	10	-	TrAxis	40	2	17
15	50	-	TrAxis	20	2	17
15	65	-	TrAxis	40	2	17
15	50	-	TrAxis	20	2	17
15	50	-	TrAxis	45	2	17
15	40	-	TrAxis	20	2	17
15	80	-	TrAxis	15	2	18
15	52	-	TrAxis	50	2	18
15	80	-	TrAxis	60	2	18
15	55	-	TrAxis	40	2	18
15	70	-	TrAxis	10	2	18
15	80	-	TrAxis	20	2	18
15	35	-	TrAxis	30	2	18
15	95	-	TrAxis	15	2	18
16	130	10	TrAxisAcc	20	20	18
16	140	20	TrAxisAcc	20	20	18
16	139	40	TrAxisAcc	20	20	19
16	120	20	TrAxisAcc	20	20	19
16	90	20	TrAxisAcc	20	20	19
16	84	20	TrAxisAcc	20	20	19
16	95	45	TrAxisAcc	20	20	19
16	100	10	TrAxisAcc	20	20	19
16	100	10	TrAxisAcc	20	20	19
16	95	25	TrAxisAcc	20	20	19
16	100	30	TrAxisAcc	20	20	19
17	20	15	Acc	40	2	19

Trend	Plunge	Feature	Height	Qual
32	22	Acc	40	2
35	22	Acc	30	1
45	28	Acc	40	2
20	14	Acc	50	2
30	20	Acc	30	2
72	20	Acc	40	2
71	23	Acc	50	2
22	15	Acc	20	2
29	15	Acc	40	2
320	25	Acc	25	1
311	15	Acc	10	2
305	20	Acc	50	2
38	14	Acc	100	2
291	21	Acc	20	2
310	12	Acc	40	2
20	5	Acc	15	2
160	15	Acc	10	2
340	28	Acc	10	2
205	10	Acc	10	2
120	40	HB Bt.	30	1
310	40	HB Up.	20	1
155	50	TrAxis	20	1
60	40	TrAxis	20	2
195	10	TrAxis	10	2
24	10	TrAxis	10	2
145	10	TrAxis	15	1
138	25	TrAxis	25	1
60	20	TrAxis	30	1
330	20	HB Bt.	30	2

Table 6 (continued)

ID	Trend	Plunge	Feature	Height	Qual	ID
19	160	20	HB Up.	30	2	21
19	165	25	TrAxis	30	2	21
19	122	40	HB Bt.	25	2	21
19	310	40	HB Up.	20	2	21
19	155	50	Acc	15	2	21
19	60	40	Acc	20	2	21
19	330	20	Acc	30	3	21
19	160	20	Acc	30	2	21
19	165	25	Sig.	25	2	21
19	195	10	Acc	15	3	21
19	24	10	TrAxis	10	2	21
19	145	10	Acc	15	1	21
19	138	25	TrAxis	25	1	21
19	60	20	TrAxis	30	1	21
20	143	15	TrAxis	5	1	21
20	162	5	TrAxis	15	1	21
20	330	10	TrAxis	10	1	21
20	183	10	TrAxis	10	1	21
20	164	20	TrAxis	15	1	21
20	60	20	TrAxis	2	2	21
20	165	25	TrAxis	20	2	21
20	187	10	TrAxis	90	1	21
20	168	25	TrAxis	5	1	21
20	80	35	TrAxis	5	2	21
20	86	22	TrAxis	10	2	21
20	185	15	TrAxis	13	2	21
20	16	20	TrAxis	15	2	21
20	60	25	TrAxis	2	2	21
20	145	20	TrAxis	15	2	21

Trend	Plunge	Feature	Height	Qual
25	25	Acc	40	1
75	25	Acc	10	1
80	45	Acc	20	1
10	25	Acc	10	1
80	30	Acc	10	1
33	25	Acc	40	1
95	25	Acc	10	2
85	45	Acc	25	2
35	25	Acc	40	2
75	25	Acc	40	3
90	45	Acc	15	2
8	25	Acc	15	2
72	30	Acc	15	2
30	25	Acc	20	2
90	25	Acc	10	2
235	18	Acc	10	2
215	8	Acc	10	2
230	20	Acc	30	2
220	20	Acc	30	2
220	15	Acc	150	2
210	14	Acc	150	2
225	20	Acc	150	2
72	30	Acc	10	1
40	25	Acc	10	1
250	25	Acc	10	1
240	30	Acc	10	1
55	20	Acc	15	2
143	15	TrAxis	5	1
162	5	TrAxis	15	1

Table 6 (continued)

ID	Trend	Plunge	Feature	Height	Qual	ID
21	330	10	TrAxis	10	1	21
21	183	10	TrAxis	10	1	21
21	164	20	TrAxis	15	1	21
21	60	20	TrAxis	2	2	21
21	165	25	TrAxis	20	2	21
21	187	10	TrAxis	90	1	21
21	168	25	TrAxis	5	1	21
21	80	35	TrAxis	5	2	21
21	86	22	TrAxis	10	2	21
21	185	15	TrAxis	13	2	21
21	16	20	TrAxis	15	2	21
21	60	25	TrAxis	2	2	21
21	145	20	TrAxis	15	2	22
21	55	20	TrAxis	10	1	22
21	50	20	TrAxis	10	1	22
21	355	30	TrAxis	10	1	22
21	85	25	TrAxis	25	1	22
21	30	20	TrAxis	20	1	22
21	90	20	TrAxis	20	1	22
21	15	20	TrAxis	30	1	22
21	30	10	TrAxis	20	1	22
21	55	40	TrAxis	20	1	22
21	40	25	TrAxis	30	1	22
21	33	45	TrAxis	10	1	22
21	10	20	TrAxis	15	1	22
21	25	10	TrAxis	15	1	22
21	35	40	TrAxis	20	1	22
21	35	25	TrAxis	20	1	22
21	33	45	TrAxis	20	1	22

Trend	Plunge	Feature	Height	Qual
60	17	TrAxis	40	1
75	16	TrAxis	30	1
265	10	TrAxis	10	3
237	5	TrAxis	20	3
165	30	TrAxis	40	2
50	18	TrAxis	5	1
73	15	TrAxis	5	1
78	10	TrAxis	5	1
58	10	TrAxis	5	1
51	15	TrAxis	20	2
85	18	TrAxis	10	1
220	10	TrAxis	10	2
305	2	TrAxis	5	2
155	18	TrAxis	10	2
160	17	TrAxis	8	2
245	4	TrAxis	10	2
140	14	TrAxis	7	2
75	9	TrAxis	20	1
215	8	TrAxis	5	2
130	25	TrAxis	25	2
320	32	TrAxis	10	2
120	12	TrAxis	10	2
130	9	TrAxis	11	2
325	16	TrAxis	10	2
325	24	TrAxis	20	2
170	13	TrAxis	5	2
220	20	TrAxis	5	2
205	16	TrAxis	7	2
175	22	TrAxis	15	2

Table 6 (continued)

ID	Trend	Plunge	Feature	Height	Qual	ID
22	155	25	TrAxis	7	2	22
22	180	22	TrAxis	5	1	22
22	260	16	TrAxis	5	2	22
22	160	22	TrAxis	5	2	22
22	310	23	TrAxis	10	2	22
22	150	16	TrAxis	7	2	22
22	190	16	TrAxis	5	2	22
22	145	6	TrAxis	12	2	22
22	140	14	TrAxis	10	2	22
22	12	20	TrAxis	10	2	22
22	220	16	TrAxis	20	2	22
22	200	18	TrAxis	19	2	22
22	20	15	TrAxis	5	2	22
22	355	18	TrAxis	3	2	22
22	210	9	TrAxis	8	2	22
22	170	9	TrAxis	11	2	22
22	215	36	TrAxis	10	2	22
22	230	18	TrAxis	10	2	22
22	55	12	TrAxis	15	2	22
22	110	9	TrAxis	18	2	22
22	222	16	TrAxis	5	2	22
22	227	26	TrAxis	30	2	22
22	196	11	TrAxis	10	2	22
22	47	15	TrAxis	4	2	22
22	240	18	TrAxis	10	2	22
22	239	22	TrAxis	10	2	22
22	192	17	TrAxis	10	2	22
22	230	13	TrAxis	4	2	22
22	215	15	TrAxis	16	2	22

Trend	Plunge	Feature	Height	Qual
40	22	TrAxis	7	2
30	30	TrAxis	11	2
190	20	TrAxis	10	2
40	24	TrAxis	5	2
30	18	TrAxis	10	2
190	30	TrAxis	10	2
345	27	TrAxis	3	2
10	3	TrAxis	5	1
30	24	TrAxis	10	2
15	12	TrAxis	5	2
200	14	TrAxis	7	2
40	24	TrAxis	7	2
230	20	TrAxis	7	2
10	22	TrAxis	0	1
235	14	TrAxis	5	2
215	22	TrAxis	10	2
200	26	TrAxis	20	2
20	25	TrAxis	10	2
160	32	TrAxis	25	2
205	6	TrAxis	15	2
25	8	TrAxis	15	1
185	7	TrAxis	5	2
345	18	TrAxis	15	2
197	18	TrAxis	18	2
40	4	TrAxis	12	2
178	20	TrAxis	10	2
200	14	TrAxis	8	2
242	14	TrAxis	4	2
160	10	TrAxis	14	2

Table 6 (continued)

ID	Trend	Plunge	Feature	Height	Qual	ID
22	322	10	TrAxis	18	2	22
22	170	12	TrAxis	10	2	22
22	177	23	TrAxis	13	2	22
22	60	10	TrAxis	8	2	23
22	67	16	TrAxis	13	2	23
22	250	10	TrAxis	15	2	23
22	235	18	TrAxis	20	2	23
22	38	22	TrAxis	10	2	23
22	140	27	TrAxis	10	2	23
22	240	10	TrAxis	13	2	23
22	170	10	TrAxis	9	2	23
22	140	10	TrAxis	5	2	23
22	132	27	TrAxis	6	2	23
22	180	12	TrAxis	8	2	23
22	200	10	TrAxis	20	2	23
22	250	31	TrAxis	18	2	23
22	230	20	TrAxis	10	2	23
22	95	6	TrAxis	20	2	23
22	10	9	TrAxis	5	2	23
22	190	7	TrAxis	12	2	23
22	55	14	TrAxis	13	2	23
22	250	12	TrAxis	10	2	23
22	87	20	TrAxis	10	2	23
22	200	14	TrAxis	10	2	23
22	40	24	TrAxis	10	2	23
22	240	20	TrAxis	15	2	23
22	13	22	TrAxis	15	1	23
22	235	14	TrAxis	15	1	23
22	218	15	TrAxis	15	2	23

Trend	Plunge	Feature	Height	Qual
186	15	TrAxis	12	2
27	16	TrAxis	10	2
78	45	Acc	20	1
35	24	PCS	5	2
55	12	TrAxis	10	2
10	22	TrAxis	15	2
85	16	TrAxis	15	2
55	10	TrAxis	11	2
355	26	TrAxis	4	2
58	9	TrAxis	16	1
62	16	TrAxis	22	2
82	16	TrAxis	24	2
350	25	Acc	40	2
75	18	PCS	22	2
79	24	Ripple	2	2
42	25	TrAxis	5	1
32	15	TrAxis	8	2
28	13	Acc	15	2
35	25	Ripple	7	2
37	12	TrAxis	8	2
342	23	TrAxis	15	2
25	14	TrAxis	18	2
35	10	TrAxis	25	2
30	22	TrAxis	15	2
0	16	TrAxis	16	2
23	7	Acc	18	2
8	18	TrAxis	19	2
50	20	TrAxis	17	2
39	24	TrAxis	20	2

Table 6 (continued)

ID	Trend	Plunge	Feature	Height	Qual	ID
23	35	30	TrAxis	23	2	23
23	75	10	TrAxis	12	2	23
23	62	20	TrAxis	13	2	23
23	65	17	TrAxis	9	2	23
23	85	30	TrAxis	25	2	23
23	62	12	TrAxis	15	2	23
23	72	28	TrAxis	20	2	23
23	45	15	TrAxis	7	2	23
23	38	24	TrAxis	40	2	23
23	22	12	TrAxis	20	2	23
23	4	28	TrAxis	22	2	23
23	30	22	TrAxis	20	2	23
23	10	12	Acc	30	2	23
23	88	15	TrAxis	20	2	23
23	25	7	TrAxis	15	2	23
23	150	45	Acc	20	2	23
23	156	15	Acc	17	2	23
23	356	16	TrAxis	19	2	23
23	85	28	PCS	23	2	23
23	15	28	TrAxis	20	2	23
23	35	10	TrAxis	18	2	23
23	55	25	TrAxis	10	2	24
23	28	32	TrAxis	17	2	24
23	45	12	TrAxis	18	2	24
23	32	18	TrAxis	20	1	24
23	68	24	TrAxis	15	2	24
23	25	15	TrAxis	15	2	24
23	46	10	TrAxis	15	2	24
23	345	18	TrAxis	15	2	24

Trend	Plunge	Feature	Height	Qual
10	10	TrAxis	5	2
25	10	TrAxis	7	2
23	20	TrAxis	5	2
100	22	Acc	60	1
130	20	Acc	7	2
100	16	Acc	40	2
125	14	Acc	35	2
65	10	TrAxis	7	1
70	10	TrAxis	15	2
55	25	TrAxis	25	2
65	18	TrAxis	18	2
32	14	TrAxis	15	2
30	14	TrAxis	17	2
12	16	TrAxis	10	2
20	25	TrAxis	10	2
13	6	TrAxis	7	2
15	10	TrAxis	17	2
120	14	Acc	35	2
16	20	TrAxis	5	2
0	8	TrAxis	5	2
125	10	TrAxis	5	2
78	45	Acc	20	1
13	25	TrAxis	10	1
72	30	TrAxis	10	1
25	25	Acc	40	1
75	25	Acc	10	1
80	45	Acc	20	1
10	25	Acc	10	1
80	30	Acc	10	1

Table 6 (continued)

ID	Trend	Plunge	Feature	Height	Qual	ID	Trend	Plunge	Feature	Height	Qual
24	33	25	Acc	40	1	-	-	-	-	-	-
24	95	25	Acc	10	1	-	-	-	-	-	-
24	55	20	TrAxis	10	1	-	-	-	-	-	-
24	50	20	TrAxis	10	1	-	-	-	-	-	-
24	355	30	TrAxis	10	1	-	-	-	-	-	-
24	85	25	TrAxis	25	1	-	-	-	-	-	-
24	30	20	TrAxis	20	1	-	-	-	-	-	-
24	90	20	TrAxis	20	1	-	-	-	-	-	-
24	15	20	TrAxis	30	1	-	-	-	-	-	-
24	30	10	TrAxis	20	1	-	-	-	-	-	-
24	55	40	TrAxis	20	1	-	-	-	-	-	-
24	40	25	TrAxis	30	1	-	-	-	-	-	-
24	33	45	TrAxis	10	1	-	-	-	-	-	-
24	10	20	TrAxis	15	1	-	-	-	-	-	-
24	25	10	TrAxis	15	1	-	-	-	-	-	-
24	35	40	TrAxis	20	1	-	-	-	-	-	-
24	35	25	TrAxis	20	1	-	-	-	-	-	-
24	33	45	TrAxis	20	1	-	-	-	-	-	-
24	91	12	TrAxis	15	1	-	-	-	-	-	-
24	35	15	TrAxis	20	1	-	-	-	-	-	-
24	0	22	TrAxis	15	1	-	-	-	-	-	-
-	-	-	-	-	-	-	-	-	-	-	-
-	-	-	-	-	-	-	-	-	-	-	-
-	-	-	-	-	-	-	-	-	-	-	-
-	-	-	-	-	-	-	-	-	-	-	-
-	-	-	-	-	-	-	-	-	-	-	-
-	-	-	-	-	-	-	-	-	-	-	-
-	-	-	-	-	-	-	-	-	-	-	-
-	-	-	-	-	-	-	-	-	-	-	-

APPENDIX E

PROVENANCE DATA

Data tables for sample numbers and descriptions (Table 7) and clast count data (Table 8) from Main Canyon.

Table 7

Sample Archive for Main Canyon

Sample ID	Interval	GPS - Latitude	GPS - Longitude	Section #	Hand Sample/Thin Section ID	Facies Description
BC DZ 1	Tibbet Canyon	37.741483°	-111.724883°	MS3	MC-TS-1	White and tan hummocky bedded fine-grained sandstone. Sample was collected from the central portion of a 3 meter thick sandstone bed. Shoreface in origin.
BC DZ 2	Calico	37.765017°	-111.716400°	MS4	MC-TS-2	White with gray and orange mottling medium to coarse-grained lenticular bedded fluvial sandstone. Individual beds range in size from 50cm to 200cm are inclined at 10-20 degrees from horizontal.
BC DZ 3	Calico estuary	37.759250°	-111.726633°	-	MC-TS-3	Fine-grained sandstone with inclined beds that contain abundant mud and organic-drapes. Laterally this more sandrich unit is discontinuous over 10's of m. Represents preserved portions of estuarine strata above the Calico sequence boundary.
BC DZ 4	Transgressive lag	37.765017°	-111.716400°	MS3	MC-TS-4	1 meter thick swaley cross stratified sandstone overlying a regional pebble conglomerate. Interpreted to be part of the proximal lower shoreface. Pebble lag represents a wave ravinement surface deposited during a rise in relative sea level

Table 7 (continued)

Sample ID	Interval	GPS - Latitude	GPS - Longitude	Section #	Hand Sample/Thin Section ID
BC DZ 5	A' shoreface	37.766186°	-111.727847°	MS3	MC-TS-5
BC DZ 6	B' shoreface	37.766186°	-111.727847°	MS3	MC-TS-6
BC DZ 7	Fluvial terrace	37.765542°	-111.717200°	MS4	MC-TS-7

Facies Description

Pebble conglomerate bearing swaley cross stratified fine-grained sandstone. Locally this unit is over 25 m thick and was deposited as part of the proximal lower shoreface. Pebbles are hypothesized to have been deposited during storms and derived from both basinward and landward sources. The land source may have been exposed portions of the Calico bed that had yet to be covered by sediment during deposition of the "A" This hypothesis explains the apparent lack of pebble conglomerates in the upper shorefaces.

Pebble free, swaley cross stratified sandstone. Proximal lower shoreface in origin.

Very well indurated upper fine to medium-grained trough cross stratified sandstone. Sandstone beds are 40-50 cm thick and are part of a 5-10 meter thick package. Unit is 2-3 m above the "B" shoreface and contains abundant concretions and is very will cemented. This high degree of diagenetic alteration suggests subaerial exposure of this unit as part of a fluvial terrace created during formation of an incised valley system. This unit is observed on the opposite side of the canyon offlapping the "B" shoreface. This unit was deposited during the FSST/LSST.

Table 7 (continued)

Sample ID	Interval	GPS - Latitude	GPS - Longitude	Section #	Hand Sample/Thin Section ID
BC DZ 8	Estuarine channel	37.766328°	-111.725236°	300 m west of MS3	MC-TS-8
BC DZ 9	Tidal barforms	37.765892°	-111.723978°	MS3	MC-TS-9
BC DZ 10	Tidal overlying 'E' shoreface	37.766756°	-111.716489°	MS4	MC-TS-10

Facies Description

Coarse-grained channelized sandstone with abundant oysters and inoceramid shell fragments. This unit erosively overlies the "B" shoreface and is very poorly cemented.

Fine to medium-grained sandstone low-angle trough cross stratification and gently inclined laminations that commonly contain mud-drapes, reactivation surfaces, and shell fragments. Unit is light tan to while in color and contains a fair amount of woody material.

Inclined, erosive based 1 meter thick fine to lower medium-grained sandstone with discontinuous shale beds. Several horizons are fossiliferous, containing oysters and sharks teeth. Bottoms are beds commonly have well rounded grey mud-rip ups in them.

Table 7 (continued)

Sample ID	**Interval**	**GPS - Latitude**	**GPS - Longitude**	**Section #**	**Hand Sample/Thin Section ID**
BC DZ 11	Bayhead delta - North Buck Hollow	37.896314°	-111.685494°	Buck Hollow - North Section	MC-TS-11
BC DZ 12	Transgressive lag	37.759250°	-111.726633°	x	MC-TS-12
BC DZ 13	Debris Flow	37.765619°	-111.717187°	MS 4	MC-TS-13

Facies Description

~20 meter thick package of channelized fine to medium grained sandstone overly a package of grey shales, carbonaceous shales, and thin coals. Sandstone beds are 2-5 m thick and commonly have cobble sized mud rip-ups and large wood fragments on the soles. Bedforms include: 10- 20 cm thick planar and trough cross stratification, massive beds, ripple laminations. In places there are Teredolites borings and well preserved oyster shells, suggesting deposition within brackish water conditions. Bayhead delta.

1 meter thick swaley cross stratified sandstone overlying a regional pebble conglomerate. Interpreted to be part of the proximal lower shoreface. Pebble lag represents a wave ravinement surface deposited during a rise in relative sea level

Similar stratigraphic interval, within estuarine fill. Collected to test the controls depositional facies has on zircon signature.

Table 7 (continued)

Sample ID	Interval	GPS - Latitude	GPS - Longitude	Section #	Hand Sample/Thin Section ID	Facies Description
BC DZ 14	Flood Tidal Delta at Mouth of MC	37.76825°	-111.6985°	MS 5	MC-TS-14	Coarse-grained trough cross-stratified lenticular bedded barforms containing abundant shell material. Bars are half meter thick. Sample was collected 2 m below white tidal sheet. Coarse-based bars fine upwards over 2 m.
BC DZ 15	E' shoreface	37.77000°	-111.698683°	MS 5	MC-TS-15	Very fine-grained sandstone with pervasive hummocky cross-stratification. Burrows and plant fragments are common. Sample collected 15-20 m above wave ravinement surface. Sandstone is 1 meter thick and very well cemented.
BC DZ 16	Upper Fluvial Deposits	37.768583°	-111.7362°	MS 5	MC-TS-16	Fine-to medium-grained sandstone deposited as a distributary channel and mouth bar. Collected at 75 m on MS-6. 5 to 10 m below heavily brecciated clinker beds.
BC DZ 17	Upper Flow Regime Sand Flats	37.7681°	-111.738967°	MS 1	MC-TS-17	Fine-grained massive sandstone w/ scattered troughs and planar laminations. Deposited as upper flow regime sand flats in the inner portions of an estuary. Overlies the lower John Henry Member Sequence Boundary

Table 8

Channel and transgressive lag clast count data

Litho	A	B mm	C	Interval
G Cht	26		45	Calico
G Cht	9		18	Calico
W Qtzt	10		18	Calico
B Qtzt	11		17	Calico
LB Cht	13		22	Calico
G Cht	11		21	Calico
G Cht	10		17	Calico
B Qtzt	15		23	Calico
B Cht	14		25	Calico
G Cht	14		24	Calico
G Cht	23		39	Calico
W Qtzt	15		26	Calico
G Cht	8		14	Calico
G Qtzt	10		18	Calico
B Cht	10		19	Calico
W Q	12		21	Calico
B Cht	15		26	Calico
G Cht	15		27	Calico
G Cht	16		38	Calico
G Cht	20		27	Calico
B Cht	20		30	Calico
B Cht	17		23	Calico
G Cht	26		33	Calico
B Cht	7		10	Calico
G Cht				Calico
W Q	12		18	Calico
W Cht	15		20	Calico
G Cht	12		16	Calico
W Q	4		6	Calico
G Cht	12		56	Calico
B Cht	21		22	Calico
G Cht	15		30	Calico

Litho	A	B mm	C	Interval
B Cht	12		21	Calico
LB Cht	10	18	21	Calico
B Cht	18	26	43	Calico
B Cht	15	19	27	Calico
W SS	12	15	28	Calico
LB Cht	11	17	20	Calico
G Cht	12	16	21	Calico
W Q	5	12	17	Calico
G Cht	4	24	30	Calico
G Cht	12	19	20	Calico
G Q	15	18	27	Calico
G Cht	16	22	28	Calico
G Cht	17	19	21	Calico
B Cht	16	22	25	Calico
W SS	10	15	18	Calico
B Cht	12	18	32	Calico
G Cht	4	16	30	Calico
G Cht	20	27	32	Calico
W Cht	10	12	17	Calico
B Cht	12	17	20	Calico
G Cht	16	24	34	Calico
S Q	12	15	20	Calico
B Cht	7	10	14	Calico
B Cht	14	15	25	Calico
G Cht	13	21	27	Calico
G Cht	23	35	46	Calico
B Cht	11	18	26	Calico
W Q	11		23	Calico
G Cht	15	19	24	Calico
G Cht	12	18	34	Calico
G Cht				Calico
B Cht	10	17	20	Calico

Litho	A	B mm	C	Interval
B Cht	-	-	-	Calico
W Cht	-	-	-	Calico
G Cht	16	26	30	Calico
W Q	11	18	25	Calico
G Cht	7	12	24	Calico
W Cht	9	11	14	Calico
G Cht	12	14	24	Calico
G Cht	8	12	14	Calico
W Q	-	-	-	Calico
G Cht	11	12	17	Calico
Granite	12	16	20	Calico
W Cht	-	-	-	Calico
B Cht	17	20	31	Calico
G Cht	12	14	17	Calico
G Cht	7	12	18	Calico
W Q	8	9	11	Calico
G Cht	13	20	26	Calico
LB Cht	11	15	22	Calico
G Cht	11	16	20	Calico
LG Cht	11	12	17	Calico
W Cht	14	18	26	Calico
G Cht	12	17	23	Calico
W Cht	5	6	9	Calico
W Q	10	17	26	Calico
G Cht	8	13	19	Calico
W Q	6	11	13	Calico
W Cht	10	13	17	Calico
W Cht	11	23	30	Calico
Tan SS	10	11	13	Calico
B Cht	5	8	11	Calico
W Qtzt	6	16	20	Calico
B Cht	7	18	20	Calico

Table 8 (continued)

Litho	A	B mm	C	Interval	Litho	A	B mm	C
G Cht	6	10	17	Calico	B Cht	13	20	26
SS	9	10	18	Calico	G Cht	8	12	15
G Cht	5	6	10	Calico	G Cht	16	22	30
G Cht	8	11	15	Calico	G Cht	14	17	19
G Cht	10	12	15	Calico	G Qtzt	14	17	24
LB Cht	8	12	15	Calico	W Q	10	17	15
S Q	6	12	18	Calico	G SS	-	-	-
G Cht	7	10	14	Calico	S Q	8	10	16
W Cht	9	10	15	Calico	W SS	20	26	35
B Cht	6	8	11	Calico	B Cht	15	18	25
G Cht	9	13	16	Calico	G Cht	5	12	17
B Cht	6	10	13	Calico	G Cht	35	40	60
W Cht	20	24	33	Calico	LB Cht	12	15	20
G Cht	5	12	26	Calico	B Cht	8	10	13
G Qtzt	12	15	17	Calico	W Q	5	9	14
Tan SS	13	15	19	Calico	G Cht	14	19	20
G Q	7	13	15	Calico	B Cht	7	8	22
W Cht	8	11	12	Calico	RB Cht	20	25	28
G Cht	12	15	21	Calico	W Q	3	3	4
B Cht	6	10	12	Calico	G Cht	15	18	22
W Cht	17	17	37	Calico	RB Cht	12	17	22
W Q	8	10	12	Calico	G Cht	12	15	17
G Q	5	6	10	Calico	G Cht	12	17	21
G Cht	7	11	17	Calico	G Cht	11	15	18
G Cht	11	13	15	Calico	B Cht	6	7	12
G Cht	4	8	10	Calico	G Cht	13	18	24
B Cht	18	19	24	Calico	G Cht	8	13	16
W Q	5	8	11	Calico	G Cht	5	12	17
G Cht	13	20	22	Calico	LB Cht	9	13	17
B Cht	8	10	13	Calico	B Cht	6	6	10
G Cht	13	20	25	Calico	G Cht	7	12	18
W Q	15	18	20	Calico	G Cht	3	10	11

Interval	Litho	A	B mm	C	Interval
Calico	W Q	4	7	8	Calico
Calico	W Q	5	7	11	Calico
Calico	LB Cht	5	8	11	Calico
Calico	B Cht	7	10	13	Calico
Calico	G Cht	20	22	32	Calico
Calico	G Cht	5	12	22	Calico
Calico	G Cht	6	9	12	Calico
Calico	LB Cht	11	11	13	Calico
Calico	G Cht	10	20	27	Calico
Calico	W Q	8	12	14	Calico
Calico	W Cht	10	13	17	Calico
Calico	G Cht	17	25	28	Calico
Calico	RB Cht	13	15	25	Calico
Calico	B Cht	6	8	10	Calico
Calico	G Cht	10	12	17	Calico
Calico	G Cht	12	15	17	Calico
Calico	W Q	9	14	17	Calico
Calico	LB Cht	7	9	17	Calico
Calico	B Cht	6	7	16	Calico
Calico	W Cht	4	6	13	Calico
Calico	G Cht	10	13	17	Calico
Calico	G Cht	4	8	9	Calico
Calico	B Cht	9	12	16	Calico
Calico	G Cht	17	21	46	Calico
Calico	W Cht	9	10	14	Calico
Calico	G Cht	9	10	15	Calico
Calico	G Cht	12	14	21	Calico
Calico	G Cht	9	12	21	Calico
Calico	LB Cht	9	13	17	Calico
Calico	B Cht	7	15	21	Calico
Calico	W Q	7	15	17	Calico
Calico	G Cht	5	6	12	Calico

Table 8 (continued)

Litho	A	B mm	C	Interval
W Qtzt	8	9	11	Calico
W Q	7	11	16	Calico
W Cht	4	9	16	Calico
G Cht	3	6	10	Calico
LB Cht	3	4	6	Calico
W Q	4	5	6	Calico
W Qtzt	6	12	16	Calico
G Cht	3	5	7	Calico
W Cht	2	4	6	Calico
W Q	3	5	7	Calico
G Cht	7	10	17	Calico
G Cht	10	15	20	Calico
W Q	4	5	7	Calico
W Q	5	7	10	Calico
G Cht	8	10	12	Calico
B Cht	7	9	16	Calico
G Cht	8	11	13	Calico
G Cht	9	11	22	Calico
LB Cht	9	10	18	Calico
G Cht	8	13	26	Calico
G Cht	7	9	12	Calico
B Cht	7	10	13	Calico
G Cht	5	7	8	Calico
W Cht	9	10	13	Calico
B Cht	4	6	9	Calico
LB Cht	5	9	16	Calico
G Cht	7	12	13	Calico
W Cht	5	8	10	Calico
W Q	6	7	11	Calico
G Cht	4	7	12	Calico
G Cht	19	20	37	Calico
W Q	6	8	10	Calico

Litho	A	B mm	C
G Cht	7	10	16
G Cht	12	14	23
G Cht	13	17	27
G Cht	7	12	15
W Q	8	9	13
G Cht	7	11	22
G Cht	12	13	17
W Cht	14	18	25
G Cht	17	23	52
B Cht	7	9	11
G Cht	7	8	13
G Cht	19	13	16
G Cht	15	17	27
G Cht	16	20	30
W Q	3	6	8
B Cht	10	18	23
B Cht	9	23	27
G Cht	15	27	28
B Cht	6	18	20
W Cht	12	25	30
B Cht	2	5	8
G Cht	8	12	16
B Cht	12	14	18
G Cht	11	15	20
W Q	5	12	13
G Cht	15	28	32
G Cht	12	30	35
G Cht	5	17	22
LB Cht	9	14	18
B Cht	14	22	30
G Cht	9	14	17
B Cht	5	8	9

Interval	Litho	A	B mm	C	Interval
Calico	B Cht	5	7	9	Calico
Calico	LB Cht	5	8	10	Calico
Calico	W Q	6	7	10	Calico
Calico	W Cht	14	15	26	Calico
Calico	G CHt	10	14	16	Calico
Calico	LB Cht	8	13	17	Calico
Calico	LB Cht	10	12	15	Calico
Calico	B Cht	17	25	28	Calico
Calico	B Cht	10	17	20	Calico
Calico	B Cht	14	17	25	Calico
Calico	LB Cht	9	14	20	Calico
Calico	G Cht	5	9	8	Calico
Calico	W Cht	8	12	17	Calico
Calico	G Cht	3	7	18	Calico
Calico	G Cht	18	23	31	Calico
Calico	LB Cht	3	10	13	Calico
Calico	B Cht	9	10	15	Calico
Calico	LB Cht	5	9	12	Calico
Calico	G Cht	12	25	30	Calico
Calico	G Cht	10	17	20	Calico
Calico	G Cht	4	5	10	Calico
Calico	LB Cht	8	8	18	Calico
Calico	B Cht	17	20	27	Calico
Calico	G Cht	5	9	9	Calico
Calico	B Cht	16	26	30	Calico
Calico	LB Cht	10	43	56	Calico
Calico	B Cht	5	8	10	Calico
Calico	LB Cht	9	10	22	Calico
Calico	G Cht	10	15	28	Calico
Calico	G Cht	10	15	25	Calico
Calico	W Q	5	8	10	Calico
Calico	W Q	5	5	10	Calico

Table 8 (continued)

Litho	A	B mm	C	Interval
LB Cht	4	4	10	Calico
LB Cht	5	9	11	Calico
B Cht	11	20	22	Calico
T SS	12	23	25	Calico
G Cht	12	17	20	Calico
G Cht	7	15	20	Calico
B Cht	8	9	17	Calico
LB Cht	10	17	18	Calico
B Cht	12	15	15	Calico
G Cht	6	17	17	Calico
W Cht	11	20	26	Calico
B Cht	12	15	18	Calico
CoarseSS	14	-	16	wRs (1)
G Qtzt	15	-	20	wRs (1)
W Qtzt	15	-	20	wRs (1)
B Cht	16	-	25	wRs (1)
G Cht	5	-	10	wRs (1)
W Qtzt	16	-	37	wRs (1)
W Qtzt	27	-	38	wRs (1)
W Qtzt	8	-	17	wRs (1)
G Cht	10	-	13	wRs (1)
W Qtzt	14	-	15	wRs (1)
P Qtzt	11	-	19	wRs (1)
B Cht	17	-	24	wRs (1)
W Qtzt	10	-	12	wRs (1)
W Cht	21	-	42	wRs (1)
W Qtzt	9	-	16	wRs (1)
R Qtzt	50	-	75	wRs (1)
G Cht	13	-	30	wRs (1)
G Cht	12	-	38	wRs (1)
P Qtzt	8	-	26	wRs (1)
W Qtzt	8	-	12	wRs (1)

Litho	A	B mm	C
G Cht	5	-	20
G Cht	9	-	22
W Qtzt	12	-	13
W Qtzt	17	-	20
G Cht	17	-	32
W Qtzt	11	-	15
G Cht	9	-	13
W Qtzt	11	-	15
LB Cht	17	-	25
G Cht	12	-	18
W Cht	17	-	39
G Cht	17	-	32
W Qtzt	18	-	15
G Cht	10	-	13
W Cht	5	-	9
W Qtzt	20	-	38
B Cht	7	-	13
W Qtzt	10	-	17
W Cht	10	-	20
LG Cht	6	-	10
L Cht	16	-	25
W Qtzt	11	-	22
LB Cht	6	-	20
W Qtzt	18	-	25
G Cht	12	-	33
B Cht	4	-	6
W Qtzt	19	-	38
W Qtzt	30	-	38
P Qtzt	15	-	22
W Qtzt	20	-	27
W Qtzt	12	-	22
W Qtzt	13	-	24

Interval	Litho	A	B mm	C	Interval
wRs (1)	W Qtzt	13	-	20	wRs (1)
wRs (1)	W Qtz	18	-	30	wRs (1)
wRs (1)	LB Qtzt	16	-	27	wRs (1)
wRs (1)	Tan Cht	12	-	20	wRs (1)
wRs (1)	P Qtzt	12	-	21	wRs (1)
wRs (1)	P Qtzt	17	-	33	wRs (1)
wRs (1)	W Cht	17	-	20	wRs (1)
wRs (1)	W Qtzt	17	-	27	wRs (1)
wRs (1)	R Qtzt	9	-	16	wRs (1)
wRs (1)	G CHt	12	-	17	wRs (1)
wRs (1)	W Qtzt	13	-	23	wRs (1)
wRs (1)	G Cht	10	-	26	wRs (1)
wRs (1)	B Cht	-	-	-	wRs (1)
wRs (1)	P Qtzt	6	-	12	wRs (1)
wRs (1)	G Cht	18	-	42	wRs (1)
wRs (1)	LB Qtzt	11	-	17	wRs (1)
wRs (1)	W Qtzt	20	-	40	wRs (1)
wRs (1)	W Qtzt	9	-	17	wRs (1)
wRs (1)	W Qtzt	15	-	23	wRs (1)
wRs (1)	G Cht	9	-	20	wRs (1)
wRs (1)	W Qtzt	15	-	16	wRs (1)
wRs (1)	P Qtzt	10	-	25	wRs (1)
wRs (1)	W Qtzt	7	-	18	wRs (1)
wRs (1)	G Qtzt	7	-	17	wRs (1)
wRs (1)	W Qtzt	20	-	32	wRs (1)
wRs (1)	G Cht	9	-	15	wRs (1)
wRs (1)	W Cht	12	-	17	wRs (1)
wRs (1)	P Qtzt	12	-	22	wRs (1)
wRs (1)	G Cht	6	-	11	wRs (1)
wRs (1)	G Qtzt	25	-	57	wRs (1)
wRs (1)	P Qtzt	17	-	21	wRs (1)
wRs (1)	G Cht	20	-	44	wRs (1)

Table 8 (continued)

Litho	A	B mm	C	Interval
P Qtzt	16	-	27	wRs (1)
B Cht	11	-	26	wRs (1)
W Qtzt	17	-	28	wRs (1)
B Cht	16	-	26	wRs (1)
W Qtzt	17	-	29	wRs (1)
W Qtzt	7	-	19	wRs (1)
LB Qtzt	16	-	29	wRs (1)
W Qtzt	11	-	20	wRs (1)
LB Qtzt	12	-	26	wRs (1)
W Qtzt	12	-	18	wRs (1)
B Cht	8	-	14	wRs (1)
TLB Qtzt	13	-	19	wRs (1)
W Qtzt	10	-	19	wRs (1)
w Qtzt	11	-	18	wRs (1)
W Qtzt	6	-	24	wRs (1)
B Cht	9	-	20	wRs (1)
MS	70	-	300	wRs (1)
P Qtzt	11	13	22	wRs (1)
LB Cht	11	18	19	wRs (1)
W Qtzt	8	12	13	wRs (1)
RB Cht	19	22	36	wRs (1)
W Qtzt	8	12	14	wRs (1)
W Qtzt	11	12	16	wRs (1)
P Qtzt	22	25	32	wRs (1)
W Qtzt	32	45	56	wRs (1)
Lb Qtzt	42	45	58	wRs (1)
G Cht	18	21	26	wRs (1)
P Qtzt	7	8	11	wRs (1)
G Qtzt	15	18	23	wRs (1)
W Cht	10	13	14	wRs (1)
W Qtzt	15	18	24	wRs (1)
W Qtzt	80	100	150	wRs (1)

Litho	A	B mm	C
P Qtzt	19	20	24
W Qtzt	32	45	56
W Qtzt	19	27	37
W Qtzt	8	10	21
W Qtzt	50	58	62
P Qtzt	6	10	16
P Qtzt	55	65	75
G Cht	5	10	12
LB Qtzt	38	40	45
G Cht	9	10	16
W Qtzt	15	35	38
BG Cht	7	10	12
W Qtzt	39	45	55
Br Qtzt	4	7	8
Br Cht	15	21	30
W Qtzt	7	11	18
G Qtzt	20	25	32
W Qtzt	6	9	10
G Cht	7	12	18
B Cht	12	18	20
P Qtzt	45	55	91
LG Cht	6	10	13
W Qtzt	20	32	38
W Qtzt	7	8	11
B Cht	23	28	32
G Cht	2	4	5
W Qtzt	30	48	58
W Qtzt	76	82	130
W Q	8	24	26
W Qtzt	32	38	42
W Cht	6	8	13
LB Qtzt	20	30	32

Interval	Litho	A	B mm	C	Interval
wRs (1)	W Qtzt	14	25	28	wRs (1)
wRs (1)	LB Qtzt	12	20	28	wRs (1)
wRs (1)	G Qtzt	12	28	30	wRs (1)
wRs (1)	W Qtzt	4	5	6	wRs (1)
wRs (1)	52	4	8	12	wRs (1)
wRs (1)	W Qtzt	5	8	10	wRs (1)
wRs (1)	P Qtzt	30	40	56	wRs (1)
wRs (1)	W Qtzt	6	7	10	wRs (1)
wRs (1)	W Cht	12	14	15	wRs (1)
wRs (1)	W Qtzt	5	7	9	wRs (1)
wRs (1)	W Cht	20	41	52	wRs (1)
wRs (1)	W Cht	2	5	8	wRs (1)
wRs (1)	B Cht	4	10	13	wRs (1)
wRs (1)	G Cht	5	7	9	wRs (1)
wRs (1)	W Qtzt	25	28	32	wRs (1)
wRs (1)	W Cht	5	6	9	wRs (1)
wRs (1)	B Cht	6	8	9	wRs (1)
wRs (1)	W Cht	28	40	50	wRs (1)
wRs (1)	G Cht	3	9	11	wRs (1)
wRs (1)	52	15	20	30	wRs (1)
wRs (1)	Q	4	8	10	wRs (1)
wRs (1)	RB Cht	7	8	10	wRs (1)
wRs (1)	B Cht	5	10	13	wRs (1)
wRs (1)	G Cht	5	7	8	wRs (1)
wRs (1)	B Cht	8	12	20	wRs (1)
wRs (1)	W Qtzt	3	8	10	wRs (1)
wRs (1)	52	5	10	12	wRs (1)
wRs (1)	G CHt	5	7	8	wRs (1)
wRs (1)	B CHt	14	15	23	wRs (1)
wRs (1)	P Qtzt	5	6	7	wRs (1)
wRs (1)	G Cht	3	5	9	wRs (1)
wRs (1)	LB Qtzt	30	40	52	wRs (1)

Table 8 (continued)

Litho	A	B (mm)	C	Interval	Litho	A	B (mm)	C
B Cht	8	10	16	wRs (1)	W Cht	9	10	15
G CHt	6	7	8	wRs (1)	G Qtzt	12	26	30
W Qtzt	12	15	17	wRs (1)	W Qtzt	9	15	17
P Qtzt	3	5	5	wRs (1)	G Cht	10	21	25
P Qtzt	3	6	8	wRs (1)	C Cht	11	15	18
W Qtzt	35	42	57	wRs (1)	P Qtzt	10	12	22
52	3	6	8	wRs (1)	B Cht	9	12	15
W Qtzt	10	12	62	wRs (1)	P Qtzt	10	16	18
LB Cht	2	3	4	wRs (1)	G Cht	10	12	12
Br Cht	4	5	6	wRs (1)	W Qtzt	10	16	22
B CHt	32	50	60	wRs (1)	LB Qtzt	10	16	20
W Cht	4	5	7	wRs (1)	W Qtzt	10	10	12
Pr Qtzt	11	12	14	wRs (1)	W Cht	11	12	19
B Cht	4	5	7	wRs (1)	52	12	15	25
W Qtzt	20	25	30	wRs (1)	W Qtzt	6	12	15
G Qtzt	16	20	30	wRs (1)	W Qtzt	40	49	82
G Cht	2	4	6	wRs (1)	52	8	13	17
W Qtzt	18	30	38	wRs (1)	W Qtzt	16	20	30
G Cht	8	10	17	wRs (1)	LB Cht	5	10	12
W Qtzt	15	20	30	wRs (1)	LB Cht	18	22	30
G Cht	15	10	25	wRs (1)	52	25	26	40
G Qtzt	12	15	20	wRs (1)	W Qtzt	21	23	25
B Cht	9	10	16	wRs (1)	W Qtzt	45	65	85
G Cht	12	15	24	wRs (1)	W	12	15	22
W Qtzt	20	25	40	wRs (1)	Q Qtz	12	13	24
G Qtzt	20	27	36	wRs (1)	B Cht	22	30	35
LB Qtzt	7	13	21	wRs (1)	W Qtzt	6	10	12
W Qtzt	25	46	56	wRs (1)	W Cht	18	30	34
W Qtzt	15	20	20	wRs (1)	G Cht	7	14	18
P Qtzt	12	16	18	wRs (1)	B Cht	10	14	18
G Cht	40	45	70	wRs (1)	RB Cht	8	9	11
W Qtzt	30	30	40	wRs (1)	W Qtzt	8	10	13

Interval	Litho	A	B mm	C	Interval
wRs (1)	W Cht	7	11	14	wRs (1)
wRs (1)	B Cht	11	12	21	wRs (1)
wRs (1)	P Qtzt	16	26	29	wRs (1)
wRs (1)	W Qtzt	27	46	50	wRs (1)
wRs (1)	W Cht	8	16	24	wRs (1)
wRs (1)	W Qtzt	26	39	63	wRs (1)
wRs (1)	W Qtzt	9	13	19	"A" SF
wRs (1)	W Qtzt	6	8	10	"A" SF
wRs (1)	W Cht	9	12	19	"A" SF
wRs (1)	W Q	6	8	10	"A" SF
wRs (1)	W Qtzt	10	11	17	"A" SF
wRs (1)	P Qtzt	8	12	17	"A" SF
wRs (1)	W Qtz	2	3	5	"A" SF
wRs (1)	W Cht	9	9	16	"A" SF
wRs (1)	W Cht	19	25	34	"A" SF
wRs (1)	W Cht	9	13	18	"A" SF
wRs (1)	W Qtzt	4	7	9	"A" SF
wRs (1)	G cht	4	7	10	"A" SF
wRs (1)	G Cht	5	7	8	"A" SF
wRs (1)	LB Cht	13	26	30	"A" SF
wRs (1)	G Cht	5	7	10	"A" SF
wRs (1)	W Cht	4	6	6	"A" SF
wRs (1)	G Cht	14	15	27	"A" SF
wRs (1)	W Cht	25	33	57	"A" SF
wRs (1)	G Cht	20	20	32	"A" SF
wRs (1)	W Cht	7	9	11	"A" SF
wRs (1)	G Qtzt	10	20	20	"A" SF
wRs (1)	W Qtzt	5	8	9	"A" SF
wRs (1)	P Qtzt	7	8	12	"A" SF
wRs (1)	LB Cht	5	8	10	"A" SF
wRs (1)	G cht	7	8	12	"A" SF
wRs (1)	W Qtzt	7	11	13	"A" SF

Table 8 (continued)

Litho	A	B mm	C	Interval
G Cht	21	28	39	"A" SF
P Qtzt	18	24	34	"A" SF
W Qtzt	10	15	16	"A" SF
W Cht	5	9	10	"A" SF
G Cht	6	10	13	"A" SF
W Qtzt	20	28	33	"A" SF
P Qtzt	18	23	30	"A" SF
W Qtzt	3	4	4	"A" SF
B Cht	8	9	11	"A" SF
W Qtzt	5	8	9	"A" SF
P Qtzt	3	5	6	"A" SF
G Cht	5	7	10	"A" SF
P Qtzt	8	10	18	"A" SF
W Qtzt	8	9	12	"A" SF
W Qtzt	9	15	18	"A" SF
W Cht	8	10	14	"A" SF
G Cht	12	15	22	"A" SF
LB Qtzt	14	17	24	"A" SF
W Cht	8	11	13	"A" SF
W Qtzt	9	11	14	"A" SF
W Cht	12	18	27	"A" SF
W Cht	4	8	14	"A" SF
W Cht	7	9	12	"A" SF
G cht	22	27	36	"A" SF
P Qtzt	9	16	22	"A" SF
W Cht	6	7	11	"A" SF
W Qtzt	7	12	14	"A" SF
G cht	14	20	29	"A" SF
LB Qtzt	5	7	11	"A" SF
W Cht	6	8	11	"A" SF
W Cht	5	8	10	"A" SF
LB Cht	12	18	25	"A" SF

Litho	A	B mm	C
W Qtzt	6	7	12
W Qtzt	7	8	9
LB Cht	6	9	10
P Qtzt	11	15	29
LB Cht	10	12	17
W Cht	11	12	16
LB Cht	4	6	8
LB Qtzt	6	9	17
W Qtzt	10	11	18
P Qtzt	7	9	14
LB Cht	6	10	14
LB Qtzt	21	22	37
W Cht	25	28	44
LB Cht	10	16	19
W Cht	6	6	11
W Q	7	9	11
RB Cht	5	8	10
W Qtzt	5	7	10
B Cht	15	22	28
W Qtzt	8	22	24
B Qtzt	13	20	28
B Cht	12	15	20
B Cht	9	13	16
W Qtzt	10	12	15
LB Cht	10	16	20
R Qtzt	18	21	42
Br Qtzt	9	27	31
LB Qtzt	5	7	8
R Qtzt	12	17	20
Lb Cht	9	10	15
LB Cht	10	17	22
W Cht	3	5	5

Interval	Litho	A	B mm	C	Interval
"A" SF	B Cht	15	18	20	"A" SF
"A" SF	LB Cht	8	10	12	"A" SF
"A" SF	W Cht	10	10	15	"A" SF
"A" SF	Br Cht	4	11	12	"A" SF
"A" SF	W Cht	7	7	10	"A" SF
"A" SF	W Cht	7	10	12	"A" SF
"A" SF	W Cht	5	9	12	"A" SF
"A" SF	W Qtzt	8	10	10	"A" SF
"A" SF	G cht	7	7	9	"A" SF
"A" SF	B Cht	5	7	10	"A" SF
"A" SF	G Cht	5	7	10	"A" SF
"A" SF	W Qtzt	5	7	12	"A" SF
"A" SF	LB Cht	7	9	10	"A" SF
"A" SF	G Cht	6	10	10	"A" SF
"A" SF	W Qtzt	7	10	15	"A" SF
"A" SF	W Cht	5	10	12	"A" SF
"A" SF	W Cht	9	13	15	"A" SF
"A" SF	W Cht	7	13	16	"A" SF
"A" SF	B Cht	6	-	8	"A" SF
"A" SF	G cht	12	25	30	"A" SF
"A" SF	W Cht	10	13	15	"A" SF
"A" SF	G Cht	13	20	27	"A" SF
"A" SF	W Cht	10	18	20	"A" SF
"A" SF	W Qtzt	7	16	20	"A" SF
"A" SF	Pu Qtzt	15	18	27	"A" SF
"A" SF	W Qtzt	10	12	17	"A" SF
"A" SF	G Cht	12	13	20	"A" SF
"A" SF	B Cht	10	15	17	"A" SF
"A" SF	Pu Qtzt	9	12	17	"A" SF
"A" SF	G Cht	10	13	15	"A" SF
"A" SF	G Cht	10	15	17	"A" SF
"A" SF	G Cht	9	17	18	"A" SF

Table 8 (continued)

Litho	A	B mm	C	Interval
B Cht	10	14	15	"A" SF
B Cht	3	5	10	"A" SF
B Cht	5	9	10	"A" SF
W Cht	5	10	12	"A" SF
W Qtzt	7	10	13	"A" SF
G Cht	5	9	11	"A" SF
G Cht	7	12	14	"A" SF
LB Cht	3	10	12	"A" SF
W Cht	5	7	10	"A" SF
G Cht	8	10	13	"A" SF
G Cht	15	16	20	"A" SF
W Cht	8	10	12	"A" SF
B Cht	5	5	8	"A" SF
W Qtzt	3	5	10	"A" SF
LB Qtzt	18	37	50	"A" SF
B Cht	15	17	22	"A" SF
W Qtzt	5	10	9	"A" SF
W Cht	10	17	25	"A" SF
W Qtzt	7	10	13	"A" SF
LB Cht	12	16	18	"A" SF
W Cht	7	9	10	"A" SF
B Cht	12	14	15	"A" SF
W Cht	5	10	11	"A" SF
B Cht	5	10	12	"A" SF
G Cht	5	10	13	"A" SF
W Qtzt	4	17	12	"A" SF
G Cht	5	10	10	"A" SF
Br Cht	3	5	8	"A" SF
W Cht	27	32	35	"A" SF
G Cht	12	16	20	"A" SF
W Qtzt	20	25	35	"A" SF
G Cht	15	17	23	"A" SF

Litho	A	B mm	C
B Cht	4	5	10
W Qtzt	12	20	22
W Cht	5	9	15
G Cht	8	12	17
G Cht	7	13	15
W Qtzt	9	12	15
B CHt	8	10	15
B Cht	6	7	10
G Cht	8	10	16
W Cht	5	7	10
G Cht	60	70	90
G Qtzt	28	40	55
G Cht	15	26	34
LB Cht	20	28	38
LB Cht	27	32	30
LB Qtzt	5	10	12
G Cht	10	15	22
G Cht	7	10	12
W Qtzt	5	17	22
G Cht	16	23	28
T SS	10	14	20
G Cht	17	22	25
W Qtzt	12	15	20
W Cht	15	20	25
W Qtzt	9	12	18
G Cht	8	10	17
G Cht	8	10	15
W Cht	10	22	28
W Qtzt	10	10	10
W Cht	8	10	15
G Cht	5	12	13
G Cht	5	7	10

Interval	Litho	A	B	C	Interval
			mm		
"A" SF	G Cht	7	10	13	"A" SF
"A" SF	W Cht	10	12	18	"A" SF
"A" SF	W Cht	12	18	20	"A" SF
"A" SF	LB Cht	4	5	8	"A" SF
"A" SF	G Cht	9	17	22	"A" SF
"A" SF	W Qtzt	10	12	21	"A" SF
"A" SF	P Qtzt	5	8	11	"A" SF
"A" SF	W Qtzt	8	12	15	"A" SF
"A" SF	B Cht	3	7	9	"A" SF
"A" SF	W Cht	4	10	11	"A" SF
"A" SF	G Cht	3	5	7	"A" SF
"A" SF	G Cht	5	11	12	"A" SF
"A" SF	W Cht	5	7	10	"A" SF
"A" SF	G CHt	3	4	10	"A" SF
"A" SF	G Cht	8	10	14	"A" SF
"A" SF	W Qtzt	9	10	14	"A" SF
"A" SF	W Cht	5	10	12	"A" SF
"A" SF	W Cht	10	10	20	"A" SF
"A" SF	W Qtzt	4	5	9	"A" SF
"A" SF	W Cht	9	10	20	"A" SF
"A" SF	G Cht	5	7	8	"A" SF
"A" SF	W Qtzt	3	7	13	"A" SF
"A" SF	W Cht	4	9	10	"A" SF
"A" SF	G Cht	8	10	14	"A" SF
"A" SF	LB Cht	7	10	10	"A" SF
"A" SF	G CHt	4	8	9	"A" SF
"A" SF	P Q	3	4	8	"A" SF
"A" SF	G Cht	11	14	23	"A" SF
"A" SF	W Qtzt	15	25	28	"A" SF
"A" SF	W Cht	13	17	22	"A" SF
"A" SF	W Qtzt	10	18	24	"A" SF
"A" SF	W Qtzt	14	19	24	"A" SF

Table 8 (continued)

Litho	A	B mm	C	Interval	Litho	A	B mm	C	Interval	Litho	A	B mm	C	Interval
P Qtzt	19	21	66	"A" SF	W Cht	7	7	13	"A" SF	W Cht	10	13	16	"A" SF
LB Qtzt	16	23	37	"A" SF	G CHt	21	36	45	"A" SF	G Cht	14	20	27	"A" SF
G Cht	9	14	18	"A" SF	G Qtzt	14	23	36	"A" SF	W Cht	10	11	16	"A" SF
G Chr	13	22	34	"A" SF	LB Cht	14	17	19	"A" SF	G Cht	6	10	12	"A" SF
W Cht	9	11	15	"A" SF	W Cht	12	17	20	"A" SF	G Cht	6	8	11	"A" SF
W Qtzt	14	15	27	"A" SF	W Cht	11	15	16	"A" SF	G Cht	9	9	12	"A" SF
P Qtzt	9	12	20	"A" SF	W Cht	6	13	18	"A" SF	W Cht	7	13	17	"A" SF
G Cht	11	13	17	"A" SF	W Cht	8	9	13	"A" SF	W Cht	9	17	21	"A" SF
W Qtzt	12	13	14	"A" SF	P Qtzt	7	8	9	"A" SF	W Cht	11	16	20	"A" SF
P Qtzt	10	11	16	"A" SF	W Qtzt	5	9	10	"A" SF	W Cht	7	8	17	"A" SF
G Cht	8	12	16	"A" SF	B Cht	9	12	14	"A" SF	G Cht	14	23	32	"A" SF
W Qtzt	11	12	16	"A" SF	W Cht	4	7	9	"A" SF	G Cht	5	7	8	"A" SF
W Qtzt	8	12	15	"A" SF	P Qtzt	6	8	9	"A" SF	B Cht	15	18	33	"A" SF
G Cht	8	10	17	"A" SF	LB Cht	6	7	16	"A" SF	G Cht	8	13	15	"A" SF
W Cht	5	8	11	"A" SF	W Cht	7	9	9	"A" SF	G Cht	10	12	18	"A" SF
W Cht	7	11	13	"A" SF	W Cht	7	14	16	"A" SF	G Cht	7	11	13	"A" SF
G Cht	8	10	12	"A" SF	G Cht	7	8	11	"A" SF	W Cht	9	15	18	"A" SF
G Cht	6	7	10	"A" SF	W Cht	5	7	11	"A" SF	W Cht	8	10	13	"A" SF
W Qtzt	7	9	10	"A" SF	G Cht	5	10	12	"A" SF	B Cht	10	15	25	"A" SF
W Qtzt	5	7	10	"A" SF	W Cht	3	3	5	"A" SF	-	-	-	-	-
W Cht	5	6	8	"A" SF	P Qtzt	6	8	11	"A" SF	-	-	-	-	-
G Cht	5	6	6	"A" SF	W Cht	6	7	15	"A" SF	-	-	-	-	-
W Cht	5	7	7	"A" SF	W Cht	6	8	9	"A" SF	-	-	-	-	-
G Cht	5	6	9	"A" SF	G Cht	3	7	10	"A" SF	-	-	-	-	-
P Qtzt	4	5	9	"A" SF	G Cht	5	6	8	"A" SF	-	-	-	-	-
P Qtzt	56	64	103	"A" SF	P Qtzt	11	16	21	"A" SF	-	-	-	-	-
W Cht	6	10	16	"A" SF	W Cht	7	13	17	"A" SF	-	-	-	-	-
G Cht	6	10	16	"A" SF	W Qtzt	13	18	24	"A" SF	-	-	-	-	-
W Qtzt	9	12	15	"A" SF	W Cht	17	31	42	"A" SF	-	-	-	-	-
W Cht	9	10	15	"A" SF	G Cht	4	5	6	"A" SF	-	-	-	-	-
W Cht	7	9	14	"A" SF	W Qtzt	5	8	9	"A" SF	-	-	-	-	-
G Cht	8	10	18	"A" SF	G Cht	9	9	13	"A" SF	-	-	-	-	-

APPENDIX F

GEOLOGIC GUIDE TO MAIN CANYON

<Zero odometers> at the intersection of N. Creek Road and Main Canyon Road, continue straight on Main Canyon Road.

<0.6 mi> The road widens and the Calico Bed is exposed at road level. A small canyon (“Tidal Gulch”) along the north side of the road provides an opportunity to discuss the regional stratigraphy and make observations on the lower John Henry Member. Time permitting, return to this spot at the end of the day and do a short hike up Tidal Gulch to look at flood-tidal delta and tidal inlet facies above the “B” shoreface

Tidal Gulch

- A short (1-2 hour) hike up a small drainage provide access to a well preserved succession through a landward migrating barrier island system.
- The lower section is similar to those at the mouth of Sunman Canyon, however, note thicker offshore package equivalent to the “A” and “B” sandstones, and thinner proximal lower shoreface sands.
- Shoreface deposits at the mouth of Main Canyon are overlain by laminated gray lagoonal mudstones interbedded with thin sandstone beds that contain landward directed ripples, small scale trough cross sets, and inclined planar laminations. These are storm beds deposited on the landward side of a barrier island as washover fans.
- Amalgamated sands and gravel barforms overlie washover fans and lagoonal fines. Tidal indicators are everywhere through this facies. Look for: reactivation surfaces, accretion sets, mud drapes, herringbone cross-stratification, sigmoidal cross sets. Do you see any trace fossils? If so what kinds are there? If not why not? These sand and gravels were deposited as a landward prograding flood tidal delta.
- As you move up through the flood-tidal delta, notice a capping white medium-grained sandstone. This records deposition within a migrating tidal inlet. Evidence for flow reversal are plentiful, look for herringbone cross-stratification. Bioturbation is scarce in this interval, probably because the high-energy setting resulted in rapidly migrating barforms and channels that were inhospitable.

- A wave ravinement surface (wRs (2)) truncates the tidal inlet and places offshore mudstones and siltstones on top of the transgressive tidal deposits. Sharks teeth scattered throughout the conglomerate.
- Further up section, tidal bars overly the "E" shoreface recording deposition on a sand-rich back-barrier platform.
- Above the tidal deposits, thick accumulations of fluvial channels form complexes in excess of 30 m. These fluvial channels record infilling and basinward progradation of the coastal plain.

Tidal Gulch Research Questions

1. How to tidal deposits at the mouth of Main Canyon differ from those to the west?
2. What were the dominate controls on reservoir architecture within transgressive deposits at Main Canyon? Is there potential for compartmentalization within these reservoirs?
3. How would you distinguish between back-barrier and estuarine deposits? Are these always mutually exclusive?
4. What processes control reservoir architecture within the upper fluvial section?

<1.5 mi> Park on right side of the road. This stop provides a nice view of large incisions into shoreface strata on the south side of the canyon.

- The "A" and "B" shorefaces amalgamate to form a > 40 m cliff.
- The eastern margin of a northeast trending incised valley is exposed on the south side of the canyon.
- Notice fluvial terraces onlapping the valley wall.
- On the north side of the canyon, heterolithic channel forms create a 25 m complex.
- Lateral to this complex, are highly channelized debris flows that record bank collapse of an incising channel.

<2.2 mi> Park on the right side of the road just past a large alluvial ledge, at the mouth of "Sun Canyon." The hike will take 3 – 4 hours; be sure to bring plenty of water, food, and sunscreen. Stick to the southeast side of the canyon to begin, make a few stops in the Calico Bed and the offshore deposits of the "A" shoreface interval. Then, drop into the canyon and make your way to the top. Petroglyphs are visible on the northeast wall.

Sunman Canyon

- Amalgamated fluvial deposits of the Calico Bed outcrop in the lower section. This unit is a regional marker "bed" within the Straight Cliffs Formation that is typically very coarse grained and bleached white from overlying carbonaceous shales and the presence of kaolinite.
- Heterolithic "estuarine" strata overly the Calico bed and contain bidirectional cross stratification, compound cross-stratification, mud/carbonaceous drapes, and marine trace fossils.
- A quartzite pebble conglomerate truncates estuarine strata and is overlain by a 1-2 m thick swaley cross stratified shoreface sandstone. This is a wave ravinement surface

(wRs (1)) generated through shoreface retreat during rising sea-level.
- ~35 m of offshore marine mudstones/siltstones equivalent to the "A" shoreface.
- Look for marine trace fossils in the hummocky cross stratified beds at the top of parasequences and thin mudstones between sand beds. Traces to look out for: *Ophiomorpha, Thalassinoides, Palaeophycus, Planolites, Chondrites, Zoophycos.* Large tidal barforms downlap onto the "B" shoreface and form a tidal ravinement surface that scours in to the shoreface.
- Coarse grained sands with scattered quartzite pebbles, inoceramid, and oyster shell fragments occur at the base of these barforms.
- These are tidal dunes and bars deposited within migrating tidal channels within a mixed tide- and wave-dominated estuary.
- Look for indicators of flow reversal. Wavy and lenticular bedding occur throughout this interval. How does this style of bedding form?
- Look for master bedding planes and accretion surfaces on these bars.
- Bioturbation is limited in these tidal deposits. What does this tell us about the environment?
- Sandy deposits grade vertically into carbonaceous shales, do you see any fossils in these fine-grained deposits? What does the fossil assemblage tell you about the environment?
- The last stop on this hike will be to look at channelized debris flows. Look across the canyon and make some rough correlations. What do these debris flows correlate with across the canyon? How would these deposits form?
- wRs (2) truncates carbonaceous shales and estuarine deposits, resulting in renewed shoreface deposition.

<u>Sunman Canyon Research Questions</u>

1. Describe the nature of the contact between the shoreface and the overlying tidal barforms.
2. Is there evidence for subaerial exposure above the "B" shoreface?
3. What are the major vertical facies trends in the lower John Henry Member?
4. How do the tidal deposits within R-T cycle 1 relate to those at Tidal Gulch? How are they similar? How are they different?

<3.1 mi > Pull off the right side of the road and discuss large tidal channel within the middle John Henry Member. These channels correlate down-dip to the northeast to tidal sheets deposited within a sand-rich back-barrier. A realively easy hike is detailed below and allows access to tidal, estuarine, shoreface, and coastal plain facies. Begin the hike by heading towards the large tidal channel in the middle of the section, which is clearly visible from the road.

Main Canyon Proper
- This hike (2-3 hours) provides an opportunity to see excellent exposures of estuarine strata within R-T cycle 1 in addition to tidal channels, tidal flats, and bayhead deltas in R-T cycles 2 and 3.
- Cross bedded gravel lags within the "A" shoreface are exposed on the way up through

the shoreface cliffs.
- Once above the shoreface, make your way to the southeast and be on the look out for tidal channels. These are estuarine sandstone bodies.
- A stop along the eastern margin of a 16 m deep incision reveals a coarse-grained lag with abundant shell debris throughout. This is evidence for tidal ravinement and modification of the lower John Henry Member sequence boundary. Tidal channels developed during the early stages of relative sea-level rise needed to have high basinal energy to remove falling stage and lowstand fluvial deposits and deposit this lag.
- Continue up the section and notice the major stratigraphic trend. Sandstones fine upwards into carbonaceous shales that are locally dissected by tidal channels.
- A wave ravinement surface separates carbonaceous shales from offshore mudstones. Look for pebbles in the float to determine its location.
- Proximal lower shoreface depsoits are truncated by tidal channels as you continue up section.
- Tidal channels grade vertically and laterally into tidal flats and lagoonal mudstones.
- If time permits, hike laterally within R-T cycle 2 and look at the large tidal channel to the northwest. *Teredolites* and small surface traces are the only bioturbation in these units, indicating high energy and/or highly brackish water.

<3.6 mi> Park near a large boulder on the right side of the road. Hike up the north side of the road to get a good look at inclined heterolithic strata that occur above the "B" sandstone. These deposits record accretion along tidally influence point-bars,and/or tidal reworking of a bayhead delta within an estuarine environment. Additionally, from this location distributary mouth bars that occur above the "A" shoreface are visible. These deposits indicate a nearby outlet of a distributary channel that would have supplied sediment to the shoreline.

Main Canyon Research Questions

1. At what interval does the largest basinward shift in facies occur, the "A" or "B"?
2. Are the incised valleys observed in Main Canyon related to the expanded section at Buck Hollow?
3. Is there evidence that estuary deposits found in Main Canyon transition down depositional dip from freshwater to marine conditions?
4. What is the origin of mud-clast conglomerates that immediately overly the incision surface?
5. What controls reservoir distribution within this interval? What is the reservoir quality of transgressive deposits of western Main Canyon vs transgressive strata to the east?
6. What caused the fluvial systems to incise into the underlying shoreface? Tectonic forcing? Drop in relative sea level? Avulsion?

Main Canyon Proper

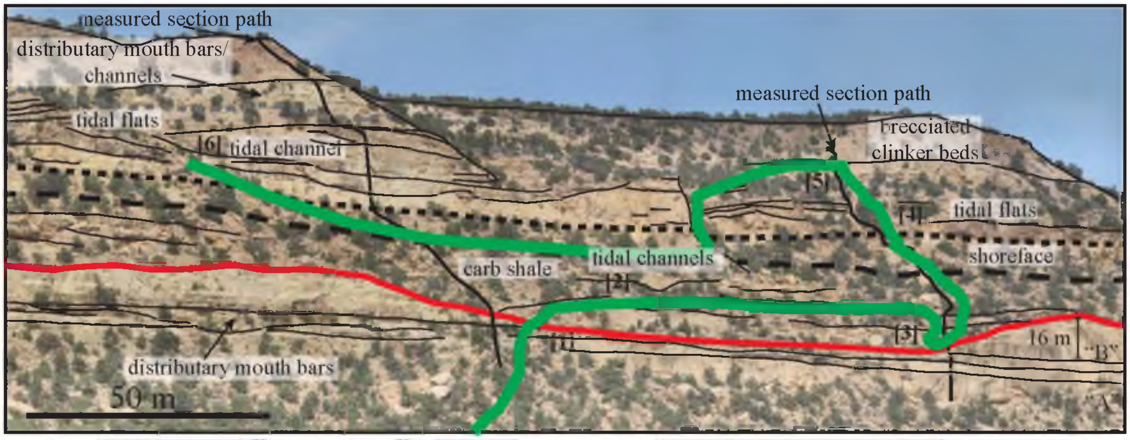

cross bedded gravels in "A" SF

tidal channels in estuarine fill

shells in gravels in shell lag (LJHMSB)

tidal flat deposits in R-T cycle 2

mouthbars and distributary channels

flank of large tidal channel

Sunman Canyon

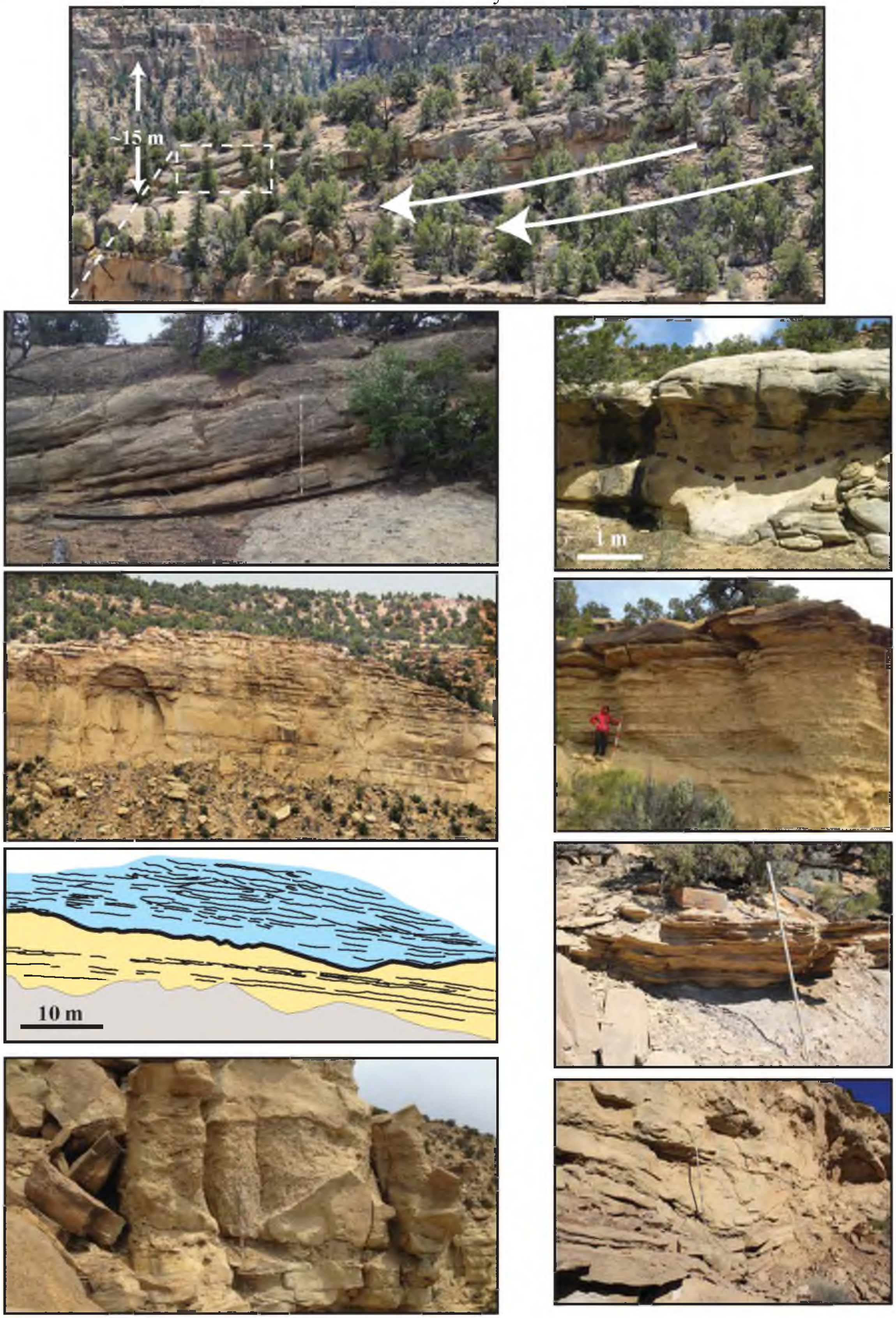

Tidal Gulch

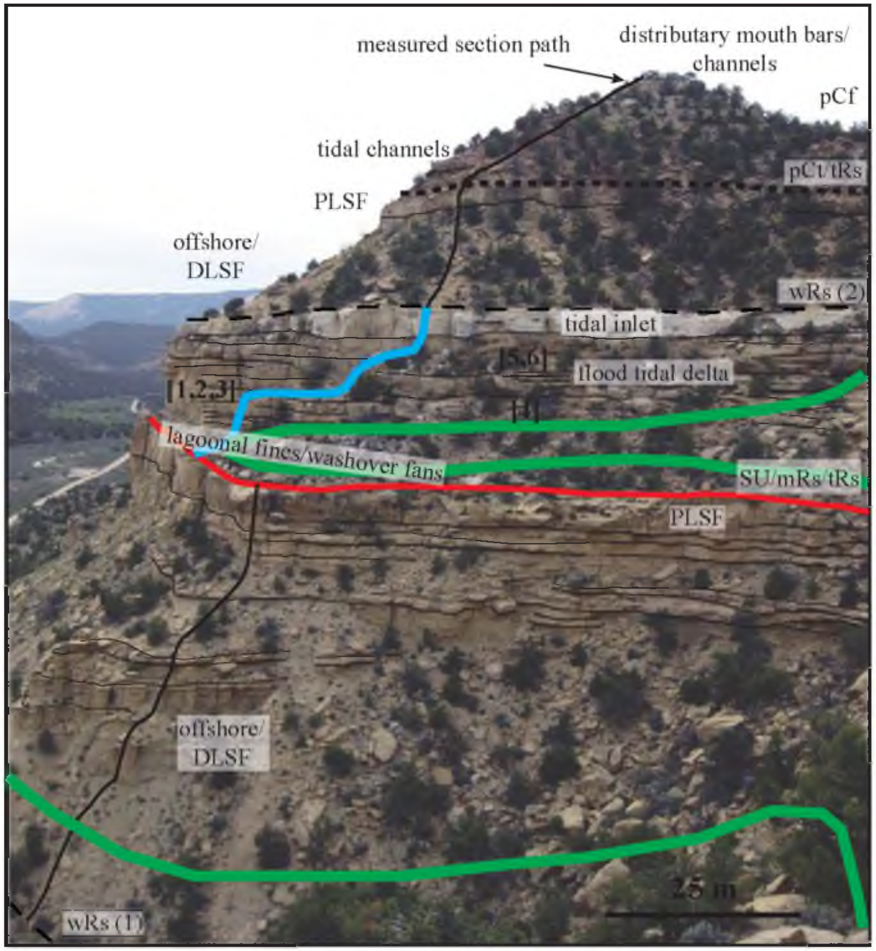

Tidal Gulch offers an opportunity to look at an excellently preserved flood tidal delta succession. Deposists coarsen upwards from grey lagoonal muds interbedded with washover fans into amalgmated gravels and sands, that are capped by a white tidal sheet recording the landward migration of the tidal inlet.

washover fans and bayfill

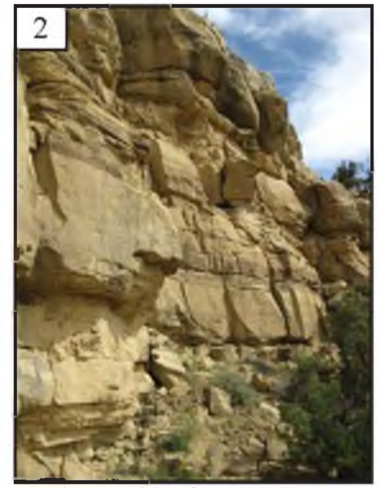

amalgmated barforms FTD

washover fans (landward flow)

tidal inlet

landward inclined accretions

herringbone cross stratification

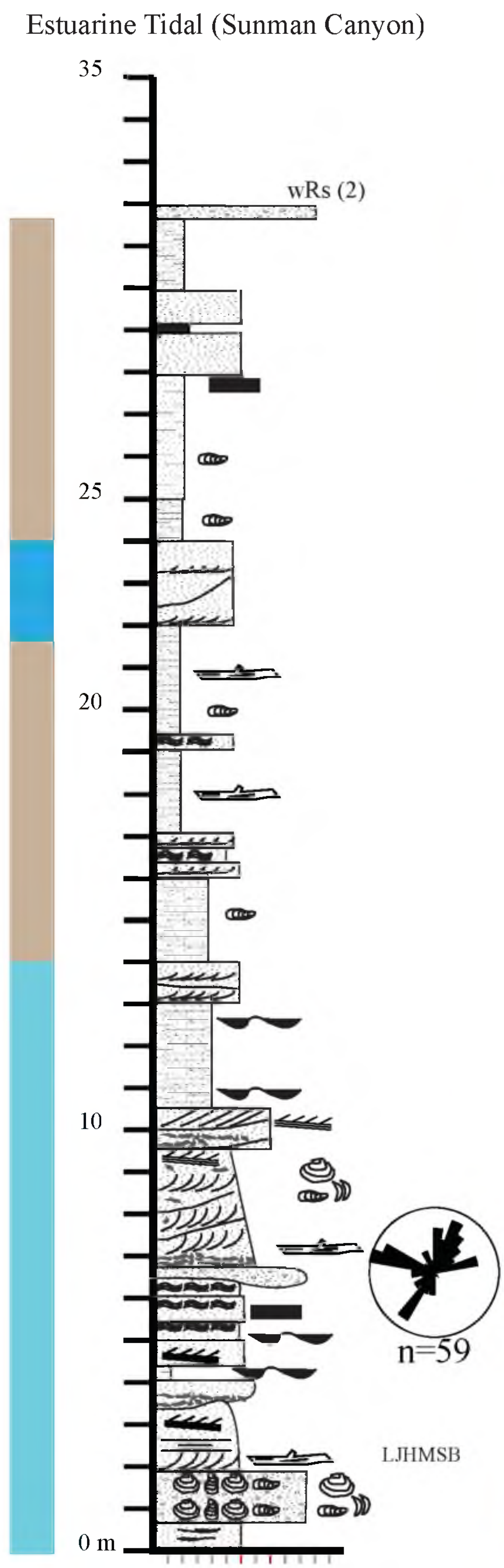
Estuarine Tidal (Sunman Canyon)
35
25
20
10
0 m
wRs (2)
n=59
LJHMSB

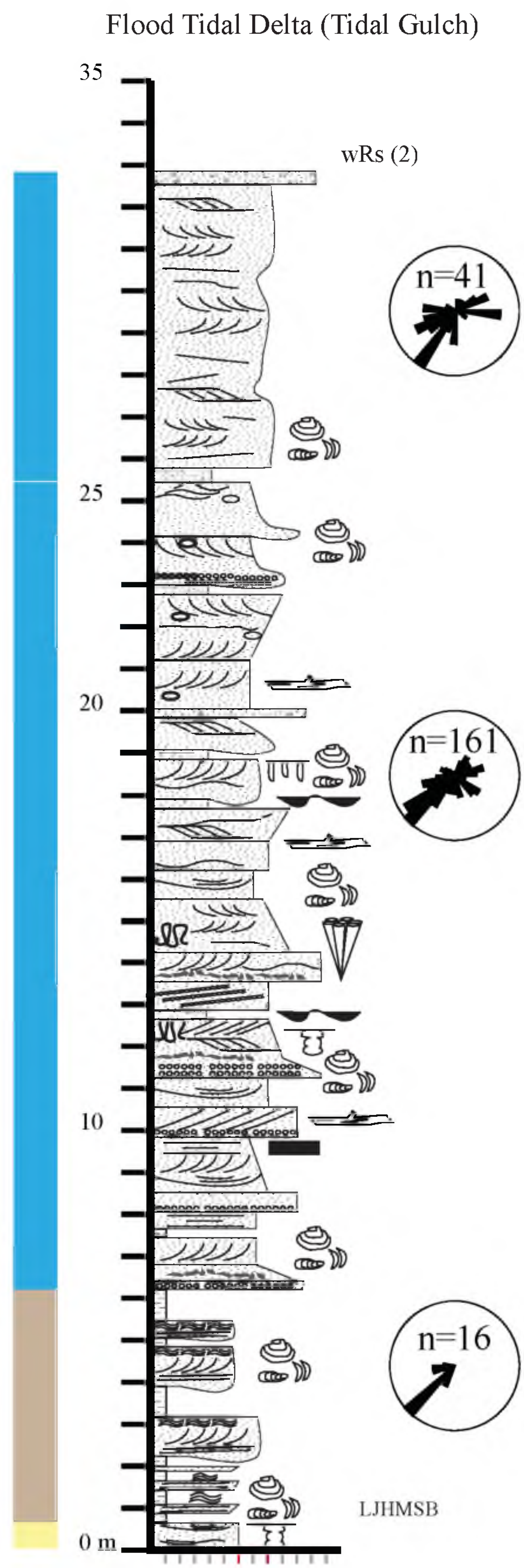
Flood Tidal Delta (Tidal Gulch)
35
25
20
10
0 m
wRs (2)
n=41
n=161
n=16
LJHMSB

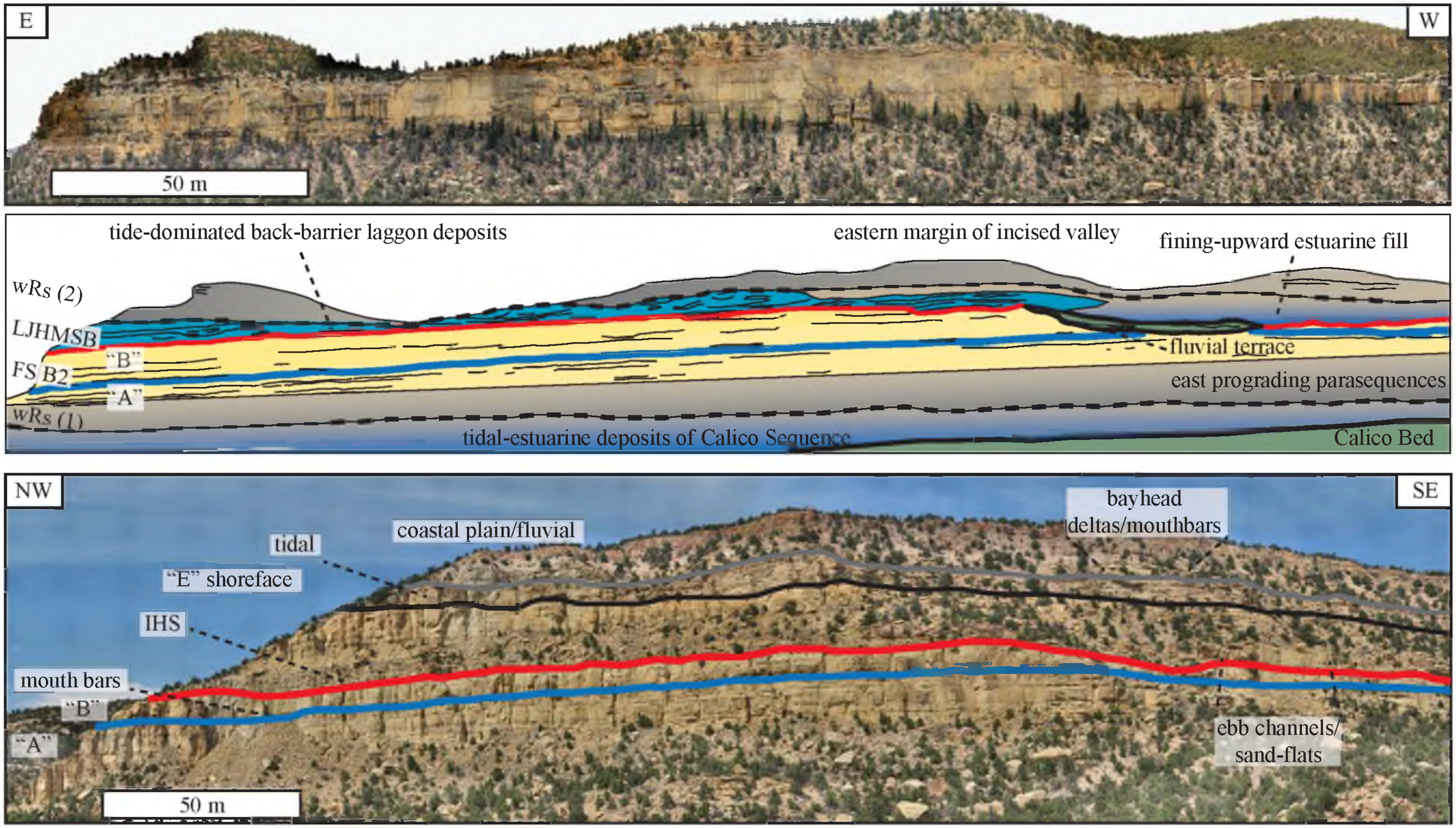
E
W
50 m
tide-dominated back-barrier laggon deposits
eastern margin of incised valley
fining-upward estuarine fill
wRs (2)
LJHMSB
"B"
FS B2
"A"
wRs (1)
fluvial terrace
east prograding parasequences
tidal-estuarine deposits of Calico Sequence
Calico Bed
NW
SE
coastal plain/fluvial
tidal
"E" shoreface
IHS
mouth bars
"B"
"A"
bayhead
deltas/mouthbars
ebb channels/
sand-flats
50 m

REFERENCES

Abdel-Fattah, S., Amin, A., Van Rijn, L. C., 2004, Sand transport in the Nile River, Egypt: Journal of Hydraulic Engineering, v. 130, p. 488–500.

Allen, G. P., 1991, Sedimentary processes and facies in the Gironde Estuary: a recent model for macrotidal estuarine systems, in D. G. Smith, G. E. Reinson, B. A. Zaitlin, and R. A., Rahmani, eds., Clastic tidal sedimentology: Canadian Society of Petroleum Geologists Memoir 16: p. 29–40.

Allen, J. L., 2009, Transgressive-regressive cycles in the John Henry Member, Straight Cliffs Formation, southern Utah, USA: University of Utah, p. 188.

Allen, J. L., and Johnson, C. L., 2011, Architecture and formation of transgressive-regressive cycles in marginal marine strata of the John Henry Member, Straight Cliffs Formation, Upper Cretaceous of southern Utah, USA: Sedimentology, v. 58, no. 6, p. 1486–1513.

Allen, J., and Johnson, C. L., 2010a, Sedimentary facies, paleoenvironments, and relative sea level changes in the John Henry Member, Cretaceous Straight Cliffs Formation, southern Utah, USA, in: S. M. Carney, D. E. Tabet, and C. L. Johnson, eds., Utah Geological Association Geology of South-Central Utah, v. 39: p. 225–247.

Allen, J. L., and Johnson, C. L., 2010b, Facies control on sandstone composition (and influence of statistical methods on interpretations) in the John Henry Member, Straight Cliffs Formation, southern Utah, USA: Sedimentary Geology, v. 230, no. 1-2, p. 60–76.

Allen, G. P., and Posamentier, H. W., 1993, Transgressive facies and sequence architecture in mixed tide- and wave-dominated incised valleys: example from the Gironde Estuary, France: Journal of Sedimentary Petrology, v. 63, no. 3, p. 378–391.

Ardies, G., Dalrymple, R., Zaitlin, B., 2002, Controls on the geometry of incised valleys in the Basal Quartz unit (Lower Cretaceous), Western Canada Sedimentary Basin: Journal of Sedimentary Research, v. 72, no. 5, p. 602–618.

Armstrong, R. L., 1968, Sevier orogenic belt in Nevada and Utah: Geological Society of America Bulletin, v. 79, no. 4, p. 429–458.

Aslan, A., Autin, W. J., Blum, M. D., 2005, Causes of river avulsion: insights from the Late Holocene avulsion history of the Mississippi River, U.S.A.: Journal of Sedimentary Research, v. 75, no. 4, p. 650–664.

Baker, E. K., Harris, P. T., Keene, J. B., Short, S. A., 1995, Patterns of sedimentation in the macrotidal Fly River Delta, Papua New Guinea, in: B. W. Flemming, and A. Bartholoma, eds., Tidal Signatures in Modern and Ancient Sediments: International Association of Sedimentologists, Special Publication 24: p. 193–211.

Barwis, J. H., McPherson, J. G., Studlick, J. R. J., 1990, Sandstone Petroleum Reservoirs, Springer-Verlag, New York: p. 583.

Bhattacharya, J. P., and Giosan, L., 2003, Wave-influenced deltas: geomorphological implications for facies reconstruction: Sedimentology, v. 50, no. 1, p. 187–210.

Bhattacharya, J. P., and Willis, B. J., 2001, Lowstand deltas in the Frontier Formation, Powder River Basin, Wyoming: implications for sequence stratigraphic models: AAPG Bulletin, v. 85, no. 2, p. 261–294.

Blum, M. D., 1993, Genesis and architecture of incised valley fill sequences: a Late Quaternary example from the Colorado River, Gulf Coastal Plain of Texas: Chapter 10: Recent applications of siliciclastic sequence stratigraphy, in: P. Weimer, and H. Posamentier, eds., AAPG Memoir 58: Siliciclastic Sequence Stratigraphy: Recent Developments and Applications: American Association of Petroleum Geologists, p. 259–283.

Blum, M. D., and Aslan, A., 2006, Signatures of climate vs. sea-level change within incised valley-fill successions: Quaternary examples from the Texas Gulf Coast: Sedimentary Geology, v. 190, no. 1-4, p. 177–211.

Blum, M. D., Martin, J., Milliken, K., Garvin, M., 2013, Paleovalley systems: insights from Quaternary analogs and experiments: Earth-Science Reviews, v. 116, p. 128–169.

Blum, M. D., and Törnqvist, T. E., 2000, Fluvial responses to climate and sea level change: a review and look forward: Sedimentology, v. 47, p. 2–48.

Bobb, M. C., 1991, The Calico Bed, Upper Cretaceous, southern Utah: a fluvial sheet deposit in the Western Interior Foreland Basin and its relationship to eustasy and tectonics: University of Colorado, p. 251.

Boyd, R., 2010, Transgressive wave-dominated coasts, in: N. P. James, and R. W. Dalrymple, eds., Facies Models 4: p. 265–294.

Boyd, R., Dalrymple, R. W., Zaitlin, B. A., 2006, Estuarine and incised-valley facies models, in: R. G. Walker, and H. W. Posamentier, eds., Facies Models Revisited, SEPM Special Publication 84: p. 171–235.

Bridge, J. S., 2003, Rivers and Floodplains: Forms, Processes, and the Sedimentary Record: Oxford, Blackwell Science Ltd.: p. 491.

Cattaneo, A., and Steel, R. J., 2003, Transgressive deposits: a review of their variability: Earth-Science Reviews, v. 62, no. 3-4, p. 187–228.

Catuneanu, O., 2006, Principles of Sequence Stratigraphy: Amsterdam, Elsevier: p. 375.

Chatanantavet, P., Lamb, M. P., Nittrouer, J. A., 2012, Backwater controls of avulsion location on deltas: Geophysical Research Letters, v. 39, no. 1, p. 1–6.

Coney, P. J., 1972, Cordilleran tectonics and North America plate motion: American Journal of Science, v. 272, no. 7, p. 603–628.

Curray, J. R., 1964, Transgressions and regressions, in R. L. Miller, ed., Papers in Marine Geology, Shepard Commemorative Volume, p. 175–203.

Dalrymple, R. W., 2010, Tidal depositional systems, in N. P. James, and R. W. Dalrymple, eds., Facies Models 4: Geological Association of Canada, p. 201–232.

Dalrymple, R. W., and Choi, K., 2007, Morphologic and facies trends through the fluvial–marine transition in tide-dominated depositional systems: a schematic framework for environmental and sequence-stratigraphic interpretation: Earth-Science Reviews, v. 81, no. 3-4, p. 135–174.

Dalrymple, R. W., Mackay, D. A., Ichaso, A. A., Choi, K. S., 2012, Processes, morphodynamics, and facies of tide-dominated estuaries, in: R. A. Davis, R. W. Dalrymple, eds., Principles of Tidal Sedimentology: Springer Netherlands, p. 79–107.

Dalrymple, R. W., Zaitlin, B. A., Boyd, R., 1992, Estuarine facies models: conceptual basis and stratigraphic implications: Journal of Sedimentary Research, v. 62, no. 6, p. 1130–1146.

Davis, R. A., and Hayes, M. O., 1984, What is a wave-dominated coast?: Marine Geology, v. 60, no. 1-4, p. 313–329.

DeCelles, P. G., and Coogan, J. C., 2006, Regional structure and kinematic history of the Sevier fold-and-thrust belt, central Utah: Geological Society of America Bulletin, v. 118, no. 7-8, p. 841–864.

Demarest, J.M., and Kraft, J.C., 1987, Stratigraphic record of Quaternary sea levels: implications for more ancient strata, in: D. Nummedal, O.H. Pilkey, S.D. Howard, eds., Sea Level Fluctuation and Coastal Evolution: SEPM Special Publication 41: p. 223–239.

Devine, P. E., 1991, Transgressive origin of channeled estuarine deposits in the Point Lookout Sandstone, northwestern New Mexico: a model for Upper Cretaceous, cyclic regressive parasequences of the U.S. Western Interior: AAPG Bulletin, v. 75, no. 6, p. 1039–1063.

Dickinson, W. R., 1974, Plate tectonics and sedimentation, tectonics and sedimentation, in: W. R. Dickinson, ed., Tectonics and Sedimentation: Society of Economic Paleontologists and Mineralogists Special Publication 22: p. 1–27.

Doelling, H. H., and Willis, G. C., 1999, Interim geologic map of the Escalante and parts of the Loa Hite Crossing 30' x 60' Quadrangles, Garfield and Kane Counties, Utah, Utah Geological Survey: Open-File Report 368.

Dooling, P. R., 2013, Tidal facies, stratigraphic architecture, and along-strike variability of a high energy, transgressive shoreline, Late Cretaceous, Kaiparowits plateau, southern Utah: University of Utah, p. 141.

Dooling, P. R., Johnson, C. L., Allen, J. L., 2012, Preservation and architecture of transgressive-regressive cycles in the Upper Cretaceous John Henry Member, of the Straight Cliffs Formation, Left Hand Collet, southern Utah, USA, Abstracts with Program: AAPG Annual Convention and Exhibition 2012, Long Beach, CA.

Embry, A. F., and Johannessen, E. P., 1993, T-R sequence stratigraphy, facies analysis and reservoir distribution in the uppermost Triassic-Lower Jurassic succession, western Sverdrup Basin, Arctic Canada, in: T. O. Vorren, E. Bergsager, O. A. Dahl-

Stamnes, E. Holter, B. Johansen, E. Lie, and T. Lund, eds., Arctic Geology and Petroleum Potential: Special Publication - Norwegian Petroleum Society, NPF, vol. 2: p. 121–146.

Ericksen, M. C., and Slingerland, R., 1990, Numerical simulations of tidal and wind-driven circulation in the Cretaceous Interior Seaway of North America: Geological Society of America Bulletin, v. 102, no. 11, p. 1499–1516.

Fielding, C. R., 2010, Planform and facies variability in asymmetric deltas: facies analysis and depositional architecture of the Turonian Ferron Sandstone in the western Henry Mountains, south-central Utah, U.S.A.: Journal of Sedimentary Research, v. 80, no. 5, p. 455–479.

Fielding, C. R., Trueman, J. D., Alexander, J., 2005, Sharp-based, flood-dominated mouth bar sands from the Burdekin River Delta of northeastern Australia: extending the spectrum of mouth-bar facies, geometry, and stacking patterns: Journal of Sedimentary Research, v. 75, no. 1, p. 55–66.

FitzGerald, D. M., and Penland, S., 1987, Backbarrier dynamics of the east Friesian Islands: Journal of Sedimentary Research, v. 57, no. 4, p. 746–754.

Gallin, W., 2010, Fluvial stratigraphic architecture of the John Henry Member of the Straight Cliffs Formation, Kaiparowits Plateau, Utah, USA: University of Utah, p. 255.

Gallin, W., Johnson, C. L., Allen, J. L., 2010, Fluvial and marginal marine architecture of the John Henry Member, Straight Cliffs Formation, Kelly Grade of the Kaiparowits Plateau, south-central Utah, in: C. L. Carney, S.M. Tabet, D.E. Johnson, eds., Utah Geological Association Geology of South-Central Utah, v. 39: p. 248–279.

Gibling, M. R., 2006, Width and thickness of fluvial channel bodies and valley fills in the geological record: a literature compilation and classification: Journal of Sedimentary Research, v. 76, no. 5, p. 731–770

Gingras, M. K., MacEachern, J. A., 2012, Tidal ichnology of shallow-water clastic settings. in: Davis, R. A., Dalrymple, R. W., eds., Principles of Tidal Sedimentology: p. 57–77.

Gooley, J. T., 2010, Alluvial architecture and predictive modeling of the Late Cretaceous John Henry Member, Straight Cliffs Formation, southern Utah: University of Utah, p. 376.

Gouw, M. J. P., and Berendsen, H. J. A., 2007, Variability of channel-belt dimensions and the consequences for alluvial architecture: observations from the Holocene Rhine-Meuse Delta (the Netherlands) and Lower Mississippi Valley (U.S.A.): Journal of Sedimentary Research, v. 77, no. 2, p. 124–138.

Hancock, J. M., and Kauffman, E. G., 1979, The great transgressions of the Late Cretaceous: Journal of the Geological Society, v. 136, no. 2, p. 175–186.

Haq, B. U., Hardenbol, J., Vail, P. R., 1987, Chronology of fluctuating sea levels since the Triassic: Science, v. 235, no. 4793, p. 1156–1167.

Hardenbol, J., Thierry, J., Farley, M. B., Jacquin, T., De Graciansky, P. C., and Vail, P.R., 1998, Mesozoic and Cenozoic sequence chronostratigraphic framework of European basins: SEPM Special Publication, v. 60, p. 3-14.

Harris, P. T., 1994, Incised valleys and backstepping deltaic deposits in a foreland-basin setting, Torres Strait and Gulf of Papua, Australia, in: R. W. Dalrymple, R. Boyd, and B. A. Zaitlin, eds., Incised-Valley Systems: Origin and Sedimentary Sequences: SEPM, Special Publication 51: p. 45–62.

Hart, B., and Plint, A., 1993, Tectonic influence on deposition and erosion in a ramp setting: Upper Cretaceous Cardium Formation, Alberta foreland basin: AAPG Bulletin, v. 77, no. 12, p. 2092–2107.

Hayes, M. O., 1979, Barrier island morphology, in S. P. Leatherman, ed., S, M.O., 1979, Barrier island morphology, in: Leatherman, S.P., ed., Barrier Islands from the Gulf of Mexico to the Gulf of St. Lawrence: Academic Pr, p. 1–28.

Hayes, M. O., and FitzGerald, D. M., 2013, Origin, evolution, and classification of tidal inlets: Journal of Coastal Research, v. 69, p. 14–33.

Helland-Hansen, W., and Gjelberg, J. G., 1994, Conceptual basis and variability in sequence stratigraphy: a different perspective: Sedimentary Geology, v. 92, no. 1-2, p. 31–52.

Helland-Hansen, W., and Martinsen, O. L., 1996, Shoreline trajectories and sequences: description of variable depositional-dip scenarios: Journal of Sedimentary Research, v. 66, no. 4, p. 670–688.

Hettinger, R. D., 1995, Sedimentological descriptions and depositional interpretation, in sequence stratigraphic context, of two 300-meter cores from the Upper Cretaceous

Straight Cliffs Formation, Kaiparowits Plateau, Kane County, Utah: U.S. Geological Survey Bulletin, report 2: p. A1–A32.

Hettinger, R. D., 2000, A summary of coal distribution and geology in the Kaiparowits Plateau, Utah, in: M. A. Krischbaum, L. N. R. Roberts, and L. R. H. Biewick, eds., Geologic Assessment of Coal in the Colorado Plateau: Arizona, Colorado, New Mexico, and Utah: U. S. Geological Survey Professional Paper 1625-B, p. J1–J17.

Hettinger, R.D., McCabe, P. J., and Shanley, K. W., 1993, Detailed facies anatomy of transgressive and highstand systems tracts from the Upper Cretaceous of southern Utah, USA: Chapter 9: Recent Applications of Siliciclastic Sequence Stratigraphy, American Association of Petroleum Geologists Memoir 58: p. 235–257.

Holbrook, J. M., and Bhattacharya, J. P., 2012, Reappraisal of the sequence boundary in time and space: case and considerations for an SU (subaerial unconformity) that is not a sediment bypass surface, a time barrier, or an unconformity: Earth-Science Reviews, v. 113, no. 3-4, p. 271–302.

Hori, K., Saito, Y., Quanhong, Z., Wang, P., 2002, Architecture and evolution of the tide-dominated Changjiang (Yangtze) River Delta, China: Sedimentary Geology, v. 146, p. 249–264.

Hughes, Z., 2012, Tidal channels on tidal flats and marshes, in R. A. Davis Jr., and R. W. Dalrymple, eds., Principles of Tidal Sedimentology: Springer Netherlands, p. 269–300.

Israel, A., 1987, A sedimentologic description of a microtidal, flood-tidal delta, San Luis Pass, Texas: Journal of Sedimentary Research, v. 57, no. 2, p. 288–300.

Jennette, D., Jones, C., Van Wagoner, J., Larsen, J., 1991, High-resolution sequence stratigraphy of the Upper Cretaceous Tocito Sandstone: the relationship between incised valleys and hydrocarbon accumulation, San Juan Basin, New Mexico, in: J.C. Van Wagoner, C.R. Jones, D.R. Taylor, D. Nummedal, D.C. Jennette, and G.W. Riley, eds., AAPG Special Publication 25: Sequence Stratigraphy Applications to Shelf Sandstone Reservoirs: p. 24–62.

Jerolmack, D. J., Mohrig, D., 2007, Conditions for branching in depositional rivers: Geology, v. 35, no. 5, p. 463.

Johnson, C.L., Stright, L.E., Benhallem, W., Pettinga, L.A., Turner, A., 2013, Metrics of stratigraphic architecture, and depositional controls on fluvial channel belt evolution:

example from the Cretaceous of Utah (USA), Abstracts with Program: 10th International Conference on Fluvial Sedimentology, Leeds, UK.

Jordan, T. E., 1981, Thrust loads and foreland basin evolution, Cretaceous, Western United States: AAPG Bulletin, no. 12, p. 2506–2520.

Kauffman, E. G., 1977, Geological and biological overview: Western Interior Cretaceous Basin: The Mountain Geologist, v. 14, no. 3-4, p. 75–99.

Kieft, R. L., Hampson, G. J., Jackson, C. A., Larsen, E., 2011, Stratigraphic architecture of a net-transgressive marginal- to shallow-marine succession: Upper Almond Formation, Rock Springs Uplift, Wyoming, U.S.A.: Journal of Sedimentary Research, v. 81, no. 7, p. 513–533.

Lane, E. W., 1955, The importance of fluvial morphology in hydraulic engineering: Journal of the Hydraulics Division, American Society of Civil Engineers: v. 81, p. 1–17.

Lawton, T. F., and Bradford, B. A., 2011, Correlation and provenance of Upper Cretaceous (Campanian) fluvial strata, Utah, U.S.A., from Zircon U-Pb Geochronology and Petrography: Journal of Sedimentary Research, v. 81, no. 7, p. 495–512.

Li, W., Bhattacharya, J. P., Zhu, Y., 2011, Architecture of a forced regressive systems tract in the Turonian Ferron Notom Delta, southern Utah, U.S.A.: Marine and Petroleum Geology, v. 28, no. 8, p. 1517–1529.

Li, Y., and Bhattacharya, J. P., 2013, Facies-architecture study of a stepped, forced regressive compound incised valley in the Ferron Notom Delta, southern central Utah, U.S.A: Journal of Sedimentary Research, v. 83, no. 3, p. 206–225.

Liu, S., Nummedal, D., Gurnis, M., 2014, Dynamic versus flexural controls of Late Cretaceous Western Interior Basin, USA: Earth and Planetary Science Letters, v. 389, p. 221–229.

Liu, S., Nummedal, D., Liu, L., 2011, Migration of dynamic subsidence across the Late Cretaceous United States Western Interior Basin in response to Farallon plate subduction: Geology, v. 39, no. 6, p. 555–558.

MacEachern, J. A., Raychaudhuri, I., Pemberton, S. G., 1992, Stratigraphic applications of the *Glossifungites* ichnofacies: delineating discontinuities in the rock record, in: S.

G. Pemberton, ed., Applications of Ichnology to Petroleum Exploration: Special Publications of SEPM: p. 169–198.

McCabe, P. J., Shanley, K. W., 1992, Organic control on shoreface stacking patterns: bogged down in the mire: Geology, v. 20, p. 741–744.

Miall, A. D., 1985, Architectural-element analysis: a new method of facies analysis applied to fluvial deposits: Earth-Science Reviews, v. 22, no. 4, p. 261–308.

Miall, A. D., 2014, Fluvial Depositional Systems: Cham, Springer International Publishing: p. 332.

Miller, K. G., Kominz, M. A., Browning, J. V., Wright, J. D., Mountain, G. S., Katz, M. E., Sugarman, P. J., Cramer, B. S., Christie-Blick, N., Pekar, S. F., 2005, The Phanerozoic record of global sea-level change: Science, v. 310, no. 5752, p. 1293–8.

Miller, K. G., Sugarman, P. J., Browning, J. V., Kominz, M. A., Hernández, J. C., Olsson, R. K., Wright, J. D., Feigenson, M. D., Van Sickel, W., 2003, Late Cretaceous chronology of large, rapid sea-level changes: glacioeustasy during the greenhouse world: Geology, v. 31, no. 7, p. 585–588

Morozova, G. S., and Smith, N. D., 2000, Holocene avulsion styles and sedimentation patterns of the Saskatchewan River, Cumberland Marshes, Canada: Sedimentary Geology, v. 130, p. 81–105.

Mulhern, J. S., Johnson, C. L., Stright, L.E., Chentnik, B. M., 2014, Implications of an expanded section and delta deposits in the Cretaceous Straight Cliffs Formation in the northern Kaiparowits Plateau, southern Utah, USA, Abstracts with Program: AAPG Annual Convention and Exhibition 2014, Houston, TX.

Nummedal, D., and Swift, D. J., 1987, Transgressive stratigraphy at sequence-bounding unconformities: some principles derived from Holocene and Cretaceous examples, in: D. Nummedal, O. H. Pilkey, and J. D. Howard, eds., Sea-Level Fluctuation and Coastal Evolution. SEPM Special Publication 41: p. 241–260.

Olariu, C., and Bhattacharya, J. P., 2006, Terminal distributary channels and delta front architecture of river-dominated delta systems: Journal of Sedimentary Research, v. 76, no. 2, p. 212–233.

Olsen, T. R., Mellere, D., Olsen, T., 1999, Facies architecture and geometry of landward-stepping shoreface tongues: the Upper Cretaceous Cliff House Sandstone (Mancos Canyon, south-west Colorado): Sedimentology, v. 46, no. 4, p. 603–625.

Peterson, F.E., 1969a, Cretaceous sedimentation and tectonism in the southeastern Kaiparowits region, Utah: USGS Open-File Report 1314, Sequence Stratigraphy and Basin Evolution of the Kaiparowits Plateau: p. 259.

Peterson, F.E., 1969b, Four new members of the Upper Cretaceous Straight Cliffs Formation in the south- eastern Kaiparowits region, Kane County, Utah: USGS Bulletin 1274-J, p. J1–J28.

Pettinga, L. A., 2013, Tectonic controls on alluvial architecture in the Upper Cretaceous John Henry Member, Straight Cliffs Formation, southern Utah: The University of Utah, p. 292.

Plink-Björklund, P., 2008, Wave-to-tide facies change in a Campanian shoreline complex, Chimney Rock Tongue, Wyoming–Utah, U.S.A., Society of Economic Paleontologists and Mineralogists Special Publication No. 90, p. 265-291.

Plink-Björklund, P., and Steel, R. J., 2006, Incised valleys on an Eocene coastal plain and shelf, Spitsbergen-part of a linked shelf–slope system, in R. W. Dalrymple, D. A. Leckie, R. W. Tillman., eds., Incised Valleys in Time and Space, SEPM Special Publication No. 85, p. 281–307.

Posamentier, H. W., 2001, Lowstand alluvial bypass systems: incised vs. unincised: AAPG Bulletin, v. 85, no. 10, p. 1771–1793.

Posamentier, H. W., Allen, G. P., James, D. P., Tesson, M., 1992, Forced regressions in a sequence stratigraphic framework: concepts, examples, and exploration significance: AAPG Bulletin, v. 76, no. 11, p. 1687–1709.

Posamentier, H. W., Erskine, R. D., Mitchum Jr., R. M., 1991, Models for submarine-fan deposition within a sequence-stratigraphic framework, in: P. Weimer, and M. Link, eds., Seismic Facies and Sedimentary Processes of Submarine Fans and Turbidite Systems SE - 6: Frontiers in Sedimentary Geology: p. 127–136.

Posamentier, H. W., Jervey, M. T., Vail, P. R., 1988, Eustatic controls on clastic deposition I - conceptual framework, in C. K. Wilgus, B. S. Hastings, C. G. Kendall, H. W. Posamentier, C. A. Ross, and J. Van Wagoner, eds., Sea-level Changes: An Integrated Approach, SEPM Special Publication 42: p. 109–124.

Posamentier, H. W., and Vail, P. R., 1988, Eustatic controls on clastic deposition II-sequence and systems tract models, in C. K. Wilgus, B. S. Hastings, C. G. Kendall, H. W. Posamentier, C. A. Ross, and J. Van Wagoner, eds., Sea-level Changes: An

Integrated Approach: SEPM Special Publication 42: Tulsa, Oklahoma, Society of Economic Paleontologists and Mineralogists, p. 125–154.

Reineck, H. E., Wunderlich, F., 1968, Classification and origin of flaser and lenticular bedding: Sedimentology, v. 11, no. 1-2, p. 99–104.

Reinson, G.E., 1992, Transgressive barrier island and estuarine systems, in: R.G. Walker, N.P. James, eds., Facies Models—Response to Sea Level Change. Geological Association of Canada Publications, p. 179–194.

Saito, Y., 1994, Shelf sequence and characteristic bounding surfaces in a wave-dominated setting: latest Pleistocene–Holocene examples from the northeast Japan, Marine Geology, v. 120, p. 105–127.

Schumm, S., 1993, River response to base-level change: implications for sequence stratigraphy: The Journal of Geology, v. 101, no. 2, p. 279–294.

Shanley, K. W., and McCabe, P. J., 1991, Predicting facies architecture through sequence stratigraphy - an example from the Kaiparowits Plateau, Utah: Geology, v. 19, p. 742-745.

Shanley, K. W., 1991, Sequence stratigraphic relationships and facies architecture of Turonian-Campanian strata, Kaiparowits Plateau, south-central Utah: Colorado School of Mines, p. 390.

Shanley, K. W., McCabe, P. J., Hettinger, R., 1992, Tidal influence in Cretaceous fluvial strata from Utah, USA: a key to sequence stratigraphic interpretation: Sedimentology, v. 39, no. 5, p. 905–930.

Shanley, K. W., and McCabe, P. J., 1993, Alluvial architecture in a sequence stratigraphic framework: a case history from the Upper Cretaceous of southern Utah, USA: Special Publication 15 of the International Association of Sedimentologists: p. 21-56.

Shanley, K. W., and McCabe, P. J., 1994, Perspectives on the sequence stratigraphy of continental strata: AAPG bulletin, v. 4, no. 4, p. 544–568.

Shanley, K. W., and McCabe, P. J., 1995, Sequence stratigraphy of Turonian- Santonian strata, Kaiparowits Plateau, southern Utah, USA: implications for regional correlation and foreland basin evolution: American Association of Petroleum Geologists Memoir 64: p. 103-136.

Simms, A., 2006, Overfilled versus underfilled incised valleys: examples from the Quaternary Gulf of Mexico, in R. W. Dalrymple, D. A. Leckie, R. W. Tillman., eds., Incised Valleys in Time and Space, SEPM Special Publication No. 85: p. 117–139.

Simms, A. R., Anderson, J. B., Blum, M., 2006, Barrier-island aggradation via inlet migration: Mustang Island, Texas: Sedimentary Geology, v. 187, no. 1-2, p. 105–125.

Sixsmith, P. J., Hampson, G. J., Gupta, S., Johnson, H. D., Fofana, J. F., 2008, Facies architecture of a net transgressive sandstone reservoir analog: the Cretaceous Hosta Tongue, New Mexico: AAPG Bulletin, v. 92, no. 4, p. 513–547.

Slingerland, R., and Smith, N. D., 2004, River avulsions and their deposits: Annual Review of Earth and Planetary Sciences, v. 32, no. 1, p. 257–285.

Steel, R. J., Plink-Bjorklund, P., Aschoff, J., 2012, Tidal deposits of the Campanian Western Interior Seaway, Wyoming, Utah and Colorado, USA, in: R. A. Davis, and R. W. Dalrymple, eds., Principles of Tidal Sedimentology: p. 437–471.

Strong, N., and Paola, C., 2008, Valleys that never were: time surfaces versus stratigraphic surfaces: Journal of Sedimentary Research, v. 78, no. 8, p. 579–593.

Swift, D. J. P., 1968, Coastal erosion and transgressive stratigraphy: The Journal of Geology, v. 76, no. 4, p. 444–456.

Swift, D.J.P., Phillips, S., Thorne, J.A., 1991, Sedimentation on continental margins: IV. lithofacies and depositional systems, in: D.J.P. Swift, G.F. Oertel, R.W. Tillman, J.A. Thorne, eds., Shelf Sand and Sandstone Bodies—Geometry, Facies and Sequence Stratigraphy. International Association of Sedimentologists Special Publication 14: p. 89–152.

Szwarc, T. S., Johnson, C. L., Stright, L. E., McFarlane, C. M., in press, Interactions between axial and transverse drainage systems in the Late Cretaceous Cordilleran foreland basin: evidence from detrital zircons in the Straight Cliffs Formation, southern Utah, USA: Geological Society of America Bulletin.

Taylor, D. R., and Lovell, R. W. W., 1995, High-frequency sequence stratigraphy and paleogeography of the Kenilworth Member, Blackhawk Formation, Book Cliffs, Utah, U.S.A, in: J. C. Van Wagoner, and G. T. Bertram, eds., Sequence stratigraphy of foreland basin deposits: outcrop and subsurface examples from the Cretaceous of North America: AAPG Memoir 64: p. 257–275.

Thomas, M., and Anderson, J. B., 1994, Sea-level controls on the facies architecture of the Trinity/Sabine incised-valley system, Texas continental shelf, in: R. W. Dalrymple, R. Boyd, and B. A. Zaitlin, eds., Incised-Valley Systems: Origin and Sedimentary Sequences: Society of Economic Paleontologists and Mineralogists, p. 63–82.

Thomas, R. G., Smith, D. G., Wood, J. M., Visser, J., Calverley-Range, E. A., Koster, E. H., 1987, Inclined heterolithic stratification-terminology, description, interpretation and significance: Sedimentary Geology, v. 53, no. 1-2, p. 123–179.

Thorne, J. A., and Swift, D. J. P., 1991, Sedimentation on continental margins; VI, A regime model for depositional sequences, their component systems tracts, and bounding surfaces, in: D. J. P. Swift, G. F. Oertel, R. W. Tillman, and J. A. Thorne, eds., Shelf Sand and Sandstone Bodies: Geometry, Facies and Sequence Stratigraphy: International Association of Sedimentology, p. 189–255.

Turner, A., Stright, L. E., Johnson, C. L., Pettinga, L.A., in review, Temporal variability in fluvial deposition and the implications for static reservoir connectivity: John Henry Member, Straight Cliffs Formation (Cretaceous, Utah): AAPG Bulletin.

Vaninetti, G. E., 1979, Coal stratigraphy of the John Henry Member of the Straight Cliffs Formation, Kaiparowits Plateau, Utah: The University of Utah, p. 292.

Van Wagoner, J. C., 1995, Sequence stratigraphy and marine to nonmarine facies architecture of foreland basin strata, Book Cliffs, Utah, USA, in: J. C. Van Wagoner, and G. T. Bertram, eds., Sequence Stratigraphy Of Foreland Basin Deposits: Outcrop and Subsurface Examples From the Cretaceous Of North America: AAPG Memoir 64: p. 137–223.

Van Wagoner, J. C., Mitchum, R., Campion, K. M., Rahmanian, V. D., 1990, Siliciclastic sequence stratigraphy in well logs, cores, and outcrops: concepts for high-resolution correlation of time and facies, in: Methods in Exploration Series 7: Siliciclastic Sequence Stratigraphy in Well Logs, Cores, and Outcrops: Concepts for High-Resolution Correlation of Time and Facies, v. 7, no. 55.

Van Wagoner, J., Posamentier, H. W., Mitchum, R. M., Vail, P. R., Sarg, J. F., Loutit, T. S., Hardenbol, J, 1988, An overview of the fundamentals of sequence stratigraphy and key definitions, in C. K. Wilgus, B. S. Hastings, C. G. Kendall, H. W. Posamentier, C. A. Ross, and J. Van Wagoner, eds., Sea-level Changes: An Integrated Approach, SEPM Special Publication 42: p. 39–45.

Walker, R. G., and Pint, A. G., 1992, Wave and storm-dominated shallow marine systems, in: R. G. Walker, and N. P. James, eds., Facies Models: Response To Sea-Level Change: Geological Association of Canada, p. 219–238.

Willis, B., 1997, Architecture of fluvial dominated valley fill deposits in the Cretaceous Fall River Formation: Sedimentology, v. 44, no. 4, p. 735–757.

Willis, B., and Gabel, S., 2003, Formation of deep incisions into tide-dominated river deltas: implications for the stratigraphy of the Sego Sandstone, Book Cliffs, Utah, USA: Journal of Sedimentary Research, v. 73, no. 2, p. 249–263.

Zaitlin, B., Dalrymple, R., Boyd, R., 1994, The stratigraphic organization of incised-valley systems associated with relative sea-level change, in: R. W. Dalrymple, R. Boyd, and B. A. Zaitlin, eds., Incised-Valley Systems: Origin and Sedimentary Sequences: Society of Economic Paleontologists and Mineralogists, p. 45–60.

Zaitlin, B. A., Warren, M. J., Potocki, D., Rosenthal, L., Boyd, R., 2002, Depositional styles in a low accommodation foreland basin setting: an example from the Basal Quartz (Lower Cretaceous), southern Alberta: Bulletin of Canadian Petroleum Geology, v. 50, no. 1, p. 31–72.

Zhu, Y., Bhattacharya, J. P., Li, W., Lapen, T. J., Jicha, B. R., Singer, B. S., 2012, Milankovitch-scale sequence stratigraphy and stepped forced regressions of the Turonian Ferron Notom Deltaic complex, south-central Utah, U.S.A: Journal of Sedimentary Research, v. 82, no. 9, p. 723–746.